Measurement of engineered nanoparticles in foods - electron microscopy method development and validation

Agnieszka Dorota Dudkiewicz

PhD Thesis

University of York

Environment Department

March 2014

Abstract

The increasing interest in use of nanotechnology by the food industry brought concerns over safety of engineered nanoparticle application in the foods and food contact materials. To aid the risk assessment in 2010 a project NanoLyse was funded by the European Union under Framework Programme 7. The project was focused on the development and validation of methods for analysing engineered nanoparticles in food matrices. The research presented in this thesis was a part of NanoLyse and was concerned with electron microscopy methods.

The aim of this research was optimization of sample preparation procedures and validation of electron microscopy as an analytical technique for engineered nanoparticle measurement in foods. Thus the comparison of different sample preparation techniques was carried out for engineered nanoparticles in food matrices. Best procedures were chosen: blotting for liquid and sedimentation of the sample onto electron microscopy grid for solid food samples. These sample preparation techniques were then included in validation of electron microscopy.

In view of unavailability of the reference materials electron microscopy results were compared against other analytical methods selected based on the literature review. These techniques were: nanoparticle tracking analysis, gas-phase electrophoretic mobility molecular analyser, centrifugal liquid sedimentation and asymmetric flow field flow fractionation. To render the comparison possible also for studied aggregated, non-spherical particles of synthetic amorphous silica, the concept of data transformation into mass equivalent diameter was developed. Thanks to this it was possible to note that electron microscopy tended to overestimate small particle number in size distribution due to the sample preparation. Subsequently sample preparation for electron microscopy was calibrated for the measurement of engineered nanoparticles of silica. Lastly remaining challenges and knowledge gaps in regards to the measurement of engineered nanoparticles in food were highlighted and discussed against NanoLyse project achievements.

List of contents

List of figures (short)

List of figures

List of figures

List of tables (short)

List of tables

Acknowledgements

I would like to express my deepest gratitude to people who helped me complete this research project.

Firstly I would like to acknowledge my supervisors: Dr Karen Tiede from Food and Environment Research Agency (FERA), Prof. Qasim Chaudhry from FERA, Prof. Alistair Boxall from University of York, Prof. Kristian Molhave from Danish Technical University and Dr Alan MacNicoll from FERA. Thank you for all your help and patience.

I would equally like to thank to people who assisted with this research.

I am especially grateful to Angela Lehner from Technical University of Vienna for providing GEMMA measurements and Dr Stephan Wagner from University of Vienna for AF4-ICP-MS data.

Great appreciation goes to Dr Stéphane Pietravalle from FERA who provided advice and help with statistical solutions especially with compositional data analysis.

I thank to my colleagues from NanoLyse project for collaboration, useful feedback and constructive criticism and especially to Dr Thomas Linsinger from Joint Research Centre (Geel, Belgium) for expert advice on validation part.

I also appreciate involvement of Dr Peter Hoffman and Dr Dirk Tiede for providing an OBIA software used through the project for nanoparticle measurements.

Special thanks go to directory, staff and students at University of York's Nanocentre. I especially am indebted to Prof Pratibha Gay and Prof Ed Boyes for making instruments available for my intensive use. I also thank to Ian Wright, Dr Michael Walsch, Dr Michael Ward and Dr Gonzalo Vallejo Fernandez for all technical help. I appreciate collaboration with Dr Leonardo Lari who invested his time in analysing meat sample by EFTEM and proposed work on presentation of this research on Electron Microscopy and Analysis Group Conference 2013 (held at University of York).

I am grateful to members of FERA staff: Dr Ping Luo, Dr John Lewis, Dr Weiqi Luo and Roy Macarthur for additional support and discussion.

Finally I would like to thank to all my family, friends and colleagues for moral support. I am sure that without you I could not make it through.

Author's declaration

Chapter 2 and Annexes 3-5 were published in peer reviewed journals. Annex 2 was published as one chapter in a book. Also parts of Chapter 1 were adapted from original introductions of the published versions of introductions of Chapter 2 and Annex 2. The publication status of all chapters is given in Table 0.1. The copyrights for published work belong to respective publishers (see Table 0.1).

All chapters regardless of publication status were formatted to fit the requirements of the thesis presentation and to avoid unnecessary repetition. All published and intended for publication chapters were written by the candidate as a lead author. Nevertheless close collaboration with co-authors allowed me to gather needed data for papers (all GEMMA measurements were provided by Angela Lehner from Vienna University and AF4-ICP-MS by Dr Stephan Wagner from the Technical University of Vienna) as well as improve the text quality. Papers presented in Annexes 3-5 were co-authored by the candidate.

The work leading to these results was performed by the candidate during four years of PhD studentship at the University of York. Most of the researchtook place at the Food and Environment Research Agency in York and the University of York's Nanocentre. Part of work (NTA data collection) was also undertaken in the Environment department of the University of York.

The research presented here was funded by EU Programme NanoLyse (FP7/2007-2013) under grant agreement n° 245162.

Table 0.1- Chapters and annexes presented in the thesis and their publication status

Chapter	Authors	Title	Status	Publication
2	Dudkiewicz A., Tiede K., Loeschner K., Soegaard Jensen L. H., Jensen E., Wierzbicki R., Boxall A. B. A. & Molhave K.	Characterization of nanomaterials in food by electron microscopy	Published (2011)	*Trends in Analytical Chemistry 30(1): 28-43*
3	Dudkiewicz A., Lehner A., Molhave K., Chaudhry Q., Boxall A., Hofmann P., Allmaier G., & Tiede K.	Evaluation of sample preparation techniques for electron microscopy- analysis of silica engineered nanoparticles in a model tomato soup matrix	In prep.	
4	Dudkiewicz A., Boxall A. B. A., Chaudhry Q., Molhave K., Tiede K., Hofmann P. & Linsinger T. P. J.	Development and validation of analytical procedures for measurement of engineered nanoparticles in food by electron microscopy	In prep.	
5	Dudkiewicz A., Wagner S., Lehner A., Chaudhry Q., Pietravalle S., Tiede K., Boxall A. B. A., Allmaier G., Tiede D., Grombe R., von der Kammer F., Hofmann T., and Kristian Molhave	Evaluation of electron microscopy against other nano-analysis methods for the measurement of aggregated silica engineered nanoparticles	In prep.	
Annex 2	Dudkiewicz A., Luo P., Tiede K. & Boxall A. B. A.	Detecting and characterizing nanoparticles in food, beverages and nutraceuticals. In edited by Qingrong Huang *Nanotechnology in the food, beverage and nutraceutical industries.*	Published (2012)	*Woodhead Publishing*
Annex 3	Lari L. & Dudkiewicz A.	Sample preparation and EFTEM of Meat Samples for Nanoparticle Analysis in Food	Published (2014)	*Journal of Physics, Conference Series 522(1): 012057*

Table 0.1- Continued

Chapter	Authors	Title	Status	Publication
Annex 4	Luo P., Morrison I., Dudkiewicz A., Tiede K., Boyes E., O'Toole P., Park S & Boxall A. B. A.	Visualization and characterization of engineered nanoparticles in complex environmental and food marices using atmospheric scanning electron microscopy	Published (2013)	*Journal of Microscopy 250(1): 32-41*
Annex 5	Grombe R., Charoud-Got J., Emteborg H., Linsinger T. P. J., Seghers J., Wagner S., von der Kammer F., Hofmann T., Dudkiewicz A., Llinas M., Solans C., Lehner A. & Allmaier G.	Production of reference materials for the detection and size determination of silica nanoparticles in tomato soup.	Published (2014)	*Analytical and Bioanalytical Chemistry 406(16): 3895-3907*

Chapter 1

Introduction

Nanotechnology is a technology employing materials with at least one dimension smaller than 100 nm (Tiede *et al.,* 2008). These materials feature different properties to their chemical bulk or ionic counterparts and thus are now or beginning to be exploited in new products in many branches of industry. A constantly updated inventory of consumer products containing nanomaterials is available from www.nanotechproject.org.

One of the industries applying nanotechnology is the food and beverage sector. The numerous applications of engineered nanomaterials or engineered nanoparticles (ENPs) in this sector are summarised in several review publications (Chaudhry *et al.*, 2008; Chaudhry and Castle, 2011; Blasco and Picó, 2011; Cushen *et al.*, 2012) and include use for improvement of shelf life, sensory quality or nutritional value of foodstuffs. Examples of types of ENPs in use in the food sector include nano-silver which is used as an antimicrobial in food packaging (Mahdi *et al.*, 2012); nano-silica which acts as a taste intensifier in dietetic beverages (MRC, 2009); nano-cellulose which is used for moisture retention (Ström *et al.*, 2013); and nano-encapsulates which render lipophilic vitamins suspendable in water (Haham *et al.*, 2012).

Alongside these new developments, recent research findings have reported the existence of ENPs in approved food additives, including titanium dioxide-E171 and synthetic amorphous silica (SAS)-E551, which have been used industrially for several decades. Nanoparticles can also be introduced to the foods as contamination resulting from the production process. For example Gatti *et al.* (2009) detected metal nano and micro contaminants on the surface of bread and biscuits. Finally food itself is composed of natural nanomaterials. Many of the compounds that make up food can be smaller than 100 nm in size e.g. casein micelles in milk (Bijl *et al.*, 2014). The presence of natural and contaminating nanoparticles in foods is expected to hamper detection and characterisation of any added ENPs.

The characterisation of ENPs in foods is important not only from the industrial new product development point of view but especially for the assessment of risks to consumers. ENPs are a new range of food additives and as such require specific regulation. Studies into the toxicity of ENPs conducted in recent years have raised

many concerns regarding potential effects on human health (Norwegian Pollution Control Authority, 2008; Fede *et al.*, 2012; Asghari *et al.*, 2012). The results of these studies indicate that for risk assessment purposes, a range of characteristics of an ENP may need to be considered, including aggregation state, surface charge, shape, structure, dissolution rate, chemical composition and mass, particle number concentration (PNC) and specific surface area (SSA) (Norwegian Pollution Control Authority, 2008; Hagendorfer *et al.*, 2012; Buffet *et al.*, 2011). The rationale for this is discussed in the following paragraphs.

Aggregation causes an increase in particle size and a decrease in the PNC and SSA of ENPs. Generally aggregation is considered beneficial from a toxicological point of view as it has been shown that smaller ENPs are taken up more easily by cells (Hillyer and Albrecht, 2001; Liu *et al.*, 2010) and thus aggregation is believed to make ENPs less toxic (Fede *et al.*, 2012). However, aggregation likely results in changes in reactivity and functionality of the ENPs, which may pose a problem in regards to the desired application of an ENP in food. Aggregation of ENPs can be prevented by electrostatic stabilisation or steric stabilisation. Electrostatic stabilisation is created by repulsive electrostatic double layer forces between charged ENPs. The charge of the ENP in the environment in which the ENP is dispersed depends on factors such as the pH and ionic strength (IS) of the environment and can be determined from the Zeta potential (ζ) of the particle. Steric stabilisation involves the use of long chain molecules as 'capping' agents on the particle surface. The capping agents provide steric hindrance for the agglomeration of particles independently of pH or IS of the dispersion environment. Examples of capping agents include surfactants, polymers and proteins. Of special interest are interactions of the ENP surface with proteins, since they may influence the fate and uptake of ENPs in an organism (Lynch and Dawson, 2008). How these interactions proceed depends on several ENP features such as the surface charge (Bouwmeester *et al.*, 2009) and the structural properties such as shape and crystallinity.

Shape is a very important factor which might influence uptake and distribution of an ENP within humans and other mammals and hence its toxicity (Norwegian Pollution Control Authority, 2008). Shape dependent toxicity might explain the toxicological effects of carbon nanotubes which, though much smaller in diameter, are shaped similarly to asbestos fibres and act in a similar manner to asbestos, causing necrosis

of the lungs in mice (Lam, 2003). It needs to be mentioned that shape is not the only explanation for the toxicity of carbon nanotubes and that a combination of properties associated with particular material used in the study may lead to different result (Donaldson *et al*., 2006).

Crystallinity has an impact on the stability of an ENP and its reactivity (Jiang *et al.*, 2008b; Barnard *et al.,* 2010). For example amorphous forms of titanium dioxide ENPs have been found to have the stronger oxidative abilities when compared to crystalline forms (Jiang *et al.*, 2008b). This property has to be considered in food industry applications since reactive oxygen species, when accumulated in the body, are harmful, sometimes resulting in carcinogenicity and causing many other disorders (Diplock *et al.*, 1998). Furthermore, reactive oxygen species may reduce the shelf life of a food product and affect its structure (Chen *et al.*, 1999).

Dissolution rate is as important as aggregation state. Ions will behave very differently than ENPs and in some instances may be more toxic (Misra *et al.*, 2012). For example the gradual dissolution of silver ENPs explains the increases in toxicity of stored dispersions to human mesenchymal stem cells (Kittler *et al.*, 2010). The functionality of an ENP, which also depends on their chemical composition, will have a strong effect on the behaviour of an ENP. The food industry uses this to their advantage when designing ENPs for use in novel products (Chaudhry and Groves, 2010).

Mass concentration can be measured for ENPs as for ‘traditional’ substances. However a more useful measure of exposure may be the PNC of SSA. PNC and SSA are closely connected to some of the other ENP features described above such as size, aggregation and dissolution and density.

A wide range of methods is available for detection and characterisation of ENPs. Numerous detailed reviews of these methods are available in the literature (e.g. Tiede *et al.*, 2008; Luykx *et al.*, 2008; Linsinger *et al.*, 2012 and Dudkiewicz *et al.*, 2012- Annex 2). Methods include chromatography based techniques, imaging techniques, spectroscopy based techniques and mass spectrometry. Nevertheless, no single method is able to measure all of the ENPs’ features described above. Table 1.1 provides an overview of different method capabilities for the characterisation of the listed ENP properties. The electron microscopy (EM) based methods are described in more detailed in Chapter 2.

Table 1.2- Use of analytical methods for characterisation of some ENP features- marked with "+" (Dudkiewicz *et al.*, 2012)

	Size & Size distribution	Aggregation	Dissolution	Chemistry	Shape	Structure	Surface charge	Particle number concentration	Mass concentration	Surface area
Chromatography	+		+							
FFF[1]	+	+	+		FFF-SLS[12], SedFFF-DLS[13]					
CE[2]	+	+	+					+		
Microscopy and coupled analytical techniques	+	+	+	+	+	+				+
Light Scattering	+	+	+	+			ELS[14]	+		
SAXS[3]	+	+			+	+				+
SANS[4]	+	+			+	+				
XRD[5]		+		+		+				
NMR[6]	+	+		+		+				
UV-Vis[7]	+	+							+	
MS[8]	SPMS			+		+			+	
Ultracentrifugation/CLS[9]	+	+	+	+	+	+			+	
Filtration	+		+							
Dialysis			+							
BET[10]										+
Particle Counters	+	+						+		
DSC[11]		+								
Raman Spectroscopy	+			+		+				

[1]Field flow fractionation, [2]Capilary electrophoresis, [3]Small angle x-ray scattering, [4]Small angle neutron scattering, [5]X-ray diffraction, [6]Nuclear magnetic resonance, [7]Ultraviolet visible spectrometry, [8]Mass spectrometry, [9]Centrifugal liquid sedimentation, [10]Brunauer-Emmett-Teller, [11]Differential scanning calorimetry, [12]Field flow fractionation coupled to static light scattering, [13]Sedimentation field flow fractionation coupled to dynamic light scattering. [14]Electrophoretic light scattering

Further challenges with characterisation of ENPs in food products include sample preparation and presence of natural and contaminating nanostructures in foods as mentioned above. Care has to be taken when preparing a food sample for analysis so that the sampling is representative. In some cases ENPs can be expected to be localized in restricted areas of the sample. For example, in the case of migration studies from food contact materials, analysts can expect that ENPs are situated on the surface of the food packed in the contact material.

For some ENPs (e.g. carbon-based ENPs), it may be difficult to distinguish the ENP from the background. For example, nano delivery systems are usually composed of lipids, proteins or polysaccharides (Luykx *et al.*, 2008), which are all naturally present in food products making detection very difficult.

It needs to be mentioned that characterisation of ENPs in general, even in a pristine dispersion, is already challenging. Size characterisation of ENPs, for example, faces two major difficulties: lack of reference materials (especially for ENPs characterised by a broad size distribution) and incomparability of the measurement results in between the methods for ENPs which are not spherical. Many of ENPs are spherical but can undergo agglomeration/aggregation after being added to food. Others might be aggregated as a result of the production process like the mentioned food additives SAS and titanium dioxide E171. For these types of ENPs size data are expressed in different ways by different methods (Table 1.2). Thus the interpretation of measurement results and comparison in between the studies is very arbitrary. Furthermore no full validation of the measurement of such ENPs can be carried out, because the accuracy of the techniques cannot be assessed. Nevertheless characterisation of the particle size distribution is very important from the toxicological as well as regulatory point of view. Recently, the European Commission (EC) issued a recommendation on the definition of nanomaterial (The European Commission, 2011). This recommendation states that a substance will be considered as a nanomaterial if 50% of the particle number within a sample is within size range of 1-100nm. Such a definition adds another challenge as very few methods are able to measure particle size distribution based on number (PNSD) rather than mass (Linsinger *et al.*, 2012; Calzolai *et al.*, 2012).

Table 1.2- Definitions of particle measurements provided by the different techniques

Measurement	Techniques providing measurement	Definition
Equivalent Circle Diameter (ECD)	Microscopy	Diameter of the circle with same projected area as the particle
Electric Mobility Diameter (EMD)	CE, SMPS[1], GEMMA[2]	Diameter of the sphere which has same electric mobility as the particle
Stoke's Sedimentation Diameter (SSD)	CLS	Diameter of a sphere with same sedimentation velocity as the particle
Hydrodynamic Diameter (HDD)	HDC[3], SEC[4], FFF. DLS, NTA[5]	Diameter of a sphere with same diffusional behaviour as the particle
Mass Equivalent Diameter (MED)	SP-ICP-MS[6]	Diameter of a compact sphere of same mass as a particle
Radius of Gyration (R_g)	SLS, MALLS[7]	Root mean square of the distances of the points on the object's perimeter to it's center of gravity

[1]Scanning mobility particle sizer, [2]Gas-phase electrophoretic mobility molecular analyser, [3]Hydrodynamic chromatography, [4]Size exclusion chromatography, [5]Nanoparticle tracking analysis, [6]Single particle inductively coupled plasma with mass spectrometry detection, [7]Multiangle laser light scattering

The European Food Safety Authority (EFSA) in their "Guidance on the risk assessment of the application of nanoscience and nanotechnologies in the food and feed chain" recommends the use of at least two methods for ENP characterisation (EFSA Scientific Committee, 2011). According to this guidance one of these methods should be EM. EM enables visualisation and characterisation of such ENP features as PNSD, shape, crystallinity and, when coupled to spectrometric techniques, also elemental composition. The great resolving power of EM is a result of the application of an electron beam with a wavelength well below the nanometer range. Optical microscopy, operating at wavelengths λ in the range of 400-800 nm and numerical aperture (NA) ~1, Abbe's diffraction limit d=λ/2NA gives a resolution of ~ 200 nm. Since the wavelength of an electron beam is much shorter than the one achieved by light, the resolution of EM will be much higher. For example, an EM working with an acceleration voltage of 100 kV allows theoretically to achieve wavelength of 0.0037 nm (Kachlicki, 2007a).

Two main EM imaging techniques are employed for ENP detection and/or characterisation, namely scanning electron microscopy (SEM) and transmission electron microscopy (TEM) (Calzolai *et al.*, 2012). The various EM methods (Figure 1.1) are briefly described below and elaborated in more detail in Chapter 2.

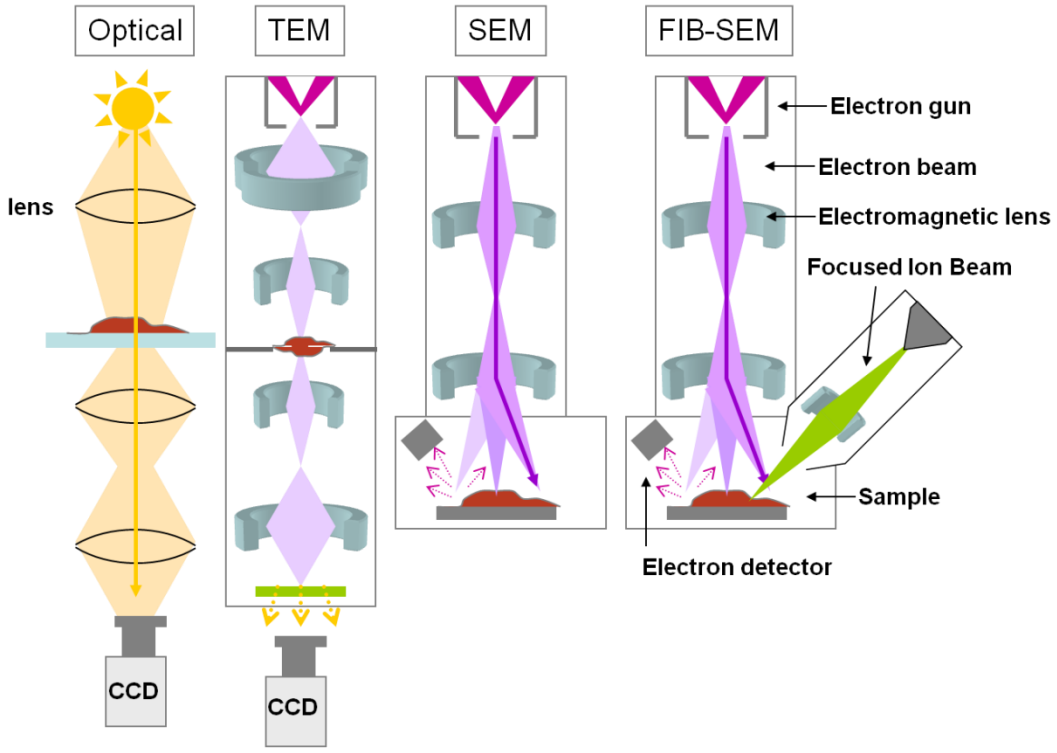

Figure 1.1- Overview of EM methods suitable for ENP characterisation in food matrices

SEM creates an image by scanning the sample surface with a low energy electron beam (1-30 keV) and detecting the scattered electrons. This technique is used for imaging of the sample surface and can provide images with great depth of field, where the whole area of the micrograph is in focus. In a focused ion beam SEM (FIB-SEM), the ion beam can cut into the material being analysed and a solid specimen can be sectioned for 3D imaging while being able to observe the process (this can also be achieved with *in-situ* microtomes) (Denk and Horstmann, 2004).

In TEM, a high energy (80-300 keV) electron beam is transmitted through a very thin layer of the sample. A fraction of the beam is scattered on the sample while some electrons can be transmitted with little change in energy or direction. Contrast in TEM is based on detection of these beam interactions with the sample, providing a

high resolution image and allowing characterisation by numerous spectrometric techniques (see Chapter 2).

Although EM has been used for decades to characterize nano-sized objects like particles, viruses and colloids in complex matrices (Bergh *et al.*, 1989; Leppard *et al.*, 1996; Doucet *et al.*, 2005; Domingos *et al.*, 2009; Tiede *et al.*, 2009c) and has advantages over other analytical methods in terms of the types and quality of information it can provide on ENPs, the technique suffers from many drawbacks. For example, it requires sample preparation, which might be complex and time consuming, as well as induce alterations to the sample (see Chapter 2). Additionally EM is only able to characterise only a very small volume of the sample at once (order of pL), which means that the limit of detection (LOD) is likely to be very high in comparison to other analytical solutions. The volume constraint also limits the number of ENPs that can be analysed in EM and may pose a challenge when it comes to representative sampling. The quantity of ENPs which need analysing to obtain reproducible data has been discussed in several papers and some authors recommend measurement of at least 500 ENPs (Linsinger *et al.*, 2013). EM is also an expensive method to use and consequently acquisition of data on so many ENPs might not always be possible from an economic viewpoint. Data on measurement reproducibility for ENPs in foods by EM methods are so far not available. Additionally for ENPs with broad size distribution and non-spherical shape it is difficult to apply other approaches which could aid assessment of ENP measurement trueness for EM because of above mentioned discrepancies in size definitions. These drawbacks require addressing, to aid the further development of appropriate guidance on the measurement of ENPs in foods using EM and to give confidence in the data generated from EM analyses of food materials.

1.1 Aim and objectives

The overall aim of this research was to develop improved procedures for the detection of ENPs in food materials by EM methodologies. This was achieved by:

1. Performing a literature review of available EM techniques and sample preparation procedures that might be appropriate for detection and characterisation of ENPs in food (Chapter 2)

2. Developing and assessing EM sample preparation protocols for liquid and solid food samples containing ENPs (Chapter 3)
3. Developing a detailed understanding of the performance of EM methods for measurement of ENPs in foods addressing such issues as: minimal measured number of particles required to produce good results, LOD and measurement precision (Chapter 4)
4. Developing of a novel approach for manipulation of nano-measurement data to allow comparison of data arising from different techniques (Chapter 5).
5. Applying the approach developed in objective 4 to assess the methods developed in objectives 2 and 3 against other available analytical approaches (Chapter 5).
6. Refining EM methods for the accurate assessment of ENP size distribution using the findings from objective 5 (Chapter 6)
7. Exploring the implications of the findings of the project for end users (Chapter 7)

The study focuses predominantly on two types of ENPs used in the food industry, namely Ag ENPs and SAS ENPs. EM images of these ENPs were contained in Figure 1.2. Ag ENPs are used in numerous food contact materials as well as some food supplements. Current EU regulations do not allow these products on the European market, nevertheless they can be purchased using the World Wide Web. There is also research ongoing on the application of Ag ENPs in automated food processing, which faces challenges in regards to microbiological cross-contamination of products.

In contrast to the Ag ENPs, the industrial application of SAS in the food industry in Europe is well established. SAS is used as an anti-caking agent or filler in foods. The material has been 'generally regarded as safe' for decades and a recent risk re-assessment (after fractions of ENPs in SAS were detected) suggests that there is no basis for concern over the consumption of SAS at current estimated daily food intakes (Dekkers *et al.*, 2010). Nevertheless SAS might fit into the description of the EC recommendation for the definition of nanomaterial (The European Commission, 2011). If it does, then foods containing it will require new labelling from December 2014 (European Commission, 2012). Nevertheless, measurement of PNSD of SAS is likely to be challenging. One of

the reasons is the shape of these ENPs. SAS is obtained by burning silicon tetrachloride using an oxygen-hydrogen flame. In the process Silica droplets are formed and collide with each other creating stable aggregates (Barthel *et al.*, 1999). Therefore, unlike Ag ENPs, SAS is comprised of particle clusters (see Figure 1.2b and d). This means that different analytical methods are likely to produce very different PNSD for SAS. Additionally as silicon is a ubiquitous element and silica particles have a low refractive index, detection especially in foods is likely to be challenging. Therefore a major part of this research was devoted to the measurement and detection of SAS.

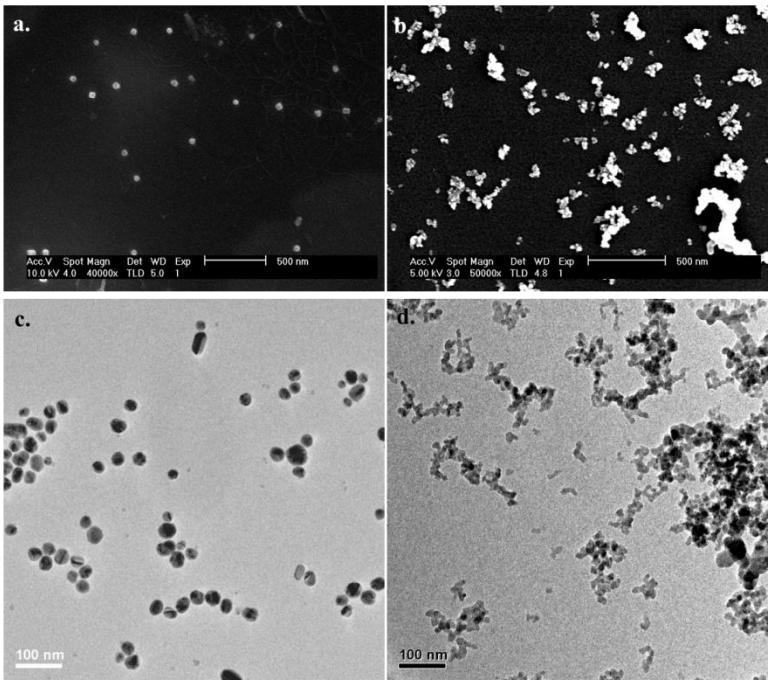

Figure 1.2- SEM (a and b) and TEM (c and d) images of Ag ENPs (a and c) and SAS (b and d)

This research was a part of EU funded NanoLyse project which focused on the development of analytical methods and reference materials for ENPs in foods. Nine institutions from Europe and one from Canada participated in the project and this research benefited from close collaboration with these institutions. Thanks to the collaboration it was possible to validate EM results against other analytical methods, such as GEMMA and AF4-ICP-MS and include in this research some of the first produced reference materials for ENPs in foods.

1.2 Structure of the thesis

The thesis content is divided in chapters, appendices and annexes. The chapters comprise the main body of the thesis and describe majority of the research done during candidate's studentship. Appendices are supporting information for the thesis which were removed from the chapters in order to preserve text coherency (Appendix 2 and 3) or/ and due to the repetition of the part of the research in different chapters (Appendix 1 and 4). Annexes are stand alone research pieces related to topic of the thesis and include work done by candidate during PhD. With the exception of Annex 1 all the annexes were published or accepted for publication. They were included in the thesis to strengthen claim of publishability of the results included in the Chapters 3-5, so far unpublished. Annex 1 includes application of findings in Chapter 5 and 6 to research results from previously generated research in Chapters 3 and 4. It was included in the thesis to highlight the importance of findings contained in Chapters 5 and 6 and their possible future applications.

Chapter 2

Characterisation of engineered nanoparticles in food by electron microscopy

2.1 Introduction

This review provides an overview of the applicability and suitability of EM techniques for characterisation of ENPs in food samples. Firstly methods of sample preparation for EM are reviewed and their limitations discussed. Then different EM imaging modes for application to samples in dry, frozen partly and fully hydrated state are introduced. Where specific techniques have not been applied yet for imaging of ENPs in food, examples have been taken from related fields such as nanomedicine, nanotoxicology and environmental nanotechnology.

2.2 Sampling and sample preparation for electron microscopy imaging

2.2.1 Sampling

The first and very critical issue of sample preparation for EM analysis is the actual sampling regime itself. Since the sample volume that can be analysed by EM is very small, obtaining a representative set of samples from a complex structured bulk is challenging. Therefore a suitable number of replicates has to be prepared for each sample and ideally a uniform distribution of the sample components should be achieved. Sampling procedures should be selected based on e.g. type of ENP and the nature of the sample matrix. Additionally the small sample volume has an impact on the LOD (number of particles that can be visualised). If number concentrations are low then the imaging analysis could be like “looking for the needle in the haystack”. The volume will also affect quantification (e.g. particle number concentration or elemental quantification by coupled spectroscopic techniques). Therefore if the concentration of ENP in the sample is not high enough, separation and pre-concentration techniques should be considered as described by e.g. Liu *et al.* 2009.

2.2.2 Sample preparation

As the standard EM instruments operate under vacuum conditions, a food sample containing water cannot be introduced into the sample chamber without prior preparation. There are three ways of dealing with hydrated samples for EM imaging:

- Chemical fixation/stabilization followed by dehydration or drying and conventional SEM or TEM
- Imaging using environmental SEM (ESEM) or liquid capsules
- Freezing followed by cryo-TEM or cryo-SEM

These are described in more detail below.

2.2.2.1 Sample preparation for imaging by scanning electron microscopy, transmission electron microscopy and focused ion beam- scanning electron microscopy

When analysing food with intact cellular structures, such as meat, fruits and vegetables the aim is to minimize changes in the sample matrix in order to be able to observe the distribution and interactions of ENP within cells and tissue in the form that they will occur in the 'real' world. In general the methods of choice for preparation of these types of matrices include fixation of the specimen (e.g. with glutaraldehyde) and post-fixation (e.g. with osmium tetroxide) followed by chemical dehydration and either critical point drying for SEM or resin embedding for TEM and FIB-SEM. Liquid samples and emulsions such as milk, yoghurt or salad dressings, can be encapsulated in agar and prepared using the same methods (Kaláb and Larocque, 1996; Egelandsdal *et al.*, 1999).

- **Chemical fixation and staining**

  By preserving protein structure with glutaraldehyde and post-fixing unsaturated lipids with osmium tetroxide it is possible to perform imaging of fat and protein based processed food with minimal impact on the sample matrix. If the post-fixation step is omitted, the fatty acids and unsaturated lipids will not be fixed. Osmium tetroxide also stains the lipids and has further impact on protein fixation. Other heavy metal stains such as uranyl acetate or lead citrate may be applied and a mordant, such as tannic acid, can be used to both enhance staining

and preservation of ultrastructures. For ENPs, the heavy metal staining may create or enhance contrast on the micrograph, if the particle material and matrix have a different affinity to the staining compound. The heavy metal can provide a negative contrast if it is moulded around the particle (or the particle coating) outlining its structure. For example, in studies of the uptake of polylactide ENPs in HeLa cells, heavy-metal staining of the cells enabled visualization of the ENPs using bright-field TEM by increasing the contrast (Musyanovych *et al.*, 2008). The negative staining technique was originally developed for imaging virus particles and bacteria (Maunsbach and Afzelius, 1999), but also organic coatings on nanoparticles can be made visible. This method has been used to reveal e.g. creatine and albumin coatings on gold nanoparticles (López-Viota *et al.*, 2009).

However, staining can also lead to difficulties in distinguishing ENPs from densely stained organic structures of the same size. In some cases an unambiguous identification can be very difficult, for example it is impossible to distinguish between polystyrene nanoparticles and vascular structures in cells (Mühlfeld *et al.*, 2007). Only a comparison of a sample that is known to contain particles with a blank sample will prevent misleading interpretation of such images and so the use of appropriate control samples is essential.

- **Chemical dehydration**

Dehydration of the sample with ethanol is considered to be the best choice for food matrices and may also improve the preservation of ENP structures compared to many other solvents that have traditionally been used e.g. acetone. Studies with silica nanoparticles have shown that agglomeration during sample preparation using this method is lower than if oven drying or freeze-drying were used (Rahman *et al.*, 2008). However, ethanol dehydration cannot be used for food products with high levels of saturated fats or especially water soluble carbohydrates. Extensive chemical treatment may also induce artefacts. For example, removal of water and fat during sample preparation can lead to a removal of ENPs that are associated with one of the phases; and reactions between the chemicals used for sample preparation and the ENPs are possible. Therefore, the effect of the dehydration treatment on ENPs in a particular sample type should be fully evaluated before the method is employed for food analysis.

- **Drying**

One approach to overcome the problems of loss of components due to chemical treatment is to use sample drying techniques. Liquid samples like soups or juices may be concentrated when dried directly on the microscopy substrate. This type of approach has previously been employed for the characterisation of ENPs in sunscreens (Lorenz *et al.*, 2010) and is about most commonly applied way of preparing ENP suspensions for EM analysis (e.g.Tiede *et al.*, 2009a; Park *et al.*, 2013; Luo *et al.*, 2013- Annex 4). Drying can be accelerated by blotting off the excess liquid using e.g. filter paper. This prevents agglomeration artefacts in dried ENP dispersions (Novak *et al.*, 2001). For food samples, drying methods can be applied, if the food matrix is liquid and its density is sufficiently low to allow the formation of a very thin film. Liquid samples may also be diluted by solvents such as methanol to increase spreading during drying, but this may influence agglomeration state of ENPs (Lorenz *et al.*, 2010).

Good spreading of the drop on the TEM grid is important to enhance the distribution of the ENPs on the grid surface. Drop spreading can be enhanced by inducing hydrophilicity of the grid coating (Hayat, 1989a). Another way of dealing with grid hydrophobicity is sedimentation of the sample on the top of the grid using ultracentrifugation (Lienemann *et al.*, 1998). This technique can be used to provide quantitative data on particle concentration (Zheng *et al.*, 1996).

Milder methods of water removal such as freeze-drying may also be used. Using this approach, the sample does not have to be chemically treated and rapid freezing can be used to preserve surface structure (5-10 μm deep) (Bozzola, 2007). Fast freezing followed by sublimation is an alternative approach for drying ENP suspensions (Domingos *et al.*, 2009). A further advantage of removing water from a sample, especially highly hydrated, is that the ENPs can be enriched in the residue which simplifies the detection and analysis. However, artefacts are more likely due to the higher density and structural change of the sample.

- **Preparation of thin sections for transmission electron microscopy imaging**

One of the most challenging steps in TEM is the preparation of a sufficiently thin sample that allows the electrons to pass through. More complex food samples can be embedded in resin and cut in 15-90 nm thin sections (Kaláb *et al.*, 1995)

by means of ultramicrotomy. Ultramicrotomy is the standard method for preparing thin sections of resin embedded biological materials by sectioning the sample with the cutting edge of a glass or diamond knife (Villiger and Bremer, 1990). The sample is mounted on an arm vertically moving with a defined speed against the knife edge. The cutting process is controlled under a binocular. Another option of thin section preparation offers FIB milling. More information about the method can be found in (Giannuzzi and Stevie, 1999). Liquid samples can be prepared as resin embedded specimen for TEM imaging without sectioning. For this purpose a water soluble melamine resin, such as Nanoplast, is added into the sample. A drop of the specimen is then deposited on the TEM grid mounted on horizontal centrifuge. Horizontal centrifugation removes excess of the liquid from the grid forming sufficiently thin layer for TEM imaging and added resin polymerizes preventing drying artefacts (Perret *et al.*, 1991; Plathe *et al.*, 2010).

2.2.2.2 Sample preparation for imaging by liquid cell technique and environmental electron microscopy

Liquid cell technique and ESEM often do not require any sample preparation, enabling imaging of the specimen in its unperturbed state. However to enhance visualisation of the fraction of interest in the sample some pre-treatment may be given to the sample. For example, Quantomix™ capsules used in the liquid SEM technique 'WetSEM™' are suitable for centrifugation, therefore this method could be used to increase adhesion of fraction of interest to the capsule membrane (Koh *et al.*, 2008). The membrane of the capsule can also be treated with substances such as gelatine or poly-l-lysine improving specimen adhesion as demonstrated for ENPs in environmental matrices and sunscreens (Lorenz *et al.*, 2010; Tiede *et al.*, 2009c).

2.2.2.3 Sample preparation for imaging by cryogenic methods

Samples can be prepared for EM imaging using "physical fixation" by freezing the sample. Water is often part of the ultra structure of biological samples or food matrices and drying the samples will change the structure dramatically. In principle, freezing is the ideal method because chemical treatment and therefore sample alteration can be avoided. The key to good sample preparation in cryo-EM is the freezing process. As ice crystals grow, only water molecules are incorporated into

the ice crystals, and the specimen is thereby segregated into crystals of water and ridges in- between containing enriched regions with the dissolved material, such as solutes and macromolecules. Formation of large ice crystals can even rupture and destroy whole cells in biological samples. The preservation of the ultrastructure is thus dependent on the avoidance of formation of ice crystals or at least preventing from growing larger than the structures of interest in the sample. Obtaining amorphous ice, so called vitrified water, from liquid water by ultra rapid freezing was first reported in the beginning of the 1980s (Bruggeller and Mayer, 1980). Even using ultra fast freezing, the thermal conductivity of water will limit the cooling rates inside specimens and vitrification of samples thicker than a few microns is impossible without addition of cryoprotectants or application of very high pressure (Dubochet, 2009).

Different freezing methods are available including plunge freezing (rapid immersion freezing), contact freezing (metal mirror/slam freezing), spray freezing (propane jet) and high-pressure freezing (Maunsbach and Afzelius, 1999; Cavalier *et al.*, 2009). The choice of method depends mainly on the dimension of the sample. In the absence of cryoprotectants, large samples with dimensions of millimetres to centimetres are not likely to be preserved without ice crystal damage. These samples have to be infiltrated with a cryoprotectant like glycerol or sucrose before they can undergo freezing. For liquid samples, like suspensions and emulsions, plunge freezing can be applied where the sample is plunged into a coolant like liquid propane, ethane or nitrogen. Instruments for plunge freezing are commercially available but also homemade solutions exist. Typically the liquid, e.g. a suspension, is pipetted on a microperforated, glowdischarged cryo-TEM grid, the excess of liquid is removed by blotting and the grid is plunged into the coolant.

If a preservation of a thin layer (5-20µm) on the sample surface is sufficient, the so called contact freezing technique can be used (Leforestier *et al.*, 1996). The sample is rapidly slammed against a cold polished metal surface with high heat conductivity. Because of the generally low heat conductivity of the samples only a surface layer is frozen with a sufficiently high speed to avoid ice crystal formation. Another method is spray freezing (Knoll *et al.*, 1982). There, the sample is placed between two plates and a jet of liquid propane cooled with liquid nitrogen is applied. The high dynamic pressure of the jet guarantees fast cooling. With high pressure freezing samples of up

to 200 µm thickness can be vitrified. The method utilizes the fact that water expands during crystallization by applying a large pressure to the sample during freezing thus counteracting ice crystal formation. The drawback of high pressure freezing is that it requires relatively expensive instrumentation, even though references of 'homemade' high pressure freezing, exploiting the expansion of water during freezing in closed containers do exist (Hayashi *et al.*, 2002; Leunissen and Yi, 2009).

Cryo-SEM might require sectioning of the sample by means of the so-called freeze-fracture method. The sample is fractured and inspected under cryogenic temperatures. Freeze-fracture provides access to the inside of a bulk sample. Samples have a tendency to break at the natural planes of weakness e.g. such as the hydrophobic interior of cellular membranes (Branton, 1966). The fracture can be succeeded by sublimation of water from the ice surface to reveal more of the embedded solid structure (Moor and Muhlethaler, 1963).

There are several possibilities to prepare cryo-fixed samples for TEM. Plunge frozen samples can be directly investigated in a TEM equipped with a cryo-sample transfer holder. Samples from contact, spray or high pressure freezing can undergo freeze substitution, i.e. dehydration at low temperatures in parallel with infiltration of a resin (Maunsbach and Afzelius, 1999). Subsequently, the sample can be treated as a chemically fixed one.

Another possibility is to fracture a sample that has been sandwiched between plates during freezing. The plates are separated in a special device and a replica of the freeze fractured surface is made for TEM investigation, typically by shadowing with platinum or gold and carbon. Thicker samples (e.g. from high pressure freezing) can be sectioned in a cryo-ultramicrotome and the frozen sections investigated in a TEM equipped with a cryo-holder. This technique is known as CEMOVIS (Al-Amoudi *et al.*, 2004).

2.2.3 Improving localisation of engineered nanoparticles in the sample

For some ENPs it is possible to use auto-metallography (AMG) or silver enhancement to increase the ENP size. In this process, silver from solution, is deposited onto existing particles so that they reach sizes visible in low magnification EM or even light microscopy. The basic principle is that silver ions adhere to the

catalytically active nanoparticle or crystal and are then reduced by electrons released from reducing molecules touching the nanoparticle. This method has successfully been applied for gold and silver ENPs, Quantum Dots (e.g. CdSe) and nanocrystals of metallic compounds generated *in vivo* (Danscher and Stoltenberg, 2006).

To get an overview of the distribution of ENPs in an inhomogeneous sample it is helpful to visualize the presence of the particles at a relatively low magnification. In correlative optical and electron microscopy specific areas are identified by screening with e.g. a confocal microscope and then re-localized at the EM level. This approach is suitable for absorbing or fluorescing ENPs with sufficient contrast in TEM like metal ENPs or quantum dots (Nisman *et al.*, 2004). Increasing the number of images and sub-samples, detection, representativeness and statistics can also be improved.

2.3 Standard Electron Microscopy methods

2.3.1 Scanning Electron Microscopy methods

Pioneer experiments leading to development of SEM method were performed in 1935 by Max Knoll. In next seven years first SEM was constructed in USA. The resolving power of the prototype was at a level of 1 μm, but soon was upgraded to 50 nm (Jóźwiak, 2007).

SEMs of today achieve resolutions of 1 nm using high resolution imaging instruments; and about 3 nm using conventional instruments. However, it has to be noted that the resolution that can be achieved strongly depends on the sample. Organic samples like food stuff need to be covered with a layer of electrical conductive substances like metal or carbon to avoid charging effects during imaging. Also, the energy of the electron beam has to be adjusted accordingly to avoid damage of the specimen.

Contrast in SEM emerges from scattering of the electron beam by the sample. SEM employs several detectors that select specific energy ranges of the scattered signal. Low energy secondary electrons (SE) primarily provide information on the surface topography while high energy backscattered electrons (BSE) can be used for mapping contrast based on differences in atomic numbers, *Z*, of elements that the sample is composed of thereby providing good contrast for heavy and light elements such as Silver ENPs in cells (Koh *et al.*, 2008). Images obtained with a BSE detector can give visible contrast when the difference between *Z* of elements is as low as 0.1

(Jóźwiak, 2007) and therefore provide simplicity of data interpretation superior to other imaging techniques.

Samples for SEM are mounted on aluminium or carbon stubs by sticking with, for example, quick setting glue, epoxy cement, wax, silver paint or double sided sticky tape. Tapes can additionally contain carbon to avoid electrical charging of the sample. Unlike TEM, in SEM, prepared samples can be introduced for imaging in bulk form as there is no need for cutting thin sections. Generally sample preparation is less challenging for SEM imaging compared to TEM. For example liquid samples can be dried directly on SEM stub as demonstrated for sunscreens (Lorenz *et al.*, 2010) or closed in agar capsules which after chemical treatment undergo incision e.g. model salad dressings (Egelandsdal *et al.,* 1999). SEM also gives the possibility of tilting the sample to allow observation from different angles and 3D imaging (Pouchou *et al.*, 2002).

The characteristic depth of field given by SEM micrographs is of great utility for food analysis as it allows the effects of ENPs on food structure to be established as well as the ENPs to be localised. The effectiveness of the technique has been demonstrated in studies on collagen cross- linking with gold ENPs for drug delivery system application (Castaneda *et al.*, 2008). In this research SEM micrographs allowed the authors to measure the effects of the ENPs on the porosity of collagen gel while TEM analysis showed organization of ENPs in the gel structure. Compiling data from micrographs by SEM as well as TEM methods is a good practice, since SEM's resolution range limits possibility of observations on ENPs morphology.

Although conventional SEM is commonly used to visualise the specimen surface, in some studies samples are also fractured for analysing the internal structure. For example, in research on beef microstructures, samples were chemically fixed and after dehydration in ethanol, cryo-fractured (Palka, 2003). This way sample alteration was minimised since frozen ethanol does not form crystals.

Another method for observation of a fractioned sample is FIB-SEM. Dual-beam FIB-SEM is a powerful alternative to TEM, when a large volume biological sample (e.g. whole cells, tissue) needs to be imaged. It is a hybrid 3D imaging technique combining FIB milling with SEM, where the two beams meet at their focal points. The ion beam is used as a cutting tool, milling slices off the sample, while the SEM

images the freshly cut surface. The third dimension is obtained by stacking of subsequent SEM images taken after each FIB sectioning of the bulk material (Principe, 2007). Resolution is limited to about 10 nm in 3D volumes and requires the particles to provide a good atomic number contrast in the extremely flat FIB-cut surface.

Compared to TEM, FIB-SEM provides five-fold lower resolution of 5 to 10 nm in the X and Y dimensions and 10 nm in Z dimension (Winter *et al.*, 2009). This allows correct imaging of organelles, cytoskeleton, nucleus, nucleolus, and vesicles, but prohibits detailed information on the lipid bilayer structure, and any single molecules. The main advantage, however, is the wide magnification range offered by SEM mode, and the available image volume of tens of micrometers: making the whole cell morphology and structure imaging easily achievable.

An image of a sample prepared by FIB-SEM milling can be seen in Figure 2.1a (stained HeLa cell).

FIB-SEM 3D images usually suffer resolution anisotropy (image anisotropy occurs when voxels (three dimensional pixels) that image is consisted of, instead of cubical are shaped in cuboids with variable edge length).This can only be avoided if the FIB-resolution is pushed to its limits: state-of-the-art FIB minimum probe size and position is stable for 10 nm slice milling (Winter *et al.*, 2009) and thus slice minimum thickness can be very close to the lateral resolution set by the SEM. However, thicker sections are often needed when higher volumes are imaged and time is constrained, which creates vertical to lateral anisotropy. Another source of lateral anisotropy is caused by the angle between the two beams. In most of the dual-beam systems, the electron beam is arranged vertically and the ion beam with an angle of 52º. Tilting of the sample stage allowing straight ion milling is commonly used.

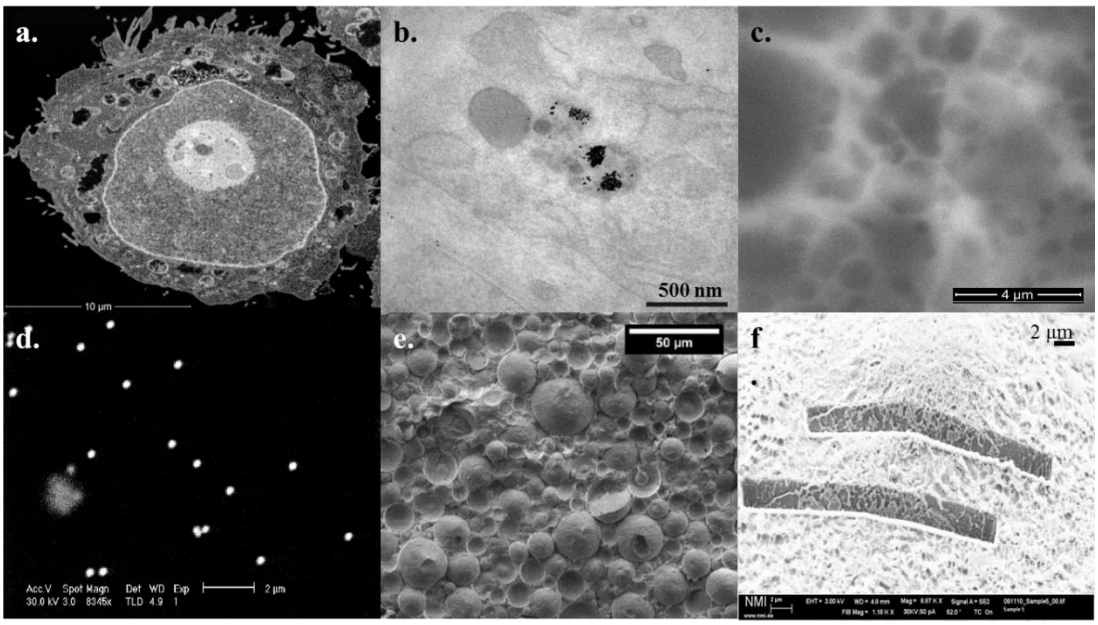

Figure 2.1-(a) SEM image of FIB-milled block face of fixed, stained and embedded HeLa cell;(b) TEM image of silver ENPs in resin embedded, unstained rat tissue; (c) liquid SEM image of unstained coffee cream (BSE detector); (d) WetSEM image of metal-based ENPs in lake water; (e) Cryo-SEM image of freeze-fractured, uncoated oil-in-water emulsion; and, (f) Cryo-FIB-SEM image of adherent cell (3T3 fibroblast) after slight sublimation. All the images originate from work of the authors.

2.3.2 Transmission electron microscopy methods

The first TEM was constructed in 1931 by Max Knoll and Ernst Ruska, later winner of Nobel Prize in Physics. Because of its high resolution and availability in many laboratories, conventional TEM is frequently used in research on nanosized objects. The technique has found application in many studies on food nanostructures (e.g. Fishman *et al.*, 1995; Auty *et al.*, 2005) and therefore is regarded as promising tool for characterisation of ENPs within food matrices. The resolution in state-of-the-art TEM is about 0.07 nm and developments are aiming to upgrade it to 0.05 nm (TEAM, 2013). For TEM, resolution is strongly dependent on the thickness of the prepared sample and the accelerating voltage for the electrons- the higher the voltage the better the theoretical resolution. For imaging of food samples, especially containing structures prone to electron damage, the optimal accelerating voltage of TEM would be limited to up to 100 kV as for most biological samples.

There are several ways of acquiring an image by means of TEM and a more detailed description of these methods can be found in the literature (Kachlicki, 2007b). For bright field TEM imaging, scattered electrons are totally absorbed by an objective lens aperture and the un-diffracted part of the beam passes through the aperture hole to form an image. The user observes a dark object on bright background with absorption or interference contrast. In TEM bright field imaging of a non-crystalline sample contrast emerges mainly from differences in the sample thickness and differences in the sample density and *Z*, with thicker sample regions and regions with higher density appearing darker. Metal based ENPs typically give significant contrast in these matrices (e.g. Lorenz *et al.*, 2010; Tiede *et al.*, 2009c) as illustrated in Figure 2.1b showing a bright field image of silver ENPs in rat tissue.

Bright field TEM is widely used technique in food research. It was applied for example in studies on morphology analysis and sizing of natural food nanostructures like starches (Fishman *et al.*, 1995) and casein micelles (Auty *et al.*, 2005).

Dark field TEM imaging is based on detection of the fraction of the beam diffracted by the sample. This method visualises a bright object on dark background. Dark field imaging employed in scanning transmission electron microscope (STEM) allows imaging of nanoparticles and biological specimens without staining and with a sub-nanometer spatial resolution (Liu, 2005). For imaging the distribution of high *Z* elements e.g. Silver or Gold in a light element matrix such as organic tissue, one can take advantage of the high angle scattered electrons in STEM that are mainly caused by the interactions of electron beam with atoms' nuclei (scattering is proportional to Z^2). Detection is achieved by the high angle annular dark-field (HAADF) detector, placed in a circle around the electron beam. HAADF was for instance used to image gold ENPs with 4 nm resolution within a cell, which amounts to several micrometers of organic matters (Niels de Jonge, 2007).

High resolution TEM (HRTEM) utilises interference contrast to provide resolutions capable of visualising atomic layers of crystalline samples and can be applied for imaging of crystalline ENPs within organic matrices such as food. For example Fayek *et al.* (2005) applied HRTEM for imaging and sizing of uranium oxide nanocrystals on the surface of bacteria. In some cases high resolution imaging enables identification of ENPs using their characteristic lattice spacing. This has for example been achieved for fullerenes (Porter *et al.*, 2007). By observation of

coherent electron nanodiffraction patterns, details of the morphology and 3-D structure of ENPs can be revealed (Liu, 2005). The three dimensional arrangement of ENPs within a matrix can be observed by electron tomography. Tilting the sample holder in the microscope a 3D image can be obtained recording images of the sample at different angles followed by a computed back-projection (McIntosh *et al.*, 2005).

2.4 Electron microscopy of hydrated samples in their original state

Imaging artefacts caused by invasive preparation methods can be partially overcome by relatively new developments in EM that allow imaging of hydrated and even fully liquid samples. A range of methods can be employed including liquid TEM, environmental TEM (ETEM), ESEM, liquid SEM/ WetSEM^{TM} and liquid scanning transmission electron microscope (Wet STEM) (Tiede *et al.*, 2008).

For example, techniques for high resolution imaging of liquid samples in TEM are being developed (resolutions of 0.3 nm have been reported by Liu *et al.* (2008) with 9 nm oxide windows and 2-5 microns of water and of 3 nm by Peckys *et al.* (2009) with 50 nm silicon nitride windows and approximately 10 microns of water). Special microfabricated chips with thin film windows that can be penetrated by the electron beam are used for this purpose. These chips allow a sample to be imaged in its fully hydrated state thus avoiding any change from staining or dehydration. Typically the microchip has a sturdy substrate of silicon for mechanical stability and an opening containing the window. The material chosen for the window must be resistant to pressure and electron transparent in such a way that the contribution to the signal from the window can be said to be negligible (Liu *et al.*, 2008; Peckys *et al.*, 2009). This method has been used to observe the synthesis of ENPs (Zheng *et al.*, 2009). It has been shown that high *Z* particles can be located in comparatively thick volumes of liquid and that the superstructure of organic composites such as cells can also be seen (Liu *et al.*, 2008; Peckys *et al.*, 2009). These devices would likely be able to provide new insights into the ENP interaction with food samples.

The liquid cell method brings many of the advantages of ETEM to a regular TEM. With ETEM a partially hydrated sample can be viewed. The main difference between the liquid cell method and ETEM is the pressure of the liquid. In ETEM the

liquid exists as vapour and can only partially hydrate the sample. In the liquid cell method the sample can be completely immersed and hydrated.

Imaging in ESEM involves detection of electrons scattered by the specimen surface and molecules of the gas in the sample chamber (Thiel *et al.*, 1997). Though ESEM does not operate under atmospheric pressure it is possible to image samples with 100% of relative humidity over the specimen surface, thus preventing water evaporation. While manipulating vapour pressure it is also possible to partially dehydrate the sample in the sample chamber. This practice may be very helpful for ENPs analysis, since e.g. in an aqueous sample imaged at 100% humidity, only the surface of the water droplet will be imaged and ENPs distributed within will not be visible (Doucet *et al.*, 2005). ESEM does not need sample coverage with an electrical conductor since ions present in the water vapour neutralize charged regions. The technique does not require extensive sample preparation and therefore is good alternative for food products imaging in their native state as demonstrated for starch-containing imitation cheeses (Noronha *et al.*, 2008). ESEM was also proven to produce high contrast images of nano and microsized inorganic contaminations in bread and biscuits (Gatti *et al.*, 2009). In studies on natural nanostructures in surface water ESEM imaging was able to provide data on the primary structures of the particles while conventional SEM imaging shown aggregated colloids and particles (Doucet *et al.*, 2005). The disadvantage of the method is worse resolution compared to conventional SEM imaging (10-100 nm) (Tiede *et al.*, 2008).

In WetSEM™ a sample is encapsulated in a special device designed by Quantomix™ allowing samples under fully liquid conditions to be imaged through an electron transparent membrane - similar to the liquid cell technique used for TEM. This method is suitable for imaging objects made of elements with high atomic numbers, which will give good contrast on the micrograph (Quantomix, 2011). Water and fat present in the sample may be clearly distinguished by this method (Quantomix, 2011; Molero *et al.*, 2009) WetSEM™ is a good option for analysis of metals and metal oxides in environmental samples in their unperturbed state (Tiede *et al.*, 2009c), therefore is also promising technique for investigation on liquid foodstuff in their native state. Figures 2.1c and 2.1d show liquid SEM image of coffee cream and WetSEM™ of metal-based ENPs suspended in lake water respectively. Like ESEM, the disadvantage of WetSEM™ is that the resolution is

lower compared to standard methods (10-100 nm) (Tiede *et al.*, 2008). Also ENPs will move in the liquid due to Brownian motion and therefore focusing can be a challenge (Lorenz *et al.*, 2010; Tiede 2009c). The capsule membranes can also be prone to damage by the electron beam (Lorenz *et al.*, 2010; Tiede *et al.*, 2009c; Tiede *et al.*, 2008). Another approach, WetSTEM, has a resolution of ~ 5 nm. For this method a drop of sample is applied on TEM grid. Then it is placed on TEM sample holder, fixed on SEM stub and inserted in an ESEM. Imagining of hydrated samples is achieved in annular dark field mode by employing BSE detector situated beneath the sample (Bogner *et al.*, 2005).

2.5 Cryo-electron microscopy

Cryogenic scanning electron microscopy (cryo-SEM) is applied for investigation of the ultra-structure of bulk samples. The samples are kept frozen by a cryo stage in the microscope and viewed under high vacuum which allows for high resolution imaging. In some cases it is possible to view uncoated samples at low acceleration voltages because the samples are to some extent protected from beam-damage by the low temperature (see Figure 2.1e).

The fracture planes in freeze-fracture are virtually impossible to control and in samples where the fracture does not reveal the structure of interest, for instance a cross section between heterogeneous materials or in cases where 3D imaging is desired it is possible to perform FIB-SEM on the frozen specimens (see Figure 2.1f). This has the advantage over ultramicrotomy that very small structures of interest can be selected by use of cryo-SEM prior to milling.

It is always wise to compare several methods to avoid conclusions made on the basis of artefacts. A number of studies have employed both cryo-SEM and ESEM to hydrated samples. Cryo-SEM has the highest resolution, whereas ESEM enables the observation of dynamic changes to the structure (James and Smith, 2009). The combination of the two is beneficial to understanding the structure, as the micrographs can sometimes be complementary (Noronha *et al.*, 2008).

Cryo-SEM is likely to be a very useful approach for analysis of foreign nanosized objects embedded in food matrices as long as their structure can be distinguished from the structure of the food product. The method has been used in characterisation of ENP bio carriers (Gomes *et al.*, 2010), polymer nanocapsules (Li *et al.*, 2009) and even in visualisation of cellular uptake of polymer ENPs (Win and Feng, 2005).

For Cryo-TEM, contrast of biological specimens is achieved by slightly under focusing the sample. By keeping the thickness of the amorphous ice film low and working at low dose conditions high resolution imaging, for example of 15 nm gold ENPs with 0.2 nm lateral resolution, is possible (Balmes *et al.*, 2006). Cryogenic samples are better able to sustain extended radiation and this results in improved image quality. In a recent paper 0.33 nm resolution was obtained in 3D on viral particles enabling 3D reconstruction of the detailed protein structure (Zhang *et al.*, 2010). The technique can be applied for imaging of ENP suspensions, like metal ENPs (Balmes *et al.*, 2006), solid lipid ENPs (Jores *et al.*, 2004) or micelles (Knudsen and Skibsted, 2010) and vesicles (Won *et al.*, 2002).

Cryogenic techniques are very useful for imaging of semi-liquid and solid food samples that cannot be fixed chemically, i.e. fat or polysaccharide based food like chocolate (James and Smith, 2009) and bread (Barcenas and Rosell, 2006), or samples where the preservation of the matrix structure is of strong interest, like meat (Larrea *et al.*, 2007).

2.6 Analytical methods coupled to electron microscopy

Analytical EM allows the determination of the elemental composition of specimen or specific areas/spots of a sample. The most common example is energy dispersive x-ray spectroscopy (EDS). EDS and wavelength dispersive spectroscopy (WDS) enable x-ray microanalysis of spectra emitted by atoms of the sample. WDS is much more precise than EDS as it also analyses light elements, but because of the high costs of the detector it is rarely used.

EDS is a helpful tool for the identification of the chemical composition of ENPs and especially to distinguish between inorganic ENPs contained in an organic food matrix. EDS can be combined with SEM, TEM, WetSEM^{TM}, liquid TEM, STEM, ESEM, ETEM and FIB-SEM.

For TEM, HAADF and energy filter imaging (EFTEM), electron energy loss spectroscopy (EELS) is usually applied for characterisation of inorganic materials, however, this methods can also be useful for the identification of carbon based ENPs. The combination of EELS and EDS together allows elemental analysis of most elements since some are mainly detected by one of the methods.

EDS is generally better suited for detecting elements of high *Z*, whereas EELS can readily detect low-*Z* elements. For instance EELS has been used to image the distribution of carbon nanotubes in cells, since the nanotube EELS spectrum is slightly different from the carbon bound in organic materials (Porter *et al.*, 2007).

2.7 Data interpretation and analysis

In most cases, the volume of a sample taken for EM is relatively small (order of pl) in comparison to the volume of the original food product or environmental material, e.g. for TEM a few µl are dried on a grid for analysis, whereas a typical bottle of soft drink contains several 100 ml. If the food product or environmental material is heterogeneous or an inhomogeneous distribution of ENPs within a homogenous material is expected, random sampling and the investigation of several samples is necessary to obtain representative results. Even if a relatively large sample volume is taken and prepared for analysis, e.g. for SEM, the volume that can be analysed is still limited. The detection of ENPs requires relatively high magnifications which limits the field of view. For biological samples, including e.g. cells and tissues, methods for sampling and quantitative analysis of ultrathin sections by TEM have been developed (Elias and Hyde, 1980; Mayhew *et al.*, 2009).

A major challenge is the analysis of samples with very low PNC of ENPs. Low PNCs can for example be expected if ENPs enter foodstuffs by migration from packaging materials. For a given mass concentration PNC of ENPs depends on their size and density of the material the ENP is comprised of. Having for example a sample with a mass concentration of silver ENPs of 0.01 % m/v, 18 ENPs could be expected per analysed volume of 1 µm³ if the particle diameter is 10 nm. In contrast, for 100 nm silver ENPs at the same mass concentration at least 55 µm³ have to be analysed to find a single particle. The LOD depends on the preparation and imaging technique and the ENP properties including, e.g. size, composition, but also on the size of the analysed volume.

One should also keep in mind that for determining the size distribution of non-spherical ENPs 3-dimensional information might be required. TEM, for example, shows only a projection of a certain orientation of the ENP, whereas, methods like FIB-SEM, tomography or single particle analysis, offer three-dimensional

information of the ENP size and shape. Nevertheless, these methods will have limitations at very low particle PNCs.

Extraction of the data from EM images in a representative and reproducible way is a challenge. Precise qualitative and quantitative image analysis is therefore required. The accuracy of determining the average particle size and the PNSD of particles contained in a sample, for example, depends on the number of particles measured and a valid statistical approach might require thousands of measurements (Tiede *et al.*, 2008; Hassellöv *et al.*, 2008). Therefore automation of image analysis is crucial for extracting data in a reproducible and objective way. Many of the available image analysis softwares are, however, based on either manual or per pixel characterisation. Manual interpretation is often inexact and tedious, whereas per pixel classification may lead to errors e.g. in the correct determination of particle boundaries, especially in presence of background noise, which is typical for EM images. Innovative object-based quantitative image analysing systems, which enable cross linking of neighboured objects, thus allowing structural and relational acquisition of information such as distance, relative positions and composition, may overcome these limitations (Tiede *et al.*, 2008). Examples for the application of automated image analysis for sizing ENPs can be found in the literature (Tiede *et al.*, 2010; Tiede *et al.*, 2009a).

2.8 Conclusions

EM methods are capable of detecting and characterising ENP in a wide range of matrices. The potential of EM for observing interactions of ENP with complex food matrices is improving with refinement of existing techniques and the development of novel techniques such as the wet state imaging systems. The traditional EM methods are promising candidates for high resolution imaging of complex 3D structures containing known inorganic ENPs. However to date not much work has been done on ENP-food studies. The main challenge for researchers is sample preparation, which may not be adequate for foodstuffs containing ENP in the structure. Careful evaluation of the various methods, considering the highly varying sample matrices and types of ENP is strongly recommended. A guiding table covering the available EM choices, based on the research covered in this review, shows the main possibilities and some pitfalls (Table 2.1).

In most cases, the use of more than one of the available techniques should be considered in order to get complementary micrographs and to determine how processes of sample preparation may alter the structure of the sample. The EM analysis should naturally be backed by other analytical methods (Tiede *et al.*, 2008). Figure 2.2 provides a potential decision tree to help the reader in selection of the most appropriate EM method(s) for a specific food sample.

It is anticipated that EM imaging techniques will mainly be applied for the validation of detection and quantification methods. The localisation of individual nanoparticles in a real world food sample by EM, is very much like "finding a needle in a haystack" due to time-consuming analysis of small sample volumes and the issue of representativeness and reproducibility, and likely also wide range of natural nanostructures present in the sample. Therefore, EM would have to be performed as a complementary analysis to separation and analytical techniques for real world samples.

Imaging of food samples containing ENP is still in the development stage. None of the discussed methods are complete and reliable just yet and the necessity of further research and validation of the methods against reference materials or/ and other type of analytical technique is highlighted by this review.

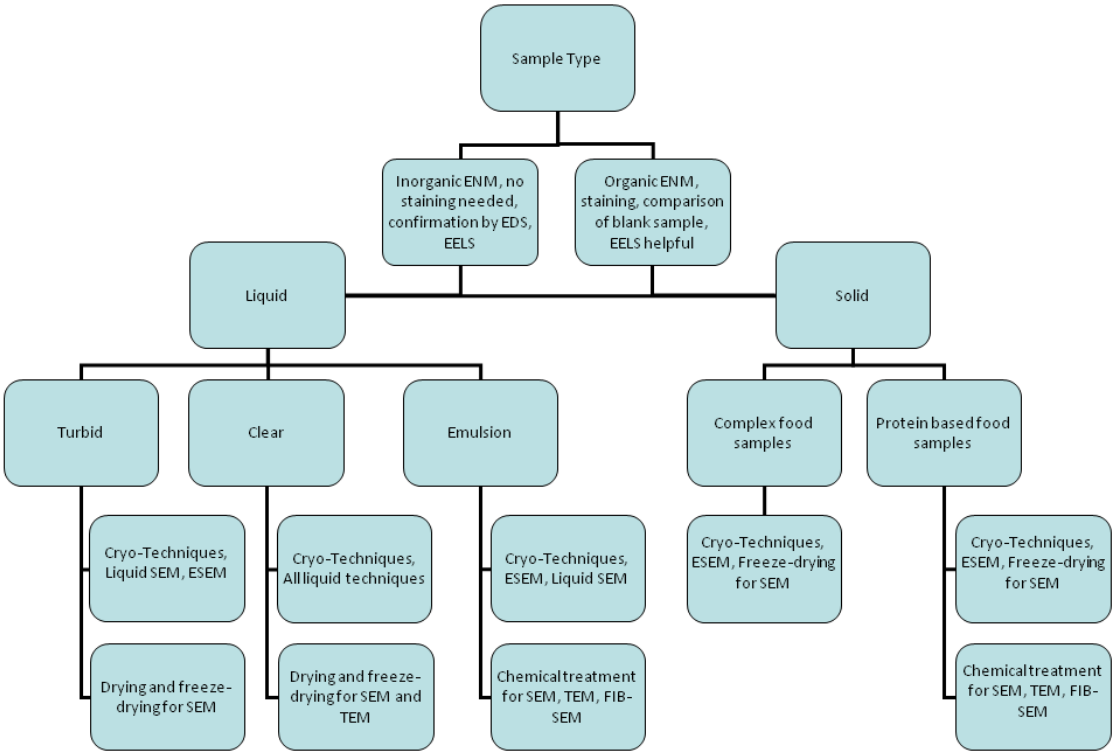

Figure 2.2- Decision tree illustrating choice of EM methods available for imaging of defined sample type

In the next Chapter, methods for sample preparation for EM imaging to support ENP analysis are evaluated in order to identify the most appropriate methods for analysis and characterisation of ENPs in food materials.

Table 2.1- Overview of discussed EM methods suitable for ENP characterisation in food matrices

Method and Approximate Resolution	Type of food matrix	Type of ENP and examples from the literature, references	Advantages	Disadvantages
SEM Resolution- 1-10 nm 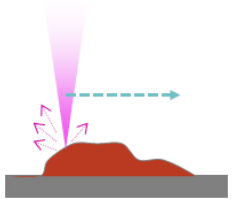 Electron beam scanned over sample. Scattered electrons detected in each pixel.	Food powders, meat, fruit, vegetables, emulsions, protein gels and protein based foodstuffs	High atomic number eg. Au(Castaneda *et al.*, 2008), Ag(Koh *et al.*, 2008) Chemically different than food matrix eg. TiO_2, ZnO(Lorenz *et al.*, 2010) Organic with heavy metal stain contrast	Imaging of food structure parameters eg. porosity (Dubochet, 2009), ENP preconcentration, ENP localisation in sample (Koh *et al.*, 2008), EDS applicable, Freeze- dried specimens may be imaged (Castaneda *et al.*, 2008) in alternative to chemically fixed ones	Water removal can alter structure of sample and induce ENP artefacts eg. aggregation Coating with conductive substance may obstruct elemental analysis, Mainly for analysis of prepared sample's surface
FIB-SEM Resolution- 10 nm in 3D 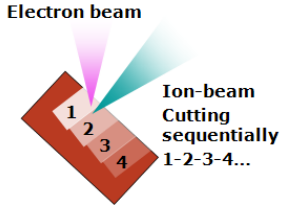 Ion beam cuts sections imaged by SEM.	Meat, fruit, vegetables, emulsions, Protein based foodstuffs	As for SEM	3D imaging of sample sections, Fracturing while imaging- controlled sectioning, ENP localization in sample, EDS applicable, FID applicable in cryo- SEMs	If not frozen sample has to be embedded in resin- artefacts, loss of components

Table 2.1- Continued

Method and Approximate Resolution	Type of food matrix	Type of ENP and examples from the literature, references	Advantages	Disadvantages
TEM Resolution- 0.07 nm 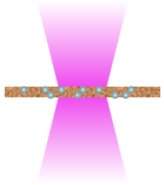 Electron beam passing through the sample.	Non- turbid liquids, without suspended solids and low concentration of dissolved substances eg. clarified juices, meat, fruit, vegetables, protein based foodstuffs	Inorganic eg. metal based ENM and quantum dots (Nisman *et al.*, 2004), metal oxides TiO_2, ZnO (Lorenz *et al.*, 2010) Organic eg. polylactide in stained matrix (Musyanovych *et al.*, 2008), fullerene C_{60} and carbon nanotubes (Porter *et al.*, 2007), differently shaped than sample components	Detail imaging of ENP and sample morphology, Simple sample preparation for liquids, EELS, EDS and tomography for 3D image applicable, Possible staining of ENP coating	Altered structure of sample ENP artefacts due to water removal, Solid samples have to be chemically treated- artefacts, loss of components, Very thin section of the sample needed- may be not representative, Particles may be damaged or misplaced during sectioning
STEM Resolution- 0.07 nm 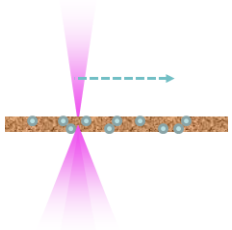 TEM electron beam scanned over sample.	Meat, fruit, vegetables, protein based foodstuffs	High atomic number ENP eg. Ag (Niels de Jonge, 2007)	HAADF detector applicable	As in case of TEM

Table 2.1- Continued

Method and Approximate Resolution	Type of food matrix	Type of ENP and examples from the literature, references	Advantages	Disadvantages
ESEM Resolution 10-100 nm (Tiede *et al.*, 2008)	Liquids, emulsions, complex solid food samples	Applicable for same as SEM if size is sufficient	Minimal sample preparation, Dynamic changes in sample may be observed No coating needed for imaging, Sample may be observed in native state (Doucet *et al.*, 2005), Controlled evaporation of water (Doucet *et al.*, 2005), EDS applicable	Resolution may be at times too low to detect ENP, FIB mode not applicable therefore only for surface analysis, Some particles may be covered by layer of free water (Doucet *et al.*, 2005)
WetSEM 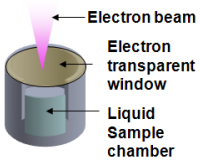 Liquid sample contained in chamber with electron transparent window	Liquids, emulsions	Applicable for same as SEM if size is sufficient eg. (Lorenz *et al.*, 2010; Tiede *et al.*, 2009c)	No sample preparation required, No artefacts related with sample preparation Water and fat phase can be distinguished (Molero *et al.*, 2009; Quantomix, 2011) EDS applicable (Bogner *et al.*, 2005), Dynamic changes may be observed	Resolution may be at times too low to detect ENP, FIB mode not applicable therefore only for surface analysis, ENP can move inside of the cell and be to far away from membrane to image them (Lorenz *et al.*, 2010; Tiede *et al.*, 2009c)

Table 2.1- Continued

Method and Approximate Resolution	Type of food matrix	Type of ENP and examples from the literature, references	Advantages	Disadvantages
Liquid TEM Resolution 0.3 nm in (Liu *et al.*, 2008) and 3 nm in (Peckys *et al.*, 2009)	Liquids without suspended solids, non-turbid	Metal based ENP and organic differently shaped than natural sample components	No sample preparation required, No artefacts related with sample preparation, Dynamic changes may be observed (Zheng *et al.*, 2009), EDS applicable, Cellular structures may be observed (Liu *et al.*, 2008; Peckys *et al.*, 2009)	Low range of products which technique may be applied for
ETEM	Liquids without suspended solids, non-turbid	Metal based ENP and organic differently shaped than natural sample components	Sample observed partially hydrated, EDS applicable,	Evaporation may alter the structure, Low range of products which technique may be applied for
Cryo- SEM Resolution- 1-10 nm	Liquids, emulsions, complex solid food samples	Organic: nano bio carriers (Gomes *et al.*, 2010), polymer nanocapsules (Li *et al.*, 2009), polymer nano particles (Win and Feng, 2005) and as for SEM	Surface structure well preserved, Freeze- fracture and FIB applicable, No artefacts connected with chemical treatment, Sample less prone to charging when frozen, Applicable for whole range of food products (Barcenas and Rosell, 2006; Larrea *et al.*, 2007; James and Smith, 2009), EDS applicable	Risk of ice damage to sample structure especially bigger samples

Table 2.1- Continued

Method and Approximate Resolution	Type of food matrix	Type of ENP and examples from the literature, references	Advantages	Disadvantages
Cryo- TEM Resolution- 0.33 nm	Liquids, emulsions, complex solid food samples	As TEM	Staining and observation of ENP coating applicable (López-Viota *et al.*, 2009), EDS applicable, Sample less prone to beam damage when frozen, No artefacts connected with chemical treatment, Applicable for whole range of food products, May achieve enough contrast without staining	Risk of ice damage to sample structure especially bigger samples

Chapter 3

Evaluation of sample preparation techniques for electron microscopy- analysis of silica engineered nanoparticles in a model tomato soup matrix

3.1 Introduction

As discussed in Chapter 2, the application of EM for the characterisation of particle size in foods, is challenging. Sample preparation of foods for EM imaging is generally unavoidable as foods typically have a high moisture content and a dry specimen is required for imaging by most EM techniques. Removal of water from the sample is however prone to introducing artefacts and may therefore alter the outcome of EM analysis. For example, some sample preparation protocols (e.g. drying) are known to induce particle agglomeration (Doucet *et al.*, 2005), whereas others, such as deposition of particles by electrostatic attraction to the microscopy grid or by adsorption, are suspected to discriminate larger size-fractions of the ENP sample (Balnois and Wilkinson, 2002; Luo *et al.*, 2013- Annex 4).

Therefore, in the Chapter, studies to identify optimum approaches for sample preparation of food materials for EM analysis are presented. In focus of this study were methods which could be used for routine analysis and hence some of more complex approaches, such as e.g. resin embedding (Kaláb and Larocque, 1996) were not included. The aims of the studies were to: 1) evaluate the applicability of standard EM sample preparation methodologies used for imaging of other biological specimens (Chapter 2) for ENPs in food samples; and 2) test the impact of this sample preparation on EM measurement of ENP size.

This was achieved by comparing the size and abundance of silica ENPs recovered from samples prepared using a range of different procedures for EM analysis with measurements provided by selected reference methods. Two reference methods able to measure ENPs directly in liquid dispersions were selected for the study, namely NTA (Carr and Malloy, 2013) and GEMMA (Bacher *et al.*, 2001). These techniques were chosen based on their ability to provide PNSD, rather than particle size

distribution weighted by mass, which is relevant to the results generated by EM analysis.

3.2 Experimental design:

3.2.1 Test particles

SAS (AERODISP® W 7520 N), made up as aqueous dispersion in NaOH at a concentration of 4% w/w, were purchased from Evonik (Hanau, Germany). An estimation of the mean particle size of 120 nm analyzed by SLS (Horiba LA 910) was provided by the manufacturer. The dispersion was further characterised, bottled and distributed by the JRC Institute of Materials and Measurement (IRMM) (Geel, Belgium), who were also a partner of the NanoLyse project. The pH of the dispersion was determined to be 8.2 and therefore a negative charge of the particles could be expected (Gun'ko *et al.*, 2001). The SAS dispersion showed a positively skewed size distribution with broad particle size range, dependant on the analytical method and measurement expression (see Chapter 5).

Two aqueous suspensions of Klebosol spherical silica ENPs, both at a concentration of 30% w/w and of nominal sizes of 12 nm (manufacturer id.: 30V12; K12) and 80 nm (manufacturer id. 30V50; K80) respectively, were kindly provided by AZ Electronic Materials (Trosly-Breuil, France). The manufacturer used the Sears' titration method to estimate particle specific surface area of which the mean number weighted diameter was derived. Further analysis by GEMMA and SEM showed a bimodal size distribution of the K80 dispersion (first peak: approximately 28 to 62 nm, second peak: approximately 70 to106 nm, see Chapter 5) and a particle size distribution with a single, resembling Gaussian peak (approximately 12 to 50 nm- see Chapter 5) of the K12 dispersion. The two dispersions were mixed (Kmix) to generate a sample showing 3 distinct size fractions during analysis. Kmix contained 3.5 % w/w of K80 and 0.04 % w/w of K12 in borate buffer at pH 8 (BB8.0). The buffer's composition was: 0.05M H_3BO_3, 0.05M KCl, 0.004M NaOH. SEM images of K12, K80 and Kmix are given in Figure 3.1.

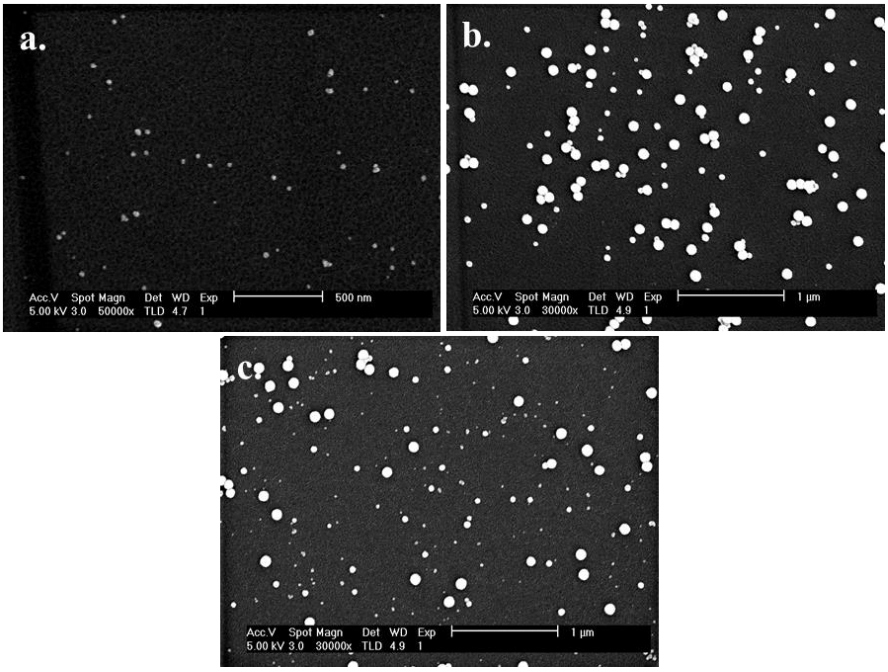

Figure 3.1- SEM images of K12 (a), K80 (b) and K mix (c), scale bars are 500 nm (a) and 1000nm (b and c).

3.2.2 Food matrix

Tomato soup was produced by JRC´s IRMM (Brussels, Belgium). It was prepared under laboratory conditions in order to avoid high background levels of silica, which might be present in a commercial product. The soup was composed of tomato pulp, beef stock, vegetables (onions, carrots) and seasoning (pepper, salt). The pH of the soup was 4.3-4.6 and the dry weight content 8 % w/w.

The food additive E551 can be added to powdered commercial food products at concentrations of up to 2 %. To allow for testing at realistic concentrations, the soup was therefore spiked with the SAS dispersion at a ratio of 1:1. The same spiking ratio was used for the Kmix sample. No sonication was used during the process; particles were simply added to the matrix by shaking to the point of visual homogeneity. No significant change of pH was recorded after spiking the soup with the particle dispersions.

3.2.3 Electron Microscopy Analysis

3.2.3.1 Imaging

SEM images were acquired using a FEI Sirion S field emission gun SEM (FEI- Hillsboro, Oregon, USA) at the York JEOL Nanocentre (University of York, York, UK). The instrument was equipped with a through the lens detector and was operated at 5 kV and spot size 3.

Standard formvar-carbon coated TEM grids (Agar Scientific- Stansted, UK) were used for sample preparation and attached to aluminium SEM stubs with carbon tape. Prepared samples were then coated with 10 nm Pt/Pd using a sputter coater (JEOL JFC-2300HR High Resolution Fine Coater) with a JEOL FC-TM20 Thickness Controller (JEOL - Tokyo, Japan). The coating was expected to increase particle size, therefore ENP size measurements were corrected for this estimated size increase (see Appendix 1).

All samples were analysed in triplicate aiming at the lowest magnification possible in order to visualise larger areas, thus improving the representativeness of the sample and tracking a higher number of particles. The images were taken from randomly selected, not neighbouring, areas towards the centre of the grid so as to avoid areas that were handled with tweezers. Twenty images were taken per replicate at a micrograph size of 29.14 μm^2 for SAS and 13.06 μm^2 for Kmix.

Blank soup samples were analysed at the same imaging conditions as the SAS to obtain reference images.

3.2.3.2 Image analysis

All images for sizing purposes were analyzed using an eCognition Architect framework (version 8.7, Trimble- Sunnyvale, California, USA) Object Based Image Analysis software (OBIA). An OBIA solution was specifically developed for semi-automated image analysis of nanoparticles in complex matrices by the Centre for GeoInformatics, University of Salzburg in Austria. Specific solutions used in this study allowed measurement of ENP agglomerates by merging particles with a common border despite the often weak contrasts at particle interfaces as well as single particles. Thus the performed measurements aimed to enable measurement of

agglomeration artefacts in the EM samples which could be related to sample preparation.

As a cut-off point for the smallest measurable particle size, 10 pixels/ particle area was chosen for Kmix samples (based on the in-house evaluation using imaging of mono-dispersed gold ENPs at decreasing magnification, data not shown), which corresponds to a 12.5 nm equivalent circle diameter (ECD). For SAS, the limit was raised to 15 pixels/ particle area (30 nm ECD) which corresponds to the NTA's size limit of detection (Size LOD). The pixel size for images of Kmix samples was 5.7 nm and for SAS samples 8.6 nm.

3.2.4 Selected sample preparation protocols for electron microscopy analysis

A variety of sample preparation protocols were selected based on their theoretical suitability for imaging of silica particles in tomato soup and also on the frequency of use in the available literature. These were: (1) drying; (2) sedimentation of the ENPs onto an EM grid by ultracentrifugation and (3) attraction of the ENPs from liquid to a charged EM grid. Standard formvar-carbon coated TEM grids (Agar Scientific-Stansted, UK) were used for all sample preparation methods and subsequent imaging by SEM. All samples were prepared in triplicate.

Initial concentrations of all stock silica ENP dispersions were high and therefore substantial dilution of samples was necessary prior to imaging. For drying and ultracentrifugation, the dilution factor was chosen so that the number of particles per grid area would approximately be equal, assuming even particle distribution on the grid. As diluents we used either demineralised water (DMW) or BB 8.0. The nominal particle concentrations for the respective sample preparation procedures are given in Table 3.1.

Table 3.1- Nominal particle mass concentration in final dilutions of samples.

Sample preparation method	Final particle concentration (% w/w)	
	SAS	**Kmix***
Drying	$6x10^{-4}$	-
Ultracentrifugation	$1.2x10^{-5}$	$2.4x10^{-6}$
Electrostatic attraction	$1x10^{-2}$	$1.8x10^{-2}$

3.2.4.1 Drying

For drying, samples were stepwise diluted with DMW. The use of BB 8.0 as diluent was not possible in this case due to the formation of salt crystals. A volume of 5 µL of the sample was placed on the surface of a TEM grid with a pipette and placed over a hotplate at 60 ^{0}C until the grid appeared dry.

3.2.4.2 Ultracentrifugation

Two triplicate series of samples were prepared for ultracentrifugation. The first series was diluted with DMW and the other one using BB8.0. A Beckman XL-100 ultracentrifuge (Beckman, California, USA) with a swing bucket rotor SW40Ti was used. Platforms made of Agar 100 resin (Agar Scientific- Standsted, UK) were placed at the bottom of the polyallomer tubes (Beckman Coulter- Oxford, UK) to provide a flat support for the grids during sedimentation. 5 mL of the diluted sample were added to the tube and then more of the respective diluent was added to the tube until the required level of 0.1-0.3 cm below the rim of the tube was reached, as specified by the manufacturer. As a last step, TEM grids were placed on the liquid surface and allowed to sink to the bottom of the tube at the beginning of ultracentrifugation process. The ultracentrifuge was operated at RCF = 100,000 g and 20 ^{0}C for 60 min for SAS ENPs and 92 min for Kmix samples. According to calculations based on Stoke's Law these parameters were sufficient to sediment silica ENPs as small as 8.7 nm and 7.0 nm, respectively, with a density of 2.65 g/mL.

3.2.4.3 Coating of transmission electron microscopy grids for electrostatic attraction of engineered nanoparticles

The samples were prepared by inducing a positive charge on the surface of the EM grid in order to attract negatively charged silica ENPs from liquid samples. For this purpose grids were coated with either: (1) a 0.1 % solution of poly-l-lysine (P8920, Sigma Aldrich, UK) or (2) a 0.1 % freshly prepared solution of gelatin from porcine skin type A (G6144-100G, Sigma Aldrich-, UK) in DMW. Both agents carry a positive charge at the pH ranges of the samples used in this study (Carr *et al.*, 1989; Raja Mohd Hafidz *et al.*, 2011). The TEM grids were coated using two different techniques independent of the coating agent:

1. TEM grids were placed floating on a drop of poly-l-lysine (T1 Lys) or gelatin (T1 Gel) for 10 s. Excess moisture was removed from the grid surface using filter paper. This procedure was repeated once more with the grid being placed on top of the sample for 30 s, or
2. TEM grids were placed floating on a drop of poly-l-lysine (T2 Lys) or gelatin (T2 Gel) for 5 min and then rinsed three times using a drop of DMW. Then the coated grids were placed on the top of the sample drop for another 2 min and subsequently rinsed using two drops of DMW. Excess moisture was removed using filter paper.

All samples used for these procedures were diluted in BB 8.0.

3.2.5 Assessment of sample preparation induced agglomeration of synthetic amorphous silica

The degree of particle agglomeration induced by different sample preparation techniques used for EM imaging of SAS was assessed by comparing EM image analysis and NTA results. Median particle sizes were compared. Particle number recovery on EM grids was also used to assess agglomeration for samples prepared by drying and ultracentrifugation. Obtained here nominal recovery was calculated based on PNC measured by NTA and thus does not reflect total recovery related to initial mass or count of particles in the dispersion. Reasons for this are possible loss of the ENPs during sample dilution and by sorption to sample container walls (as suggested by Tiede *et al.* 2009b) as well as limited range of NTA measurements (30-1000 nm HDD).

NTA was chosen for the evaluation of the degree of agglomeration as this technique allows for the fast measurement of unperturbed samples of ENPs in complex liquid matrices, if a simple approach for background correction is applied (e.g. Gallego-Urrea *et al.*, 2011; Luo *et al.*, 2013- Annex 4). NTA provides values for the particles' HDD, rather than the ECD derived from EM imaging. Generally HDD is expected to be larger than the ECD (Linsinger *et al.*, 2012).

3.2.5.1 Nanoparticle tracking analysis

NTA analysis was performed using an LM20 (software version 2.2, NanoSight Ltd, Amesbury, UK). Prior to analysis the samples were diluted to reach a concentration of SAS at $2x10^{-5}$ % w/w using either BB 8.0 or DMW. Three replicates of each sample were analysed and three measurements per replicate were obtained. Recorded videos were 60s long.

3.2.5.2 Data analysis

Sigma Plot (version 12) was used for statistical evaluation and curve fitting of the data. The PNCs of SAS in soup and stock dispersions diluted with DMW and BB8.0, respectively, were compared using t-tests.

In order to conclusively evaluate the influence of sample preparation as well as the matrix effect on size measurements, the median of the particle ECD obtained from SEM micrographs ($\leq$ 60 readings per sample) and the median HDD of each NTA video (9 readings per sample) were calculated. The raw data for particle size measurements were not compared because the high number of measured particles (up to a few thousand) made the statistical tests very powerful and as a consequence statistically significant differences between particle sizes were not only observed between different sample treatments but also in-between replicates of the same treatment/sample.

The majority of the SAS data used for statistical evaluation did not conform to a normal distribution and therefore non-parametric tests were applied, namely the Kruskal-Wallis test with Dunn's post hoc test. The NTA data of samples diluted with DMW or BB 8.0 were compared to EM data of samples, for which the same diluent was used. Finally, to evaluate the change of particle size before and after SAS was added to the soup, the Mann-Whitney U rank sum test was used (for all EM and NTA data).

For all statistical tests a significance level (p) of 0.05 was assumed.

3.2.6 Assessment of the size distribution of spherical silica engineered nanoparticles

Experiments were carried out using preparation procedures minimising particle agglomeration. These were selected based on the results of the study on SAS. The experiment was carried out using samples of Kmix in BB 8.0 as well as spiked into soup. Here, GEMMA was chosen as a comparative analytical technique over NTA as: (1) NTA analysis provides poor peak resolution for different size fractions present within a sample (Filipe *et al.*, 2010; Anderson *et al.*, 2013; Wagner *et al.*, 2013; Chapter 7), (2) silica ENPs smaller than ~30 nm (manufacturer's claim) cannot be detected by NTA and (3) quantification of example silver ENPs by detector coupled to GEMMA was previously proven to be accurate (Kesten *et al.*, 1991), which implies that the method was a good reference for the measurement of PNSD. In this study it was found that smallest particle in the HDD distribution of SAS measured on average ± s.d.: 27 ± 8 nm therefore 30 nm seemed a good approximation. Nevertheless it should be noted that the accuracy of particle size related LOD in NTA especially for such ENPs as silica (characterised by low refractive index, resulting in low light scattering intensity) suffers from contribution of the background noise due to strein of the instrumental settings, such as camera gain and shutter during video acquisition. Unfortunately, Kmix samples dispersed in tomato soup could not be analysed by GEMMA, as the non-volatile substances of the sample interfere with the non-selective GEMMA analysis resulting in false positives. The method is limited to pure particle suspensions containing only volatiles and analysed particles. Even the Kmix stock dispersion required major purification prior to GEMMA analysis in order to remove large contaminating solids that could clog instrument's capillaries and ions from BB8.0 which were interfering with the measurement. For coarse purification the samples were centrifuged at 5000 rpm for 5 min at 20^0C (Universal 30 RF, Hettich Zentrifugen, Newport Pagnell, UK). Subsequent spin filtration was performed using Nanosep Centrifugal Filters (Pall Port Washington, New York, US) with a molecular weight cut-off of 30 kDa and a modified polyethersulfone membrane: 60 µL of the Kmix was applied to the membrane filter and 340 µL of Ammonium Acetate (0.02 M, pH 8) (AA 8.0) was

added. The sample was then centrifuged for 5 min at 14000 g using a 1-14 Sigma table top centrifuge (Osterode am Harz, Germany) until only about 60 µL of supernatant was left on top of the membrane. The eluate was discarded, 400 µL of AA 8.0 were added to the membrane and the centrifugation step was repeated once more. The supernatant was pipetted into a vial and AA 8.0 was added diluting the sample in total 500 fold. The sample was prepared for analysis in duplicate.

3.2.6.1 Gas-phase electrophoretic molecular analyser setup

A GEMMA instrument as described by (Weiss *et al.* 2012) was used in this experiment. Applied settings were: air sheath flow for the nano electrospray process: 0.5 L/min.; sheath flow in the nano differential mobility analyzer: 3 L/min (this allows for a particle separation in the diameter range of 4 to 164 nm); voltage during the electrospray process: 2.5 kV (current of 500-585nA). The Kmix ENPs were approximately spherical (see Figure 3.1) and therefore it could be expected that the ECD derived from SEM would give very similar measurement to GEMMA derived EMD.

3.2.6.2 Data analysis

For comparative purposes SEM raw Kmix ECD measurements were grouped in histograms matching the GEMMA data output. The histograms were divided into four particle size groups: 12.5-30.1 nm (GI), 30.4-61.8 nm (GII), 62.4-106 nm (GIII), 107-163 nm (GIV). Groups GI-GIII corresponded to particle populations from the initial stock dispersions (K12 and K80), whereas GIV was comprised of particle agglomerates. Peak areas of the four particle size groups were integrated and % fractions of particle numbers in each size group were calculated.

The abundance of particles in size groups GI-GIV was prepared for statistical comparison of EM sample preparation methods and GEMMA, as well as of soup and stock samples using additive log-ratio (*alr*) transformation for compositional data as described by (Aitchinson, 1982 and 2013). The data transformation is necessary to avoid the issue of the sum-to-one constraint in the compositional data analysis (Aitchinson, 2013). The transformed data were obtained by dividing the relative particle number in GI, GII and GIII by the relative particle number in GIV and acquiring natural logarithms for the respective quotients.

The statistical comparisons were done using Multivariate Analysis of Variance (MANOVA). If significant differences were detected then ANOVAs and Tukey post-hoc tests were run for the *alr* GI-GIII between data of the different EM sample preparation techniques and GEMMA. T-tests were used for comparison of *alr* GI-GIII of ENPs between stock and soup.

Additionally the effect of particle abundance of different size fractions on the median ECD from full size distribution of Kmix in stock and soup was investigated, the median ECD measurements were compared using ANOVA and Holm-Sidak post hoc test.

All tests were run at $p \leq 0.05$ using the IBM SPSS Statistics 21 software.

Due to the nature of *alr* transformation it is not possible with a certainty to determine which variable given in nominator or denominator of natural logarithm is responsible for a detected statistical difference. This can be only discussed based on the comparison with the original data and this is how the results were interpreted here.

3.3 Results and discussion

3.3.1 The effect of sample preparation on the agglomeration behaviour and particle count of synthetic amorphous silica

3.3.1.1 Quantification of synthetic amorphous silica by nanoparticle tracking analysis prior to sample preparation

Particle recovery is a measure to assess the degree of sample alteration during sample preparation and the subsequent impact on analysis results. Thus, PNCs in the samples containing SAS were analysed by NTA prior to sample preparation for EM imaging. These PNCs were then used as a basis for the calculation of particle nominal recoveries of samples prepared for and analysed by EM (see section 3.3.1.2). Total, mass particle recovery of the SAS (based on the mass concentration in the initial stock dispersion) could however not be estimated due to complexity of particle shape (the issue is further discussed in Appendix 1). PNC measurements for SAS in the stock dispersion and the soup matrix (diluted with DMW and BB8.0, respectively) by NTA are shown in Figure 3.2.

A decrease in PNC after spiking SAS into a sample can in general imply (1) particle-particle agglomeration, (2) particle interactions with the matrix (agglomeration, dissolution, sorption), or (3) particle loss during sample handling (sorption to containers, pipettes, filters and other lab ware) as discussed in e.g. Tiede *et al.* (2009b).

Samples of both, SAS stock dispersions and SAS in soup, show higher PNCs after dilution with BB8.0 than with DMW. The PNC of particles in the stock and soup increased significantly in samples diluted with buffer (PNC = 4.05 x 10^8 and 1.71 x 10^8 particles/mL respectively) in comparison to those diluted with water (PNC = 3.22 x 10^8 and 0.86 x 10^8 particles/ mL respectively) (t-test, $p<0.05$). PNCs of SAS in soup were generally much lower to PNCs of SAS in the stock dispersion (t-test, $p<0.05$). For the SAS in soup prepared with BB8.0 the decrease in mean PNC was 58%, whereas for samples of SAS in soup diluted with water the mean particle loss reached 73%.

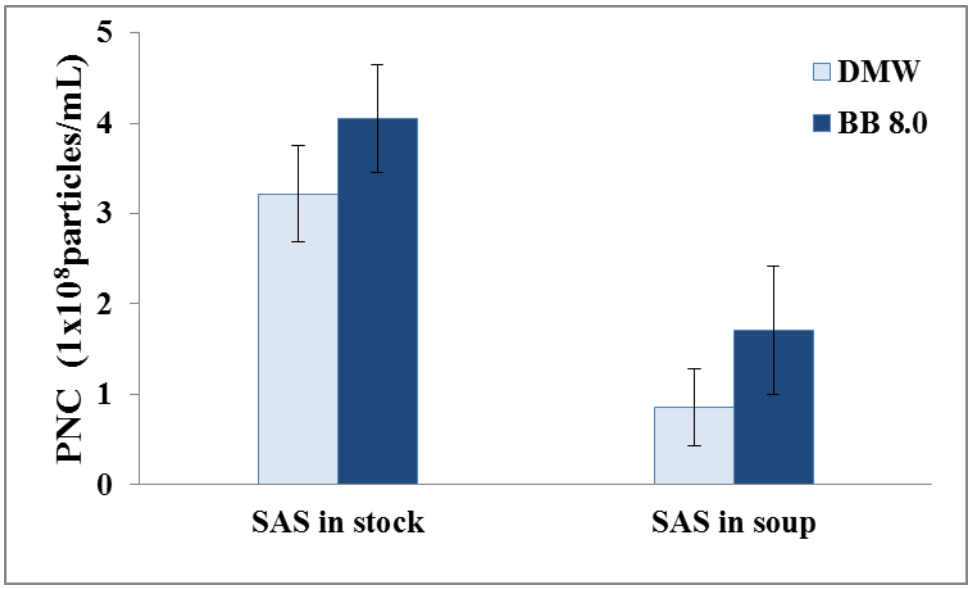

Figure 3.2-Average PNC (columns) and standard deviation (error bars) for SAS containing samples measured by NTA

The decrease of PNC in soup is assumed to be associated with silica ENP interactions with suspended solids as well as with particle agglomeration due to e.g. charge effects, trapping, change of pH and high ionic strength This behaviour of silica colloids has been known for decades and is used in beverage fining (Fede *et al.* 2012).

It has to be noted that a particle loss as high as > 50 % may also have an impact on size measurement and size distribution as it cannot be ruled out that a specific size fraction of particles is selectively affected. However, the overall higher PNCs when using BB8.0 as diluent rather than DMW are well pronounced and thus BB8.0, which apparently stabilised the SAS, was preferentially used in the subsequent experimental work and is in order to minimise particle losses.

3.3.1.2 Agglomeration behaviour of synthetic amorphous silica in soup

Figure 3.3 shows representative SEM images of soup samples with (Figure 3.3d-j) and without SAS ENPs (Figure 3.3a-c). Some EM images obtained from pure soup samples show patterns, which could not be observed in soup samples containing SAS. There also were no structures of matrix components visible that could possibly be mistaken for SAS or Kmix ENPs. In fact most EM images obtained from the pure soup samples did not show anything at all. Subsequent EM image analysis of SAS and Kmix samples were thus assumed to be unbiased in this respect.

The results of particle size measurements and counted particle numbers for all samples obtained by SEM image analysis and NTA are presented in Figures 3.4 & 3.5. A decrease in particle numbers and a simultaneous increase in the particles' diameter was indicative of particle agglomeration. Particle numbers of samples prepared by means of electrostatic attraction could not be compared to PNC obtained by NTA as the sample volume when using this specific sample preparation technique is unknown.

Figure 3.4 shows that among tested sample preparation methods the largest median particle sizes for both SAS ENPs in soup and stock were obtained for samples that were prepared by drying (102 and 121 nm respectively) and ultracentrifugation in DMW (114 and 240 nm respectively). Statistical comparison indicated that these measurements were not significantly different to ones obtained by NTA (Dunn's post-hoc, $p>0.05$), where median HDD of SAS in stock was 108 nm and in soup 117 nm. However, the number of the particles that could be found on the EM micrographs for samples prepared according to these two procedures was very low (Figure 3.5).

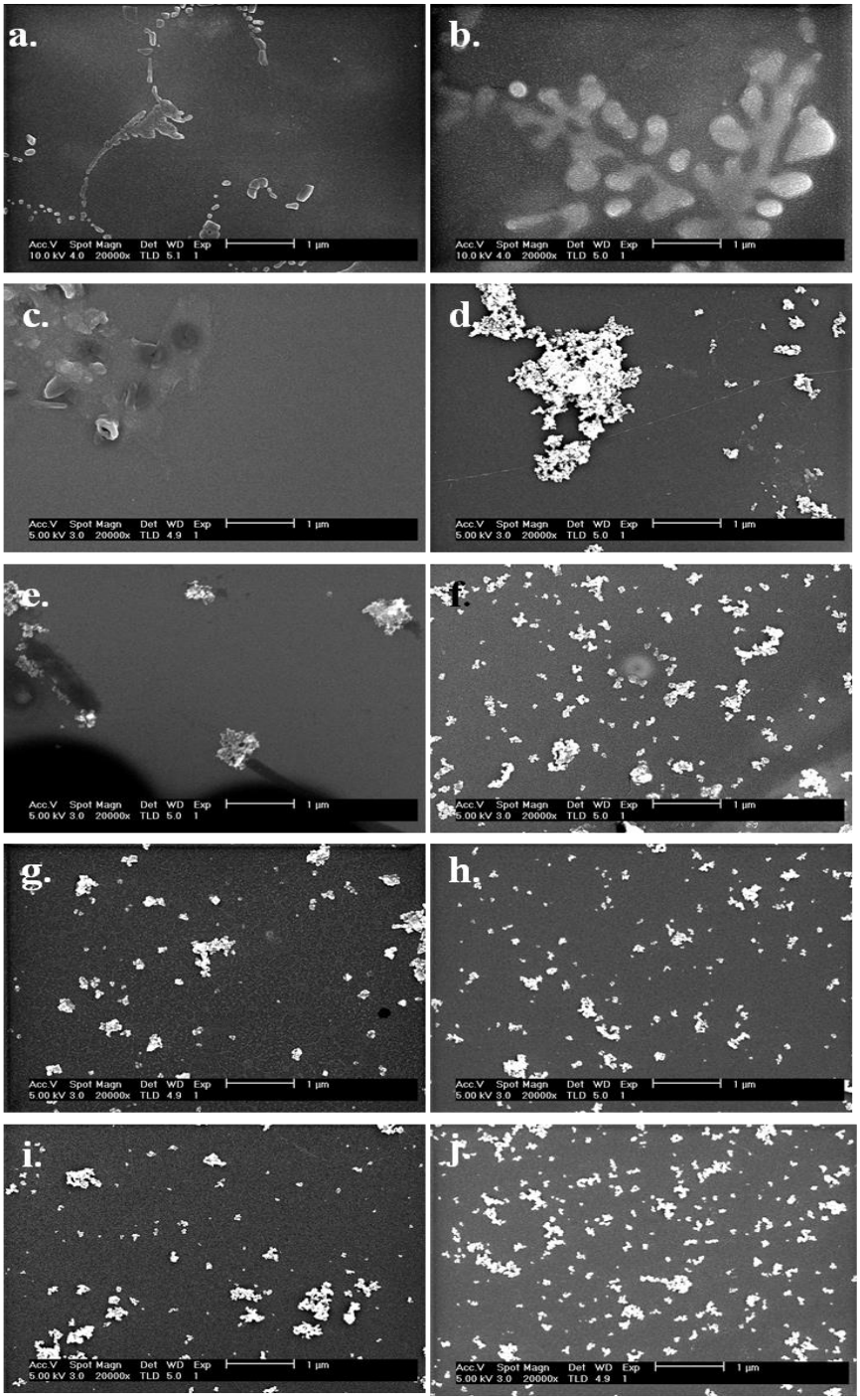

Figure 3.3- (a- c) SEM images of tomato soup without SAS particles. Samples were prepared using following protocols: (a) Ultracentrifugation (in BB8.0), (b) T1 Gel, and (c) T2 Gel. (d - j) SEM images of tomato soup spiked with SAS. Samples were prepared using the following protocols: (d) Drying, (e) Ultracentrifugation in DMW, (f) Ultracentrifugation in BB 8.0, (g) T1 Gel, (h) T2 Gel, (i) T1 Lys, (j) T2 Lys. The length of the scale bar is 1000 nm.

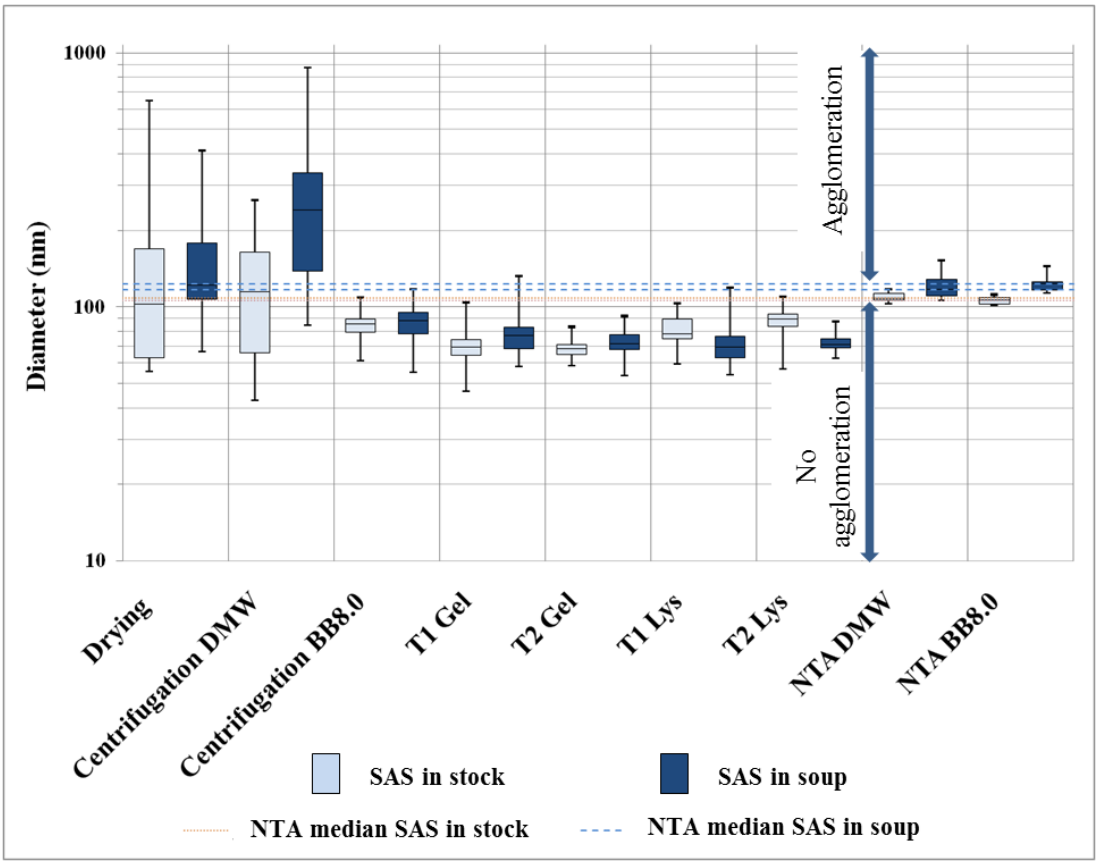

Figure 3.4 -Box plot showing distribution of median SAS measurements per reading (SEM image/ NTA video). The dashed lines present the prolonged medians obtained from NTA videos (lower- diluted with DMW, higher- diluted with BB8.0).

Particle number recoveries of SAS from stock and soup were 5 and 18% respectively for drying and 1 and 50% respectively for ultracentrifugation in DMW. The result points out that the agglomeration of SAS due to these sample preparation procedures might have taken place. Strong agglomeration of natural colloids as an effect of sample drying was previously reported by e.g. Doucet *et al.*, (2005). For ultracentrifugation similar findings were so far not reported. Drying is to date one of the most commonly applied sample preparation techniques as it is a simple procedure allowing pre-concentration of the sample on the grid. In most studies, where the focus lies on regularly shaped and relatively monodispersed particles (unlike studied here SAS or Kmix), image analysis tools can be used for automated particle separation and measurement (e.g. Tiede *et al.*, 2009a).

Ultracentrifugation was used in the literature, for the enumeration of viruses and particles allowing to obtain a linear relationship between initial PNCs and the

number of sedimented particles (Zheng *et al.*, 1996; Lienemann *et al.*, 1998). As in section 3.3.1.1 it was shown that SAS losses were found to be lower during the dilution process when using BB8.0 instead of DMW, the sample preparation by Ultracentrifugation was repeated using BB8.0.

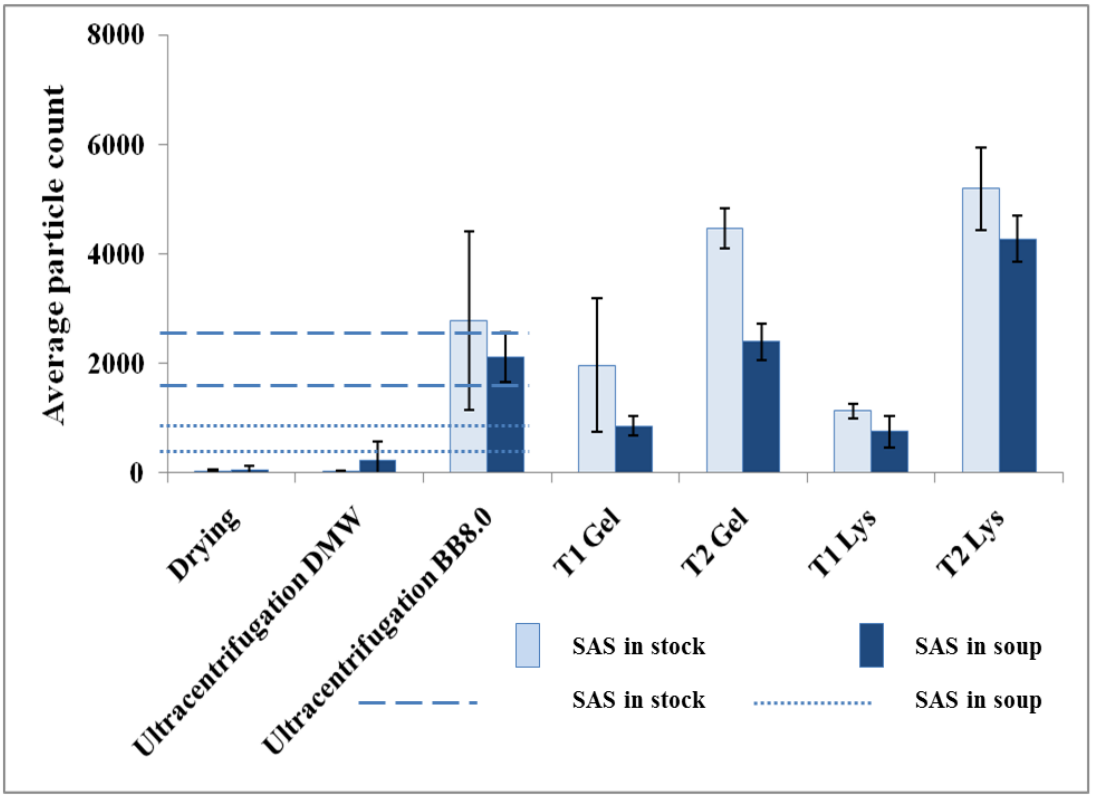

Figure 3.5- Average particle counts of SAS spiked samples prepared by selected sample preparation techniques for EM, error bars represent s.d. between replicates. The expected particle counts based on PNC measured by NTA are presented as lines. Lower lines are expected particle count after diluting the sample with DMW and the higher lines after dilution with BB 8.0.

For both samples the SAS in stock dispersion and soup prepared by ultracentrifugation in BB 8.0 ECDs were smaller (86 nm for particles in stock dispersion and 88 nm for particles in soup) compared to HDDs (106 nm for stock dispersions, 123 nm for soup samples), although the difference was not statistically significant (Dunn's post hoc, $p > 0.05$). The nominal recovery when using BB8.0 was much higher compared to the PNC for DMW dilutions (see Figures 3.3f and 3.5): The mean nominal recovery of SAS in stock and soup was determined to be

120 % and 221% respectively. Nominal recovery values of > 100 % were somewhat unexpected, however it needs to be born in mind that PNC measurements from NTA, on which the nominal recovery calculations were based, as well as the particle count obtained from SEM image analysis showed relatively high s.d. (Figures 3.2 and 3.5). Furthermore, issues related to accuracy of determination of smallest measurable silica ENP and lowered detection efficiency toward small particle sizes in NTA (see Chapter 5) as well as incomparability of SEM and NTA given measurements (ECD and HDD respectively) contributed to error in the estimation of nominal recovery.

All procedures based on electrostatic attraction of particles allowed to obtained smaller median ECD measurements for SAS in soup and stock when compared to NTA derived HDD (Figure 3.4). The only treatment for which a statistical significance was not determined was the T2 Lys with a median ECD of 89 nm for SAS in stock dispersion compared to a 106 nm median HDD (Dunn's post hoc, $p>0.05$).

It was also found that sample preparation methods using gelatin showed significantly smaller ECD measurements for SAS in stock dispersion (T1 Gel: 69 nm, T2Gel: 68 nm) compared to poly-l-lysine treatments (T1 Lys: 78 nm, T2 Lys: 90 nm) (Dunn's post hoc, $p < 0.05$). All methods provided similar ECD values for SAS in soup (T1 Gel: 77 nm, T2 Gel: 72 nm, T1 Lys: 69 nm, T2 Lys: 71 nm) (Dunn's post hoc, $p>0.05$).

EM images obtained from samples prepared using T2 protocols revealed a higher number of SAS than those samples prepared using T1 protocols (Figures 3.3 g-h, and 3.5). In treatment T1, gelatin attracted more particles to the grid than poly-l-lysine, but in treatment T2 the opposite effect was observed. Similar protocols are usually used for preparing biological specimen for EM analysis (Hayat, 1989a; Mast and Demeestere, 2009) and more recently also for immobilizing ENPs on TEM grids (e.g. Micheel *et al.*, 2008; Doren *et al.*, 2011). However, factors such as the chosen coating agents, duration of the treatment and the amount of water used to wash the grids vary between these studies. Here it was shown that small changes in a protocol can have a major impact on the measurement results and potential reproducibility in between the studies.

3.3.1.3 Matrix effects on particle size and particle count

Nearly all EM results, regardless of the sample preparation method (except for Ultracentrifugation of particles in DMW), indicated that SAS were less abundant in the soup than in stock dispersions (Figure 3.5). These results confirm the outcome of the previous NTA analysis. As well as the observed reduction in particle number, NTA also indicated a significant increase in particle size due to the matrix presence (Mann-Whitney U, $p < 0.05$) (Figure 3.4). However, the tendency of an ECD increase of SAS in soup when compared to the stock dispersion was not always the case for all of tested sample preparation procedures. For example for samples prepared by T1 Lys and T2 Lys, a significant decrease of the ECD after spiking particles into soup was observed (Mann-Whitney U, $p < 0.05$). It is assumed that the potential alteration of particle surface chemistry (e.g. surface charge) in the soup matrix could result in change affinity of SAS to poly-l-lysine.

3.3.1.4 Techniques minimising agglomeration during sample preparation

In conclusion, the results obtained for SAS show that the following protocols have the potential to minimise agglomeration of SAS during sample preparation and provide a representative number of the particle population of the sample:

(1) Ultracentrifugation in BB 8.0,

(2) T1 Lys,

(3) T1 Gel,

(4) T2 Lys, and

(5) T2Gel.

However, differences in the SAS median ECD values for the different preparation technique were found (Kruskal-Wallis test, $p < 0.05$). Significantly higher ECDs were obtained for SAS in stock and soup samples when prepared by ultracentrifugation in BB8.0 rather than by electrostatic attraction (Dunn's post-hoc, $p < 0.05$). Significant differences between ECD measurements from different electrostatic attraction protocols were also observed as discussed previously. Thus in the following section these sample preparation methods were subjected to further evaluation using spherical Kmix particles featuring 3 distinct modal particle sizes.

The purpose of this exercise was to determine if the selected five sample preparation methods could cope with different ENPs proportions in selected size fractions.

3.3.2 Impact of electron microscopy sample preparation on the particle size distribution of spherical silica particles

3.3.2.1 Abundance of Kmix particles in different fractions of size dsitribution

Figure 3.6 shows data of the respective particle size distributions obtained by GEMMA and SEM image analysis, as well as the results from the peak area integration for the chosen size fractions (groups GI-GIV) for differently prepared samples.

The triple-modal pattern of the Kmix PNSD was preserved in both stock dispersion and soup samples regardless of the sample preparation technique and analytical method applied (SEM, GEMMA). Tailing was also observed for all samples and is associated with particle agglomeration.

Relatively poor peak separation of the selected particle size groups (GI-GIII) was seen for samples prepared by Ultracentrifugation in BB8.0 and subsequently analysed by SEM, which suggests some degree of particle agglomeration. ECD distributions for the electrostatic attraction protocols (T1 Gel, T2 Gel, T1 Lys and T2 Lys) suggest that these protocols induce less or no particle agglomeration as the three size fractions were more distinct for both matrices, the stock dispersion and soup, than in case of ultracentrifugation in BB8.0.

Statistical comparisons of relative particle abundance in GI-GIV between sample preparation procedures and the reference method as well as between samples of spherical silica ENPs in soup and stock are given in Table 3.2.

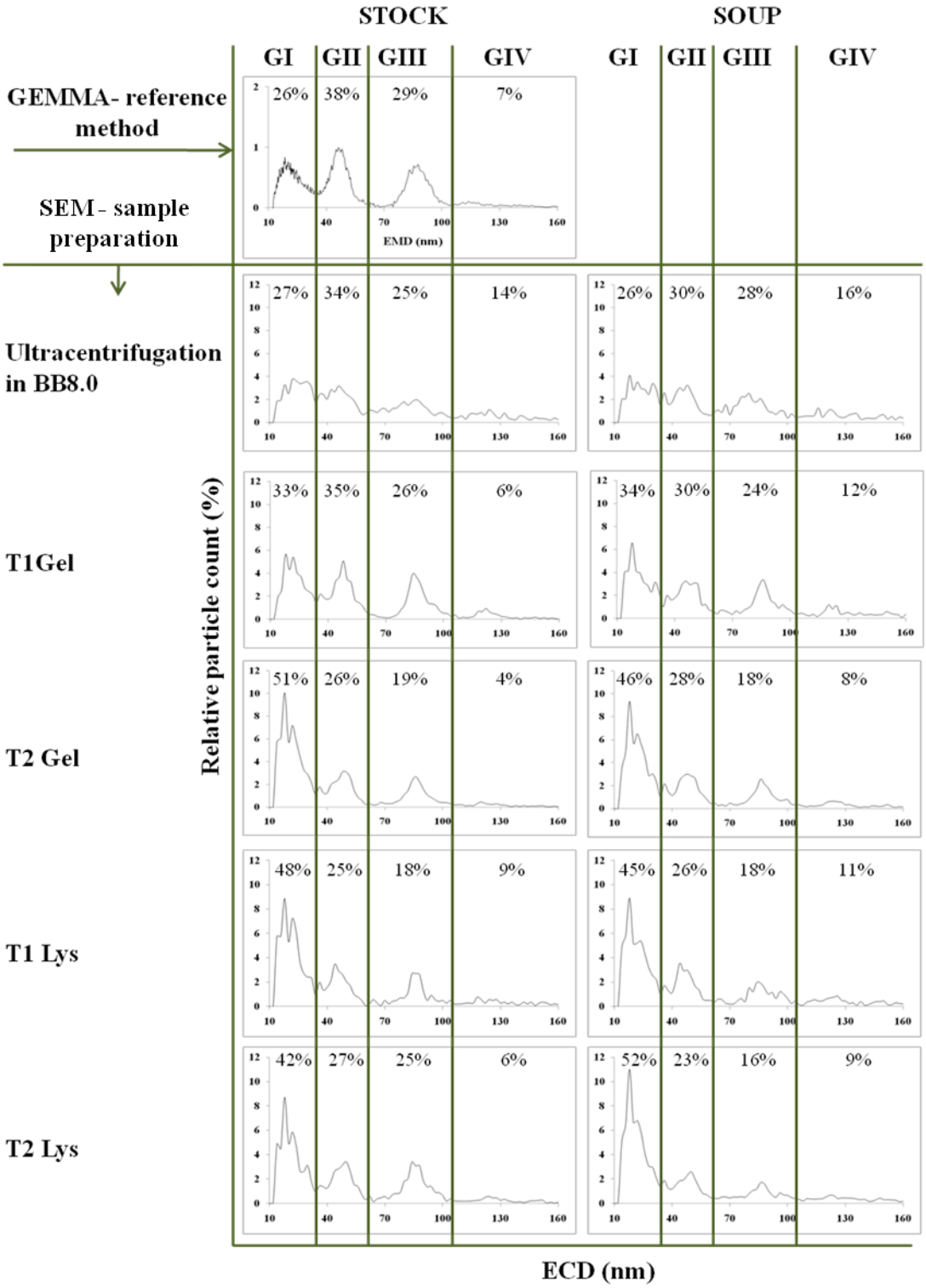

Figure 3.6- Size distribution of Kmix particles dispersed in stock and tomato soup obtained from GEMMA (reference methods) and SEM image analysis. The data shows % of the number of particles present within the respective size group (GI-GIV) (particle size range: 12.5-160 nm)

Table 3.2- The results of statistical analysis on *alr* transformed relative particle counts in selected particle size ranges (GI-GIV) of size distribution of Kmix in stock and soup

	Mean (s.d.) of *alr* transformed relative particle counts in particle size groups GI-GIII (significantly different results between: 1) sample preparations/ reference are marked by different letters, 2) soup and stock are marked with *)					
	stock dispersion			**Soup**		
	ln (GI/ GIV)	ln (GII/ GIV)	ln (GIII/ GIV)	ln (GI/ GIV)	ln (GII/ GIV)	ln (GIII/ GIV)
GEMMA	1.36^{AB} (0.41)	1.75^{A} (0.35)	$1.50^{A\ B}$ (0.27)	-	-	-
Ultracentrifuga-tion BB8.0	0.73^{A} (0.09)	0.78^{B} (0.07)	0.57^{A} (0.11)	0.47^{A} (0.09)	0.55^{A} (0.09)	0.53 (0.09)
T1 Gel	1.58^{AB*} (0.07)	1.65^{A*} (0.06)	$1.44^{B\ C}$ (0.17)	$0.91^{A\ C*}$ (0.16)	$0.98^{A\ B*}$ (0.36)	0.86 (0.43)
T2 Gel	2.57^{C} (0.26)	1.89^{A} (0.15)	1.53^{B} (0.16)	1.86^{B} (0.32)	1.39^{B} (0.3)	0.99 (0.33)
T1 Lys	1.33^{AB} (0.25)	0.88^{B} (0.11)	$0.65^{A\ C}$ (0.48)	$1.20^{C\ D}$ (0.1)	$0.84^{A\ B}$ (0.12)	0.62 (0.34)
T2 Lys	1.65^{BC} (0.62)	1.31^{AB} (0.41)	$1.23^{A\ B}$ (0.41)	$1.42^{B\ D}$ (0.11)	0.63^{A} (0.18)	0.24 (0.23)

There were significant differences detected between particle abundance in GI-GIV measured by SEM and GEMMA (MANOVA, $p<0.05$). The Tukey post hoc comparison revealed that out of five SEM sample preparation protocols only two: T1 Gel and T2 Lys did not yield significantly different results from GEMMA. Differences in relative particle abundance between GEMMA and the other treatments were found for the T2 Gel (ln(GI/GIV)), the T1 Lys and ultracentrifugation in BB8.0 (ln(GII/GIV) both) (Tukey's post-hoc, $p<0.05$). The pre-transformed data (Figure 3.6) show a twofold higher abundance of particles in size group (GI) of the sample prepared according to T2 Gel (52%) when compared to GEMMA (26%). Additionally, fewer particles were found for the T2 Gel treatment

in size group GIV (4 % in comparison to 7 % for GEMMA). This suggests that the T2 Gel method was selective towards smaller particles and possibly did not induce particle agglomeration. In the case of the T1 Lys and ultracentrifugation in BB8.0 lower percentages in particle abundance were observed for size group GII (25% and 34%, respectively) when compared to GEMMA (38%), while higher abundances in size group GIV were noticed (ultracentrifugation in BB 8.0 - 14 %, T1 Lys 9%, other sample preparation methods 4 – 6 %). Here the results imply that these methods were either more prone to cause agglomeration and/or attract preferntially larger particles to the grid.

The comparison of particle abundance in different size fractions between stock and soup samples showed significant difference only for the T1 Gel prepared sample (MANOVA, $p<0.05$). This result needs to be interpreted with caution. The relative abundance of particles in GIV increased after spiking Kmix in soup for all sample preparation methods, therefore it is very likely that differences would be noted if more replicates would be measured for statistical comparison.

3.3.2.2 Median Equivalent Circle Diameter of Kmix

The selectivity of specific methods towards certain particle size fractions is bound to affect median size measurements. The results of median size comparison for full size distribution of the Kmix particles ares summarised in Table 3.3.

Significant differences in the median ECD of Kmix particles in soup and in stock were detected in between the SEM sample preparation techniques as well as EMD derived from GEMMA (ANOVA, $p < 0.05$). The T2 Gel method indicated smaller median ECD (29 nm) compared to median EMD (47 nm) for Kmix in stock dispersion (Holm-Sidak post hoc, $p < 0.05$). This was a result of high numbers of particles in the smallest size fraction after T2 Gel preparation for SEM. The median ECD of Kmix particles in stock dispersion prepared by T1 Gel (46 nm) and T2 Lys (43 nm) were comparable to median EMD (47 nm) (Holm-Sidak post hoc, $p > 0.05$) and as previously indicated there was no significant difference in particle numbers between the size fractions. Median ECD for sample prepared by ultracentrifugation in BB 8.0 (51 nm) and T1 Lys (ECD 36 nm) in stock dispersion also did not differ significantly from the median EMD (47 nm) (Holm-Sidak post hoc, $p > 0.05$), even though previously it was suggested that these sample preparation methods induced

particle agglomeration. The reason for this outcome was balancing effect of particle relative abundance in other size groups.

Table 3.3- Median sizes of Kmix ENPs in stock and soup samples (prepared by different techniques) as obtained by GEMMA and SEM analysis (significantly different results between: 1) sample preparations/ reference are marked by different letters, 2) soup and stock are marked with *)

	Mean (s.d.) of median size measurements in Kmix samples (nm)	
	Stock dispersion	**Soup**
GEMMA	47^{A} (1)	-
Ultracentrifugation BB8.0	51^{A*} (3)	60^{A*} (1)
T1 Gel	46^{AC} (2)	46^{B} (1)
T2 Gel	29^{B} (2)	36^{CD} (6)
T1 Lys	36^{BC} (7)	39^{D} (3)
T2 Lys	43^{AC*} (5)	30^{C*} (1)

There were also differences found for ECD median measurements of Kmix samples in stock and soup when using the same SEM sample preparation method (t-tests, $p < 0.05$). The ultracentrifugation in BB8.0 resulted in larger Kmix ECDs in soup than in stock (60 and 51 nm respectively), whereas T2 Lys preparation yielded contrary effect- particles in soup had a smaller median size than in stock (30 and 43 nm respectively). Although the results of previous statistical comparison on the particle abundance in different size fractions did not indicate significant differences between stock and soup samples prepared by means of these two methods, it is clear that selective deposition of particles from small size fraction (T2 Lys) and agglomeration (ultracentrifugation in BB8.0) affected the Kmix particles after spiking in soup. This result agrees with previous observation for SAS.

3.3.3 Optimal electron microscopy sample preparation techniques for measurement of silica particle size distribution

Overall it was found that sample treatments using electrostatic attraction was most favourable technique in terms of limiting sample preparation artefacts while drying seemed to alter samples the most. Preparation by ultracentrifugation in DMW also caused high losses of particles and possibly agglomeration. These results were considerably improved when DMW was substituted with BB8.0 as a diluent. Based on these findings ultracentrifugation in BB8.0 helps to avoid great particle losses, although it appears to have some effect on agglomeration as shown by the results for Kmix.

Within the set of protocols for electrostatic attraction of particles to the surface of a TEM grid, methods with longer exposure of the sample to the poly-l-lysine or gelatin (T2 treatments) were preferred as higher particle numbers for SEM analysis could be achieved. With regards to the impact of sample preparation on the particle size distribution only one of the methods, T1 Gel, showed a similar particle abundance in the different size groups of Kmix compared to the reference GEMMA measurement. Therefore it seemed that the T1 Gel sample preparation protocol could be recommended for the size characterisation of silica ENPs in pristine dispersions and complex matrices. The results also suggested that the T2 Gel method could be used for the accurate estimation of PNSD for silica ENPs larger than 30 nm. This is because for SAS ENPs with measured particle cut-off at 30 nm both T1 and T2 Gel methods yielded similar median size, but for Kmix ENPs with a part of the PNSD in size range of 12.5-30.1 nm (GI) a clear overestimation of particles number in this size region could be observed. Thus for the measurement of particles larger than approximately 30 nm, T2 Gel protocol was preferential due to a higher particle number recovered from the sample compared to the T1 Gel.

3.4 Conclusions

Here, the impact of different sample preparation techniques on the characterisation of silica based ENPs in a real soup matrix by EM was assessed. In general, it was found that sample dilution is an important factor to consider and a higher silica ENP nominal recovery can be achieved when a stabilizing diluent (BB8.0) was used rather than DMW. Commonly applied sample preparation techniques with their

advantages and disadvantages were discussed and the most suitable ones for EM analysis of silica ENPs in complex food matrices minimising preparation artefacts, such as particle agglomeration, specific to certain size fractions and low particle recoveries, were identified. This was achieved by comparison of size measurement results obtained by selected treatment protocols with each other as well as complementary analytical techniques (NTA and GEMMA).

It needs to be noted that absence of a uniform measurement expression for SAS particles hampered the comparison of PNSD generated by SEM and NTA. Therefore the interpretation of results in this and previously published studies on measurement methods comparisons (e.g. Domingos *et al.*, 2009; Grombe *et al.*, 2014- Annex 5; Loeschner *et al.*, 2013a) posed an analytical challenge. However, since the applied reference methods did not require removal of the particle suspending environment (liquid), it is believed that the obtained ENP size measurements are a good basis for identification of artefact-prone EM sample preparation methods. The availability of reference materials of ENPs featuring broad size distribution and certified not only for particle size, but also for the PNC could overcome this problem.

The study suggested that the best sample preparation techniques for silica ENPs in liquid food matrix were electrostatic attraction protocols. These protocols allowed to limit the agglomeration of silica ENPs in the course of sample preparation. Additionally T1 and T2 Gel electrostatic attraction protocols allowed to obtain silica ENPs measurements in closest relation to the reference methods. Of these two methods T2 Gel may be more suitable for further evaluation due to higher particle numbers recovered from samples.

The suitability of the identified sample preparation techniques for the accurate assessment of particle size not only in freshly spiked materials but also in ageing and/or processed food products has yet to be assessed (Chapter 4). Further research efforts are therefore needed to develop and validate EM methods for the analysis of real life samples and to ensure transferability to different types of ENPs. Studies on validation of EM methods and their application to real life samples are therefore presented in the following chapter.

Chapter 4

Development and validation of analytical procedures for measurement of engineered nanoparticles in food by electron microscopy

4.1 Introduction

The risk assessment studies for ENPs in foods are in need of analytical methods that would allow the reliable characterisation of ENPs in complex samples (Buffet *et al.*, 2011). It is well understood that ENP characteristics can change after spiking into complex matrices (e.g. Pan *et al.*, 2012; Fede *et al.*, 2012; Luo *et al.*, 2013- Annex 4; Park *et al.*, 2013) and thus methods which could measure ENPs directly in foods are needed (EFSA Scientific Committee, 2011).

Currently EM is recommended for the measurement of ENPs in food in support of risk assessment studies (EFSA Scientific Committee, 2011). This is because, as discussed in Chapter 1, EM allows the characterisation of more features of ENPs compared to other techniques. In the previous chapter, EM sample preparation procedures allowing minimal manipulation and near in-situ imaging of ENPs in food matrices were presented and this provides a big step forward in understanding how to prepare samples.

However, sample preparation is only one part of the story and very limited guidance is available on how to produce robust analytical data for ENPs using EM methods (Calzolai *et al.*, 2012). For example, the current understanding in regards to EM LOD for ENP concentration and the errors associated with different steps of food sample analysis is poor. This chapter therefore describes experimental studies that were performed to gain a detailed understanding of the performance of EM for measurements of ENPs in liquid and solid food matrices. Reference materials of ENPs in respective matrices were obtained for the study. To test robustness of the obtained data from analysis of reference material featuring liquid food sample, also a commercially available food product with declared content of SAS ENPs was analysed here. The studies presented in the Chapter address four main questions - 1) how many nanomaterials need measuring to obtain reliable data on particle size distribution? 2) what is the level of background noise from natural nano-structures

present in foods and how could this impact the detection of ENPs? 3) how precisely can particles be measured by EM? and 4) which step(s) in the analysis contribute most to the measurement uncertainty? By having a better understanding of the method performance, it should be possible to develop improved guidance on how to apply EM methodologies to food analysis.

4.2 Experimental design

4.2.1 Materials

The materials included in the study as well as characterisation information provided by the manufacturer or determined in-house are listed in Table 4.1. Two groups of reference food materials spiked with ENPs were used. These were chicken paste (Meat 1, Meat 2 and Meat Blank), and tomato soup (Soup 1, Soup 2 and Soup Blank). The development of these materials is described in (Grombe *et al.*, 2014- Annex 5; Grombe *et al.*, In preparation). Meat reference materials contained Ag ENPs (described in Lari and Dudkiewicz, 2014- Annex 3) and soup reference materials contained SAS ENPs at the spiked concentrations listed in Table 4.1.

Along with the reference materials, JRC IRMM also provided pure suspensions of the respective ENPs that had been used in the preparation of the reference materials. These were also studied to provide information on the original characteristics of ENPs prior to spiking into foods. Additionally, a commercial soup powder (Soup COM) with a declared content of E551 was obtained from a local supermarket. As a control for the Soup COM, SAS powder (SAS COM)- NM203 from the JRC-IHCP Nanomaterial Repository for Toxicology Testing was used.

Prior to the study, Soup COM and SAS COM were suspended in aqueous media using a magnetic stirrer. Soup COM was mixed at a ratio of 11:100 with boiling tap water. The SAS COM was mixed at a ratio 2:98 with BB 8.0 (same buffer as used in Chapter 3).

Table 4.1- List and size characteristics of the materials used in the studies described in this Chapter

Sample	Type of particles	Concentration of core particle % w/w	Declared average particle size	Median (nm)[a]	Interquartile range (% of median)[a]
Meat Blank	Blank	-	-	-	-
Meat 1 (NanoLyse13)	Ag coated with PVP[b]	0.01	-	27	45
Meat 2 (NanoLyse14)		0.05	-	26	39
Ag ENPs 1 (NanoLyse03)		0.02	42±10 nm by TEM	30	38
Ag ENPs 2 (NanoLyse04)		0.1	42±10 nm by TEM	32	34
Soup Blank	Blank	-	-	-	-
Soup 1 (NanoLyse09)	SiO_2 fumed stabilized with NaOH	0.5	-	42	57
Soup 2 (NanoLyse10)		2	-	41	50
SAS 1 (NanoLyse01)		1	120 nm by SLS	57	70
SAS 2 (NanoLyse02)		4	120 nm by SLS	60	82
SAS COM	SiO_2 (E551)	~2	-	53	107
Soup COM		0.28[c]	-	57	71

[a]values obtained by characterisation with TEM (Ag ENPs containing samples) and SEM (SAS containing samples) based on intermediate precision study data (for full size distribution and EM images see Appendix 2, Figure A2.1), [b]Polyvinylpyrrolidone, [c]refers to powder, measured using ICP-MS Thermo Axiom instrument at Food and Environment Research Agency, UK.. NanoLyse labeling provided to allow comparison of results with (Grombe *et al.*, 2014; Grombe *et al.*, In preparation)

4.2.2 Electron microscopy and energy dispersive x-ray spectroscopy

Two different EM methods were selected for imaging depending on the sample's matrix type (solid/liquid) and chemistry of the ENPs. The SAS have generally weak contrast in EM, however for imaging in SEM, samples can be coated with a nanometric layer of metal to improve contrast and minimize charging. Thus the use of coating potentially results in reduction of size measurement uncertainty related to imaging and image analysis of the uncoated materials. Ag ENPs could be best visualized using TEM as these ENPs were embedded in a layer of the meat sample. Therefore for imaging of SAS and Ag ENPs containing samples, SEM and TEM were selected respectively. The previously evaluated methods described in Chapter 3 and (Lari and Dudkiewicz, 2014- Annex 3) for sample preparation were used for the EM sample preparation. A number of additional steps prior to the preparation were applied. Liquid food samples and respective ENP dispersions were stirred for at least 5 min on a magnetic stirrer and were subsequently diluted in BB 8.0. Soup 1 and 2 were diluted 100 fold and all SAS dispersions 200 fold. The Soup COM was not diluted, but instead adjusted to pH 8.0 using 0.4 M NaOH. The samples were then mixed on the magnetic stirrer for 6 hours (equilibration). Equilibrated samples were prepared for imaging using T2 Gel protocol described in Chapter 3.

The prepared grids were attached to the conventional aluminum SEM stubs using a carbon tape and conductively coated as described in Chapter 3. The thickness of the coating was subtracted from the measurements as described in Appendix 1.

Frozen meat samples were defrosted in a water bath at approximately 35^0C for 5 min. The samples were then diluted 400 fold in BB 8.0. Ag ENPs suspensions were diluted 800 fold in order to match the concentration levels in respective meat samples. Then same protocol as described in (Lari and Dudkiewicz, 2014- Annex 3) was used for preparation of both sample types.

The SEM images were taken using an FEI Sirion S field emission gun SEM equipped with a through the lens detector and EDS from Thermo Fisher (NS7 system S/N 0409235 with NSS112E NORAN operating software). For imaging, an operating voltage of 5 kV and spot size 3 were used. The EDX spectra of point

analyses were recorded at spot size 4 and 5 kV for 30 s from the selected areas corresponding to objects of interest, primarily to measure the 1.8 kV Si peak.

The TEM images were acquired with a JEOL JEM 2011 TEM operating at 200 kV. The microscope was equipped with a digital camera (Gatan 794) and EDS system (Thermo Fisher NS7 system S/N 0409237 operated by NSS112E NORAN).

4.2.3 Data acquisition and image analysis

All provided particle size measurements refer to the ECD. The data acquisition parameters used in this study are summarised in Table 4.2.

Table 4.2- Data acquisition parameters

Technique	Area of a single image (µm x µm)	Pixel size (nm)	Smallest particle		Volume analysed per replicate (ml)
			Area (no. of pixels)	ECD (nm)	
SEM	6.3 x 4.73	8.7	15	30	Cannot be specified
TEM	1.6 x 1.6	1.6	80	16	2.8×10^{-9} [e]

Ten images per sample replicate were taken from randomly selected places (predetermined coordinates) of the grid. SEM and TEM image areas were adjusted to allow capture and measurement of maximal number of particles for the respective sample types (imaging at relatively low magnifications). The micrograph area was relatively large in proportion to the measured ENPs. The smallest measurable ENP size was experimentally estimated for SEM as described in Chapter 3, for TEM the smallest measurable particle size was chosen based on visual assessment allowing limiting background interference during image analysis.

The acquired images were analysed using OBIA software (described in Chapter 3).

4.2.4 Quantification of uncertainty in particle size measurements related to measured particle number and broadness of the size distribution

An approach previously described by Jarvis and Hedges (2011) was used to derive dependence of ECD measurement uncertainty in relation to a given number of

randomly selected particles from a population of known size distribution. Five of the samples listed in Table 4.1 (Meat 1, Ag ENPs 1, Soup 1, SAS 1 and SAS COM) were selected to cover different interquartile ranges of particle sizes (given as relative to median- *IQR%*). For each of these samples, 200 images generated in the intermediate precision study (see section 4.2.6) were used. For each sample, 1388 particles were randomly selected from 200 images. These 1388 particles from each sample referred to as the 'population' were subjected to simulations without replacement in order to derive a relationship between measured particle number and measurement uncertainty of median particle ECD. This was done by randomly selecting either 25, 50, 75, 100, 150, 200, 250 and 500 particles from the particle population of each sample, and the process was repeated 500 times for each sample and particle sampling number. Median particle sizes and relative standard deviations (*RSD%*) between them were then estimated from the 500 sets for each sample and particle number. In order to investigate the magnitude of *RSD%* increase with increase of *IQR%,* the obtained *RSD%* values were plotted against the *IQR%* values for each particle sampling number (see section 4.3.1).

4.2.5 Limit of detection

The approach used for LOD estimation was based on detected levels of matrix interference (LOD_{matrix}).

Samples of Meat and Soup Blank were prepared in duplicate and imaged using the methodologies described above. The resulting micrographs were visually assessed to determine the presence or absence of particles or structures which looked similar to Ag ENPs and SAS used in the study. If potentially interfering particles or structures were observed then a further 18 replicates of the sample were prepared and imaged. These images and the original duplicate images were analysed using the OBIA software tool to determine the interfering particle concentration for each replicate. The LOD_{matrix} was then estimated from the mean interfering particle concentration using Eq. 4.1 and 4.2. The assumption was that the particle distribution followed a Poisson distribution similar to a study on quantification of bacterial cells in food reference material (in 't Veld *et al.*, 1996).

$$LOD_{matrix}=N+1 \text{ for } N>s \text{ with } P<5\% \qquad \textbf{Eq. 4.1}$$

$$P = \frac{e^{-s} \times s^{N}}{x!} \quad \textbf{Eq. 4.2}$$

Where:

x- number of false positive particles

P- probability of the sample containing *x* of the false positive particles

N- consecutive number of particles

s- mean number of particles found per replicate for a blank sample

4.2.6 Intermediate precision and expanded uncertainty of particle size measurements

The materials listed in Table 4.1 were used to determine the inter-laboratory reproducibility of size measurement- intermediate precision. The study setup was based on the routine protocol for analytical method validation as described in (Boque *et al.*, 2002). For this, samples were prepared and imaged in duplicate on 10 different days spread through a period of four weeks.

Different vials of Meat 1 and 2 were prepared and analysed every day. However, for Soup 1 and 2 it was decided to use only 1 jar over the 10 testing days due to the variability of the pH in between the received jars (5.2-6.5), which could potentially affect particle size distribution. The opened jars were not refrigerated for the duration of the test. The Soup COM was freshly prepared on each day. Respective particle stock dispersions were sampled from one bottle during the whole test.

Data acquired from this test were used to calculate *RSD*% of the median particle ECD measurements for repeatability (RSD_r), day to day variation (RSD_{dd}), and intermediate precision (RSD_{ip}):

$$RSD_r = \frac{100 \times \sqrt{MSW}}{s} \quad \textbf{Eq. 4.3}$$

$$RSD_{dd} = 100 \times \frac{\sqrt{\frac{(MSB - MSW) + MSW}{n} \times e^{-\frac{MSB}{MSW}}}}{s} \quad \textbf{Eq. 4.4}$$

$$RSD_{ip} = \sqrt{RSD_r^2 + RSD_{dd}^2} \quad \textbf{Eq. 4.5}$$

Where:

MSW- ECD mean squares of replicates measured on the same day

MSB- ECD mean squares of replicates of all 10 days

s- mean ECD of the median measurements between replicates

The *MSW* and *MSB* were calculated by one way ANOVA using Microsoft Office Excel 2007.

Eq. 4.4 was adapted from Federer (1968) as suggested in (Linsinger *et al.*, 2001) to allow calculation of RSD_{dd} for results, where *MSW*>*MSB*.

The RSD_r and RSD_{ip} obtained for two levels of concentrations of ENPs in food matrices and relevant stock dispersions were compared using the F-test at significance level (p) of 0.05. The F-test was also used to compare pairs of concentrations related to relative uncertainties for stock dispersions and ENPs spiked in the food matrix.

The expanded uncertainty (U_{exp}) is obtained by combining all the sources of measurement uncertainty and multiplying by the coverage factor (k=2 for approx. 95% confidence interval) (ISO/IEC Guide 98-3:2008). In this study the U_{exp} was derived combining RSD_{ip} and trueness (RU_t) according to Eq. 4.6

$$U_{exp} = k \times \sqrt{RSD_{ip}^2 + RU_t^2} \quad \textbf{Eq. 4.6}$$

The RU_t values were 1.4% and 1.9% for TEM and SEM respectively and were calculated using the procedure described in the (Linsinger, 2010). The trueness assessed in this study reflects solely the 'goodness' of instrument calibration, determined by ENP reference material (NIST 30 nm gold nanoparticles, manufacturer's id: 8012) characterised by very narrow size distribution. It is expected that for the ENPs characterised by a broad size distribution and/ or spiked in food the RU_t would be higher than estimated here.

4.2.7 Influence of data acquisition stages on intermediate precision

As the data acquisition from EM is more complex than many other analytical methods, estimation of the relative uncertainty for each of the stages in the process was of interest. The experiment was performed using four selected reference materials: SAS 1, Soup 1, Ag ENPs 2 and Meat 2. For this, four separate experiments were performed to assess *RSD* attributed to sampling (RSD_s), sample preparation (RSD_{sp}), imaging (RSD_i) and image analysis (RSD_{ia}). The following experiments were performed:

1) Sampling - 10 different portions of a sample were prepared on the same day and imaged within one day;

2) Sample preparation - 10 replicates of the same subsample were prepared on the same day, then imaged within a day;

3) Imaging - a single replicate was imaged on 10 different days; and

4) Image analysis – the same set of 10 images was analysed 10 times (returning image analysis settings to default every time).

Experiments 1-3 resulted in *RSD* values (RSD_1, RSD_2, RSD_3 respectively). Obtained this way *RSD* values were a combined uncertainty of several factors and not only sought uncertainty values for specific data acquisition stages. The RSD_1 and RSD_3 except of respective RSD_s and RSD_i values did not exclude RSD_{ia} and RSD_{pn} (standard relative uncertainty related to measured number of ENPs see section 4.3.1). Additionally RSD_1 was also inclusive of RSD_{sp}. Therefore to calculate interesting *RSD* values the root-sum-square manner subtraction of inclusive uncertainties from RSD_1, RSD_2 and RSD_3 as proposed in (Boque *et al.*, 2002) was used Eq. 4.7-4.9.

$$RSD_s = \sqrt{RSD_1^2 - (RSD_{sp}^2 + RSD_{ia}^2 + RSD_{pn}^2)} \quad \textbf{Eq. 4.7}$$

$$RSD_{sp} = \sqrt{RSD_2^2 - (RSD_{ia}^2 + RSD_{pn}^2)} \quad \textbf{Eq. 4.8}$$

$$RSD_i = \sqrt{RSD_3^2 - (RSD_{ia}^2 + RSD_{pn}^2)} \quad \textbf{Eq. 4.9}$$

Total *RSD* (RSD_{total}) was obtained by adding all *RSDs* attributed to all the sources of measurement error according to Eq. 4.10:

$$RSD_{total} = \sqrt{RSD_s^2 + RSD_{sp}^2 + RSD_i^2 + RSD_{ia}^2 + RSD_{pn}^2} \quad \textbf{Eq. 4.10}$$

The RSD_{pn} for RSD_{total} calculation was derived from the median count of particles per replicate and the *IQR%* from the precision results of the studied samples. The RSD_{total} ideally should be equal to RSD_{ip} estimated in the intermediate precision study.

4.3 Results and discussion

4.3.1 Quantification of uncertainty in particle size measurements related to measured particle number and broadness of the size distribution

Linear relationships were obtained between *IQR%* and *RSD%* of median ECD measurements depending on the measured number of particles (*N*) (Fig. 4.1a). Fits between R^2= 0.973 to 0.997 were achieved with an expected intercept of 0.0 and were described using Eq. 4.11. The slope coefficient *a* in Eq. 4.11 clearly depended on the number of particles, therefore dependence of *a* to *N* was shown in Fig. 4.1b. This dependence followed a power curve and was well described (R^2=0.998) by Eq. 4.12.

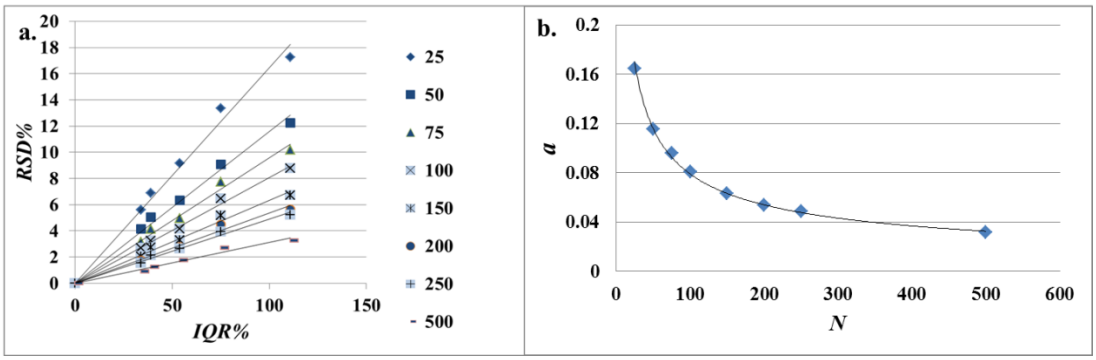

Figure 4.1- (a) Dependence of median size measurement *RSD%* of the sample size *N* to *IQR%* and (b) Relationship between slope coefficient *a* of Eq. 4.11 and *N*

$$RSD\% = a \times IQR\% \quad \textbf{Eq. 4.11}$$

$$a = 1.0071 \times N^{-0.553} \quad \textbf{Eq. 4.12}$$

The expected measurement uncertainty for samples with known *IQR%* and a defined sample size can be calculated using following derived Eq. 4.13.

$$RSD\% = 1.0071 \times N^{-0.553} \times IQR\% \quad \textbf{Eq. 4.13}$$

The ISO guideline draft (Draft ISO/WD 14411-2, In preparation) describing the relationship between the uncertainty of particle size measurement and the required number of measured particles aims to include the theoretically derived equation for Gaussian PNSDs adapted from unpublished work of Professor Hideto Yoshida, Hiroshima University, Japan. A comparison of this theoretical approach to the experimental approach developed in this study (Eq. 4.13) was done. It was found that both approaches do not give significantly different level of the *RSD%* for a given sample size and *IQR%*. Nevertheless, as the empirical Eq. 4.13 does not assume any particular particle size distribution (for theoretical approach a Gaussian distribution is accepted), it is considered more practical for the materials studied here.

Using Eq. 4.13 for calculation of *N* for samples with different *IQR%*, and *RSD%* at the level of 5 and 1%, results shown in Table 4.3 were obtained.

Table 4.3- Calculated (Eq 4.13) smallest number of measured ENPs needed to obtain a desired *RSD%* level depending on given for ENP population with specific *IQR%*

IQR%	**Numbered of particles needed for targeted *RSD%***	
	***RSD%*=5**	***RSD%*=1**
34	38	994
39	49	1630
54	91	5260
75	170	17166
111	359	70424

This shows that the minimum number of particles to achieve *RSD%* at the level of 5% is smaller than 500 particles previously suggested (Linsinger *et al.*, 2013), even for a sample with the broadest *IQR%* (111). To achieve a lower uncertainty of 1%, particle numbers need to be much higher due. However, the acceptability of the *RSD%* threshold will ultimately depend on other contributing factors during data acquisition. This is further discussed in subsequent sections where Eq. 4.13 was used to calculate RSD_{pn}.

4.3.2 *Nominal recovery and limit of detection*

Data regarding the count of particles per sample replicate (from the intermediate precision test, 20 replicates), nominal recovery, and LOD are summarised in Table 4.4. As in most cases particle number distributions between replicates of ENPs spiked in food did not conform to the Gaussian distribution, the median value gave a better representation of particle number in the sample. Therefore the median number of particles was used to calculate ENP nominal recovery and *LOD.*

Table 4.4- The number of measured particles in 20 sample replicates, nominal recovery and the *LOD*

Sample id	Number				Nominal recovery (% particle number)	LOD_{matrix} (% mass)	LOD_{ENP}[c] (% mass)
	Median	Mean	*RSD%*	Min[a]			
SAS 1	1361	1431	41	633	-	-	-
SAS 2	5640	5603	24	706	-	-	-
Soup 1	264	515	96	65	19	0.010	0.008
Soup 2	909	1531	114	170	16	0.013	0.010
SAS COM	1190	1266	33	724	-	-	-
Soup COM	305	461	81	98	19	-	0.003
Ag ENPs 1	47	46	53	14	-	-	-
Ag ENPs 2	163	177	28	102	-	-	-
Meat 1	32 (34)[b]	30 (33)[b]	52	3 (10)[b]	68	None detected	0.003
Meat 2	83	88	57	24	51	None detected	0.002

[a] Smallest number of particles found in one replicate of 20, [b] Number of particles found at random selection of the micrographs, in parentheses number of measured particles in precision test (some areas selected randomly did not contain any ENPs. In such a case, nearby area with at least 1 particle present was imaged instead for estimation of precision) [c] Limit of detection based on number of ENPs found at analysed concentrations.

The nominal recovery was expressed as a median particle count in the food reference material relative to median particle count in respective stock dispersion. Recoveries for SAS in Soup 1 and 2 and Soup COM did not exceed 20% of the stock particle number. For Meat 1 and 2, Ag ENPs recoveries were much higher at 51 and 68% of the stock particle number respectively. The sample preparation protocol used for Soup 1 and 2 was previously tested on tomato soup freshly spiked with silica (Chapter 3) whereas the Soup 1 and 2 were tested after over a year from manufacturing. In freshly spiked samples, the particle nominal recovery was as high

as 50% of particle number. If particle mass rather than particle nominal recovery was considered (see Annex 1), these values would be different because in both Soup 1 and 2 the particles were ~20 nm smaller than in the respective stock dispersions (median ECDs in Table 4.1). There are several possible reasons for the low nominal recovery, such as transformation of the particle surface over time leading to reduced adsorption to the grid, a higher loss of larger particles, and/or a partial dissolution of the SAS and Ag ENPs.

The *RSD%* values were relatively high (28-114%) when compared to the previously published work using EM for quantification of viruses in aquatic systems (10.2%) (Bettarel *et al.*, 2000), biological suspensions (~5-30%) (Zheng *et al.*, 1996) and when set with other analytical approaches for particle quantification e.g. NTA 3.1-6.9% (Du *et al.*, 2010). This led to a difficulty with use of standard protocol for estimation of *LOD* for smallest detectable analyte concentration (Vogelgesang and Hädrich, 1998). To give an idea on lowest detectable particle mass concentration, LOD_{ENP} values were calculated dividing particle mass concentration in the initial food sample (Table 4.1) by Number/Min value from Table 4.4. For Meat 1 and 2 LOD_{ENP} was at the level of 0.003 and 0.002% mass respectively. For Soup 1 and 2 0.008 and 0.01% mass respectively.

The estimation of *LOD* related to presence of interfering particles in blank matrix LOD_{matrix} was also carried out. The EDS analyses did not confirm the presence of Ag in Meat Blank or Si in Soup Blank (see Appendix 2 Figure. A2.2). In Meat Blank, no objects were found that could be mistaken for Ag ENPs. Some nanometric sized globular structures were present but they had a very low contrast compared to Ag ENPs (Figure 4.2 a, c). These natural nano-structures within the matrix were also not suitable for measurement using OBIA. Therefore, no matrix related errors such as false positives could be expected when analysing Ag ENPs in meat samples.

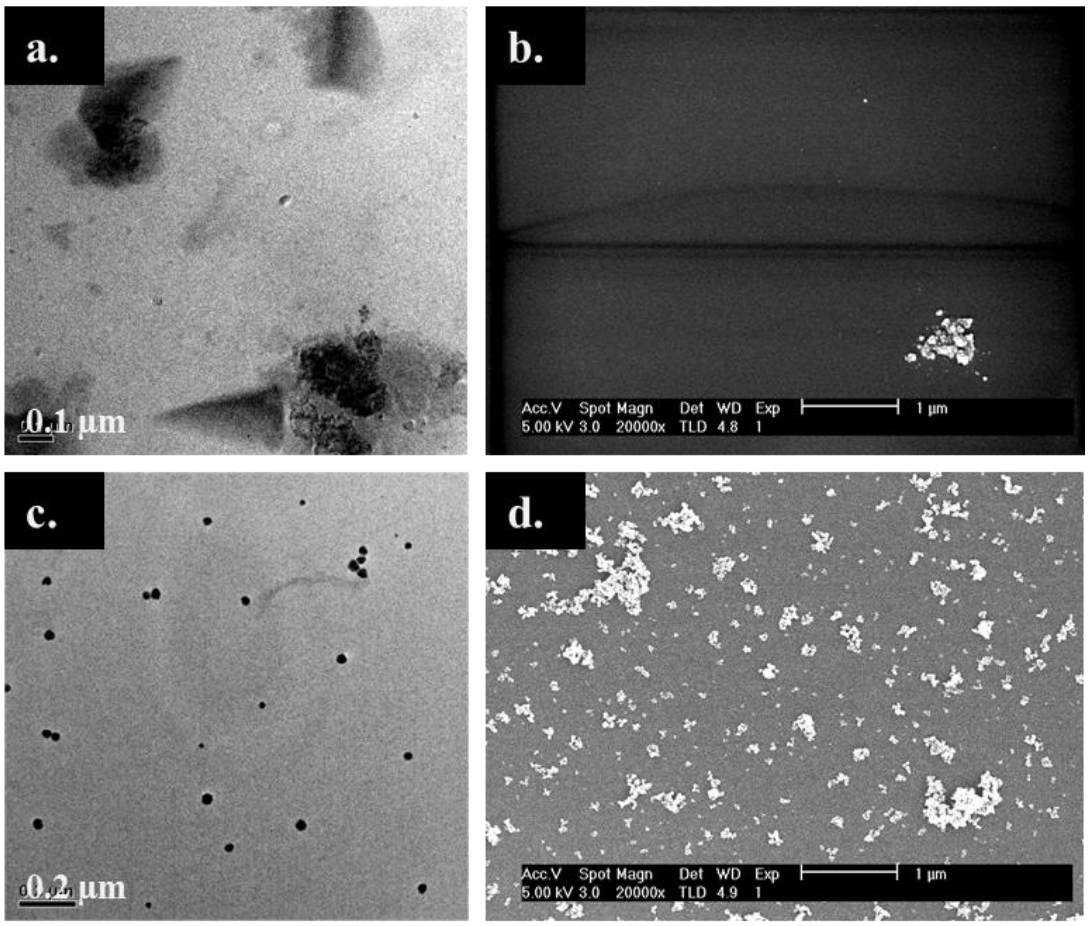

Figure 4.2- EM images of (a) Meat Blank, (b) Soup Blank, (c) Ag ENPs 2 and (d) SAS 2

Soup Blank contained some irregularly shaped ENPs which were similar in appearance to SAS (e.g. Figure 4.2b) and could potentially be mistaken for SAS. These ENPs and the ones close to the cut-off ECD value were accounted for as interference, because in this study and others (Tiede *et al.*, 2009c; Lorenz *et al.*, 2010) identification of the EDS spectra for nanometric particles was typically carried out as a confirmation on single particle basis rather than on full measured sample. In different study examples, such confirmation was not carried out at all and estimates were based on expert knowledge of the particle appearance (Weir *et al.*, 2012; Luo *et al.*, 2013- Annex 4). The average number of interfering ENPs per replicate in Soup Blank was 5, which after calculation (according to Eq. 4.1 and 4.2) gave LOD_{matrix} of 10 particles and an equivalent of concentrations of 0.01-0.013% mass for Soup 1 and 2. Because LOD_{matrix} for SAS in soup had higher values than respective LOD_{ENP} it became clear that background noise is likely to be a key limiting factor for detection of these ENPs in foods.

The estimated 0.013 % mass LOD_{matrix} is sufficient for analysis of E551 in commercial food products as the typical E551 concentrations in food powders range from 0.06 to 0.54 % mass (Dekkers *et al.*, 2010). However, this statement is only valid at assumption that commercial food samples are less or equally abundant in natural nanostructures as studied here Soup Blank.

It needs to be emphasized that the LOD_{matrix} and LOD_{ENP} values estimated here are not robust and applicable only to study setups with same samples, and micrograph sizes at a random selection of imaged areas.

4.3.3 Intermediate precision and expanded uncertainty of particle size measurements

The results of the uncertainties of particle ECD measurements were summarised and compared to RSD_{pn} values calculated for median sample size (Table 4.4) and sample specific *IQR%* (Table 4.1) in Figure 4.3.

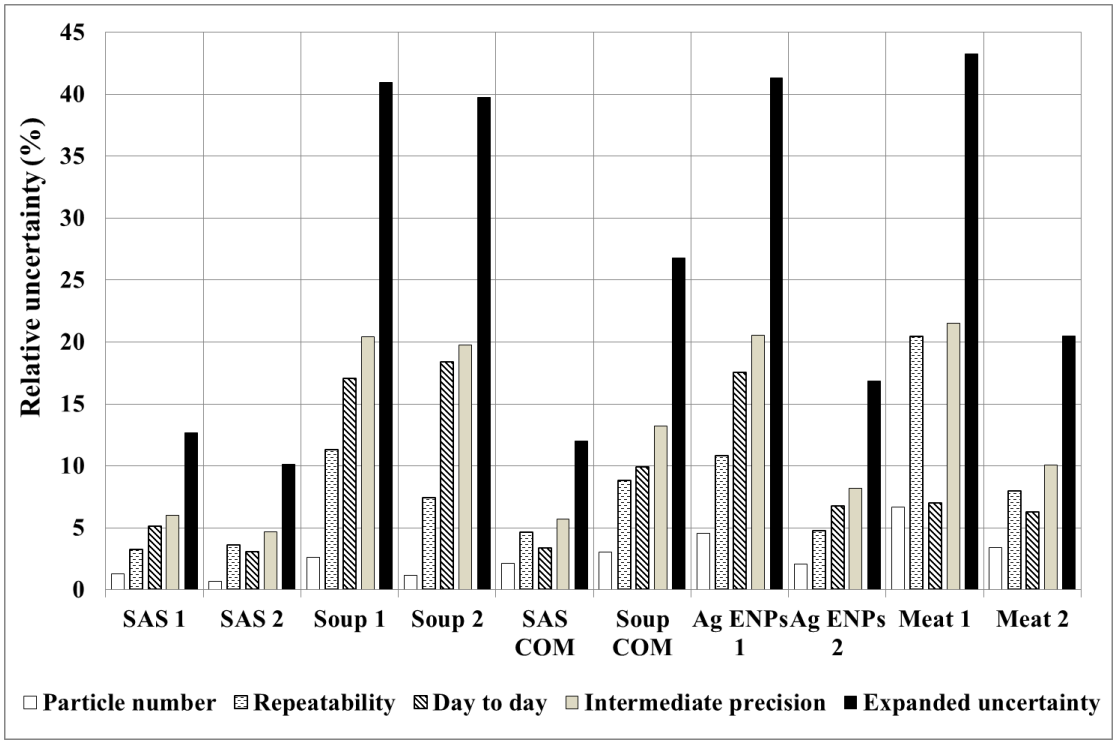

Figure 4.3- The median ECD particle number, repeatability, day to day, intermediate precision and expanded uncertainty for ENPs measured in respective samples

The values of U_{exp} for food samples containing ENPs ranged from 21% (Meat 2) to 43% (Meat 1), whereas for the stock dispersions the range was 10% (SAS 2) to 41%

(Ag ENPs 1). The obtained U_{exp} for the stock dispersions with the exception of Ag ENPs 1 corresponded well with the expanded uncertainty of 16% that was previously proposed for CLS measurement method of pure ENP suspensions (Braun *et al.*, 2011). This result points out that EM has the potential for producing equally reliable results as other analytical methods.

The RSD_{pn} for all measured samples was significantly lower (1-7%) than RSD_{ip} obtained in the experiment (5-21%) (F test, $p<0.05$). This is in agreement with the published data on characterisation of the reference materials for ENP measurement. For example in the study (Braun *et al.*, 2012), ENP with *IQR%* ~ 20 and 500 particles measured per replicate was characterized by EM in 11 different facilities. The RSD_{ip} measured between the laboratories ranged from 1.2 to 8.5 whereas calculated for this material from Eq. 4.13, RSD_{pn}=0.6. The result suggests that factors other than particle size distribution broadness and sample size affected the measurement uncertainty.

For samples containing SAS, the presence of soup matrix significantly increased the uncertainty of the measurements (RSD_{ip} ranging 13-21%) when compared to the stock dispersions (RSD_{ip} ~5%) (F test, $p<0.05$). Contrary to this result, the RSD_{ip} were similar for Ag ENPs in stock and meat dispersions at respective concentrations, i.e. 21-22% for lower concentration and 8-10% for higher one (F test, $p>0.05$). Therefore the presence of the matrix hampered reproducibility of measurement of ENPs only in soup samples. The uncertainty increase for the measurement of SAS in soup, when compared to stock dispersions, seemed to depend on the nature of the sample. SAS in the Soup COM were measured with 13% RSD_{ip}, whereas for Soup 1 and 2 RSD_{ip} exceeded 20%. The increased RSD_{ip} for Soup 1 and 2 when compared to Soup COM were attributed to high RSD_{dd} rather than to RSD_r. For Soup 1 and 2, only one jar of the sample for the 10 testing days spread over period of four weeks was used. However, the trend of changing particle size toward smaller or larger values with sampling time was not confirmed within the experiment (see Appendix 2, Figure A2.3). Thus either a) subsamples taken at the same time point had a higher chance of being closely related by size, or b) imaging the samples on different days introduced a major error to the measurement. To address these aspects, the effect of the different stages involved in the data acquisition process was also explored.

4.3.4 Influence of data acquisition stages on the intermediate precision

The results of further experiments on the uncertainty level introduced by individual stages in the analytical process are summarized in Tables 4.5 and 4.6.

Table 4.5- The contribution of the stages in the data acquisition process to the RSD_{total} of SAS containing samples

	Sampling	Sample preparation	Imaging	Image analysis	Particle number	Total
Soup 1	11%	7%	2%	2%	2%	14%
SAS 1	1%	1%	6%	1%	2%	7%

Table 4.6- The contribution of the stages in the data acquisition process to the RSD_{total} of AgENPs containing samples

	Sampling	Sample preparation	Imaging	Image analysis	Particle number	Total
Meat 2	8%	3%	3%	3%	3%	10%
AgENPs 2	negligible	9%	negligible	2%	3%	9%

The highest *RSD* for Meat 2 and Soup 1 were attributed to the sampling (8 and 11% respectively). At the same time the sampling had a very small *RSD* value (up to 1%) for respective ENPs in the stock dispersions.

Such results were partly expected. The EMs can analyse only a very small volume of the sample at a time (order of few pl), and it is not possible to make food products so homogenous that it is representative at the small sample scale. Therefore it can be expected that each portion of the sample will contain a varying population of the particles and as shown here not only by number, but also by size.

The high RSD_{sp} (9%) Ag ENPs 2, when compared to Meat 2 (3%), suggested that the presence of the meat matrix may have prevented random particle clustering in the sedimentation process, but this might have taken place during preparation of Ag ENPs 2.

The imaging, sample preparation, and image analysis were each expected to influence the RSD_{total} of the Meat 2. This is because the particles were suspended in meat matrix at different depths and it was not possible to fully focus on all of the particles within the field of view. Additionally, the sample layer obtained in the preparation procedure was thick (approximately 100 nm) and not uniform (up to 33 *RSD%* of the sample thickness between different images) (based on Lari and Dudkiewicz 2014- Annex 3). This inevitably affected the definition of particle boundaries and consequently the results of image analysis. It also means that the instrumental performance had limited influence on the RSD_i for Meat 2.

Imaging of the SAS 1, yielded higher (6%) RSD_i than of Soup 1 (2%). It is possible that for this sample the instrumental or operator performance on a day-to-day basis and certain particle features (shape, size) may have had a significant impact on the measurements. As with the increase of the size (on median particles in SAS 1 were characterized by longer ECD than in Soup 1- see Table 4.1), the particle perimeter becomes larger, the possible instrumental or operator variations in alignment, noise from the microscope surroundings (stage drifting), may cause a shift in the particle boundaries and affect size measurement more than in case of small, nearly spherical particles.

The RSD_{total} for all the samples (Table 4.5 and 4.6), with the exception of Soup 1, corresponded very well to the previously obtained RSD_{ip} (Fig. 4.3, a difference of 1%) with the exception of Soup 1. The estimated RSD_{total} for Soup 1 (14%) had closer value to previously estimated RSD_{ip} of Soup COM (13%) rather than of Soup 1 (20%). It is hypothesized that the degradation of liquid soup matrix over the precision test duration (four weeks) caused dynamic changes in the particle size. Particle random agglomeration and release from complexes with soup solids due to the bacterial/ oxidative activity, pH and ionic strength changes could result in a very high day to day size measurement variation. The result also emphasizes robustness of derived RSD_{ip} value for the measurement of SAS ENPs in different food products.

It is worth reminding that E551 food additive is mainly used in food powders and therefore RSD_{ip} derived for Soup COM relates to the case of this additive better than Soup 1 and 2. Nevertheless, for other types of ENPs, the obtained information in study of Soup 1 and 2 might be useful in relation to liquid foods, where the matrix

changes will have to be considered as one of the factors that might influence particle size and measurement precision.

4.4 Conclusions

In this study, an attempt to validate the two main EM methods - SEM and TEM, for the measurement of ENPs in solid and liquid food matrices was made. Doing so, the issues of measurement uncertainty, limit of detection, nominal recovery and minimal sample size required for adequate EM measurements were addressed.

It was found that the EM methods were able to measure ENPs in food with an expanded uncertainty of typically approximately 21-27% accounting for different samples (solid and liquid food matrix, ENPs with narrow and broad size distribution, different imaging conditions and sample preparation methods). This study will therefore be useful in predicting uncertainties associated with the measurement of ENPs in complex matrices by EM, where the ENPs are relatively stable. For samples containing particles that are undergoing constant transformation e.g. aggregation and/or dissolution, much greater expanded uncertainties may be expected. For example, an expanded uncertainty of 43% was derived in this study for liquid soup samples containing SAS that were analysed at different time points.

The study also showed that a number of factors can influence uncertainties in the particle size measurements by EM methods. The results indicated that the number of measured particles and broadness of the particle size distribution were only secondary contributors to the ENPs size measurement uncertainty in foods. The major factor was found to be the sampling step. Most food samples are inherently inhomogeneous, and could not be homogenized to the nanoscale. As a result, different sub-samples of the same sample may vary a lot in terms of particle number and shown here also particle size. Thus it may not be possible to achieve a reproducible particle quantification and adequate estimation of the concentration LOD and recovery in food samples. To overcome the sampling issues and to lower the LOD by increase of particle recovery, a viable option may be to digest the food matrix or extract the particles, instead of the homogenization steps tested in this study. However, it is also possible that such pre-treatment may change particle characteristics and may lead to inaccurate results.

Another possibility for improvement of particle size measurement precision is to increase the sample replication during routine analysis. As it is shown here, the particle quantities necessary to obtain reliable data on median size measurement would depend on broadness of the size distribution and the desired measurement confidence level, which can be calculated from a simple dependence outlined in this chapter- Eq. 4.13. Therefore cutting the number of measured particles to an essential minimum, and increasing the number of replication instead, would allow acquisition of more precise information on the particle size and a better characterisation of the sample.

In summary, the EM were found to be suitable for screening on ENPs in food and delivering information on the ENP size and shape. There are however uncertainties over the results of the characterisation of size distributions of aggregated and polydispersed ENPs. Therefore in the next chapter a novel approach for normalizing sizing data from different methods is presented and then applied to compare the results from EM analysis with results from other nano-analysis methodologies.

Chapter 5

Evaluation of electron microscopy against other nano-analysis methods for the measurement of aggregated silica engineered nanoparticles

5.1 Introduction

The characterisation of PNSD of aggregated silica ENPs, such as SAS poses analytical difficulty. One challenge is detection of these ENPs. Silica ENPs have a low refractive index making them difficult to detect using light scattering and absorption methods. Additionally silicon is an ubiquitous element and background noise from element detection methods may hamper the analysis. The general lack of data on the Size LOD does not allow one to properly understand measurement outputs or estimate a method's measurement accuracy. Another analytical difficulty arises from the shape of SAS. Instruments measuring ENPs are generally calibrated with spherical particles, but as pointed out in Chapter 1 use different principles and expression units for the measurements. This leads to incomparability of the measurements between different types of instruments for non-spherical materials (e.g. Bowen, 2002; Domingos *et al.*, 2009).

One way of achieving the measurement comparability is to transform the results from different analytical methods from instrument equivalent spherical diameters (IED) into a standardised mass equivalent diameter (MED). The MED is the diameter of a compact sphere having the same mass as the analysed aggregated particle. The dependence of MED on the IED has been previously described for techniques measuring aerosol particles (Kasper, 1982; DeCarlo *et al.*, 2004). However, so far, the approach has not been used for ENPs in aqueous suspensions. One way considered previously in the literature for generating MED-IED relationships for ENPs was the the dynamic shape factor. The dynamic shape factor in particle measurements depends on the nature of the flow within the measuring instrument (free molecular, transition or continuum) as well as specific particle shape. Some values for the dynamic shape factors have been derived for differently regularly shaped particles and flow regimes (DeCarlo *et al.*, 2004), but for particle

aggregates these values were restricted by the conformation of the particles within the aggregate e.g. chains (Kasper, 1982). If the conformation of the particles is random (as in case of SAS) obtaining value of dynamic shape factor becomes laborious and difficult as for example described by Zelenyuk *et al.* (2006). Nevertheless, the literature provides some evidence that the IED can be related to the aggregate fractal structure (e.g. Gmachowski, 2000; Maricq and Xu, 2004; Boldridge, 2010) and thus to the number of primary particles within aggregates. Once the number of primary particles within the aggregate is known, the aggregate mass and subsequently MED can be calculated. Use of fractal geometry could therefore provide a way of ommiting a need of experimental estimation for dynamic shape factor of ENP aggregates.

The aim of this study was to use MEDs to compare results for SAS PNSD generated by EM and other techniques. Several techniques that produce particle size data in different ways (see Chapter 1, Table 1.2) and which have been used widely in the literature were selected. These techniques included:

1. methods that measure particle ECD – i.e. SEM and Wet-SEM;
2. methods that measure measure HDD – i.e. NTA and assymetric flow field flow fractionation with ICP-MS detection (AF4-ICP-MS); and
3. methods that measure SDD – i.e. CLS and measuring EMD- GEMMA.

The principles of particle measurements by these techinques have previously desribed in (e.g. Chapter 2; Tiede *et al.*, 2008; Dudkiewicz *et al.*, 2012- Annex 2; Linsinger *et al.*, 2012; Anderson *et al.*, 2013; Tiede *et al.*, 2009c; Carr and Malloy, 2013; Loeschner *et al.*, 2013b; Braun *et al.*, 2011; Bacher *et al.*, 2001). Thus here only brief general information helping to understand derived relationship between IED's and MED's will be given.

In order to achieve the aim this study attempted to address between-method discrepancies in the size measurements for these ENPs using their fractal characteristics. Prior to investigation of SAS, spherical silica ENPs were also analysed to characterise method specific size LODs and limits of quantification in terms of particle size (size LOQ). The chapter also discusses the potential of the

methods for accurate measurement of PNSD of silica ENPs and for addressing the EC recommendation for the definition of nanomaterial (The European Commission, 2011).

5.2 Silica engineered nanoparticles

Three different silica ENP dispersions were used in the study- two of them K12 and K80 contained approximately spherical ENPs (see Chapter 3) and SAS was composed of particulate aggregates (see Chapter 1). The same silica ENP dispersions as used in Chapter 3 were analysed in the experiments described in this chapter. The K12 sample contained very fine particles (on average 12 nm diameter by Manufacturer's claim) and was used for estimation of methods size LOD. The K80 sample contained both smaller and larger ENPs and a bimodal PNSD. This sample was used for determination of differences between the methods for quantification of particles in two size fractions corresponding to the modes. This was done to aid the conclusion on method sensitivity for quantification of small and large particles in the distribution. The SAS is a fractal aggregate (Boldridge, 2010), which means that its geometry can be described by the fractal scaling law (Eq. 5.1).

$$N = k_0 \left(\frac{2R_g}{d_{pp}}\right)^{D_f} \qquad \text{Eq. 5.1}$$

Where:

N-number of primary particles within the aggregate

d_{pp}- primary particle diameter

D_f- Fractal dimension

k_0- Fractal prefactor of lacunarity

The characterisation of the aggregated fractal structure of the SAS is described in Appendix 3 and the experimentally derived parameters are: d_{pp}=9 nm, D_f=2.11 and k_0=1.17.

All silica ENPs dispersions used in this study are not sold for use as food additives but for food application (e.g. clarifying beverages). The SAS example was used solely for analytical method development rather than indicating whether the SAS would be regarded a nanomaterial according to EC recommendation.

5.3 Principles of measurements and data transformation

For spherical particles, MED is equal to the particle size measurement directly derived from the instrument. For fractal aggregates MED calculations were derived using various relationships adapted from the available literature as described below.

5.3.1 Scanning electron microscopy in high vacuum and liquid setup

There is a variety of measurements that can be acquired from analysis of the images, but one of the most common ones is ECD. ECD is obtained using Eq. 5.2

$$ECD = \sqrt[2]{\frac{4S}{\pi}} \qquad \text{Eq. 5.2}$$

The relationship of ECD with MED for fractal aggregates was derived using dependencies commonly used for calculation of primary particle number within these structures from EM images.

The particle number can be calculated from two dimensional projection on the imaged particle area according to Eq. 5.3 (Boldridge, 2010):

$$N = 1.15\left(\frac{4S}{\pi d_{pp}^2}\right)^{1.09} \qquad \text{Eq. 5.3}$$

Substituting *S* in Eq. 5.3 with the solution from Eq. 5.2 relationship between ECD and *N* was obtained. Thus calculated *N* was then substituted into relationship of MED and *N* (Eq. 5.4) and Eq. 5.5 was obtained.

$$MED = d_{pp}\sqrt[3]{N} \qquad \text{Eq. 5.4}$$

$$MED = \sqrt[3]{1.15 ECD^{2.18}\, d_{pp}^{0.82}} \qquad \text{Eq. 5.5}$$

5.3.2 Gas-phase electrophoretic mobility molecular analyser

The instrument measures electrical mobility of the particles in the gas phase at ambient pressure. Based on this, the spherical equivalent diameters were obtained using Eq. 5.6

$$EMD = \frac{ne_eC_c}{3\pi\eta_aZ_c} \quad \text{Eq. 5.6}$$

Where:

n-number of electric charges on the particle

e_e- elementary charge

C_c- Cunnigham slip correction factor

η_a- viscosity of air

Z_c- electric mobility

The MED of the fractal aggregates can be related to EMD using the mass balance Eq. 5.7 and calculation of effective density (ρ_{pe}) from Eq. 5.8 (Maricq and Xu, 2004)

$$\rho_{pe}\frac{\pi EMD^3}{6} = \rho_{SiO2}\frac{\pi MED^3}{6} \quad \text{Eq. 5.7}$$

Where:

ρ_{SiO2}-density of silica

$$\rho_{pe} = \rho_{SiO2}\left(\frac{EMD}{d_{pp}}\right)^{D_f-3} \quad \text{Eq. 5.8}$$

Substituting ρ_{pe} in Eq. 5.7 with Eq. 5.8, Eq. 5.9 describing relationship of MED and EMD was obtained

$$MED = d_{pp}\sqrt[3]{\left(\frac{EMD}{d_{pp}}\right)^{D_f}} \quad \text{Eq. 5.9}$$

5.3.3 Centrifugal liquid sedimentation

The instrument estimates particle SSD based on sedimentation time (t_s) of particles from sample administration to reaching the detector. SSD of the particles is estimated by the instrument's software according to Eq. 5.10 (CPS Instruments, Inc., 2005)

$$SSD = \frac{18x\eta_s}{\sqrt[2]{t_s a(\rho_{SiO2} - \rho_f)}} \quad \text{Eq. 5.10}$$

η_s-viscosity of sucrose gradient

x- distance from the injection point to the detector

a-centrifugal acceleration

ρ_f- density of the sucrose gradient

Particle mass concentration is estimated based on light absorption corrected for Mie scattering solution (Wriedt, 2012). Thus the obtained particle mass concentration over the size distribution is then transformed into PNSD by calculation (CPS Instruments, Inc., 2005). The non-spherical shape of any particles slows down their sedimentation velocity when compared to spheres of the same mass. To correct for velocity change, adjustment of the density value of the particles in Eq. 5.10 have been suggested (e.g. Kamiti *et al.*, 2012). The corrected particle density (ρ_{ps}) can be estimated by means of two CLS measurements in two media of different density. For estimation of ρ_{ps} of the SAS studied here, the so called 'zero velocity approach' was used (Woehlecke *et al.*, 2013). This approach is based on Archimedes law. The particle velocity is measured in a medium of lower and higher density than the particle of interest. Then the density of the liquid in which particle would not sediment (have a velocity equal to 0) is calculated. This density is equal to $\rho_{ps.}$ The Eq. 5.11 summarising relationship of MED and SSD was obtained from equality of t_s, η_s, *x* and *a* for the particles with ρ_{ps} and ρ_{SiO2}.

$$MED = SSD \sqrt[2]{\frac{\rho_{SiO2} - \rho_f}{\rho_{ps} - \rho_f}} \quad \text{Eq. 5.11}$$

5.3.4 Nanoparticle tracking analysis

The measurement of an ensemble of absolute mean displacements of the individual particles due to the Brownian motion obtained from NTA allows for subsequent calculation of the diffusion coefficient (*D*). The *D* is then used to obtain HDD from the Stokes-Einstein dependence (Eq. 5.12)

$$HDD = \frac{k_B T}{3\pi\eta_w D} \quad \text{Eq. 5.12}$$

Where:

k_B- Boltzman constant

T- temperature

η_w- viscosity of the medium that ENPs are suspended in (here water)

This approach is only suitable for spherical particles (principle of the Stokes-Einstein equation), although there are publications discussing hydrodynamic behaviour of fractal aggregates. For example Melas *et al.* (2012) derived relationship between hydrodynamic and gyration radius (R_g) of the fractal aggregates with variable *N*, D_f and k_0. Using the data generated in the cited study for this sample of SAS with average N=84±9 and k_0=1.17, the dependence of R_g and HDD can be approximated with Eq. 5.13.

$$HDD = 2.2R_g \quad \text{Eq. 5.13}$$

Combining general Eq. 5.1 and Eq. 5.13, Eq. 5.14 allowed the MED to be calculated.

$$MED = d_{pp} \sqrt[3]{k_0 \left(\frac{HDD}{1.1 d_{pp}}\right)^{D_f}} \quad \text{Eq. 5.14}$$

5.3.5 Asymmetric flow field flow fractionation with inductively coupled plasma spectrometry detection

In AF4 the cross flow drives the particles towards the so-called accumulation wall covered with a membrane. The smaller particles diffuse further back into the channel and form diffusional clouds (Messaud *et al.*, 2009). The thickness of the clouds depends on the *D* of the particles and the cross flow. The larger the *D*, the larger the resulting cloud thickness. Due to the carrier flow profile, the higher the cloud, the larger the mean travel velocity of the respective particles, so small particles elute before larger ones. The particle-retention expressed as retention time (t_r) is related to the *D* of the particles through Eq. 5.15 (Wahlund and Giddings, 1987).

$$t_r = \frac{w^2}{6D} \ln\left(1 + \frac{V_c}{V_{out}}\right) \qquad \text{Eq. 5.15}$$

Where:

w- channel thickness

V_c- cross-flow volumetric flowrate

V_{out}- volumetric outlet flowrate

Substituting *D* in Eq. 5.15 with Eq. 5.12 the HDD can be calculated for AF4 measurements according to Eq. 5.16.

$$HDD = \frac{2t_r k_B T}{\pi \eta w^2 \ln\left(1 + \frac{V_c}{V_{out}}\right)} \qquad \text{Eq. 5.16}$$

In this study, AF4 theory was not chosen for the determination of the PNSD of the investigated nano-structured materials. Instead, an independent size measurement by a calibration with spherical particle size standards of known size was applied. This was regarded as a better approach, because the t_r was also shown to be affected by other factors, such as additional focusing stage after sample injection (Loeschner *et al.*, 2013a) or particle-membrane interactions, which cannot be avoided even under close to ideal conditions. Optimisation of the AF4 channel for size calibration by standards allows a correction for these additional factors to be made.

Using multi angle light scattering (MALS) coupled to AF4 it was possible to verify the relationship between HDD and R_g. Ratios between HDD/R_g ranged from 2.0 to 2.34 through entire PNSD of SAS. This proved that the 2.2 value from (Melas *et al.*, 2012) used previously to derive Eq. 5.14 was a very good approximation.

5.4 Instruments and measurement conditions

5.4.1 Scanning electron microscopy in high vacuum and liquid setup

SEM and Wet-SEM images were acquired using a FEI Sirion S field emission gun SEM equipped with a through-the-lens detector. The instrument was operated at spot size 3 and voltage of 5kV for high vacuum and at 20 kV for Wet-SEM imaging. For high vacuum imaging the samples were prepared according to T2 Gel protocol and Pt/Pd coated as specified in Chapter 3. The adjustment for coating thickness was made as well (Appendix 1).

For liquid state imaging, Quantomix™ capsules (QX-102) were used. Prior to application of the sample, each capsule was treated with 0.1% solution of poly-l-lysine (P8920, Sigma Aldrich, UK) according to the protocol available on the manufacturer's website (Quantomix, 2011).

Particle visibility could be improved by exposure of the capsule membrane to the electron beam for approximately 1min at low 5000x magnification. It was noted that with time of the beam exposure, particles were gradually attracted closer to the capsule membrane, increasingly populating the irradiated area (Figure 5.1a and b). The particles were apparently moving at the increased magnification required for the measurement consequently creating zig-zag patterns on the images (Figure 5.1c). Therefore only objects which looked approximately spherical were measured.

Example Wet-SEM images used for the measurement of silica ENPs in respective samples are presented in Figure 5.2.

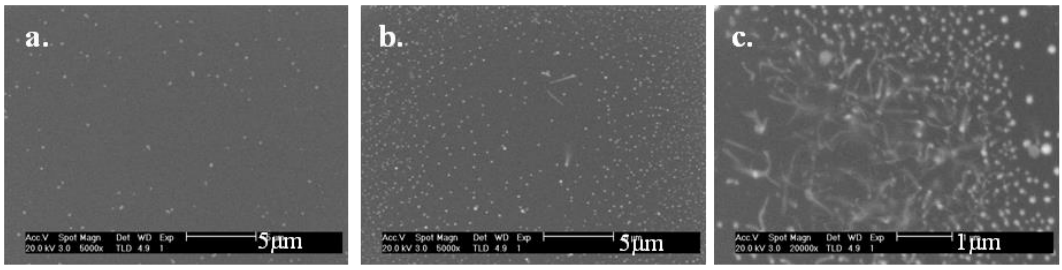

Figure 5.1- Wet-SEM images of silica ENPs (a) taken at the start point, (b) same area as (a) after 1min exposure to the beam and (c) movement of attracted particles at increased magnification

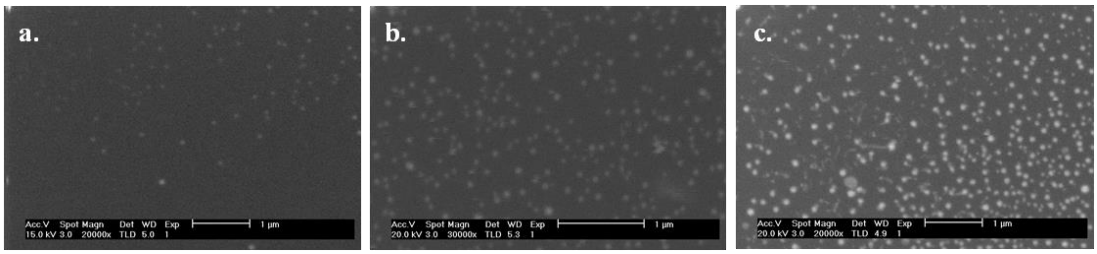

Figure 5.2- Wet-SEM images of silica ENPs (a) K12, (b) K80, (c) SAS (scale bar on every image is 1000 nm)

The particles of K12 and K80 had visibly lower contrast to SAS. Additionally it was observed that it was not possible to discriminate between the shape of spherical particles and SAS. All the images for sizing purposes were analysed using OBIA and particle size measurements were grouped into a histograms of 2 nm bin width. All samples were diluted with BB8.0 prior to preparation and imaging.

The SEM and Wet-SEM imaging setup (sample dilution factor, micrograph size, pixel size, smallest measurable particle and number of replicates) is summarised in Table 5.1.

Table 5.1- Data acquisition properties for SEM and Wet-SEM

Sample	K12		K80		SAS	
Method	**SEM**	**Wet-SEM**	**SEM**	**Wet-SEM**	**SEM**	**Wet-SEM**
No of replicates	3	2	3	2	3	2
Dilution ratio	1:149.999	1:9	1:1999	1:9	1:399	1:1
Single micrograph area (μm^2)	3.98	29.14	13.06	13.06	3.98	29.14
Pixel edge (nm)	3.4	8.6	5.7	5.7	3.4	8.6
Smallest measurable particle- ECD (nm)*	4.2	37.7	12.5	20.5	7.0	37.7
Number of particles measured per replicate- mean (s.d.)	465 (129)		1165 (342)	544 (398)	1291 (628)	

*The values given refer only to cut-off point during image analysis, for SEM particles with ECD <8 nm were excluded from the statistical analysis due to the thickness of conductive coating (see Appendix 1)

All the analysed images of the same sample in SEM were taken at constant magnification allowing measurability of main visualised particle population. It was noted that for SAS only ENPs up to approximately 300 nm were measured, although a low content of larger particles (up to 1 micron) was also detected at lower magnification in a previous study (Chapter 4, Appendix 2- Figure A2.1). For Wet-SEM imaging the magnification was limited by the mobility of the particles in the liquid. It was found that at increased magnifications, particles would drift away from the membrane within a short time. This time varied between the samples, making capture of the image difficult at higher magnifications than given in Table 5.1.

5.4.2 Gas electrophoretic mobility molecular analyser

A GEMMA system previously described in (Weiss *et al.*, 2012) was applied for this study. The data were obtained analysed and interpreted by Angela Lehner from Technical university of Vienna. The samples were analysed after diluting in 0.4M ammonium acetate buffer pH 8.0 (K12 and K80) and pH 7.4 (SAS). The dilution ratios were: K12- 1:36.999, K80- 1:9.999 and SAS 1:199. SAS prior to dilution was additionally filtered using 0.2µm Minisart syringe filter (Sartorius- Vienna, Austria)

to avoid clogging instrument's capillaries due to a presence of very large aggregates. Each sample was prepared and analysed in triplicate running 10 (K80 and K12) or 7 (SAS) scans per replicate. Median calculation between scans was used for final data presentation. Macrolon flows of 0.5 L/min filtered air (table-top compressor, Dürr-Technik, Biegigheim-Bissingen, Germany) and 0.1 L/min CO_2 (99.995%, Air Liquide, Schwechat, Austria) were used for nano-ESI and a sheath flow of 3 L/min in the DMA. Voltage in the nano-ESI was set at 2.5kV resulting in a current of 500-585 nA. The measurements covered the size range 4.43-163.3 nm. The PNSD was calculated as described in (Hallar *et al.*, 2011).

5.4.3 Centrifugal liquid sedimentation

A CPS DC24000 UHR centrifuge (Analytik- Cambridge, UK) operating at a maximum rotational speed of 24000 rpm was used in this study. All silica ENPs were analysed in triplicate. Assessment of dilution requirement was carried out based on the visual turbidity of the sample. Only K80 was opaque and required 10 fold dilution with BB8.0. Samples were centrifuged in 8-24 % sucrose gradient, as specified in the instrument manual (CPS Instruments, Inc., 2005). As a calibration standard polyvinyl chloride particles (PVP) of 476 nm diameter were used, as provided by instrument's manufacturer. The ρ_{SiO2} required for the CLS procedure run was set at 2.2 g/cm^3 for all Silica ENPs. The ρ_{ps}=2.01 g/cm^3 for SAS was acquired from (Woehlecke *et al.*, 2013).

The run included readings for data points from approximately 700 down to either 8 nm (K12) or the point in which negative values for absorption were obtained (K80, SAS). The 8 nm cut-off point was dictated by the length of sample analysis- to get down to this small size approximately 2.5 h was necessary for analysis of a single sample. The temperature of sucrose gradient increases with the time of the centrifugal run, therefore manufacturer recommends that single sample run does not exceed 40 min, after which re-calibration is carried out.

The data output were histograms with irregular bin width starting at 0.1 nm from the smallest particle diameter to 13 nm for largest.

5.4.4 Nanoparticle tracking analysis

An NTA instrument LM14 from NanoSight (NanoSight Ltd, Amesbury, UK) was used in the study. All samples were diluted with BB8.0 prior to analysis 6.000 (K12), 1.000.000 (K80) and 100.000 (SAS) fold. Samples were prepared in triplicate and 3 recordings per replicate were performed. Recorded videos were 1 min long and were taken at maximal camera shuttle and gain settings. Acquired videos were processed with the Nanosight 2.3 software according to the manufacturer's specifications. The raw data output for each single track recorded was used to generate PNSDs presented in the study. The bin width for the created histograms was 2 nm.

5.4.5 Asymmetric flow field flow fractionation with inductively coupled plasma mass spectrometry detection

The AF4 system consisted of a Wyatt Eclipse^{TM} 3+ flow control module (Wyatt Technology Europe GmbH, Dernbach, Germany) with a flat AF4 separation channel (Superon GmbH, Dernbach, Germany, length 275 mm, wide spacer). The channel was equipped with a 350 µm spacer and a 10 kg•mol^{-1} nominal cut-off regenerate cellulose membrane (Millipore®, USA) as the accumulation wall. Flows were controlled using an Agilent Technologies 1200 Series quaternary pump equipped with a micro-vacuum degasser. All injections were performed using an autosampler (Agilent Technologies 1200 Series, large volume kit). The hyphenated detection sequence consisted of a MALS (MALS Dawn Heleos II, Wyatt Technology, Santa Barbara, US) and an inductively coupled plasma mass spectrometer (ICP-MS, Agilent Technologies 7700x).

Size calibration of the AF4 channel was done with NIST traceable latex beads at 50, 100 and 150 nm (Thermo Fisher Scientific, Dreieich, Germany), due to the lack of certified silica reference materials of different sizes. The eluent for size calibration was composed of 0.025% FL70 as a biodegradable detergent (Fisher Scientific, US) and 3 mM NaCl (analytical grade, Sigma Aldrich) which was slightly different to one used for separation of silica ENPs (mixture of 0.025% FL70 and 0.25 mM NaCl). This was necessary because the particle behaviour in the channel is strongly related to the surface properties of the particles and so eluent concentration needs to be adjusted to a given material. The elution and analysis conditions were

experimentally derived by Dr Stephan Wagner and Dr Samuel Legros from University of Vienna.

All samples were injected at concentrations of 100 ppm SiO_2. For quality control, samples were analysed as triplicates. Total Si recovery ratios for SAS, K12 and K80 were 0.99 ± 0.06; 1.14 ± 0.03 and 1.04 ± 0.01, respectively. A previous study on gold ENPs recovery rates for AF4 found much lower recovery in the range 0.04-0.69 (Gray *et al.*, 2012). Here, the procedure was optimized for analysis of silica ENPs in AF4-ICP-MS and thus we expected the best achievable accuracy in terms of PNSD as well.

Simultaneous MALS detection was used for the examination of the size separation and as an indicator of the particle size.

The generated size distributions of silica ENPs were mass-size based and were transformed into PNSD by calculations assuming particle sphericity and ρ_{SiO2}=2.2 g/ml. For MED based distributions this calculation was done following transformation of HDD into MED as in Eq. 5.13.

All AF4-ICP-MS data were obtained analysed and interpreted by Dr Stephan Wagner from University of Vienna.

5.5 Results and discussion

The results obtained in the study relate to 1) measurement of nearly spherical silica ENPs and 2) aggregated SAS particles. The measured particle sizes were compared between the methods, in terms of modal, median or mean values. The nominal values given by the manufacturer were also considered in the comparisons. Additionally for K12, size values at 5^{th} and 95^{th} percentile, and for SAS also at 25^{th} and 75^{th} percentile, were reported together with *RSD%* between replicates to allow between-method comparison and assess particle size measurement repeatability at different points of the PNSD. Where raw data (measurements for each single particle) were not available (as in the case of GEMMA, AF4-ICP-MS and CLS) the measurement values were derived from the histograms given by the methods and therefore are meant to be approximate whilst assuming an even distribution of all the size data points in each bin of the histogram. To minimise probability of type I statistical errors, all measurement methods were compared for the values of given modal sizes in K80, percentiles in K12, and SAS PNSDs using MANOVA. If a significant

statistical difference was detected ANOVAs followed by relevant post-hoc test (specified in the result section) were run in order to determine the methods which gave significantly different measurements. All the tests assumed a *p* of 0.05.

5.5.1 Measurement of spherical silica engineered nanoparticles

The particle size distributions derived from different techniques are presented in Figure 5.1. The PNSD of K80 sample was divided into 3 arbitrary chosen size groups: primary particles: I (18-62 nm), II (63-106 nm) and agglomerates III (107-160 nm). These groups served for comparison of relative particle abundance within the PNSD between the methods using the statistical evaluation described previously in Chapter 3. The comparison of modal size measurements from all the techniques against SEM was used here to define accuracy of the techniques, as EM has been applied in most research papers for characterisation of ENPs (Calzolai *et al.*, 2012) and is recommended as a reference method for particle size measurement (EFSA Scientific Committee, 2011; Linsinger *et al.*, 2012).

5.5.1.1 Ability of measurement methods for characterisation of sample featuring polymodal size distribution

Two out of the six methods (NTA and Wet-SEM) did not provide a level of resolution necessary to distinguish the two particle populations in K80 PNSD (Figure 5.3). For NTA, similar results were previously reported (Mahl *et al.*, 2011) (Anderson *et al.*, 2013). However, there was no comparable study on liquid imaging techniques carried out so far. Two hypotheses can be used to explain why Wet-SEM did not provide sufficient resolution between the two particle size populations:

1. Beam broadening during membrane passage and in aqueous environment might have an effect on the particle size in the same way as positioning of specimen out of focus
2. Subsequent image analysis of such blurred and low contrast images might be inaccurate. Therefore it is possible that the error introduced by the image analysis is simply too large to deliver reliable image statistics.

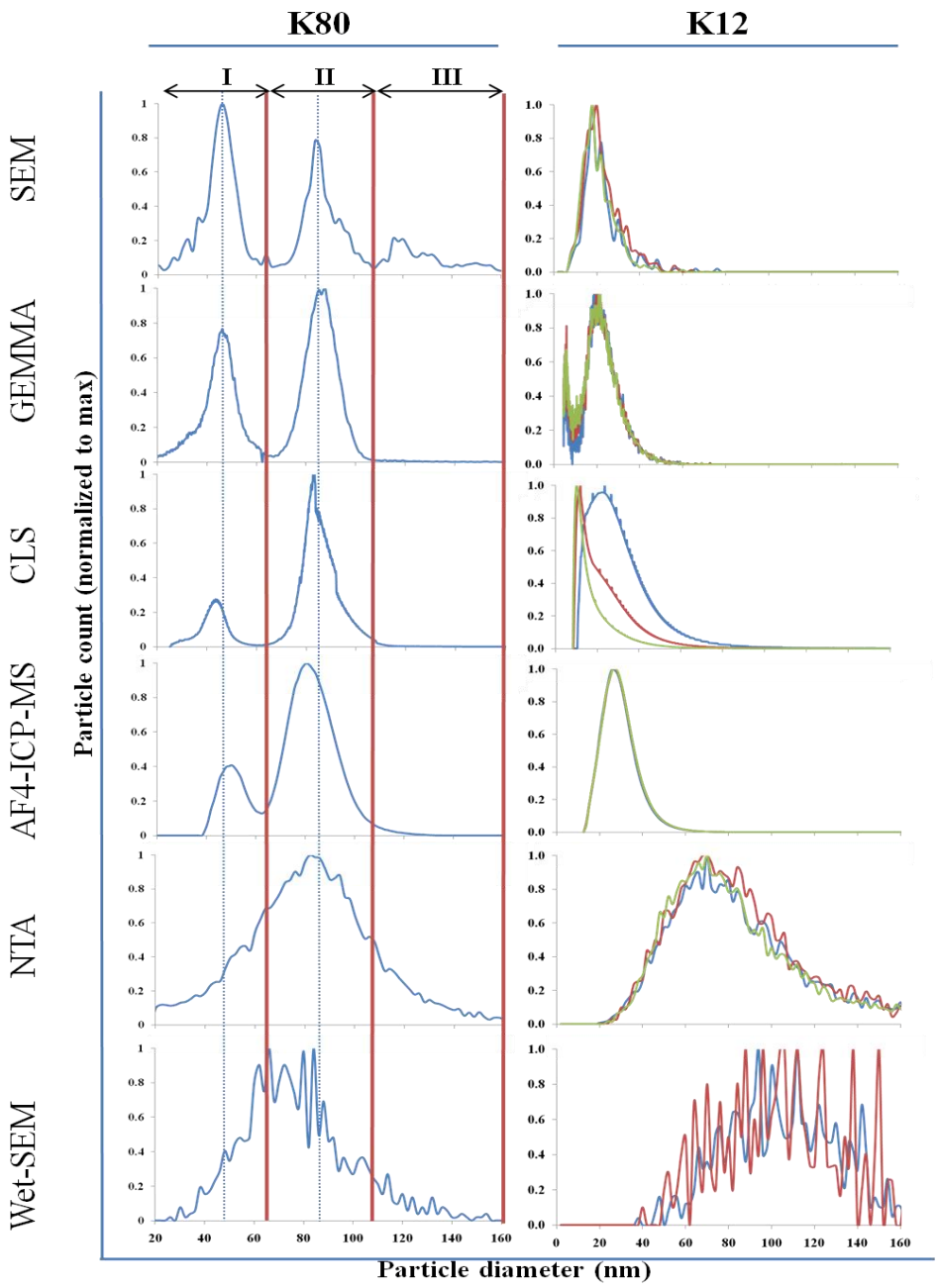

Figure 5.3- Number-size distribution of K80 and K12 samples measured by different techniques, K80-measurments given as total particle size distribution from 3 replicates (SEM, NTA, Wet-SEM), mean (GEMMA) or selected single replicate (CLS, AF4-ICP-MS), K12- measurements from 3 replicates shown (and 2 replicates for Wet-SEM)- different colors show different replicates

The remaining four methods SEM, GEMMA, CLS and AF4-ICP-MS were able to resolve the bimodal PNSD, but exhibited size related differences in particle abundance (see section 5.5.1.2).

5.5.1.2 Measurement method dependant differences in particle abundance through size distribution

Table 5.2 provides a summary of modal and mean measured particle diameters in determined points of the PNSD and relative particle abundance in predetermined size groups I-III.

Table 5.2- Mean and modal diameters of particles in the size distribution of K80 and relative abundance of particles in predetermined size groups (I-III)

Method	Size (s.d.)			Relative particle abundance (%)		
	Mean	Mode I	Mode II	I	II	III
SEM	76.1 (3.4)^{AB}	47.3 (1.8)	84.7 (1.3)	48	36	16
GEMMA	69.3 (0.8)^{C}	46.1 (1.3)	86.5 (1.8)	41	58	1
CLS	77.2 (0.6)^{AB}	43.7 (0.2)*	83.6 (0.7)	20	79	1
AF4-ICP-MS	75.7 (0.9)^{ABC}	51.3 (1.0)*	81.1 (1.3)*	23	74	3
NTA	82.2 (1.7)^{A}	N/A	N/A	22	62	16
Wet-SEM	74.6 (5.6)^{BC}	N/A	N/A	26	64	10

$^{A-C}$Same letter in column with mean size value of K80 sample marks that no significant difference was detected between measurement methods (Tukey's test, $p>0.05$), *Significant difference detected in comparison to SEM measurement (Dunnett's test, $p<0.05$).

Significant differences were detected between methods relative abundance within the predetermined size groups I-III (MANOVA, $p<0.05$). The small particles in group I of the PNSD were found most abundant in SEM (48%) and least abundant in CLS and AF4-ICP-MS (20% and 24% respectively). Aggregates (group III) were also most abundant in PNSD derived by SEM (16%) when compared to GEMMA, CLS (1% both) and AF4-ICP-MS (3%). These differences had an obvious effect on the particle mean size. CLS, SEM and AF4-ICP-MS mean diameter measurements (77.1, 76.2 and 75.7 nm respectively) were not significantly different from each other (Tukey's test, $p>0.05$) and comparable to declared by manufacturer diameter

(80 nm). The GEMMA derived mean diameter was significantly smaller at 69.3 nm (with the exception of AF4-ICP-MS).

However, it is unclear which of the methods measured the sample more accurately. In case of SEM, evidence produced in Chapter 3 suggests that method may suffer from some level of overestimation of small sized particle number as a consequence of sample preparation. This artifact is thought to be a consequence of the sample preparation which may selectively remove larger ENPs from the EM grid. Issue is further investigated in Chapter 6. The CLS method was previously reported to closely follow particle number proportions in PNSD to the expected values (Anderson *et al.*, 2013) and in this study also provided similar particle abundance proportions in group I and II as AF4-ICP-MS (based on statistical evaluation as in Chapter 3). As pointed out previously in Chapter 3, data available in the published literature suggest that GEMMA could provide accurate quantification of particles through PNSD. GEMMA's particle detection unit features exponential growth to maximum of particle registration efficiency from smaller to larger sizes. It has been shown that for the used model the near to maximal registration efficiency (approximately 0.95) was obtained after reaching EMD of 4 nm for silver ENPs (Kesten *et al.*, 1991). Furthermore data are also available on the determination of monomodal PNSD of spherical gold ENPs by several analytical methods including GEMMA and TEM (Small and Watters, 2012; Kaiser and Watters, 2007a; Kaiser and Watters, 2007b). These reports show, that the PNSDs of gold ENPs generated by GEMMA and TEM had similar shape and size range, thus there is no evidence that GEMMA is more specific for measuring particles of smaller or larger sizes.

5.5.1.3 Method's particle size measurement accuracy

Shown in Table 5.2 particle modal diameters in K80 determined by GEMMA (Mode I: 46.1, Mode II: 86.5) were not significantly different to SEM measurements (Mode I: 47.3, Mode II: 84.7 nm, Dunnett's test, $p>0.05$), providing more confidence that the size measurements were accurate. CLS results also compared well to SEM measured particle size in Mode II (83.6 nm, Dunnett's test, $p>0.05$), but significantly smaller in Mode I (43.7 nm, Dunnett's test, $p<0.05$). However, AF4-ICP-MS showed particles larger in Mode I (51.3 nm) and smaller in Mode II (81.1 nm, Dunnett's test, $p<0.05$) than SEM. Although size differences between SEM and AF4-ICP-MS or CLS were small (less than 10% of the SEM measured diameter),

given that for AF4-ICP-MS and CLS original data outputs are particle mass-size distributions transferred by calculation into PNSD, some error in calculated particle number could be expected.

5.5.1.4 Ability of analytical methods to detect and measure small sized silica nanoparticles

Measurements of the particle size at chosen points of size distribution for K12 sample are summarized in Table 5.3.

Table 5.3- Mode and percentile diameter in the PNSD of K12

Method	Min[a]	Mode (s.d.)	5% (s.d.)	50% (s.d.)	95% (s.d.)
SEM	8.0	15.1 (1.9)	10.6 (0.4)	19.3 (0.7)	37.6 (3.4)
GEMMA	8.0	23.2 (1.9)	12.1 (1.3)	22.3 (0.3)	40.0 (0.6)
CLS	9.2 (1.2)	15.2 (7.3)	10.9 (2.2)	20.7 (6.4)	50.2 (9.4)
AF4-ICP-MS	6.5 (0.3)	26.8 (0.7)	17.5 (0)*	28.0 (0.7)*	44.2 (0)
NTA	22.8 (0.8)	69.7 (0.6)	42.0 (0)*	77.3 (1.2)*	152.0 (5.3)*
Wet-SEM	38.3 (0.9)	94.3 (0.7)	60.3 (5.1)*	100.2 (3.8)*	174.0 (14.8)*

[a]Diameter of smallest detected particle, except SEM and GEMMA where the values represent cut-off point accepted for the analysis, *Significant difference detected in comparison to SEM measurement (Dunnett's test, $p<0.05$).

It was found that none of the methods studied, provided size measurement for K12 sample close to the nominal 12 nm given by the manufacturer (Table 5.3). It became apparent that Wet-SEM and NTA did not allow measuring the main population of ENPs in K12 sample (see Figure 5.3), and instead detected only larger particles (median: 77.3 and 100.2 nm respectively), the presence of which was not reflected in PNSD by other methods The CLS method showed a very high measurement uncertainty noticeable in PNSD generated from each replicate (Figure 5.3), and high s.d. values for subsequent percentiles (Table 5.4). Interestingly, a previous study with the same model of instrument and setup was able to obtain very reproducible results for silica ENPs with 20 nm modal diameter (expanded uncertainty <5%) (Braun *et al.*, 2012). The K12 ENPs studied here were characterised by a slightly shorter modal diameter (15.1 nm by SEM). Therefore it can be concluded that silica ENPs smaller than 20 nm cannot be accurately measured by CLS.

Comparing the PSND of K12 from SEM and GEMMA indicated that the artefacts introduced by agglomeration in SEM analysis of group III in K80 were not apparent in K12.

The use of the K12 sample was aimed at testing the size LOD. However, accurate estimation of size LOD for most of the methods was not possible. For SEM, a cut-off point (8 nm) was based on a thickness of conductive coating (4 nm), as for particles with radius smaller than the thickness of the coating, only a part of the particle could be visualized. The smallest observed particles were smaller than 8 nm and hence hindered the exact size LOD characterization. In GEMMA an additional peak starting at approximately 8 nm and continuing toward lower size values was observed in PNSD. This peak was attributed to the background noise (presence of dissolved substances in the sample e.g. dissolved Si, or NaOH) and was also noticed during examination of the K80 sample (starting at 10-14 nm therefore not shown in the Figure 7.3). Thus the size LOD in GEMMA will also be dependent on the level of contamination in the test sample.

It was not possible to accurately estimate the size LOD for Wet-SEM either. The observed minimal particle size was 38.3 nm, which was above the set cut-off point for the K12 sample analysis (see Table 5.1). However, for the K80 sample, imaging at higher magnification was possible (see Table 5.1) and particles down to 27.1 nm diameter could be detected. This indicated that the size LOD in Wet-SEM was affected by particles drifting away from the membrane at higher magnifications (see Instruments section above) and probably sample matrix features such as IS.

The CLS detected particles at or close to a given size cut-off point (8 nm) for the two replicates but for third replicate the size distribution terminated at 10.5 nm (see Figure 5.3). Therefore the size LOD could not be unambiguously determined. It should be mentioned that in this study we used a very concentrated K12 dispersion (30% mass of SiO_2). At 10 fold dilution, no response could be detected from this sample (data not shown) and therefore it could be concluded that in fact the majority of the particles in PNSD of K12 was under the size LOD for CLS.

For the AF4-ICP-MS and NTA, the smallest measured particle size could be clearly identified (6.5 and 22.8 nm respectively). Thus Silica ENPs size LOD for NTA was identified. However, for AF4-ICP-MS this value could be even lower than the

smallest detected particle size, as it was not possible to confirm with other techniques that particles smaller than 6.5 nm were not present in the sample.

Interestingly, it was also found that PNSD of K12 from NTA and Wet-SEM before reaching the size of the smallest detected particles, displayed a gradual decay of particle abundance rather than rapid cut-off particle population as for example previously reported in study on SP-ICP-MS (Laborda *et al.*, 2013). This result suggests that some analytical methods for ENPs may not only be bound by the size LOD but also size LOQ- size below which particle count is no longer accurate. The size LOQ was likely a reason for detection of significant differences in particle abundance in groups I-III of K80 PNSDs derived by different analytical methods and is further discussed in the section below.

5.5.2 Size characterisation of synthetic amorphous silica featuring a broad size distribution

5.5.2.1 Improvement of measurement comparability between techniques after data transformation into mass equivalent diameter

As expected, PNSDs of SAS reported as IED differed strongly depending on the analytical technique used (Figure 5.4a, Table 5.4). The broadest and the narrowest IED weighted PNSD were obtained by NTA and CLS, respectively with differences of 182.2 nm for NTA and 53.1 nm for CLS between the 95^{th} and 5^{th} percentile. Particle median sizes were in the range of 40.4 nm for SEM to 115.4 nm for NTA and PNSDs and fractions were also found to vary widely with NTA and Wet-SEM displaying an approximately normal PNSDs and CLS, GEMMA and AF4-ICP-MS showing positively skewed PNSDs. The variation in PNSDs shape may suggest method's selectivity to certain particle size fraction, but also may be a result of different measurement expression.

Transformation of the IED into MED (Figure 5.4b, Table 5.5) resulted in narrower PNSD for all the methods with exception of CLS (difference between 95^{th} and 5^{th} percentile for IED 53.1 nm, for MED 57.3 nm). The difference between 95^{th} and 5^{th} percentile in MED distributions was ranging from 42.7 to 58.6 nm among the measurement methods and was smallest for AF4-ICP-MS and largest for NTA.

Wet-SEM, NTA and CLS showed similar MED weighted PNSDs (Figure 5.4b) resulting in a similarity between median MED (55.9; 53.3 and 50.8 nm respectively) (although Tukey's test, $p<0.05$ for CLS and Wet-SEM). Furthermore, the IQR of NTA and CLS analysis gave similar results of 23.3 nm and 21.9 nm, respectively, whereas the IQR of the Wet-SEM analysis was more narrow (16.2 nm), probably due to the cut-off point as well as the size LOQ.

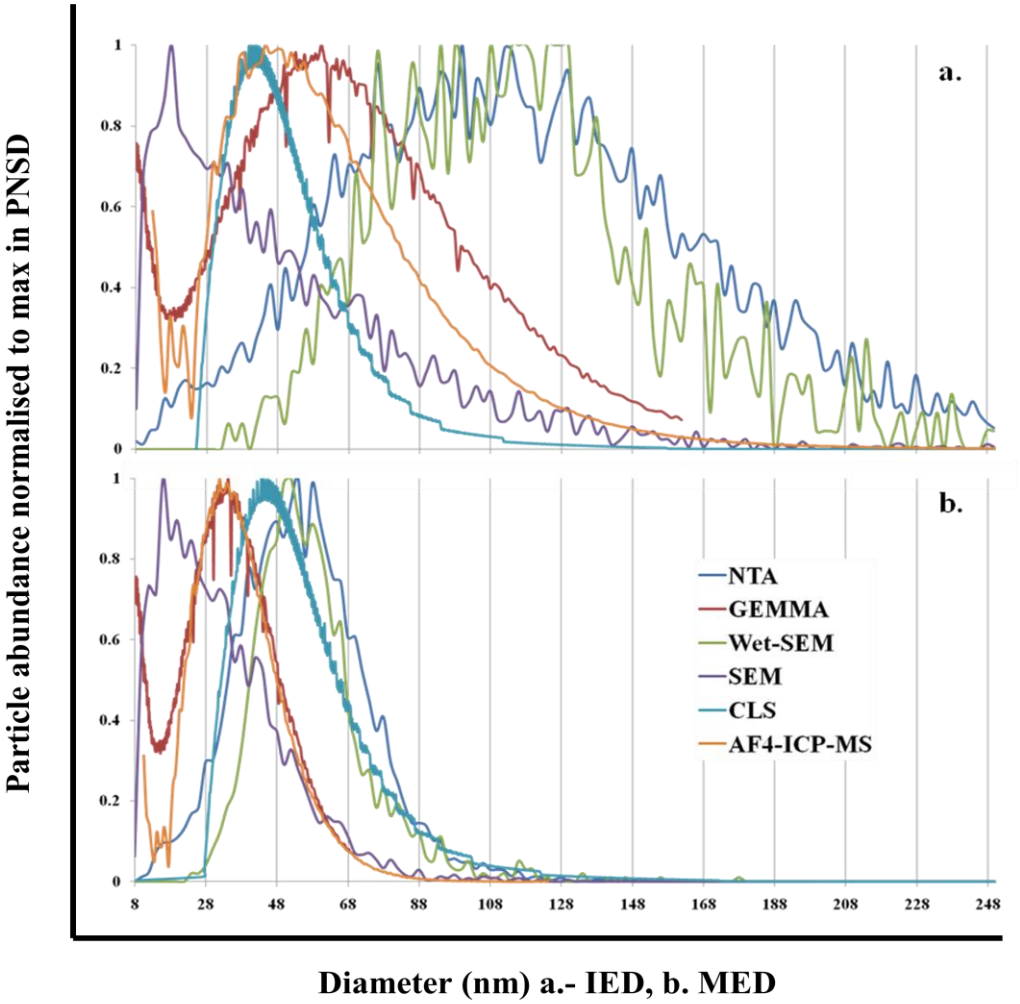

Figure 5.4- Particle number size distribution of SAS obtained by different analytical methods

Even better correspondence of MED transformed PNSDs was achieved for GEMMA and AF4-ICP-MS (Table 5.6; Figure 5.4a and b). The PNSDs of SAS from these two methods were in a good agreement already for IED measurements (Table 5.5), however it can be noticed that the transformation improved the correspondence of results especially in the central part of the curve (Figure 5.4 a and b). This can be noticed looking also at the difference of median diameter between GEMMA and

AF4-ICP-MS measurements in Table 5.5, which decreased after MED transformation from 14 to 3% (as relatively to GEMMA given median).

Thus it can be concluded that the MED transformation generally improved PNSD comparability between the methods.

Table 5.4- Mode and percentile diameter in the particle number size distribution of SAS given as method IED

Method	5%	25%	Mode	50%	75%	95%
SEM (ECD)	10.9 (0.7)^{A}	22.0 (2.2)^{A}	13.9 (2.8)	40.4 (2.7)^{A}	68.3 (3.3)^{A}	123.9 (6.3)^{A}
GEMMA (EMD)	15.5 (1)^{A}	44.4 (1.5)^{B}	71.6 (2.6)	65.8 (0.6)^{B}	90.5 (0.5)^{B}	131.2 (0.7)^{AB}
CLS (SSD)	29.7 (1.3)^{B}	38.3 (0.7)^{C}	42.4 (2.9)	47.1 (0.6)^{AC}	58.7 (0.5)^{A}	82.8 (0.6)^{A}
AF4-ICP-MS (HDD)	16.0 (2.8)^{A}	39.6 (0)^{BC}	44.9 (6.7)	56.4 (0.7)^{BC}	78.8 (0)^{AB}	123.0 (0.7)^{A}
NTA (HDD)	43.4 (2.6)^{C}	81.8 (3.7)^{D}	156.8 (36.8)	115.4 (5.4)^{D}	153.4 (5.6)^{C}	225.6 (8)^{C}
Wet-SEM (ECD)	62.3 (4.1)^{D}	84.9 (2.2)^{D}	94.9 (3.0)	104.3 (7.5)^{E}	126.6 (14.4)^{D}	182.2 (57.9)^{BC}

Table 5.5- Mode and percentile diameter in the particle number size distribution of SAS given as MED

Method	5%	25%	Mode	50%	75%	95%
SEM	10.9 (0.3)^{A}	18.1 (0.8)^{A}	12.9 (1.8)	28.2 (1)^{A}	41.1 (1.3)^{A}	63.5 (2.1)^{A}
GEMMA	13.2 (0.6)^{A}	27.7 (0.7)^{B}	39.4 (0.4)	36.5 (0.2)^{B}	45.6 (0.2)^{AB}	59.4 (0.4)^{A}
CLS	32.2 (1.3)^{B}	41.4 (0.8)^{C}	43.6 (0.8)	50.8 (0.7)^{C}	63.3 (0.6)^{C}	89.5 (0.7)^{B}
AF4-ICP-MS	21.2 (0.1)^{C}	29.9 (0)^{B}	32.5 (1.1)	37.6 (0)^{B}	46.8 (0)^{B}	63.9 (0.2)^{A}
NTA	26.8 (1.2)^{D}	41.9 (1.3)^{C}	65.9 (11.1)	53.3 (1.8)^{CD}	65.2 (1.7)^{C}	85.5 (2.1)^{B}
Wet-SEM	38.5 (1.9)^{E}	48.2 (0.9)^{D}	52.2 (1.2)	55.9 (2.9)^{D}	64.4 (5.3)^{C}	83.5 (19.4)^{B}

$^{A-F}$Same letter in column with percentile size value in Table7. 4 and 7.5 means that no significant difference between measurement results was detected (Tukey's test, $p>0.05$).

5.5.2.2 Causes of remaining discrepancies in between mass equivalent diameter distributions given by different methods

Despite the improvement, a complete comparability of the MED weighted PNSDs for SAS by different methods was not achieved. For example, the median MED for SEM was not comparable to any other median MED and although SEM covered similar 5th to 95th percentile size ranges to GEMMA (10.9 to 63.5 nm for SEM and 13.2 to 59.4 nm for GEMMA), the 25th percentile and median sizes were smaller for

SEM (18.1 and 28.2 nm, respectively) compared to GEMMA (27.7 and 36.5 nm, respectively). This provides further evidence for more selectivity of SEM sample preparation (see Chapter 3 and section 5.5.1.2) towards smaller particles.

The incomparability of the SAS MED PNSD derived from Wet-SEM, NTA and CLS to those derived from GEMMA and AF4-ICP-MS was most likely a consequence of the particle size LOD and LOQ. Based on the modal MED (Table 5.5) the size LOQs proposed for CLS, NTA and Wet-SEM are 43.6 nm, 65.9 nm, and 52.2 nm respectively. These values correspond with the data for the K80 apparently underestimating the particle population in the size fraction 18 to 62 nm (see Table 5.3, group I in section 5.5.1.2). It could be observed that for NTA estimated modal diameters of the K12 and SAS (MED) differed less than one s.d. from each other. Hence it can be assumed that the size LOQ identified here could be generally proposed for silica-based ENPs. A comparable relationship between the modal sizes of K12 and SAS measured by Wet-SEM and CLS was not obtained. In case of Wet-SEM, this is probably due to the behaviour of the ENPs during imaging, whereas for CLS the K12 sample's PNSD was not reproducible, and thus potentially below size LOQ.

It was expected that AF4-ICP-MS will also have size LOQ for SAS because, for K80, a significant underestimation of particle number in group I was detected when compared to GEMMA (Tukey $p<0.05$, analysis based on procedure in Chapter 3, data not shown). The concentration LOD of ICP-MS detection was estimated at 10 µg/l and it was found that a part of the data points in K80 and SAS PNSDs were below this concentration (K80 particles smaller than 39 nm and SAS particles smaller than: IED 22nm, MED 17 nm). Deriving LOD for analyte concentration was out of the scope of this work, however it had to be mentioned for accurate interpretation of the results.

The good comparability of GEMMA and AF4-ICP-MS derived PNSDs for SAS, indicates that these two methods were not subjected to the size LOQ limitation and so the characterisation of SAS is likely most complete among the tested techniques.

5.6 Conclusions

This study determined PNSDs for silica ENPs by different analytical techniques. The findings enabled development of a concept of data transformation to derive

comparable particle size distributions across different methods. The PNSD of SAS could not be fully characterised in this study due to measurement outputs being restrained by the size LOD, and for some methods a gradual decline in the detection sensitivity prior to reaching the size LOD. Particle sizes below which the method sensitivity was decreasing (size LOQ) were determined for CLS, Wet-SEM, and NTA. Remaining methods were limited in relation to small sized particle detection by the background noise (GEMMA), sample preparation (SEM), or concentration LOD (AF4-ICP-MS). The sample preparation steps used for SEM seemed to overestimate particle number in the small size region, and in one studied sample, also induced apparent agglomeration. Wet-SEM, although required minimal sample preparation, was impaired by the high size LOQ and inability to distinguish between two particle populations in a bimodal size distribution. This result points out that more work needs to be undertaken on the evaluation and development of sample preparation methods for the high vacuum electron microscopy, such as corrections for overestimation of small sized particle number within PNSD (Chapter 6).

The described set of relationships, allowing conversion of IED for the case of SAS fractal aggregate into MED, allowed interpretation and comparison of PNSDs produced by different methods. The MED is one of possible ways of interpreting the data outputs from measurement techniques and it is worth emphasising that CLS provides means for this measurement without the necessity of knowing the particle fractal structure, that is as long as particle size range does not fall below the specified size LOQ and no chemical speciation is required in the study.

The MED unit could be recommended for normalization of measurement expression in between studies on ENPs and could be also considered for implementation in emerging nanomaterial definitions and regulations. By means of MED transformations presented in this study, the measurements from different techniques can be related and thus distributions transformed from one into another equivalent diameter.

Two additional benefits from expression of data as MED arise

1. regardless of particle shape, a total recovery calculation based on mass of individual ENPs can be performed

2. validation of results in between methods for samples such as e.g. fractal aggregates, where no reference materials was so far available became possible

Extend of these benefits application was presented using data generated in Chapters 3 and 4 in Annex 1. Described benefit 2 could lead to the development of required reference materials which would aid farther ENP measurement method development and validation.

In summary MED could be used as a basis to provide a uniform way of expressing particle size measurements to support future research on nano-sized or nano-structured materials.

Chapter 6

Refinement of electron microscopy sample preparation and measurement analysis for the engineered nanoparticles with broad size distribution

6.1 Introduction

In previous Chapter 5 it was pointed out that EM sample preparation introduces a significant error in ENP size measurement. Figure 6.1 recalls a comparison of SEM, and GEMMA measured PNSD of SAS ENPs from Chapter 5 to illustrate overestimation of small particle number in PNSD derived by SEM.

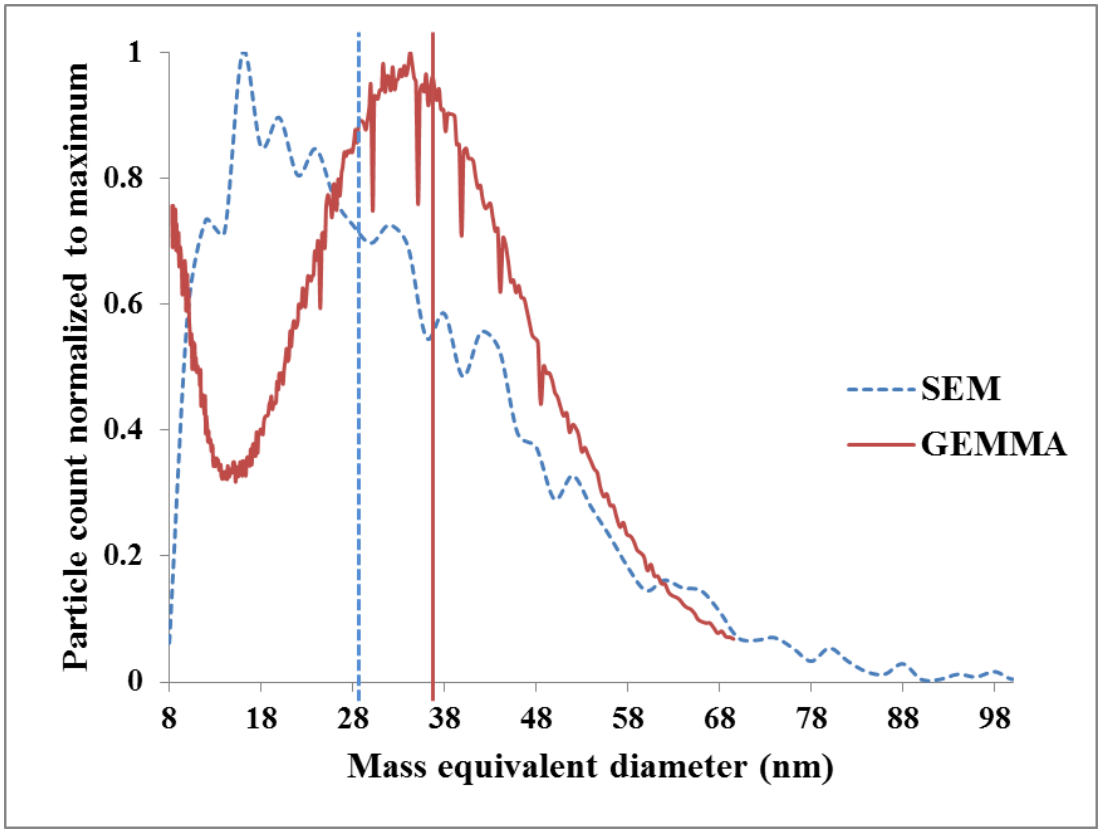

Figure 6.1- Measurement of SAS PNSD by GEMMA and SEM given as MED. Vertical lines are marking median of respective PNSDs.

The quantification of the median measurement error resulted from overestimation of small particles in SAS PNSD was presented in Annex 1. There it was shown that expanded measurement uncertainty for SAS in pristine dispersion was boosted from

10-12 to 37-40% due to flawed trueness. Thus it became clear that errors of this magnitude requires correction if EM shall be used for characterisation of ENPs featuring broad PNSD range.

The overestimation of number of small particles in PNSD as a consequence of the sample preparation used in Chapters 4 and 5 may be explained by smaller particles being more firmly attached to the microscopy substrate than the larger ones. Such supposition is justified by smaller particles having larger % surface area in contact with the microscopy substrate. As a consequence a selective removal of larger ENPs from the sample during washing of the microscopy substrate and blotting may have place as suspected in previous works (Balnois and Wilkinson 2002; Luo *et al.* 2013). The so far unanswered questions are: 1. Is this artifact solely a consequence of particle size? 2. Can it be corrected for?

To answer these two questions here a calibration approach for the sample preparation method used through the study (Chapters 4 and 5) was presented and discussed. As a calibration material citrate coated Au ENPs and spherical silica ENPs (Kmix) characterised by a polymodal distribution were selected. These two chemically different ENPs were chosen to verify whether except of size also composition of ENPs had an impact on shape of calibration curve. Derived calibration was then applied to correct MED expressed PNSD of SAS generated previously in Chapter 5.

6.2 Materials and methods

6.2.1 Calibration approach

The calibration approach was based on the measurement of the ENP PNSD by EM and a reference method. As a calibrant, spherical ENP samples featuring polymodal distribution were prepared in order to cover a need for a broad PNSD and allowing between method comparison of particle abundance in smallest to largest size fractions of PNSD. Quotients of particle abundance in assigned particle size fractions of EM to reference method derived PNSDs were used to generate a calibration curve. From this curve a size dependent correction factor (*f*) for particle counts in PNSD was obtained. This correction factor was then used to correct SAS PNSD expressed as MED.

Two reference methods were used for obtaining calibration curve: CLS and GEMMA. CLS was selected as a reference for Au ENPs PNSD and GEMMA for Kmix PNSD. Evidence in the literature suggested that both methods quantify ENPs accurately (Kesten *et al.*, 1991; Anderson *et al.*, 2013). Additionally, in-house performed assessment of CLS for quantification of Au ENPs verified that the method provided accurate results.

Kmix sample was characterised previously in Chapter 3 by means of SEM and GEMMA and these data were re-used in this study. Au ENPs were characterised as described below.

6.2.2 Engineered nanoparticles

Au ENPs were selected to confirm whether the calibration curve was transferable for chemically different ENPs. Citrate coated Au ENPs of 5 different sizes were purchased from BB International (Cardiff, UK). In previous studies it was found that the particle number overestimation was highly apparent for particles with diameters under 30-40 nm (Chapter 3 and 5). Therefore dispersions of monomodal Au ENPs (Mono Au ENPs) of nominal diameters: 10, 15, 20, 30 and 50 nm were selected. These 5 dispersions were mixed at concentrations given in Table 6.1 using DMW to obtain a well-defined polymodal sample (Poly Au ENPs).

The Kmix sample was previously described in (Chapter 3): the sample was divided in 4 size fractions (ranges given in Chapter 3) with modal sizes of 15.1; 47.3; 84.7 and 120.3 nm, respectively. These size fractions (with numbers given I to IV) were previously characterised by % abundance of particle numbers per size fraction by GEMMA (26, 38, 29 and 7%, respectively) and by SEM (51, 26, 19 and 4% respectively). SEM analysis was preceded by the T2 Gel sample preparation (see Chapter 3).

The SAS was previously characterised in Chapter 5, section 5.5.2: The PNSD of this sample was broad, with the main population of particles ranging from ~8 to 120 nm and some particles (agglomerates/aggregates) reaching a few hundred nm in MED. MED based PNSDs of SAS obtained by GEMMA and SEM were compared and it was found that due to the applied sample preparation method the fraction of particles in the range of 8 nm to 24 nm was overestimated by SEM resulting in a shift in the median diameter from 36.5 nm (GEMMA) to 28.2 nm.

Table 6.1- Size and concentration data of Au ENPs obtained by CLS and EM and provided by the manufacturer

Particle nominal size (nm)	10	15	20	30	50
Particle mean diameter (nm)[a]	9.5	14.9	20.9	30.7	48.6
Gold concentration in initial dispersion (μg/ml)[b]	57.6	47.7	56.6	1090	853
Gold concentration in Au ENPs sample analysed by EM (μg/ml)	1.152	4.77	11.32	54.5	170.6
PNC in Au ENPs sample analysed by EM (particles x 10^{11}/ ml)[c]	1.32	1.42	1.23	2.07	1.48
Expected particle abundance in Au ENPs sample (%)	18	19	16	27	20
CLS given proportions based on measurements of initial stock dispersions	17.6	21.2	19.7	23.3	18.2

[a]measurement derived by TEM, [b]data provided by the manufacturer, [c]values determined by calculation based on Au mass concentrations provided by the manufacturer and mean diameter obtained by TEM

6.2.3 Electron microscopy

A JEOL-JEM 2011 TEM operating at 200 kV (Nanocentre, University of York, UK) was used for the image acquisition of Mono Au ENPs and Poly Au ENPs. Additionally Mono Au ENPs were imaged by SEM (FEI Sirion S FEG SEM-Nanocentre, University of York). The SEM was operated at 5kV, spot size 3 and through lens detection.

Subsequent image analysis for the particle size measurement was carried out using OBIA. All particle size measurements for spherical ENPs (all studied ENPs, with exception of SAS) were expressed as ECD. The SAS's size was expressed as MED. The ECD is equivalent to the MED, if particles are spherical. Thus here a hypothesis was made that a calibration using spherical ENPs would be valid for non-spherical ENPs if their size is expressed as MED.

6.2.4 Gas-phase electrophoretic mobility molecular analyser measurements

Kmix and SAS sample measurements previously generated in Chapters 3 and 5 by GEMMA were adapted in this study. The data were used for comparison and discussion of robustness of the calibration obtained by Poly Au ENPs as reference material.

6.2.5 Centrifugal liquid sedimentation

The CLS instrument (CPS DC24000, Analytic, Cambridge, UK) was operated at a maximum speed of 24000 rpm. The analytical procedure settings were adjusted following the instrument manufacturer's guideline: 1. gold ENPs density: 19.3 g/cm^3, 2. gold ENPs refractive index: 0.47. The measured particle size range was set on 5-150 nm.

The spinning disc was filled with a gradient of sucrose solution (8-24%) and topped with dodecan to prevent the water from evaporation (according to the manufacturer's guideline). All Mono Au ENPs as well as Poly Au ENPs were measured by CLS.

Size calibration of the instrument was carried out before each sample run. As a calibrant citrate coated Au ENPs were used: 8012 Gold Nanoparticles Nominal 30 nm Diameter from NIST (Gaithersburg, US) instead of the polyvinyl chloride beads (PVC) proposed by the manufacturer. According to carried out in-house assessment the PVC beads were found to compromise particle size measurement trueness, which had an impact on the readings of particle number concentrations (data not shown). The calibration settings were: 1. Half peak width: 6nm and 2. Peak diameter: 27 nm (estimated based on the NIST report of investigation) (Kaiser and Watters, 2007a).

6.3 Results and discussion

6.3.1 Characterisation of calibrant- gold nanoparticles using electron microscopy and centrifugal liquid sedimentation

The PNSD of Mono Au ENPs analysed by CLS, TEM and SEM as well as CLS and TEM measurements of Poly Au ENPs are presented in Figure 6.2. It can be noticed that a certain level of diameter overlap was present in between particle populations from Mono Au ENPs in all the analyses. However in TEM and CLS derived PNSDs

this level was low (Figure 6.2a and b respectively), whereas for SEM it was very significant (Figure 6.2c), especially between gold ENPs with nominal diameters 10, 15 and 20 nm.

The broadening of PNSD observed by SEM analysis compared to TEM analysis was previously noticed by (Luo *et al.*, 2013- Annex 4). However, other sources e.g. reports of investigation of monomodal gold ENPs using both types of EMs do not confirm this information (Small and Watters, 2012; Kaiser and Watters, 2007a; Kaiser and Watters, 2007b). Ultimately, the instrument's operating parameters such as voltage, current and detection type can potentially influence the PNSD. In this study it was found that the broadening of PNSD determined by SEM was particle size dependent. The IQR within the PNSD of Mono Au ENPs of 50 nm nominal diameter was 1.53 times higher in SEM than in TEM. It was found that the discrepancy of IQR between two microsocopes was increasing with decrease of particle size and was highest in case of nominal diameter 15nm Mono Au ENPs (2.80 times higher in SEM than in TEM). The PNSD of Mono Au ENPs with a nominal diameter of 10 nm was limited by the cut-off point within the SEM analysis- 8 nm (Chapter 5, section 5.5.1.4). Thus for this sample IQR was only 1.86 times longer in SEM than in TEM.

The comparison of PNSD broadness between various analytical methods was previously carried out in other studies. For example Anderson *et al.* (2013) suggested that the method which reveals narrower PNSD is likely to be correct, as particle swelling can take place under different analytical conditions (in quoted study CLS provided narrower PNSDs of polystyrene particles than TEM analysis). Following this reasoning here TEM analysis could be considered more trustworthy in terms of PNSD measurement in comparison to SEM.

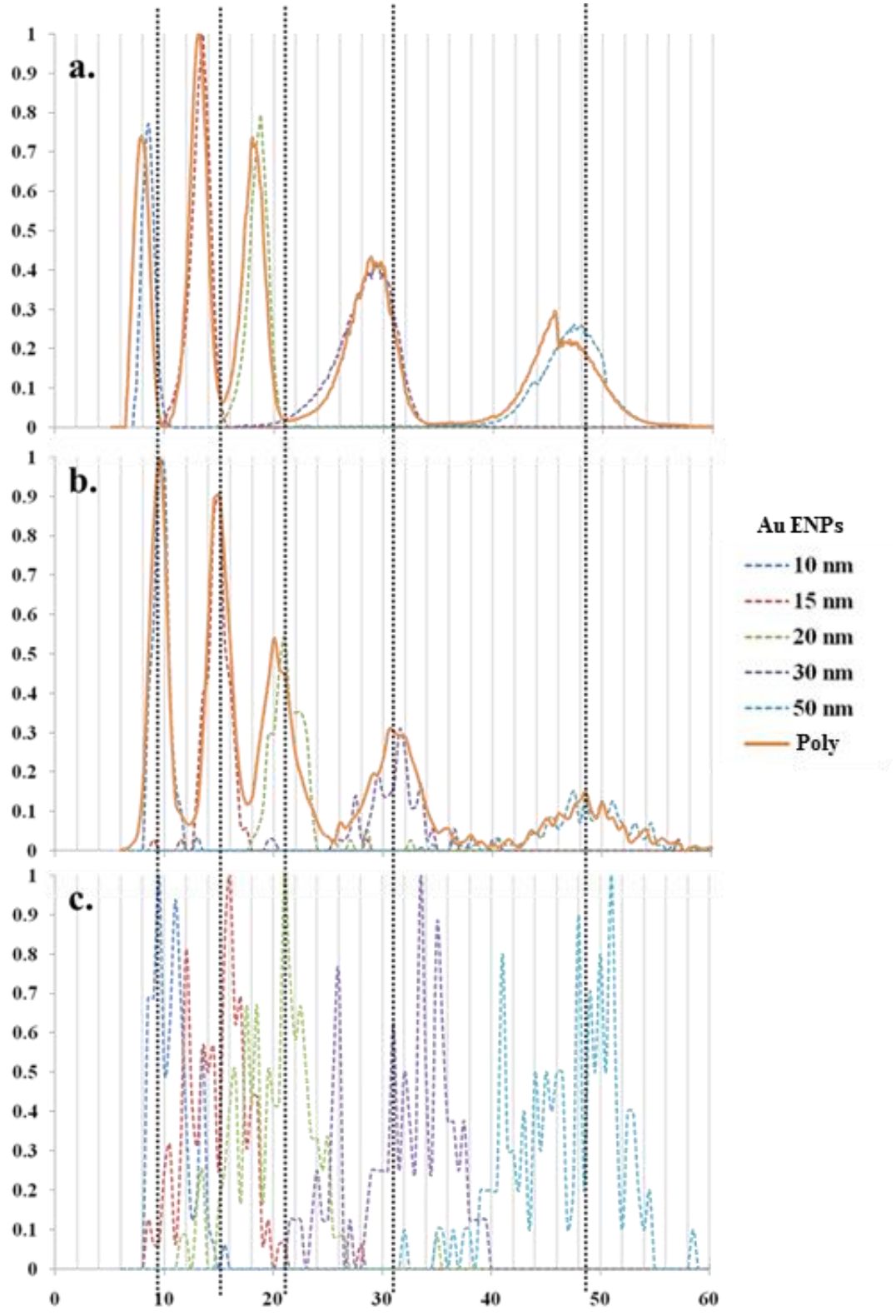

Figure 6.2- PNSD of Mono Au ENPs (dotted lines) and Poly Au ENPs (continuous lines) measured by a) CLS, b) TEM, c) SEM (Poly Au ENPs not measured). Black dotted reference lines point mean diameter of Mono Au ENPs measured by TEM.

In order to allow distinction between particle populations originating from different Mono Au ENPs, Poly Au ENPs was analysed by TEM rather than SEM. However, for the measurement of silica ENPs SEM was used, due to a very poor contrast of these ENPs in TEM (see e.g. Figure A1.2a in Appendix 1). Thus in further result discussion the PNSD broadening in SEM was also brought up to explain possible differences of PNSD between SEM and a reference method (GEMMA).

The Poly Au ENPs PNSD from TEM and CLS displayed in Figure 6.2a and b as expected (Chapter 3 and Chapter 5) clearly differed in terms of particle abundance. For the quantitative comparison the PNSDs for Poly Au ENPs obtained from both techniques was divided into five groups (GI-GV). As there was an overlap between particle populations, the size ranges of the size fraction groups GI-GV were not in complete agreement with the initial Mono Au ENPs. The cut-off points of the size fractions were chosen based on the minimal particle counts between the peaks. These points were different for CLS and TEM derived PNSDs (see Table 6.2), because it was found that the CLS tends to underestimate particle sizes compared to TEM, especially if measured particles are smaller than the calibrant particles (here 30 nm). This can be explained by the relative increase in the amount of stabilizing agent on the particle surface with decrease in size, which results in a lower density of the particles. The decrease in density decelerates the particle sedimentation velocity in CLS, which in turn results in smaller measured particle diameters, as demonstrated by (Zook *et al.*, 2011).

Table 6.2- Size range of groups GI-GV for Poly Au ENPs and relative particle abundance

Method		**GI**	**GII**	**GIII**	**GIV**	**GV**
CLS	Diameter range (nm)	6.0-10.2	10.3-15.7	15.8-22.0	22.1-36.5	36.6-60.0
TEM		8.0-12.5	13.0-17.5	18.0-25.5	26.0-36.0	36.5-60.0
CLS	Particle abundance (%)	16.0	23.4	20.3	23.0	17.3
TEM		22.6	26.5	20.8	18.1	12.0

The % particle abundance of Poly Au ENPs for each chosen size factions (GI-GV) as characterized by CLS and TEM are summarised in Table 6.2. The % particle abundance for all groups GI-GV determined by CLS was in good agreement with the

previous CLS estimation of particle abundance in Mono Au ENPs- Table 6.1 (1-2% of difference). Therefore it can be concluded that the overlap of the PNSD of the Mono Au ENPs and the chosen size fraction cut-offs did not influence the quantification of Poly Au ENPs significantly and also that agglomeration of the Poly Au ENPs was minor.

TEM results show higher % abundance of particles in size fractions GI and GII compared to CLS (16.0 and 23.4 for CLS and 22.6 and 26.5% for TEM, respectively). The % abundance of particles in groups GIV and GV was lower in TEM (18.1 and 12.0%, respectively) compared to CLS (23.0% and 17.3 %, respectively).

6.3.2 Generating calibration curve

In order to calibrate the sample preparation method for the measurement of ENPs with broad size distributions (Poly Au ENPs and Kmix) the quotients of % particle abundance obtained by EM analysis and the reference method (*f*) for each size group were plotted against mean (Poly Au ENPs) and modal (Kmix) ECDs (Figure 6.3a and b). Modal rather than mean diameters were chosen for Kmix sample because it was not possible to measure initial monomodal stock dispersions for this sample (one of them- K80 was already bimodal). For all Mono Au ENPs the PNSD was following approximately a Gaussian distribution therefore mean size measurements derived were approximately equal to modal size measurements.

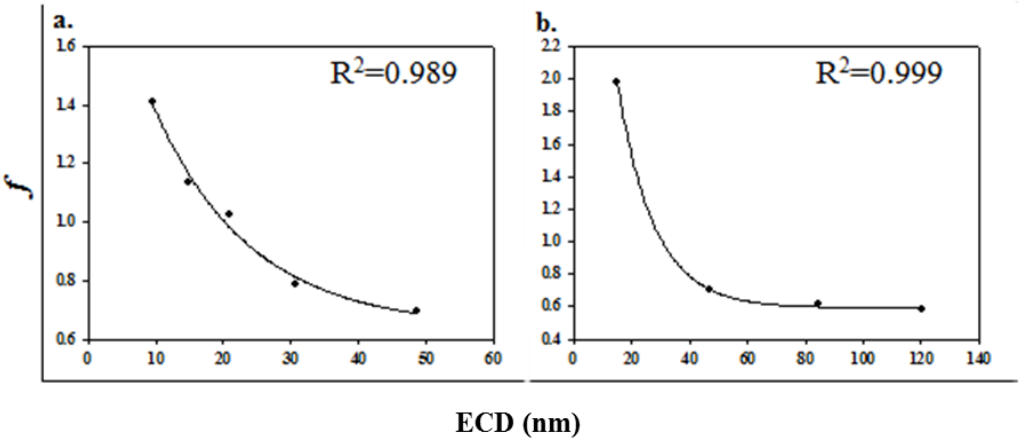

Figure 6.3- PNSD calibration curves for ENPs featuring a broad size distribution (dependence of the *f* to ECD using a.) Poly Au ENPs and b.) Kmix particles

The relationship between ECD and f for both Poly Au ENPs and Kmix was not linear. If particle size was the only factor affecting % particle abundance, then the % of total particle surface in contact with the TEM grid gelatin coating could be a factor affecting a chance of the particle being removed during the sample preparation. The dependence of % surface of the particle in contact with the TEM grid from diameter at assumption of particle sphericity can be derived from spherical cap and sphere surface equations and is given by Eq.6.1:

$$\%s = 100 \times \frac{2h}{ECD} \qquad \text{Eq. 6.1}$$

%s- fraction of particle surface area in contact with the gelatin coating on the TEM grid (%)

h- thickness of the gelatin coating (equals height of the spherical cap) (nm)

This dependence is shaped as a power curve. However, for both types of ENPs Poly Au ENPs and Kmix the f increased more rapidly with the decrease of particle diameter than expected from power law (Figure 6.2a). Therefore, better correlation and thus description of the calibration curve was obtained using exponential decay- Eq. 6.2 (for Poly Au ENPs) and 6.3 (for Kmix) than a power law. For both Poly Au ENPs and Kmix, R^2 of 0.99 was obtained for exponential decay fit, compared to R^2 of 0.98 and 0.91 for power fit respectively.

$$f = 0.639 + 1.4954 \times e^{-0.0704d} \qquad \text{Eq. 6.2}$$

$$f = 0.5924 + 4.5908 \times e^{-0.0791d} \qquad \text{Eq. 6.3}$$

It could be noticed that the obtained calibration curves (Eq. 6.2 and 6.3) derived for Poly Au ENPs and Kmix samples were different. The overestimation of small particle size fraction was larger in the case of Kmix (at *d*=15.1 nm, *f*=1.98) than Poly

Au ENPs (at d=14.9 nm, f=1.13). This implies that the particle chemistry affected the calibration. Differences in the physicochemical characteristics at the particle surface (see Figure 6.4) could provide a clue to the underlying reasons. The silica molecules at the surface of Kmix are likely to carry a higher overall negative charge due to the oxygen atoms bound to silicon on the surface (electronegativity difference of Si-O bond = 1.6 eV in Pauling scale), compared to citrate modified surface of Poly Au ENPs (electronegativity difference of C-O bond = 0.9 eV in Pauling scale). In view of these differences in surface characteristics, silica ENPs are likely to be more strongly attracted to the positively charged amino group of gelatin than citrate coated gold ENPs.

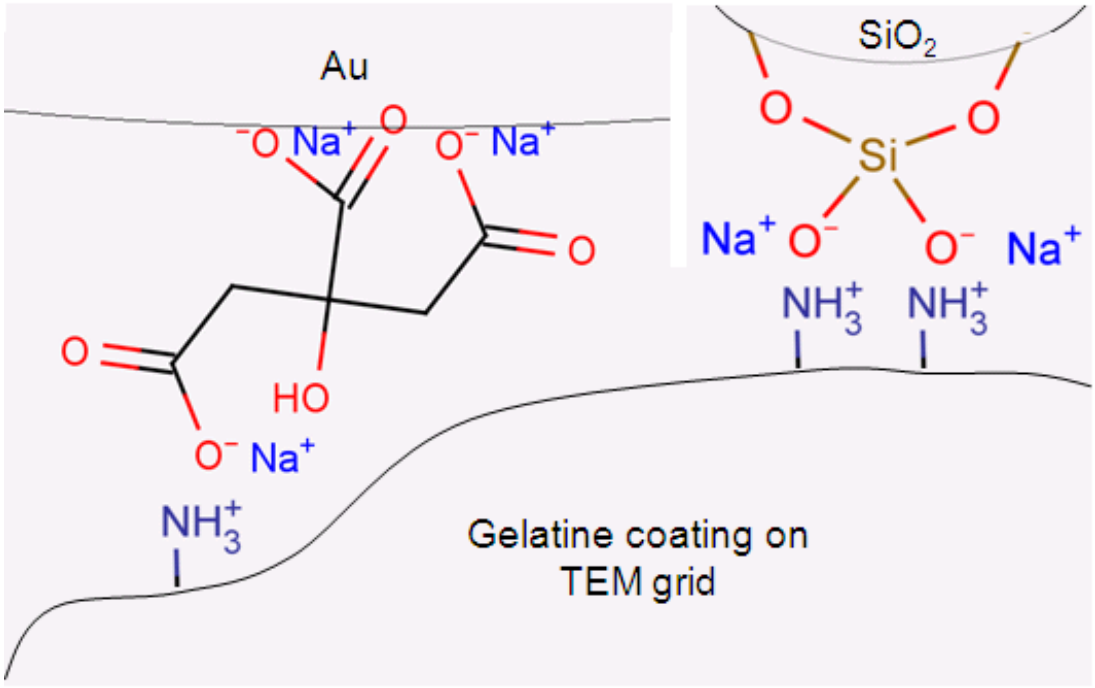

Figure 6.4- Interaction of gold and silica ENPs stabilized with citrate and sodium hydroxide respectively, with gelatin coating on the TEM grid

6.3.3 Calibration of particle size distribution of synthetic amorphous silica

In conclusion the calibration curve generated from Kmix sample was considered more appropriate for correction of PNSD of SAS because of the similarities in particle surface chemistry. To generate calibration corrected PNSD of SAS the particle counts for respective diameter measurements were divided by f values

generated from Eq. 6.3. The Figure 6.5 presents SEM and reference method (GEMMA) derived PNSDs of SAS expressed as MED.

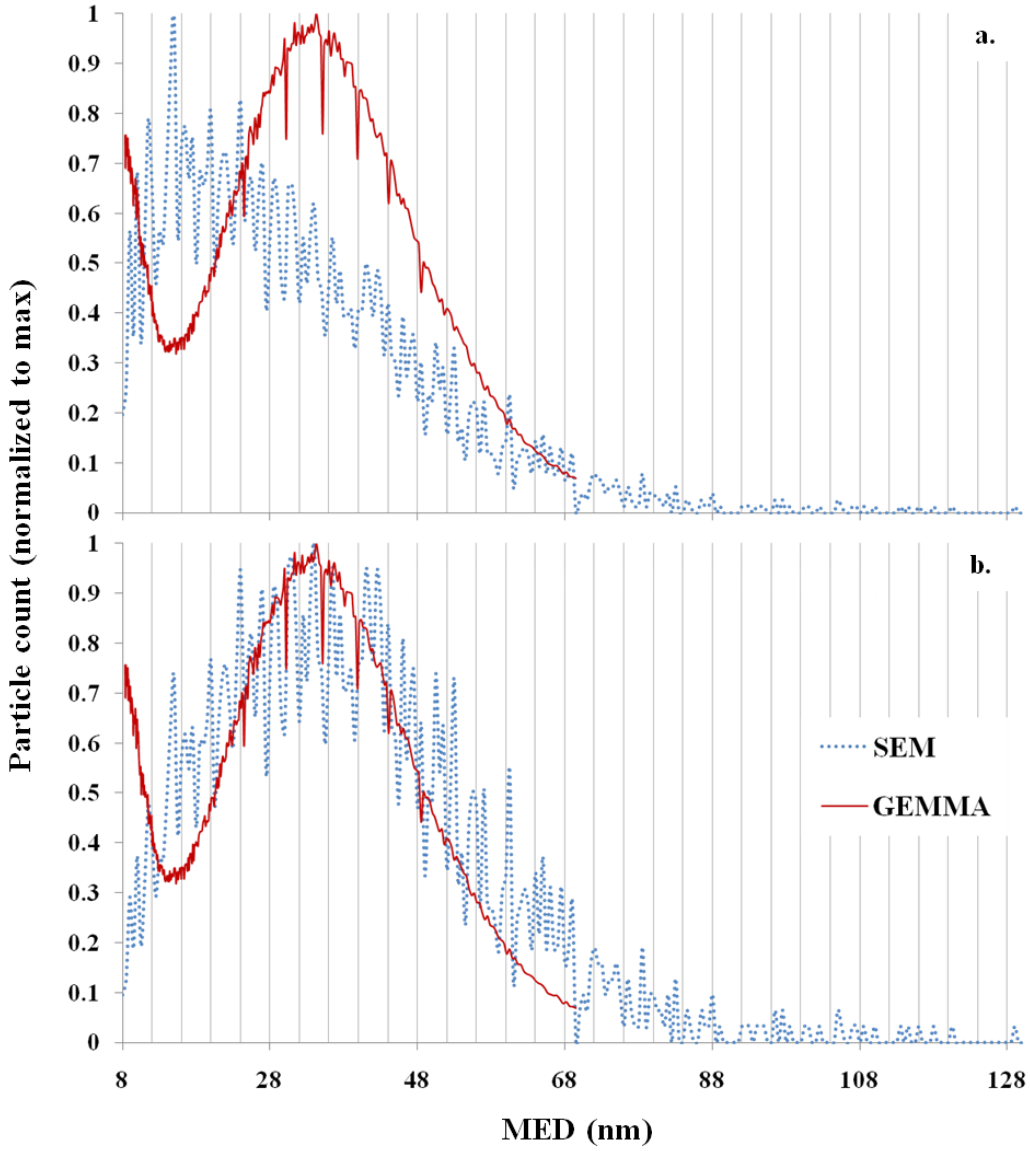

Figure 6.5- The PNSD of SAS measured by GEMMA and SEM a) initially, b) after correcting SEM result for calibration Eq. 6.3

It can be noticed that the correction resulted in a shift of median SAS size from 28.2±1.0 nm to 36.3±0.6 nm. The median size derived from SEM after correction was similar to that estimated by GEMMA reference method: 36.5±0.02 nm (t-test, p>0.05). However, it was also noticed that the IQR of PNSD in SEM distribution was 1.31 times broader (23.5 nm) in comparison to GEMMA (17.9 nm). It is anticipated that except of the previously mentioned instrument's operating settings and particle size, the chemical composition of the ENPs, can also affect PNSD

broadness. The reason might be the electron beam penetration depth in the material, which depends on the chemical composition of the sample and electron beam voltage (Molhave, 2004). As all the samples were imaged at same instrumental settings, the deeper penetration depth of the electron beam within silica, compared to gold ENPs, potentially allowed to reduce the PNSD broadening effect. Interestingly, previously it was found that for a monomodal sample of spherical silica ENPs with relatively narrow IQR=9.9 nm in SEM was similar to that generated by GEMMA: IQR=10.1 nm (K12 sample in Chapter 5). Therefore it is anticipated that the difference in particle shape could also influence the broadness of PNSD. The SAS materials were composed of the primary particles measuring on average 9 nm (Chapter 5). The boundaries of such small objects could have been affected by the instruments resolution (approximately 2 nm), which might have affected accuracy of the measurement resulting in broadening of PNSD.

However, despite the difference in particle shape between the calibration material (spherical Kmix) and a sample (aggregated SAS), it was possible to obtain PNSD of SAS that was not biased by the sample preparation method.

6.4 Conclusions

In this chapter an approach for the correction of particle size underestimation due to overestimation of small particle counts by the sample preparation, was introduced. The method used multimodal particle systems. It was shown that spherical particles can be successfully applied to calibrate the PNSD of aggregated ENPs, when the PNSD is expressed as MED. It was also found that particles with different surface chemistry can have an effect on calibration. This is a disadvantage, especially of concern, if ENPs in complex matrices are assessed. In such cases particles can undergo surface chemistry transformation in unpredictable ways. In a previous study (Chapter 4) the pH of the sample was adjusted to stabilize SAS using a buffer (BB 8.0) to avoid this problem. Other sample preparation approaches, where ENPs are separated from the matrix could also be considered.

Here the correction for introduced size measurement artefacts by sample preparation for citrate coated gold and silica ENPs was presented. Research needs to include calibration approaches for different type of particles, potentially leading to a highly

useful generalization of calibration equations for a broader group of particles with different surface chemistries.

Chapter 7

General discussion and conclusion

7.1 Introduction

The increasing application of nanotechnology in the food industry raises demand for the risk assessment of the new products before they can be introduced to the market.

A frequently studied property of the ENPs after spiking into complex matrices is size. This is because size can determine the uptake of the ENPs into the cells and their toxicity (Jiang *et al.*, 2008a; Fede *et al.*, 2012). Thus the accurate estimation of the ENPs size distribution in foods is important.

EM is recommended and used as a reference method for the measurement of ENPs in general (Hagendorfer *et al.*, 2012; Tiede *et al.*, 2009a; Linsinger *et al.*, 2012; Calzolai *et al.*, 2012; Anderson *et al.*, 2013) and also in food and feed (Dekkers *et al.*, 2010; Weir *et al.*, 2012; EFSA Scientific Committee, 2011). Although the application of the method is widespread still not much is known on how accurate the results of ENP measurements are, especially in the case of materials characterised by a broad size distribution and non-spherical ENPs. Another challenge is the unavailability of standardized protocols for preparation of food samples containing ENPs. Therefore the research presented in this thesis aimed to develop and validate EM-based approaches (sample preparation, imaging and image analysis) for determination of ENP size distribution in foods. This chapter will firstly give a brief summary of the research achievements and then explore the implications of these achievements for current guidance on risk assessment of ENPs in foods. Suggestions on further work on method development will also be given.

7.2 Key findings of the research study

In this work the EM methods were evaluated and developed for the measurement of ENPs in food matrices. In Chapter 3, potentially suitable sample preparation protocols which were previously used for food and biological sample preparation (Chapter 2) were evaluated. It was found that the ENPs in liquid food matrix were prone to changes due to the sample preparation. These alterations included agglomeration or discrimination of large ENPs number in the PNSD. Agglomeration

of colloids and ENPs was previously reported in numerous studies (Balnois and Wilkinson, 2002; Doucet *et al.*, 2005; Tiede *et al.*, 2008), but discrimination of particle size fraction was so far rather a supposition than a fact supported by clear scientific evidence (Balnois and Wilkinson, 2002; Luo *et al.*, 2013). In Chapter 3 such evidence was obtained using an ENP sample featuring polymodal size distribution and by comparing EM results against a reference method (GEMMA) which was previously shown to accurately quantify ENPs (Kesten *et al.*, 1991). Unfortunately a sample preparation method which would not induce any of the two artefacts (either agglomeration or overestimation of small particle number) was not found. Thus a method which, whilst not optimum, was thought to be the most suitable, based on recovery of ENPs from food samples and minimized agglomeration was selected for further validation. The validation described in Chapter 4 was a first attempt of obtaining data on reliability of EM measurements of ENPs in foods. It was also the first study evaluating the contribution of subsequent stages in the data acquisition process to the measurement precision for such samples. Chapter 4 also emphasized that measurement trueness for SAS ENPs in tomato soup could not be estimated. This was due to the unavailability of either reference materials or methods against which the EM measurements could be compared. The problem was a consequence of inherent SAS properties. SAS was characterised by aggregated structure and because of this, each of the analytical methods, which employ different measurement principles were generating different measurement outputs (see Chapters 1 and 5). Comparison of size measurements of such randomly aggregated ENPs between methods was so far not possible (Kasper, 1982; DeCarlo *et al.*, 2004). Nevertheless the literature provided evidence that particle behaviour on which measurements were based could be linked to its fractal geometry (e.g. Boldridge, 2010; Melas *et al.*, 2012; Maricq and Xu, 2004). Using this concept in Chapter 5 a series of calculations for MED- the diameter of a compact sphere having the same mass as an ENP aggregate was developed. MED values for SAS were then derived from the measurements of ECD, HDD, SSD and EMD given by SEM, NTA and AF4-ICP-MS as well as CLS and GEMMA respectively. This is the first known study linking measurements of randomly aggregated ENPs in between the methods. It was found that AF4-ICP-MS and GEMMA measurements of SAS after MED transformation were in excellent agreement. Nevertheless SEM overestimated particle number in the small size region, which was also confirmed by observations

for spherical silica in Chapter 3. Thus in Chapter 6 correction for small particle number overestimation in was developed. Using spherical silica ENPs it was possible to successfully correct the measurement of aggregated SAS ENPs expressed as MED.

Overall the study identified problems connected to the measurements of ENPs also in foods and provided some valid solutions. Nevertheless results also show that more research is needed for routine application of the method and identified some inherent problems with addressing current guideline for the risk assessment of ENPs in foods (EFSA Scientific Committee, 2011). These challenges are described in the sections below.

7.3 Implications and recommendations for further method development

A general challenge in the measurement of ENPs is the availability of reference materials. Certified reference materials for ENPs size are available on the market for few decades, however so far no materials with certified particle number as well as size have been developed. These are obviously required for the determination of accuracy of the PNSD measured by the method. In view of the non-availability of these materials many authors use confirmatory techniques for result validation in the studies (e.g. Chapter 3; Tiede *et al.*, 2009a; Dekkers *et al.*, 2010; Peters *et al.*, 2012; Loeschner *et al.*, 2013a; Park *et al.*, 2013). The problem with this approach is incomparability of the measurement outputs for non-spherical particles (Kasper, 1982; Naito *et al.*, 1998; Bowen, 2002; DeCarlo *et al.*, 2004; Domingos *et al.*, 2009; Chapter 5). Authors have discussed application of the dynamic shape factor or effective density to correct for particle shape and express particle size MED (Kasper, 1982; Kousaka *et al.*, 1996; DeCarlo *et al.*, 2004; Kamiti *et al.*, 2012; Woehlecke *et al.*, 2013). However, each of the methods following different flow regime require estimation of a separate dynamic shape factor or effective density and is problematic for some of the ENP shapes like e.g. aggregates. An alternative solution for deriving MED of particle aggregates was described in Chapter 5 using as an example SAS. SAS was difficult in detection for some of the studied methods. High size LOD and size LOQ's for light scattering and absorption methods did not allow full comparison of SAS PNSD between all methods. Therefore a study featuring different ENPs with

higher refractive index, e.g. titanium dioxide could be considered to validate given methodology for these methods. Additionally further validation of MED transformation approaches could be supported with a method which measures MED in a direct way, such as SP-ICP-MS.

The further development of MED transformations for other analytical techniques and other types of ENPs is of importance when reporting results from the studies where ENP size is crucial. Such uniform expressions are lacking so far in the literature. This so far hampered interpretation of the data and developments of reference materials as well as full validation of measurement methods for ENPs of broad size distribution and non-spherical shape.

Shown in this research EM validation (Chapter 4) emphasized problem with defining ENP size measurement trueness due to lack of reference materials or methods for ENPs characterised by a broad PNSD and non-spherical shape. In Chapter 5 comparison of EM with other techniques for such sample was carried out and it was found that EM introduced a significant shift of the distribution toward smaller ENP sizes. Thus the trueness of EM measurements for ENPs with broad size distribution was compromised. In Annex 1 it was shown that the ENP measurement trueness error was very significant. It is therefore suggested that calibration (e.g. presented in Chapter 6) is applied to correct PNSD from EM.

Although the calibration was proven to be successful, it was also shown that surface chemistry of ENPs is likely to affects calibration. The chemical transformation of the particle surface in a food matrix may lead to difficulties with the application of the calibration approach and more research is needed to address these difficulties.

Extremely small sample intake in EM when compared to other analytical techniques was another concern emphasized in this study. Only a volume of few pl can be analysed at once. Linsinger *et al.*, pointed out the necessity of measuring very high numbers of particles and proposed that 500 measurements were needed for obtaining reliable information on particle size (Linsinger *et al.*, 2013). Some practical solutions to this problem are described in Chapter 4 and ISO draft guidance (Draft ISO/WD 14411-2, In preparation) showing that this number can be high (over 500) or low (less than 50) depending on the broadness of PNSD in particle population and desired level of confidence. Nevertheless, small sample intake in EM still poses a problem in the representative sampling of particle populations when dealing with

ENPs in food samples (Chapter 4). Thus for further method validation removal of the matrix prior to preparation is advised in order to improve the measurement certainty. Summarising, the measurement of ENPs even in pristine dispersions is still challenging although advances were made in recent years in this field. Thus the further considerations for measurement of ENPs in complex matrices needs to be based on this state-of-the-art knowledge and requires further detailed considerations described below.

7.4 Implications for current guideline on risk assessment of engineered nanoparticles in foods

EM offers a distinct advantage over other analytical approaches when it comes to analysis of ENPs in foods and other complex matrices. This is because visualisation of the sample (with certain exception of e.g. organic ENPs) allows identification of association of the ENPs with the matrix components (e.g. Tiede *et al.*, 2009c). In other analytical techniques this association may lead to difficulties in result interpretation. Authors working on analytical method development for Ag ENPs in complex matrices reported incomparability of PNSD derived from EM micrographs versus AF4-ICP-MS, SP-ICP-MS (Loeschner *et al.*, 2013a) and HDC-ICP-MS (Tiede *et al.*, 2010). In both cited studies, Ag ENPs used were approximately spherical. Thus results suggested that association of these ENPs with matrix (meat (Loeschner *et al.*, 2013a) and activated sludge (Tiede *et al.*, 2010) had a significant effect on particle elution time in AF4 and HDC as well as ionization of single ENPs in SP-ICP-MS. Nevertheless successful application of methods which do not allow distinguishing between ENPs and matrix nano-structures for the measurement of ENPs in foods like e.g. NTA (Chapter 5; Gallego-Urrea *et al.*, 2011; Luo *et al.*, 2013- Annex 4) indicate that association of the ENPs with the matrix components is not always the case. However, challenges related to characterisation of ENPs in complex matrices lead to development of guidances in which use of more than one analytical method is recommended. EFSA recommends that the results of ENPs measurements in food are always verified with EM (EFSA Scientific Committee, 2011).

Nevertheless, confirming results using EM can be challenging. This is because the sample pre-treatments for EM and other techniques vary. The preparation might

involve only sample dilution however, even dilution changes sample matrix, altering content of suspended solids, dissolved substances, pH and IS. All of these factors can affect particle agglomeration state (Jiang *et al.*, 2008a; Peters *et al.*, 2012; Park *et al.*, 2013). While dilution with DMW is commonly practiced, some authors appreciated the use of other agents, having on mind stability of the ENPs or mimicry of the sample matrix. For example (Lienemann *et al.*, 1998) used a synthetic electrolyte of 1.5 mM $Ca(HCO_3)_2$ for diluting ENPs of Fe_2O_3. These ENPs were then used for EM method calibration where the content of colloids was measured in natural waters. In Chapter 3 it was shown that the use of borate buffer at pH 8.0, stabilised ENPs of SAS and resulted in higher particle numbers recovered from stock dispersions and a soup sample following dilution process when compared to the same samples diluted with DMW. This was because the buffer had a stabilising effect on SAS ENPs. Thus use of stabilising ENPs diluents could be recommended if dilution is necessary in sample preparation. However, the issue of matrix changes and possible change of ENPs agglomeration state after dilution in comparison to original in the undiluted food matrix still remains unresolved.

The sample preparation of the foods or complex matrices containing ENPs may require use of more invasive steps than sample dilution, namely ENPs extraction or matrix digestion (e.g. Grombe *et al.*, 2014- Annex 5; Grombe *et al.*, In preparation; Loeschner *et al.*, 2013a). These actions aim to remove ENPs from the original matrix and by doing this may contribute to the changes of the particle size. Different variants of sample preparation for EM involving sample dehydration were shown to introduce various artifacts to the PNSD of ENPs (Chapter 3). These drawbacks were primarily related to the EM preparation of ENPs in liquid food samples and liquid suspensions. In solid samples where ENPs were strongly bound to the matrix e.g. tissues from uptake studies (e.g. Loeschner *et al.*, 2011) the ENPs could be preserved in the unchanged form thanks to well developed standard sample preparation techniques such as resin embedding or freezing described in detail in (Hayat, 1989b; Cavalier *et al.*, 2009; Chapter 2) which allow the preservation of the matrix structure. An alternative to these sophisticated sample preparation methods for TEM was described in Lari and Dudkiewicz (2014- Annex 3). It involved dilution of the solid meat sample containing Ag ENPs by a high factor and homogenization, then sedimentation of the obtained sample onto a TEM grid. Although this technique was

matrix destructive (due to sonication used in homogenization step), comparison with simple swab of the sample surface with TEM grid and imaging electron transparent sample portion, showed no difference in particle agglomeration state for studied in Chapter 6 reference material of Ag ENPs in meat - see Figure 7.1 a and b.

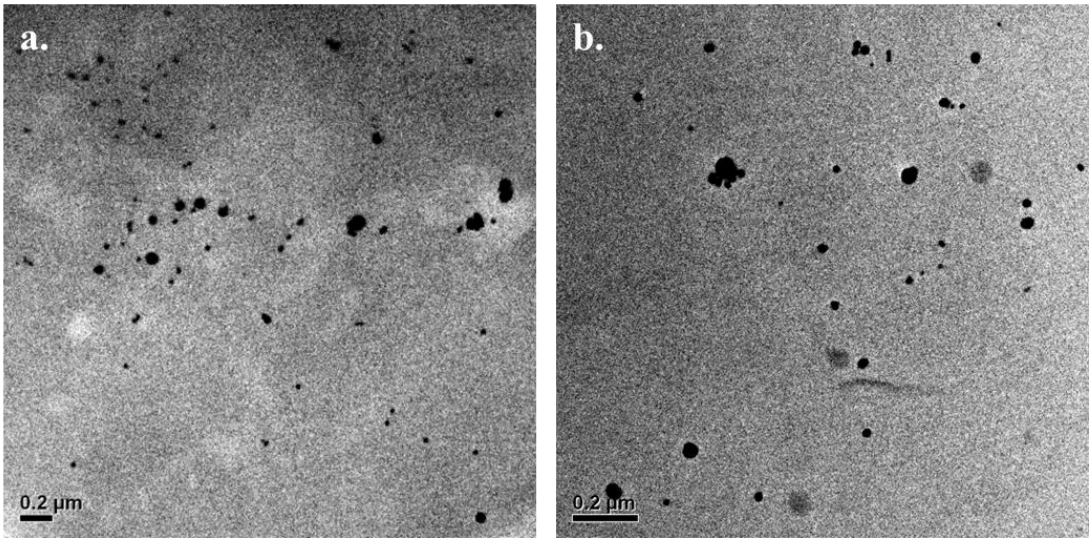

Figure 7.1- TEM images of Ag ENPs in meat prepared by a. swabbing grid over sample surface and b. ultracentrifugation

The technique was used in Chapter 4 for validation and it was found that only negligible agglomeration of Ag ENPs in meat was present. This contrasted with result of SP-ICP-MS analysis in (Grombe *et al.*, 2014- Annex 5), where Ag ENPs measured in same material occurred to have approximately twice longer diameter than measured by TEM in Chapter 4. Providing a nearly spherical shape of these ENPs the comparability of TEM and SP-ICP-MS measurements was expected. This measurement discrepancy can be again attributed to the difference in the sample preparation and measurement technique. While in TEM the presence of the meat matrix layer does not affect the measurement much (Chapter 4), in SP-ICP-MS the small particles of the matrix with few non-agglomerated Ag ENPs 'sitting' on it will be detected and interpreted as one Ag ENP. The actual agglomeration/ aggregation of Ag ENPs could also take place in process of sample preparation for SP-ICP-MS. This based on enzymatic digestion protocol (Loeschner, *et al.*, 2013a), due to liquidation of the matrix could result in a complete freeing Ag ENPs and subsequent agglomeration of initially single particles.

Figure 7.2 summarises which of the transformations that ENPs can undergo in the food products are likely to affect the PNSD measurement using various analytical

techniques. Out of these aggregation and dissolution can be measured. However agglomeration and association with food matrix components affect the measurement in a way which does not allow to predict behaviour of ENPs in measuring instrument.

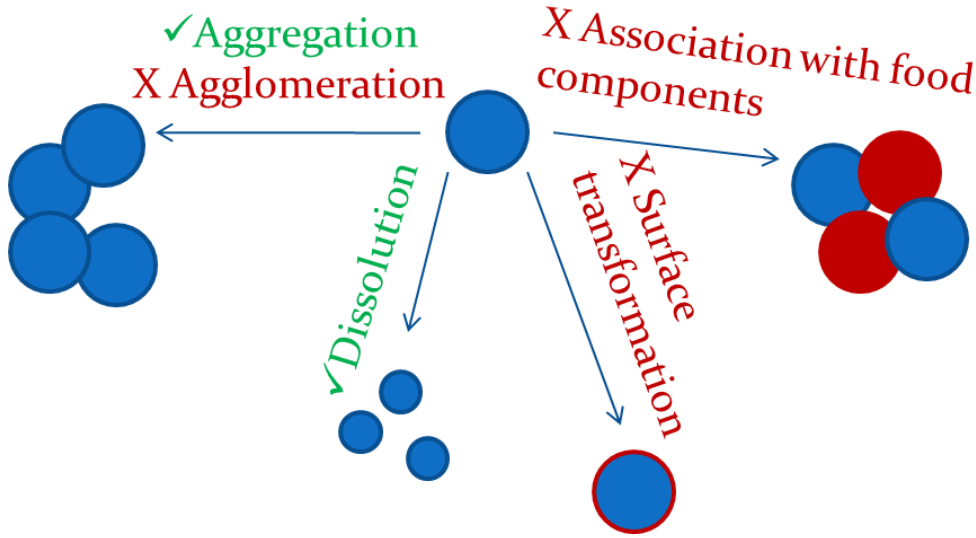

Figure 7.2- Possible transformations of ENPs in the food matrix, marked with thick allow comparable measurement of particle size across the characterisation methods while marked with cross do not

Additional drawback of measuring ENPs directly in foods is high measurement uncertainty when compared to the stock dispersions (Chapter 4). It has been shown that over 40% of median size value uncertainty could be expected for SAS spiked in tomato soup (Chapter 4) and measured by SEM. Such high values of the expanded uncertainty of measurement were attributed to random changes of these ENPs on different sampling days and could have been a result of changes in the soup matrix. Thus one of the major difficulties with the real food samples are the dynamic changes occurring in them with time and perhaps even locally in separate subsamples.

Taking into consideration the number of scenarios of ENPs fate during sample preparation and in the food product as well as incomparability of the results from different analytical techniques, it became clear that addressing measurement of particles in the food matrix as recommended (EFSA Scientific Committee, 2011) may not be possible. The only exception to this is a special case of solid food samples which can trap firmly analysed ENPs and subsequently be prepared for

TEM. On the other hand the toxicological studies show that the conditions in which ENPs are at different points of experiment change multiple times and affect ENP size. For example Peters *et al.* showed that silica ENPs can agglomerate and deagglomerate in human digestive track depending upon pH present at different stages of digestion system (Peters *et al.*, 2012). Thus, it could be argued that as long as the sample matrix pre-treatments are not invasive for the ENPs of interest (do not cause aggregation or dissolution) a toxicologically relevant information on the particle size can be extracted.

In view of the future guidelines for research on ENP fate in food and human digestive tract these results highlight a necessity of further development of acceptable study designs for the risk assessment. Such guideline should take into consideration possible changes to the ENPs in course of sample preparation, set acceptable practices as well as consider food stimulants with much simpler composition to allow uniformity of particle behaviour in whole sample volume. Meanwhile the research on analytical methods for the measurement of ENPs in foods is on-going (NanoDefine project will continue work of NanoLyse) and hopefully will allow to address knowledge gaps necessary for setting guideline.

7.5 Summary on recommendation for analysing of ENPs in foods using EM

This recommendation is based on today's state-of-the-art knowledge to which above presented research contributed. Figure 7.2 presents a decision tree, potentially useful for EM users interested in analysing of ENPs in foods. Figure 7.3 depicts a course of action in terms of sample preparation and data interpretation depending on nature of the matrix as well as type of ENPs' PNSD. This course of action assumes sphericity of ENPs. If ENPs are non-spherical or aggregated additionally mesurements should be expressed as MED. The protocol for liquid food samples and ENPs featuring broad size distribution is at the moment laborious and time consuming. Thus further developments are needed to improve it and either develop sample preparation, which will allow to exclude the necessity of calibration or develop more calibration curves that could be generalized.

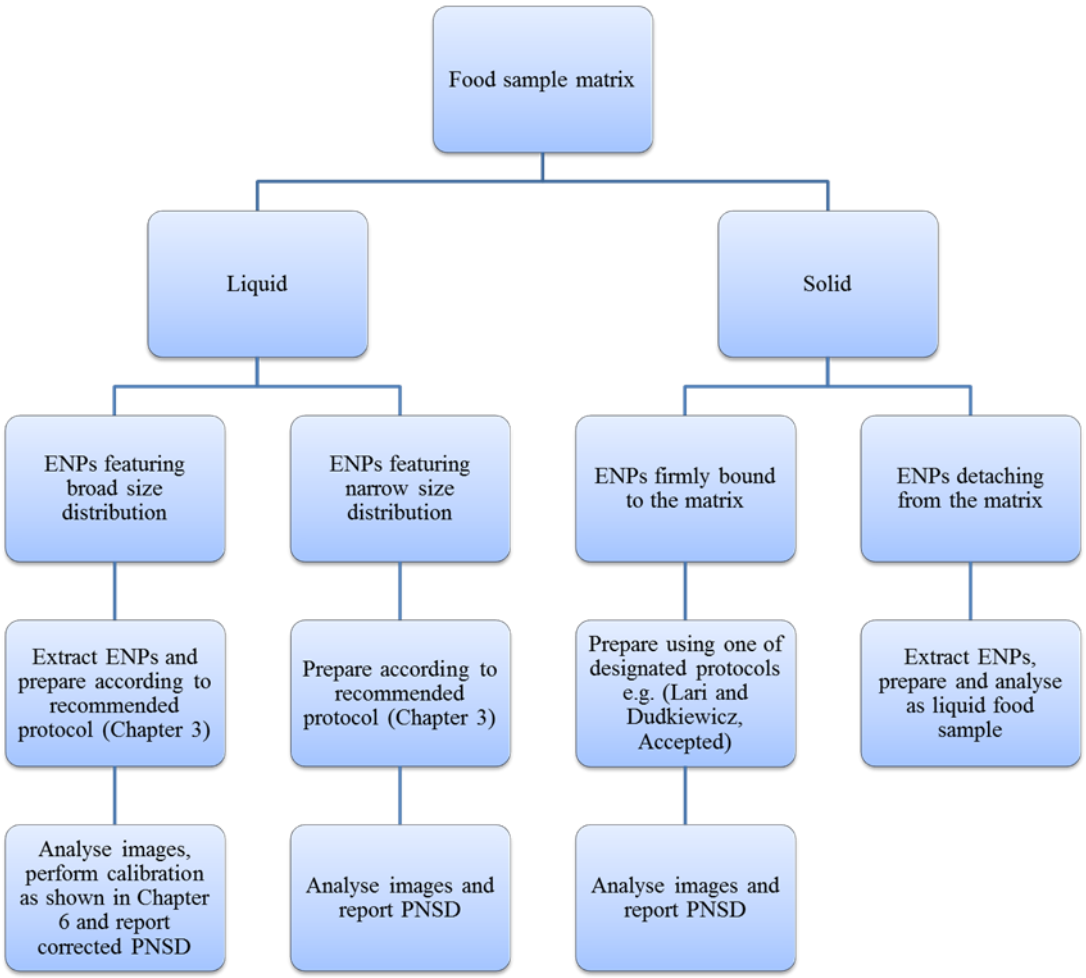

Figure 7.3- Course of action for analysis of spherical ENPs in foods

7.6 Conclusion

Overall this study presented first attempt of EM method development and validation for the measurement of ENPs in foods. The findings allowed addressing challenges related to sample preparation and incomparability of ENP measurements between analytical methods. Nevertheless also some drawbacks of the method were highlighted, such as a need of calibration and high measurement uncertainties for ENPs in foods. These might be improved on by further research efforts.

Appendix 1

Particle size increase due to conductive coating

Methodology

The measurements were conducted using two types of particles- SAS (see Chapter 3) and citrate coated spherical Au ENPs with nominal diameter 30 nm available from NIST (manufacturer's id: 8012). As, compared to the SAS, the Au ENPs were spherical and fairly monodispersed. Samples were prepared according to T2 Gel protocol described in Chapter 3, SAS (3 replicates) sample was diluted 100 fold with BB8.0 and Au ENPs (5 replicates) undiluted. Both ENPs were measured before and after coating using SEM imaging and OBIA analysis as specified in the main text. The SAS were imaged at two magnifications lower than one used in the study. The micrograph settings were summarised in Table A1.1.

Table A1.1- SEM imaging settings for measurement of particle ECD increase due to coating

Sample	Number of micrographs	Micrograph area (µm x µm)	Analyzed area per replicate (μm^2)	Pixel size	Smallest particle ECD (nm)
SAS	4	6.3 x 4.73	119	8.6	38
SAS	16	3.15 x 2.37	119	4.3	19
Au ENPs	10	1.56 x 1.18	18	2.2	8

To visualise the thickness of the coating additionally samples of coated Au ENPs and SAS were imaged by TEM.

Result

The Au ENPs increased in median size by 7.8 ± 0.8 nm (mean increase between replicates ± standard error). The result was confirmed by imaging of the coating in TEM (see Figure A1.1). Measurement of the coating thickness of SAS imaged in TEM was difficult due to a very poor contrast of the SAS (see Figure A1.2a) which resulted in poor distinction of the particle boundary (see Figure A1.2b), but a vague Pt/Pd shell seems to be present in a similar fashion as in the Au ENP coating.

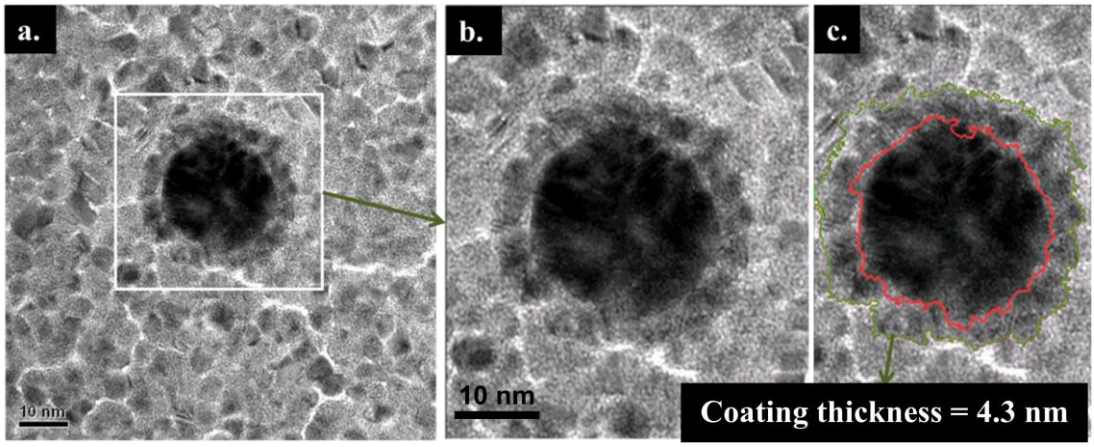

Figure A1.1- TEM images of coated Au ENPs (a) Original image (scale bar 10 nm), (b) Zoomed on the particle, (c) Result of image analysis

Figure A1.3 presents the size distribution of all measured particles for coated and uncoated ENPs.

The full size distribution of Au ENPs was clearly shifted toward higher values, whereas the sizes of SAS did not include the small size tail of the distribution and hence it is difficult to make an obvious conclusion about any shift in distribution. An increase of total measured particle number in coated SAS samples when compared to uncoated ones close to the cut-off ECD value was observed (Figure A1.3b). The median measurements of coated and uncoated SAS were not significantly different (Mann-Whitney rank-sum test, p=0.136- lower magnification and 0.214- higher magnification). Neither of the magnifications taken in this study was able to cover fully the size distribution of SAS and this was the reason for similarity in particle ECD measurements between coated and uncoated samples.

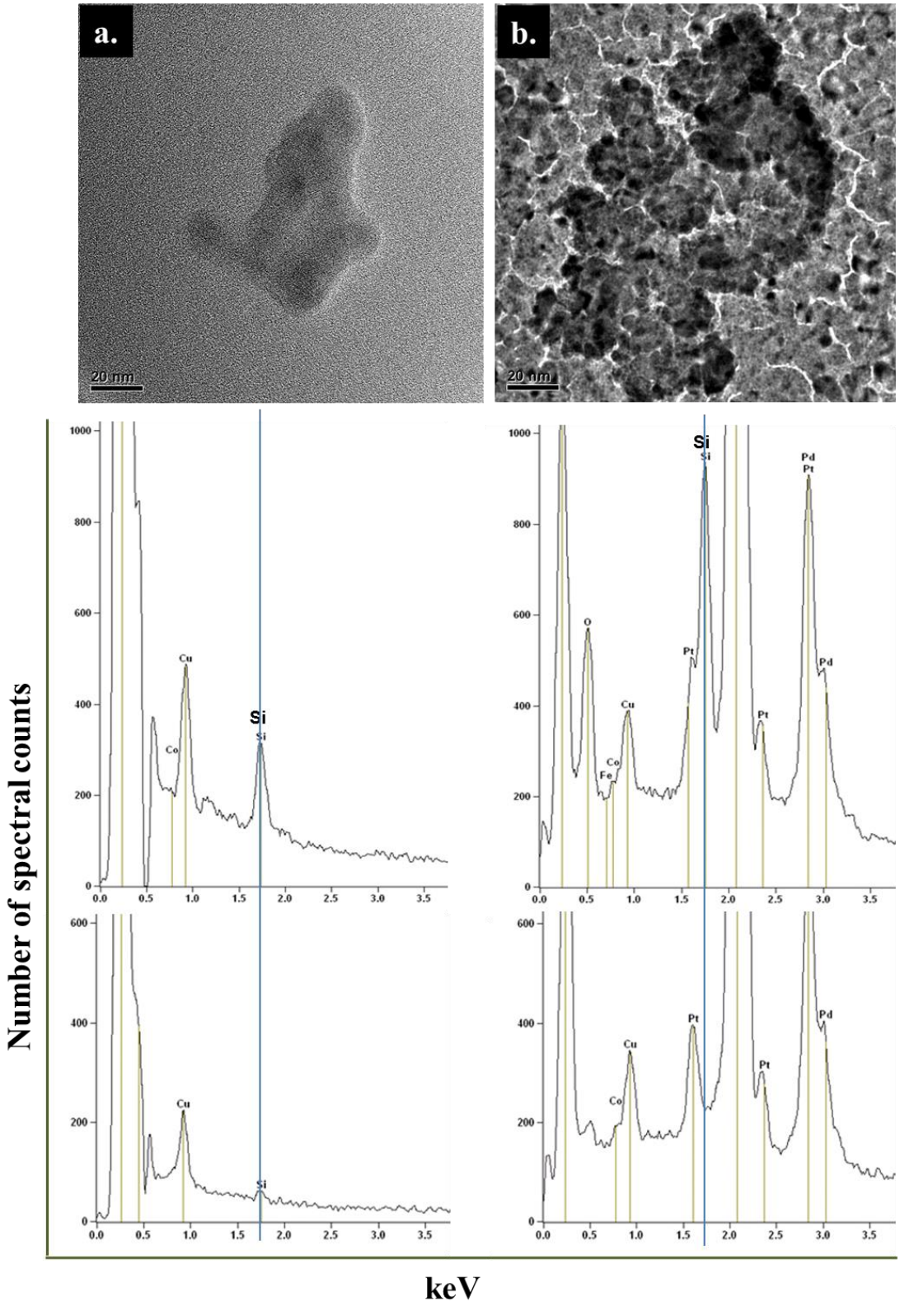

Figure A1.2- TEM images of a uncoated and b coated SAS and below EDS spectra of imaged particle (upper spectrum) and measured away from the particle background (lower spectrum). Thin blue line marks position for Si spectrum.

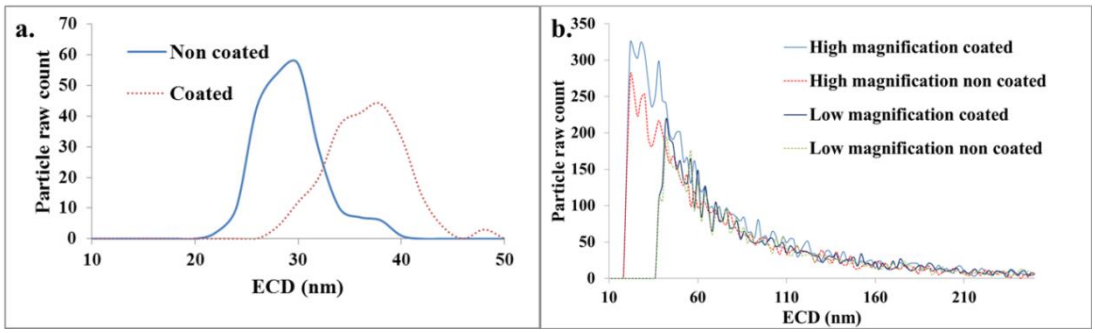

Figure A1.3- Size distribution of the ENMs before and after conductive coating (a) Au ENPs, (b) SAS

Based on the indication of a Pt/Pd shell in the TEM image (Figure A1.2b) for SAS, it is reasonable to expect that the size of the individual particles of SAS also increases by at least 8 nm as found for Au ENPs, and this is supported by the fact that shifting the size distribution of the uncoated to match the coated sample with around 10 nm will make the two curves roughly match. The 8 nm is not exact as the particles of SAS had non spherical shape and thus longer perimeter than Au ENPs. This means that we would expect longer ECD increase for SAS especially for larger particles because the compactness of particles decreased with the size. Indeed the increase in size could be noticed for large particles- the 75th percentile of SAS (corresponding to coated ECD 131 ± 2 nm in coated particle size distribution) imaged at lower magnification was increased by 8.8 ± 1 nm. For higher magnification the size increase was not reproducible- two of the replicates had shifted 90th percentile (ECD 156 ± 9 nm) toward larger values, but in one replicate smaller particles were measured after coating. It is anticipated that in case of higher magnification images the charging of uncoated sample though not apparent could affect the result. The uncoated particles of SAS were generally more difficult to discriminate from the background in comparison to coated ones due to the poor contrast (see Figure A1.4). Coating allowed defining boundaries of SAS particles better.

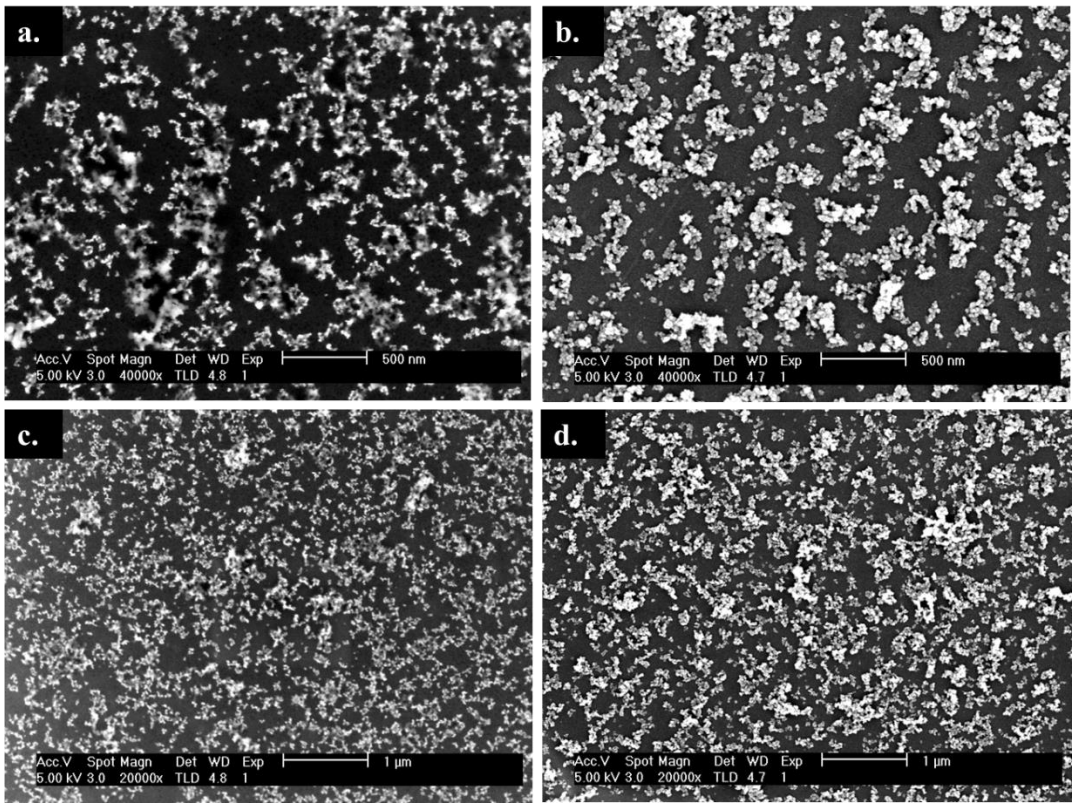

Figure A1.4- SEM images of SAS without coating (left) and coated (right) at high (a), (b) and low (c), (d) magnification

Therefore the 8 nm subtraction from the particle size was applied for all the SAS for which measured ECD increase due to the coating was smaller or equal to 8nm. Based on size distribution of coated SAS imaged at lower magnification the ECD at which measured size increase was 8 nm equaled to 116 nm. Therefore for larger particles than 116 nm the linear curve was fitted to measured particle ECD increase at five size points corresponding to range of percentiles (between 73rd to 95th) within size distribution of coated SAS from lower magnification (see Figure A1.5). The particle size increase for coated particles with ECD>116 nm was then calculated from the equation of the fitted curve and subtracted accordingly.

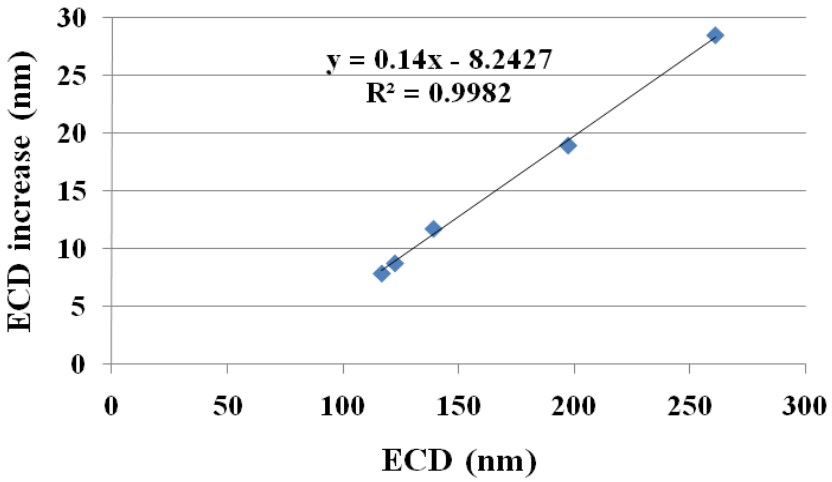

Figure A1.5- The relationship between SAS ECD increase due to the presence of conductive coating and measured ECD of coated particles

Appendix 2

Additional figures for Chapter 4

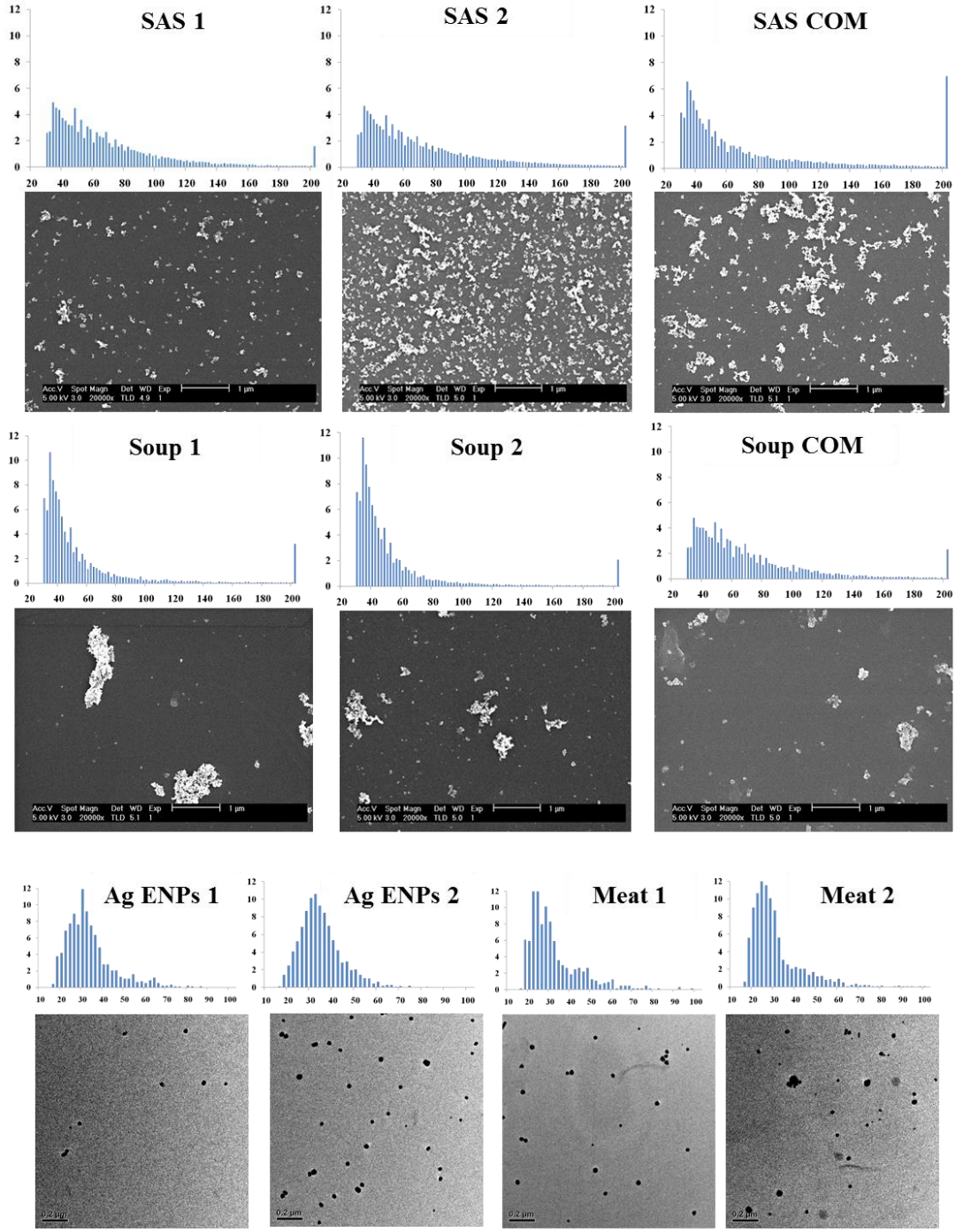

Figure A2.1- Particle size distribution (x axis- ECD, y axis- % of particle count) and below respective EM images of the studied samples (SEM scale bar- 1 µm, TEM scale bar- 0.2 µm), last bin in the size distribution of samples containing SAS corresponds to quantity of particles larger than 200 nm

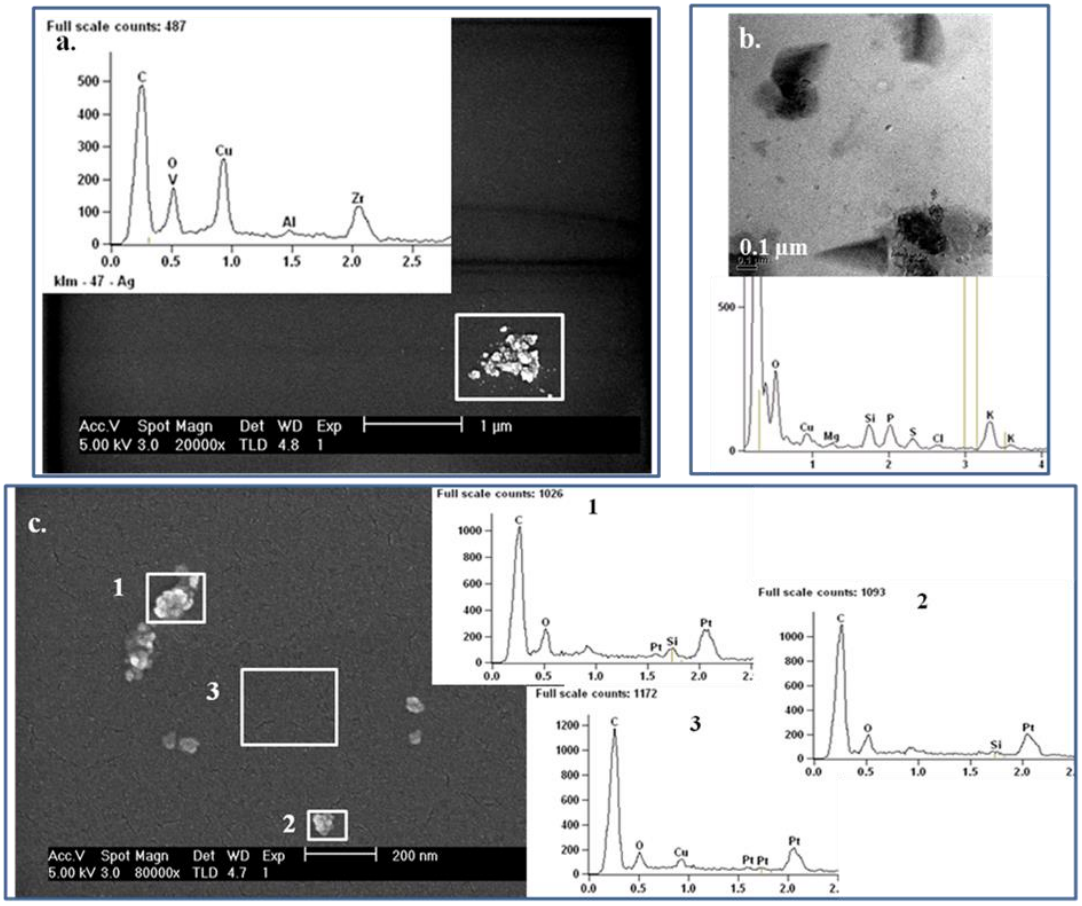

Figure A2.2- EM images and respective EDX spectra (x axis- keV, y axis- number of counts) of a Soup Blank, b Meat Blank, c Soup 1, d and e Meat 2

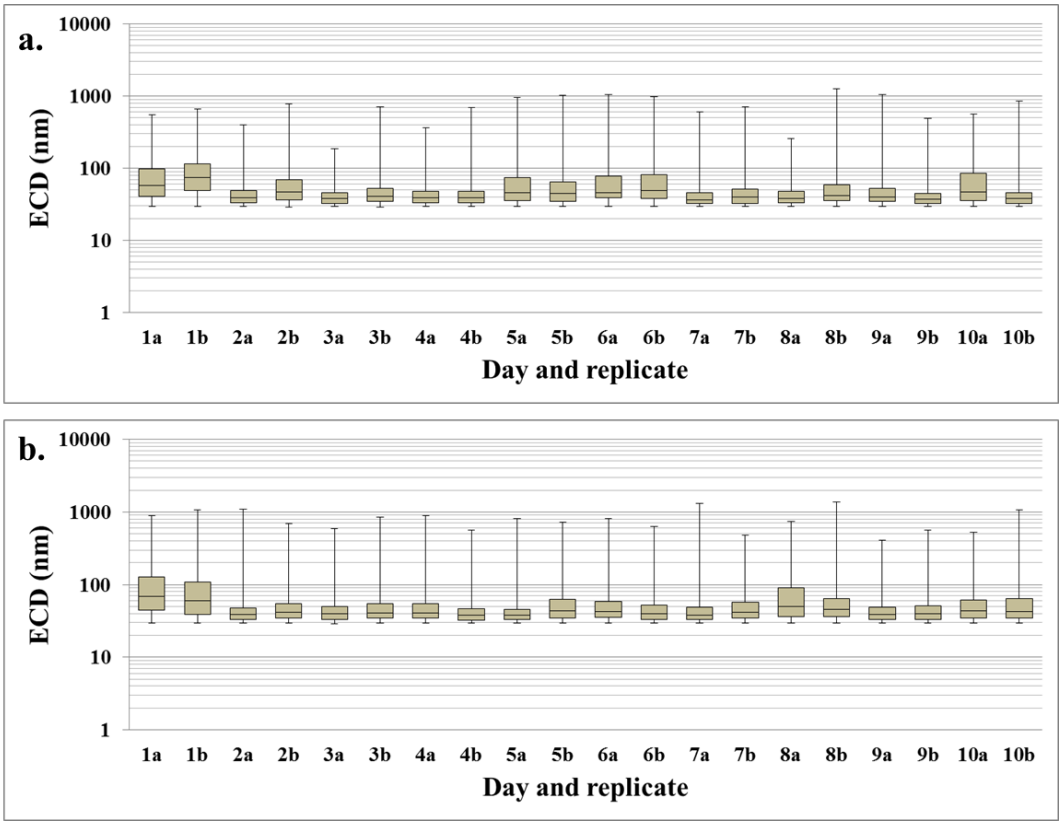

Figure A2.3- The box plot (median, IQR, max and min values) of the particle size distribution in respective replicates of a Soup 1, b Soup 2

Appendix 3

Definition of fractal dimension and fractal prefactor of lacunarity for studied synthetic amorphous silica

The studied SAS sample has an aggregated structure that can be characterised as a fractal aggregate as described in (Boldridge, 2010). The main parameters are the D_f and k_0, that relates the number of primary particles in an aggregate with the primary particle diameter and R_g through Eq. 7.1 described in Chapter 5.

Methodology

The mean primary particle diameter (d_{pp}) value was estimated from nonaggregated residual single particles using identification of these particles by OBIA. Mean value of d_{pp}= 9 nm was used for calculating SAS fractal characteristics as described in (Boldridge, 2010).

In total 3791 SAS aggregates were measured. If the ECD of measured SAS particle was $\leq d_{pp}$, it was assumed that N=1. In larger SAS aggregates the number of primary particles was calculated according to Eq. 5.3 provided in Chapter 5. The D_f and k_0 were derived by plotting linear dependence of ln (N) from ln (d_{max}/d_{pp}) (Figure A3.1). The d_{max} was Ferret's diameter directly measured from the SEM images and reduced by 8 nm to correct for the conductive coating thickness.

Result

The plot of ln (N) from ln (d_{max}/d_{pp}) is presented in Figure A3.1.

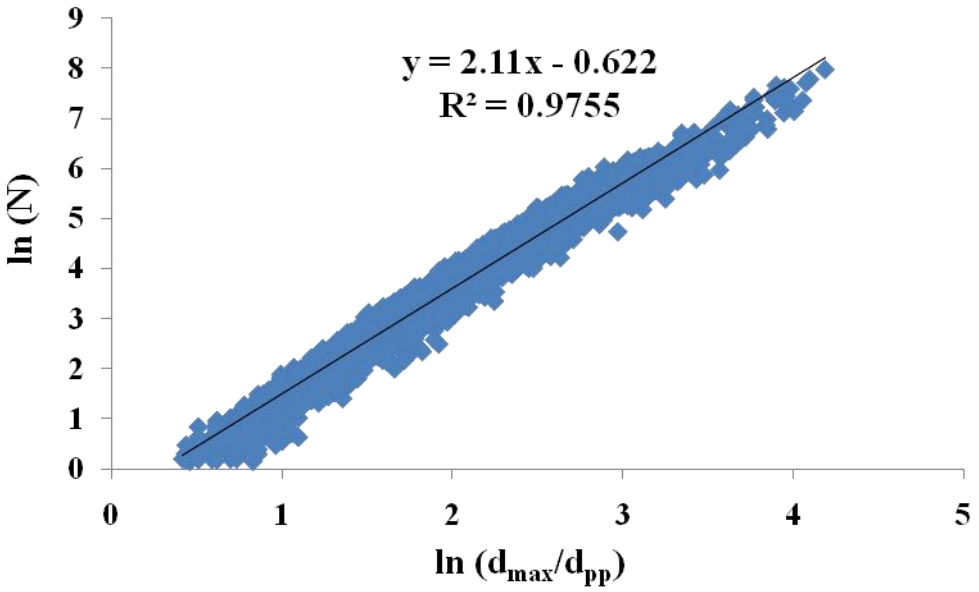

Figure A3.1- Linear curve fit to dependence of ln (N) from ln (d_{max}/d_{pp})

The D_f was equal to the slope of the linear curve (2.11) and k_0 was calculated from Eq. A3.1 (Boldridge, 2010) and gave value of 1.17.

$$k_0 = 0.69^{-D_f} e^b \qquad \text{Eq. A3.1}$$

Where:

e- mathematical constant

b- the linear curve coefficient determining the intercept

The generated curve was based on the measurement of all aggregates in 3 sample replicates. The maximum difference in between replicates in estimate of D_f was 0.06 and k_0 0.08.

Appendix 4

Glossary

Abbreviation/ symbol	Full length name
A	Centrifugal acceleration
AA 8.0	Amonnium acetate buffer pH 8.0
AF4	Assymetric flow field flow fractionation
ANOVA	Analysis of variance
BB 8.0	Borate buffer pH 8.0
BET	Brunauer-Emmett-Teller
BSE	Back scattered electrons
c_c	Cunnigham slip correction factor
CE	Capillary electrophoresis
Cryo-	Cryogenic
d	Diameter
D_f	Fractal dimension
DLS	Dynamic light scattering
d_{max}	Ferret's diameter
DMW	Demineralized water
d_{pp}	Primary particle diameter
DSC	Differential scanning calorimetry
e	Mathematical constant
EC	European Commission
ECD	Equivalent circle diameter
EDS	Energy-dispersive X-ray spectroscopy
e_e	Elementary charge
EELS	Electron energy loss spectroscopy

Appendix 4 Glossary

EFSA	European Food Safety Authority
EFTEM	Energy filtered transmission electron microscopy
ELS	Electrophoretic light scattering
EM	Electron microscopy
EMD	Electric mobility diameter
ENP	Engineered nanoparticle
ESEM	Environmental scanning electron microscopy
ESI	Electrospray ionisation
ETEM	Environmental transmission electron microscopy
f	Particle number overestimation factor
FFF	Field flow fractionation
FIB	Focused ion beam
GEMMA	Gas-phase electrophoretic mobility molecular analyser
HAADF	High angle annular dark field
HDC	Hydrodynamic chromatography
HDD	Hydrodynamic diameter
HRTEM	High resolution transmission electron microscopy
h_s	Sample thickness
ICP	Inductively coupled plasma
IED	Instrument equivalent diameter
IQR	Interquartile range
IQR%	Relative to median interquartile range
IS	Ionic strength
k	Coverage factor
k_o	Fractal prefactor of lacunarity
LOD	Limit of detection (concentration)
LOD_{ENP}	Lowest detectable nanoparticle mass concentration
LOD_{matrix}	Mass concentration limit of detection for nanoparticles in food

	matrix related to matrix interference
MALLS	Multiangle laser light scattering
MALS	Multiangle light scattering
MANOVA	Multivariate analysis of variance
MED	Mass equivalent diameter
MS	Mass spectrometry
MSB	Mean squares of measurements obtained on different days
MSW	Mean squares of measurements obtained on same day
N	Number
n	number of electric charges on the particle
NMR	Nuclear magnetic resonance
OBIA	Object based image analysis
p	Statistical significance level
P	Probability of the sample containing given number of the false positive particles
PNC	Particle number concentration
PNSD	Particle number- size distribution
PVC	Polyvinyl-chloride
R_g	Radius of gyration
RSD%	Relative standard deviation
RSD_{dd}	Standard measurement uncertainty of measurements performed on different days
RSD_i	Standard measurement uncertainty of imaging
RSD_{ia}	Standard measurement uncertainty of image analysis
RSD_{ip}	Standard measurement uncertainty of intermediate precision
RSD_r	Standard measurement uncertainty of repeatability
RSD_s	Standard measurement uncertainty of sampling
RSD_{sp}	Standard measurement uncertainty of sample preparation

Appendix 4 Glossary

RSD_{total}	Total standard measurement uncertainty
S	Mean number of particles found per replicate for a blank sample
s	Mean
s.d.	Standard deviation
SANS	Small angle neutron scattering
SAS	Synthetic amorphous silica
SAXS	Small angle x-ray scattering
SEC	Size exclusion chromatography
Sed-FFF	Sedimentation field-flow fractionation
SEM	Scanning electron microscopy
size LOD	Limit of detection (particle size)
size LOQ	Limit of quantification (particle size)
SLS	Static light scattering
SP-ICP-MS	Single particle inductively coupled plasma mass spectrometry
SMPS	Scanning mobility particle sizer
SSA	Specific surface area
SSD	Stoke's sedimentation diameter
STEM	Scanning transmission electron microscopy
TEM	Transmission electron microscopy
t_s	Sedimentation time
U_{exp}	Expanded uncertainty
UV-VIS	Ultraviolet- visible spectrophotometry
W	Channel thickness
WDS	Wavelength-dispersive X-ray spectroscopy
Wet-	Prefix prior to imaging method meaning liquid imaging
x	Distance from the injection point to the detector in CLS
XRD	X-ray diffraction
Z	Atomic number

Appendix 4 Glossary

Z_c	Electric mobility
ζ	Zeta potential
η_a	Viscosity of air
η_w	Viscosity of water
η_s	Viscosity of the sucrose gradient
λ	Wavelength
π	Mathematical constant
ρ_f	Density of the sucrose gradient
ρ_{pe}	Effective density
ρ_{SiO2}	Density of silica
V_c	Cross-flow volumetric flowrate
V_{out}	Volumetric outlet flowrate
k_B	Boltzmann constant
D	Diffusion coefficient
T	Temperature
H	Viscosity of dispersing medium

Discussion on interpretation of the measurement results of synthetic amorphous silica in view of mass equivalent diameter transformation and small particle abundance correction.

Introduction

The transformations of measurements outputs from different techniques into MED for the fractal aggregate of SAS allowed uniform expression and result comparison (Chapter 5). Thanks to this, it was also possible to calibrate the sample preparation method for SEM in order to correct for its specificity toward small particle size fraction (Chapter 6). However, in previous Chapters 3 and 4 the SAS measurements from EM were given as ECD. This did not allow to relate EM measurement against the reference method HDD from NTA in Chapter 3 or calculation of the particle mass recovery (Chapters 3 and 4). Another highlighted issue in the previous work (Chapter 4) was inability of the estimation of measurement trueness for SAS due to lack of certified reference material and/or measurement technique against which the result could be compared. The problem was a consequence of the particle shape.

The aim of this chapter was to use MED transformation and corrective calibration for selected EM sample preparation in order to address the issues raised in Chapters 3 and 4. Therefore the data from these two chapters are interpreted again in regards to comparison against reference method, recovery and trueness assessment.

Methodology and data

The NTA and SEM measurements of SAS in stock dispersion and soup generated in previous Chapters 3 and 4 were used in this study. The respective HDD and ECD measurements were transformed into MED as described in Chapter 5 to allow discussion on their comparability. Based on thus transformed data mass recoveries in relation to initial sample concentration were calculated. The calculation of total recovery was not possible for blotting techniques because of unspecified sample volume. The recovery for SAS particles in soup using blotting techniques was discussed instead as relative to the mass of the particles acquired from the stock dispersion. Additionally all the results where T2 Gel sample preparation protocol was used (part of Chapter 3 and whole chapter 4) were corrected for specificity of the method toward smaller particles using Eq 6.3 developed in Chapter 6. The

correction was carried out using MED transformed particle measurements grouped in the histograms of bin width 1 nm. This correction allowed the discussion on the trueness of the particle size measurement and comparison of SEM MED measurements of SAS against reference method- NTA. For trueness assessment it was assumed that the corrected median size measurement using Eq. 6.3 was the true median size of SAS PNSD measured in the study. This assumption was taken because as shown in Chapter 6, using correction it was possible to obtain median MED measurement for SAS, which was not significantly different to GEMMA used as reference method. The trueness was calculated for ECD and MED based PNSDs of SAS according to (Linsinger, 2010) using instead of the certified reference measurement the value measurement corrected for the initial overestimation of the particle number in small size fraction Eq. 6.3.

Results and discussion

Comparison of mass equivalent diameters of synthetic amorphous silica derived by electron microscopy and nanoparticle tracking analysis from Chapter 3

The comparison of SEM and NTA measurements given as IEDs in Chapter 3 aimed to verify which of the sample preparation procedures for SEM caused agglomeration of SAS ENPs. The assumption was that NTA will give a larger or even median measurement to SEM if no agglomeration occurred. The transformation of SAS measurements into MED ideally would allow one to obtain not significantly different results from both techniques. However, in previous chapters it was determined that NTA was subjected to Size LOQ (Chapter 5) and some of the sample preparation methods for SEM were specific toward particles of small size (Chapter 3 and 5). Thus generally it could be still expected that the median MED of PNSD of SAS from NTA could be larger to this of SEM. Only T2 Gel sample preparation method was calibrated and corrected for overestimation of small particle number in the PNSD. Thus in Figure 1 full MED weighted PNSD of SAS in soup and stock as measured by NTA and SEM preceded by T2 Gel preparation are compared.

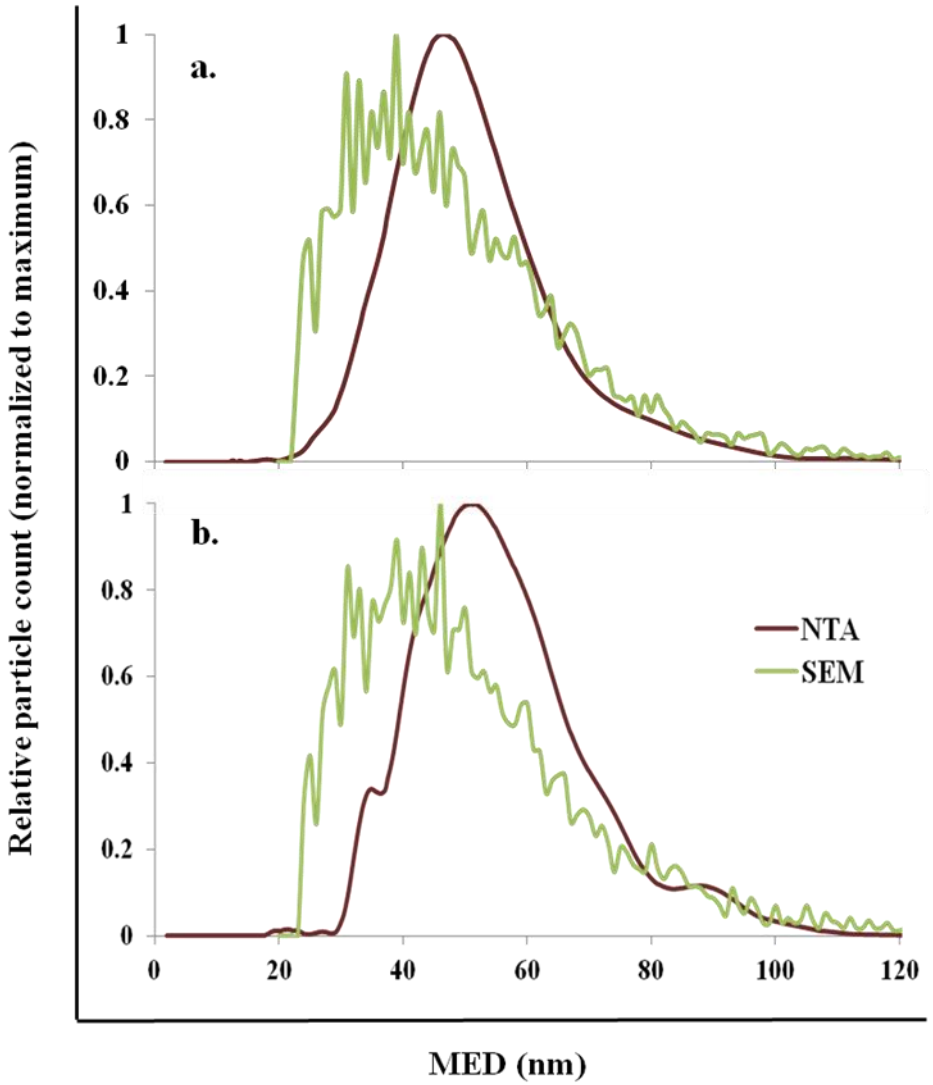

Figure 1- PNSD of SAS in a) stock and b) soup as revealed by NTA and SEM using T2 Gel sample preparation

Both methods show similarities in PNSDs in terms of size range. However, it can be noticed that PNSD from NTA has nearly Gaussian distribution whereas from SEM is positively skewed. This was a result of Size LOQ in NTA given PNSD, which was (mean ± s. d.) 47±3 nm and 50±5 nm for SAS in stock and soup respectively. These Size LOQ's between soup and stock were not significantly different from each other (Holm-Sidak $p>0.05$), but lower than previously indicated stock dispersion of SAS in Chapter 5 (66±11 nm, Holm Sidak $p<0.05$)). This was likely attributed to the model of the NTA, which was different in Chapters 3 and 5.

Despite the presence of Size LOQ in NTA given PNSD the statistical comparison of MED transformed results for SAS measured by NTA and SEM after preparation by different methods was carried out. This was done to verify conclusion in Chapter 3

on the sample preparation methods for SEM which did not induce particle agglomeration.

Figure 2 presents the box and whiskers plot of SAS MED distribution between readings from single SEM (images) and NTA (videos). The figure is a counterpart of Figure 3.4 presented in Chapter 3, which was based on ECD measurements. Same statistical analyses were run on the MED transformed data as previously described for ECD measurements in Chapter 3.

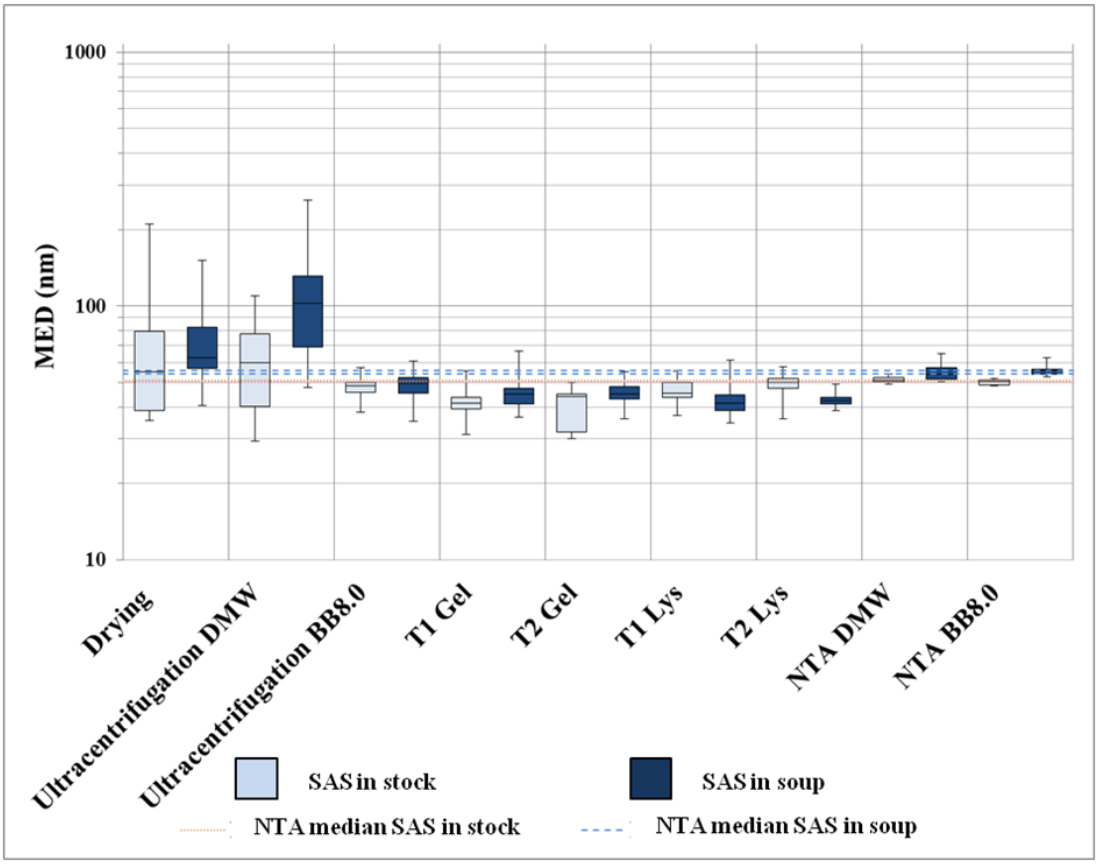

Figure 2- Box and whiskers plot of median MED measurements per reading (Image-SEM and Video-NTA). The figure is a counterpart of the Figure 3.4 where all the measurements were expressed as ECD.

The MED transformation generally did not change results of statistical comparison of the SAS measurements generated by SEM and NTA. The only exception was SAS in stock prepared using T1 Lys protocol. This measurement was now not significantly different to NTA (Tukey, $p>0.05$). This slight difference was attributed to generally decreased difference in between PNSD of SEM and NTA measurements expressed as MED in comparison to IED's as previously discussed in Chapter 5. Here it was found that for all the sample preparation methods the difference between

median MED of NTA and SEM decreased at least 1.7 times relatively to NTA given MED when compared to IED.

Nevertheless it was confirmed that sample preparation methods for SEM, which did not induce SAS ENPs agglomeration were previously correctly assessed in Chapter 3.

Total mass recovery of silica in nanoparticle tracking analysis and scanning electron microscopy in Chapter 3

Previously (Chapter 3) the PNC measured by NTA was used to calculate particle number recovery of SAS in SEM analyses preceded by 3 sample preparation techniques: Ultracentrifugation in DMW, BB8.0 and drying. However, total recovery in relation to the particle concentration in the initial, undiluted sample could not be calculated. The transformation of the measurements into MED, allowed to calculate total recovery (in relation to initial manufacturer claimed mass of ENPs in dispersion) for SAS in stock and soup samples analysed by NTA and SEM. The results are shown in Figure 3.

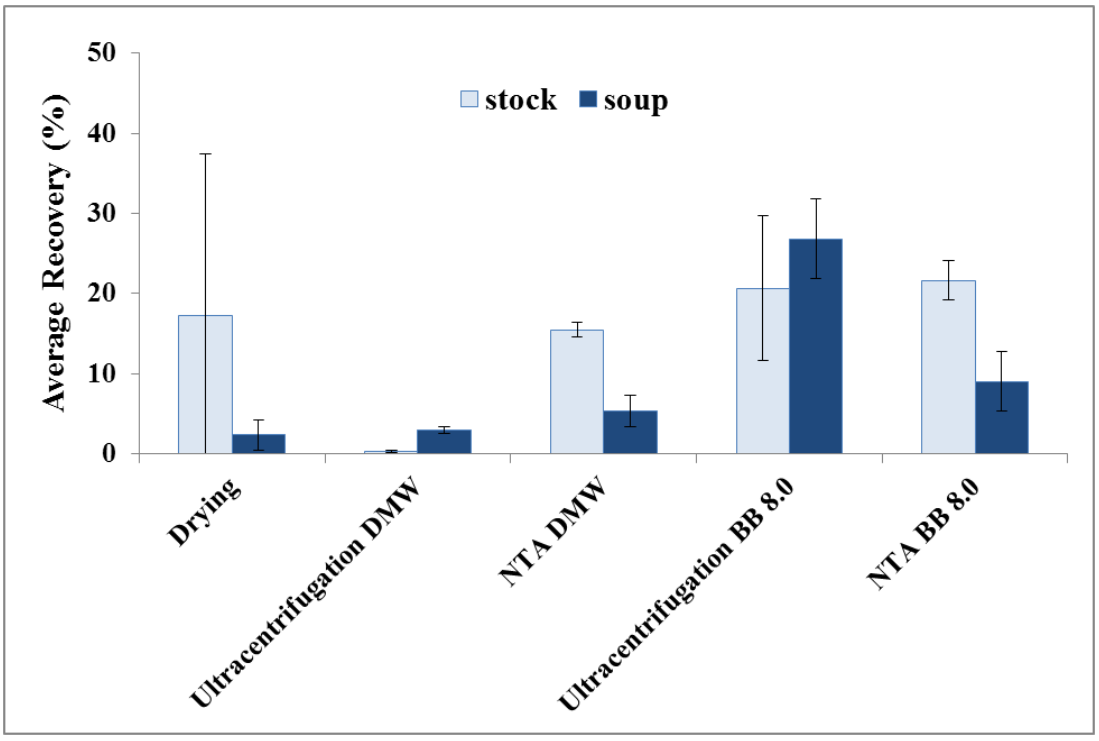

Figure 3- Particle mass recovery in relation to used sample preparation in SEM and as revealed by NTA (error bars are s.d.)

It can be noticed that for all SEM and NTA analyses on average less than 30% of particles was recovered when compared to initially claimed mass concentration in the samples. The low recoveries could be partly attributed to Size LOQ in NTA and cut-off point in SEM analyses (MED 22 nm). However, based on corrected distribution of particles in MED range of 8 to 22 nm (Chapter 6) constituted only about 1% of total measured particle mass.

Again it needs to be emphasized that NTA and SEM are also affected by the largest measurable particle size (up to 1000 nm) and are based on single particle measurement. Thus omitting a fraction of very large but not abundant particles, which have a high contribution to the total particle mass could have place bringing the recovery down by a very significant value.

Statistical analysis did not prove any significant differences in recoveries of SAS particles within stock dispersions (ANOVA $p>0.05$) measured by NTA and SEM preceded by different sample preparation methods due to very high variability in measured particle number (see Chapter 3, Figure 3.5) and thus mass recoveries variability. The recovery of SAS in soup was significantly higher for the sample prepared by ultracentrifugation in BB 8.0 (Holm-Sidak $p<0.05$) in comparison to other sample preparations and NTA analyses. This was expected as previously reported (Chapter 3) particle number recovery for this sample and sample preparation was high (120% for SAS in stock and 221% for SAS in soup). The mass recoveries of SAS particles in both types of samples (soup and stock) were not different between NTA measurements in BB 8.0 and DMW. This was contrary to what could be expected based on measurement of PNC by NTA in Chapter 3, where it was concluded that the DMW inflicted higher losses of SAS particles in the dilution process than BB 8.0.

Recoveries of synthetic amorphous silica from fresh and aging soup using electrostatic attraction preparation for electron microscope

The total SAS mass recoveries from EM for a range of techniques using electrostatic attraction for sample preparation could not be calculated. Therefore the discussion is limited to the mass recovery of the SAS particles from soup samples in relation to the SAS stock dispersions prepared by same means. Within this research two types

of samples were used for analysis: soup freshly spiked with SAS (Chapter 3) and aging together with particles (Chapter 4). The mass recoveries of particles from soup samples freshly spiked with particles were ranging on median from approximately 60 to 110% (Figure 4), which was higher than could be expected from particle counts in soup relatively to stock dispersions (see Figure 3.5, Chapter 3).

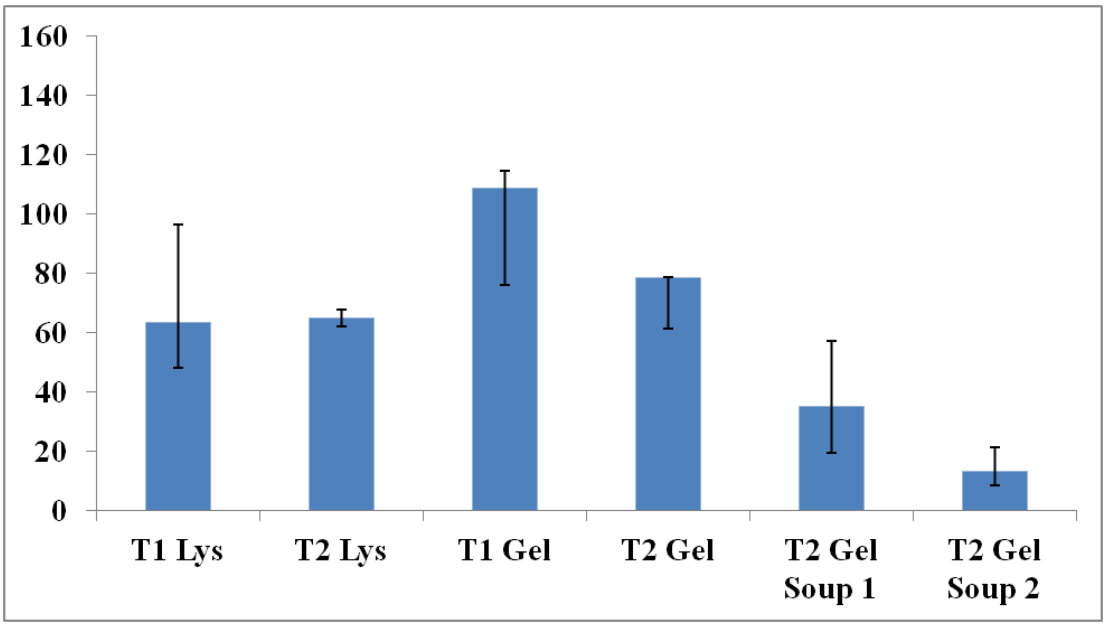

Figure 4- Median mass recoveries and IQR (error bars) of SAS particles from soup relatively to stock dispersions, columns corresponding to T1 Lys, T2 Lys, T1 Gel and T2 Gel are derived from data in study on soup freshly spiked with particles (Chapter 3), while T2 Gel Soup 1 and Soup 2 from the study where matrix was aging with the particles prior to analysis (Chapter 4)

The results also confirm that the recoveries of SAS particles from aging soup were generally lower than for freshly spiked one (Chapter 4). However, significant difference was only confirmed for Soup 2 sample (Dunn's test $p<0.05$). The mass recoveries of SAS from aged soup were expected to be lower than the number recoveries discussed in Chapter 4 (calculated based on number of particles obtained from stock dispersions analyses), because the particles were on median smaller in Soup 1 and 2 samples when compared to the respective stock dispersions. However, this was only the case for Soup 2. Mass recovery of SAS particles from Soup 1 was actually higher than reported in Chapter 4 particle number recovery (38% and 19% respectively). This was likely a result of particle aggregation in soup and rapid increase of mass particle recovery by inclusion of few large aggregates in total mass

calculation (max MED of SAS in stock: 210 nm and in soup: 311 nm). The mass recovery of particles in Soup 2 was lower than in Soup 1 (although not significantly: Dunn's $p>0.05$) because the measured median size of SAS 2 particles was larger than SAS 1 as a result of grid saturation with particles and potential overlap during image analysis (See Figure A2.1 Appendix 2).

The assessment of scanning electron microscopy measurement trueness for synthetic amorphous silica

Previously in Chapter 4 estimates of ECD measurement uncertainty for SAS in soup and stock dispersion was obtained. The total expanded uncertainty (U_{exp}) did not inlude the estimate of the measurement trueness for polydispersed particles of SAS. Only 'goodness' of instrumental calibration was assessed using nearly monodispersed, spherical gold ENPs. Developed in Chapter 6 calibration allowed to estimate the measurement trueness for SAS. Results are summarised in Figure 5. Additionally intermediate precision (RSD_{ip}) and U_{exp} previously reported in Chapter 4 for SAS in stock and soup dispersions at concentrations 1 and 2 were included in the graph. The results for SAS COM and Soup COM (also Chapter 4) were not included in this discussion because they would require separate definition of fractal characteristics in order to be subjected to MED transformation.

The RSD_{ip} of the median ECD was higher after correcting for small particle abundance for all the samples with exception of SAS 1. The uncertainty increase was expected as the correction could only be applied to the results after MED transformation and thus some error related to multiple data transformation needed to be included. The RSD_{ip} increase was however minor (1-5%) and thus not significant (F test $p>0.05$).

The estimated trueness of ECD measurements was similar for all four samples (F test $p>0.05$) ranging from 17% to 22%. These values were much higher than previously reported 'goodness of calibration' trueness (1.9%) and in comparison to RSD_{ip} were significantly higher for SAS 1 and 2 (F test $p<0.05$) and not different for Soup 1 and 2. This meant that the trueness was bound to significantly increase the U_{exp} budget. The increase of U_{exp} was most pronounced for SAS measurements in stock dispersions, where it was higher than two fold in comparison to the initially estimated in Chapter 4 (Figure 5).

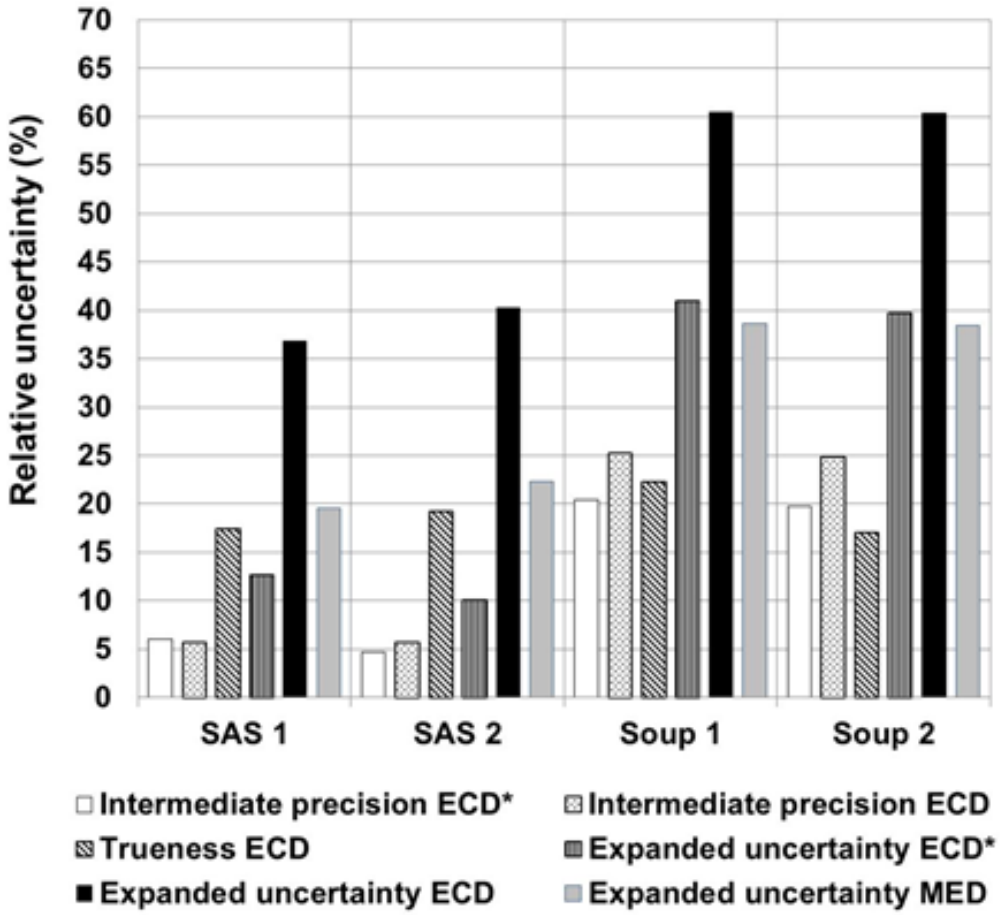

Figure 5- Errors introduced to the measurement of SAS and combined expanded uncertainty of median measurements.*-initial results quoted from Chapter 4

The U_{exp} calculated for the MED median measurements was generally lower than one related to ECD (37% to 60%) and ranged from 20 to 44% although this difference was proven to be significant only for SAS 1 and 2 (F test, $p<0.05$). This improvement on measurement certainty is attributed to the general narrowing of PNSD after MED transformation (Chapter 5).

Conclusions

Thanks to the data transformation form ECD into MED transformation it was possible to confirm that the previous classification of sample preparation methods to inducing and non-inducing agglomeration (Chapter 4) for SAS in stock and soup dispersions was correct. It was also possible to obtain total mass recovery of SAS in stock and soup for SEM and NTA analyses. Additionally applied correction for the sample preparation method specificity to small particle size fraction allowed to

correct previously reported measurement uncertainty (Chapter 4) for trueness value. The trueness occurred to be a significant factor affecting U_{exp}. This result points out that the EM should not be used for the measurement of ENPs characterised by a broad size distribution not only in foods but also in pristine dispersions unless calibrated as demonstrated in Chapter 6. This was so far neglected in the studies on ENPs measurements. The MED transformation was found to bring down the measurement uncertainty. This is another useful argument in using MED as means of uniform measurement expression for fractal aggregates from different measurement techniques.

In summary future work should focus either on sample preparation development or/ and calibration for polydispersed ENPs as this thesis only provided solution for specific case of silica ENPs. However, means of obtaining information on the measurement accuracy from EM was given, providing a tool for future research.

3

Detecting and characterizing nanoparticles in food, beverages and nutraceuticals.

A. Dudkiewicz, University of York, UK and Food and Envrionment Research Agency, UK, P. Luo, university of York UK, K. Tiede, Food and Environment Research Agency, UK and A. Boxall, University of York, UK

Abstract: While nanotechnology offers a number of benefits to the food sector, the use of nanoparticles (NPs) in food may also cause risks. In order to understand the risks of NPs, it is essential to have access to good quality analytical methods that are able to detect and characterise NPs in a wide range of media. This chapter provides an overview of the characteristics of NPs that will need to be measured in food materials and describes methods that are available to derive these characteristics. The advantages and drawbacks of each method are described and the challenges for the development of new methods for NP analysis in food materials are highlighted.

Keywords: characterization, nanoparticles, food, analytical methods, sample preparation

3.1 Introduction

Nanotechnology is increasingly being applied in the food and pharmaceutical industry and provides a wide range of benefits. However, due to the fact that we know very little about the behaviour of nanoparticles (NPs) in food items and their interactions with the human body, there are concerns that the use of nanotechnology may pose a risk to food quality and consumer health.

One of the factors that is limiting the development of our knowledge of the behaviour of NPs in food and potential toxicity to humans is the availability of validated techniques for NP analysis within food matrices. Analytical method development for detection and characterization of nanoparticles has been recognized by international organizations, including the European Food Safety Authority (EFSA, 2009) and the US Food and Drug Administration (U.S. FDA, 2010), as one of the major issues that needs addressing concerning the risks of NPs. A number of research projects are therefore currently tackling this issue (CORDIS, 2010). The biggest challenge concerning the detection and characterization of NPs is that, unlike 'traditional' chemicals, we are not only interested in the concentration of the NP but also other characteristics such as particle size distribution, particle shape and the characteristics of the surface coating (Norwegian Pollution Control Authority, 2008). No single analytical method can currently provide information on all of these details at once.

The majority of food products comprise complex structures and usually some form of sample preparation is required before an NP can be detected and characterized. Many of the potential pre-treatments that food samples might undergo, prior to analysis, are known to have an impact on the NP structure. For example, drying may cause aggregation of NPs and hence, if this approach is used for analysis of particle size distribution in a food product, misleading results will be obtained (Domingos *et al.*, 2009; Doucet *et al.*, 2005). NPs also occur naturally so a further challenge is how to distinguish between NPs that are man-made and NPs that are naturally present in food stuffs.

This chapter therefore provides an overview of the available methods that are potentially suitable for the characterization of NPs in food and nutraceuticals and discusses the advantages and limitations of the different methods for food analysis. More detailed reviews can be found in Tiede *et al.* (2008) and Dudkiewicz *et al.* (2011).

3.2 Detecting and characterizing- but what?

Results of many toxicological studies indicate that for risk assessment, a range of characteristics of an NP may need to be considered, including aggregation state, surface charge, shape, structure, dissolution rate, chemical composition and mass and particle number concentration.

Aggregation causes increases in size and a decrease in the particle number concentration (PNC) of an NP, which may result in changes in reactivity and functionality of these particles. Aggregation of NPs can be prevented by electrostatic stabilisation or steric stabilisation. Electrostatic stabilisation is created by repulsive electrostatic double layer forces between charged NPs. The charge of the NP in the environment in which the NP is dispersed depends on factors such as pH and ionic strength (IS) of the environment and can be determined from the zeta potential (ζ) of the particle. Steric stabilisation involves the use of long chain molecules as 'capping' agents on the particle surface. The capping agents provide steric hinderance for the agglomeration of particles independently of pH or ionic strength of the dispersion environment. Examples of capping agents include surfactants, polymers and proteins. Of special interest are interactions of the NP surface with proteins, since they may influence the fate of NPs in an organism (Lynch & Dawson, 2008). How these interactions proceed depends on several NP features such as the surface charge (Bouwmeester *et al.*, 2009) and structural properties such as shape and crystalinity.

Shape is a very important factor which might influence uptake and distribution of an NP within humans and other mammals and its toxicity (Norwegian Pollution Control Authority, 2008). Shape dependent toxicity might explain the toxicological effects of carbon nanotubes which, though much smaller in diameter, are shaped similarly to asbestos fibres and act in a similar manner to asbestos, causing necrosis of the lung in mice (Lam, 2003).

Crystalinity has an impact on the stability of an NP and its reactivity (Jiang *et al.*, 2008; Barnard *et al.*, 2010). For example amorphous forms of titanium dioxide NPs have been found to have the strongest oxidative abilities when compared to crystalline forms (Jiang *et al.*, 2008). This property has to be considered in food industry applications since reactive oxygen species (ROS), when accumulated in the body, are harmful, sometimes resulting in carcinogenicity and causing many other

disorders (Diplock *et al.*, 1998). Furthermore ROS may reduce the shelf life of a food product and affect its structure (Chen *et al.*, 1999).

Dissolution rate is as important as aggregation state. Ions will behave very differently than NPs and in some instances may be more toxic e.g. the gradual dissolution of silver NPs explains the increases in toxicity of stored dispersions to human mesenchymal stem cells (Kittler *et al.*, 2010). The functionality of an NP, which also depends on their chemical composition, will have a strong effect on the behaviour of an NP. The food industry uses this to their advantage when designing NPs for use in novel products (see chapter 1 and (Chaudhry & Groves, 2010)).

Mass concentration can be measured for NPs as for 'traditional' substances. However a more useful measure of exposure may be the particle number concentration (PNC). PNC is closely connected to some of the other NP features described above such as size, aggregation and dissolution, density.

3.3 Challenges in detecting and characterizing nanoparticles in food products

There are three major challenges that need to be addressed in order to analyse NPs in food items. Firstly, the characterization of the NP itself is challenging and, although a range of validated methods exist, none of them can provide information on all of the characteristics of an NP required to assess risks to human health. Some of the characteristics can also be extremely difficult to determine, requiring sophisticated instrumentation. Table 1 provides an overview of which techniques are able to characterize specific features of an NP. Method development for NP characterization is an on-going issue and a subject of extensive current research. Secondly, food products are made up of complex matrices. Therefore care has to be taken when preparing a food sample for analysis so that the sampling is representative. In some cases NP can be expected to be localized in restricted areas of the sample. For example, in the case of migration studies from food contact materials, analysts can expect that NPs are situated on the surface of the food packed in it. For some NPs (e.g. carbon-based NPs), it may be difficult to distinguish the NP from the background. Thirdly, food matrices will also contain natural NPs (e.g. casein micelles, whey proteins, fat globules and particulate material that may have deposited onto e.g. a crop from the atmosphere) making interpretation even more problematic (Peters *et al.* in press). For example, nano delivery systems (NDS) are usually composed of lipids, proteins or polysaccharides (Luykx *et al.*, 2008), which are all naturally present in food products making detection very difficult.

To overcome some of these issues it may be necessary to exclude or limit the presence of food components from the analysis by using extraction methodologies. The use of extraction methods adds additional complications as the method used can cause a change in the NP characteristics meaning valuable data might be lost or, in some cases, incorrect results are obtained. It will also be necessary to develop approaches that can distinguish between man-made particles and particles that occur naturally.

Table 3.1- Use of analytical methods for characterization of relevant features

	Size & Size distribution	Aggregation	Dissolution	Chemistry	Shape	Structure	Surface charge	Particle number concentration	Mass concentration	Surface area
Chromatography	+		+							
FFF	+	+	+		FFF-SLS, SedFFF-DLS					
CE	+	+	+					+		
Microscopy and coupled analytical techniques	+	+	+	+	+	+				+
Light Scattering	+	+	+	+			ELS	+		
SAXS	+	+			+	+				+
SANS	+	+			+	+				
XRD		+		+		+				
NMR	+	+		+		+				
UV-Vis	+	+							+	
MS	SPMS			+		+			+	
Ultracentrifugation/AN UC	+	+	+	+	+	+			+	
Filtration	+		+							
Dialysis			+							
BET										+
Particle Counters	+	+						+		
DSC		+								
Raman Spectroscopy	+			+		+				

3.4 Methods for detection and characterization of nanoparticles in food products

3.4.1 Chromatography based techniques

Chromatography and related techniques are routinely used in food analysis for separation and characterization of food components and contaminants. These methods have been also applied to the needs of nanotechnology in order to separate NPs out from each other as well as from interfering materials based on size differences (Tiede *et al.*, 2009a; Brewer & Striegel, 2010).

The chromatography-based techniques typically used for size separation of nano-sized objects are size exclusion chromatography (SEC), hydrodynamic chromatography (HDC) and field flow fractionation (FFF). Determination of parameters like concentration or chemical composition of eluting substances is achieved by on-line coupling of these methods to other analytical techniques such as UV detection or light scattering techniques (see section 4.3). Selective qualitative analysis of particles is possible when chromatography is combined with methods employing mass spectrometers (see section 4.4) such as inductively coupled plasma-mass spectrometry (ICP-MS) (e.g. Chan *et al.*, 2010; Tiede *et al.*, 2009a; Tiede *et al.*, 2010; Dekkers *et al.*, 2010). ICP-MS coupled to HDC has been used for NP analysis in complex food samples such as food concentrates as well as in complex environmental matrices (Tiede *et al.*, 2009a; Dekkers *et al.*, 2010). It is also possible to install a fraction collector on the chromatographic system. Separate fractions can then be then analyzed by any technique, which cannot be coupled online to chromatography.

In SEC, the stationary phase consists of porous beads. The space in the pores is easily accessible for smaller particles, which are therefore retained for longer end elute from the column more slowly than larger particles. This process enables separation of NPs by their size or molecular mass. SEC allows separation of particles where molar masses are at least 10% different from each other (Meyer, 2000). The size separation range in SEC depends on the pore size distribution.

HDC separates particles depending on their hydrodynamic radius. Unlike SEC, separation is based on flow velocity in flow channels created by non-porous beads. The size separation range for HDC depends on the length of the column and for commercially available instruments is 5-1200 nm (Tiede *et al.*, 2008).

FFF instruments separate particles ranging in size from 1 nm to a few micrometers (Dubascoux *et al.*, 2010). Partitioning takes place in a thin channel with an applied field, which affects the flow of particles moving through it. There are many types of field that can be used including flow, thermal, electrical and sedimentation. Each field type will influence fractionation of particles depending on the characteristics of the particle. For example differences in diffusion coefficients of particles are used as a basis for separation in flow FFF, while sedimentation FFF separates particles by volume and buoyant mass (Von Der Kammer *et al.* in press). In FFF, unlike HDC and SEC, separation results in elution of smallest particles first (Tiede *et al.*, 2008; Dubascoux *et al.*, 2010).

Electrophoretic methods can also be used. Capillary electrophoresis (CE) employs quartz capillaries filled with a buffer (Cieślik *et al.*, 2008). The flow of the buffer is induced by applying a high voltage. Particles then move with different speeds, depending on their charge and size. This method can also be coupled to numerous

detectors and can be used for the detection and characterization of natural food nanostructures such as nucleic acids, proteins and polysaccharides. CE in food analysis is regarded as an alternative and complementary method to chromatography (Cieślik *et al.*, 2008).

3.4.2 Microscopy based techniques

Microscopy as an analytical technique has found many applications in food science. It is regarded as the most relevant of available methods for food structure analysis (Kaláb *et al.*, 1995) and for last few decades has been extensively used in studies on natural food nano- and microstructures e.g. starches (Fishman *et al.*, 1995), casein micelles (Auty *et al.*, 2005), whey proteins and fat globules (Relkin *et al.*, 2006). Imaging methods are currently applied broadly in NP analysis as they can give information on many features of the NP characteristics which the coupled chromatography techniques described above cannot. Imaging provides data on NP morphology, distribution in the sample, agglomeration, chemical composition, presence and thickness of associated substances. Furthermore it can be used to help to understand the fate of NP in food products and determine the influence of their presence on sample structure (Castaneda *et al.*, 2008). Imaging is also important for validation of other analytical methods which aim to characterize NPs (Tiede *et al.*, 2009a) and natural food nanostructures (e.g. Fishman *et al.*, 1995).

Light microscopy is not usually suitable for NP visualization because its resolving power is limited to 200 nm. The exception is near- field scanning optical microscope (NSOM) where resolutions as low as 12 nm can be obtained (Betzig *et al.*, 1991). In NSOM, the nanometric tip of an optical probe is positioned close to the sample surface, interacting with it. The method is also suited for detection of fluorescent nano objects (e.g. Zhong *et al.*, 2008).

The fluorescence characteristics of some NPs may allow their detection by confocal laser scanning microscope (CLSM; e.g. Lewinski *et al.*, 2010). This type of microscope is capable of optical sectioning of the sample by scanning across it with a focused beam of light. The resolving power of CLSM is usually limited to 200 nm, however, a recent application for 3D, real time tracking of fluorescent particles was able to obtain a lateral resolution of 15 nm and an axial resolution of 50 nm (Katayama *et al.*, 2009).

X-ray microscopes (XRM) can resolve up to 30 nm and, when combined with x-ray microtomography, 3D images can be obtained. In X-ray microtomography, images are obtained from sections of a sample using penetrating X-rays. XRM can be coupled to analytical techniques based on x-ray fluorescence for determination of a samples chemical composition. X-ray fluorescence microscopy has been used for example in studies on secretion and accumulation of intracellular Zn in mammary glands of mice where it enabled imaging and quantification of Zn transferred through the gland (McCormick *et al.*, 2010)

Another way of non-invasive imaging of a sample containing NPs is atomic force microscopy (AFM). This technique employs a nanometric mechanical probe which is scanned over the sample surface, recording its shape. AFM offers resolution down to 0.1 nm (Tiede *et al.*, 2008). If a functionalized probe is used, data can also be generated on the chemical characteristics of an NP. This method is known as chemical force microscopy (CFM). CFM measurement is based on chemical interactions of the tip with the sample, enabling characterization of chemical heterogeneity of the imaged surface on a nanometric level (Ito *et al.*, 2010).

The most commonly applied microscopy approaches for NP imaging are Transmission Electron Microscopy (TEM) and Scanning Electron Microscopy (SEM). In TEM, the electron beam is accelerated with high voltage (80-400 kV) and passes through the nanometric layer of the sample. The resolution of these instruments can go down to 0.07 nm (Dudkiewicz *et al.*, 2011). SEM offers a lower resolution of 1-3 nm but also a different image pattern in comparison to TEM. Images are formed by the detection of electrons scattered by the sample surface. Additionally, SEM can be coupled with focused ion beam (FIB-SEM), which enables sample sectioning and 3D imaging. Similar to SEM, scanning transmission electron microscope (STEM) scans the sample with a focused beam of electrons. However in STEM signal is obtained as in TEM from the electrons transmitted through the ultrathin specimen, and as in TEM, resolution of STEM reaches atomic level.

Electron microscopes (EMs) in conventional modes operate under vacuum. Therefore food samples cannot usually be imaged without previous preparation (discussed in section 4.5). However, by modifying the way in which the sample is introduced to the conventional EM, imaging of food can be achieved. A range of approaches are available for doing this including cryo- and liquid EM. For cryo techniques (cryo- TEM, cryo- SEM, cryo- FIB-SEM), the sample is imaged when frozen. Liquid EM employs capsules (e.g. WetSEM^{TM}) and chips which separate the hydrated sample from the vacuum chamber of conventional instruments. The sample is then imaged through electron transparent windows. Cryo-, environmental and liquid EM have been shown to be useful for analysis of ENPs in cosmetics, food and environmental media (Noronha *et al.*, 2008; Tiede *et al.*, 2009b; Lorenz *et al.*, 2010), they do however have a lower resolving power in comparison to conventional TEM and SEM.

An alternative approach to analyzing hydrated food samples is to use environmental SEMs and TEMs (ESEM, ETEM) which also allow a sample to be imaged in its original state. In these techniques, imaging takes place under a lower pressure than in conventional instruments. One limitation of these methods is that they do not operate under atmospheric pressure and so, only partially hydrated specimens can be viewed.

Chemical characterization of the sample is possible by means of coupled spectrometers. The electron beam employed in EM excites the atoms with a specimen resulting in the emission of x-rays. The chemical composition of the sample can therefore be characterized based on the detection of x-ray radiation energy using energy dispersive spectroscopy (EDS) or wavelength dispersive spectroscopy (WDS). The energy loss of the electrons transmitted through the sample can also provide information on sample characteristics, this is the basis of electron energy loss spectrometry (EELS). Unlike EDS and WDS, EELS cannot be coupled to most types of EMs and is only compatible with TEM.

3.4.3 Spectroscopy-based techniques

Given the quick and easy sample preparation, a wealth of spectroscopic methods is widely applied for food residue analysis and quality control (Karoui & Debaerdemaeker, 2007). Some of these techniques can also provide information on the characteristics of NPs in food samples, including concentration, size, and structure (Valous *et al.*, 2010). This section provides an overview of all the different spectroscopy-based methods that could be used to characterize nanoparticles in food matrices.

Scattering spectroscopy is the most common method applied to date for particle analysis (Dodds *et al.*, 2004). It measures the amount of light that a substance scatters at certain wavelengths, incident angles, and polarization angles, where the interference patterns can be detected to measure the molecular weight and/or particle size. Dynamic light scattering (DLS, 3 - 1000 nm) is the main scattering techniques used for NP size measurements in liquids (Brar & Verma, in press) and provides data on PNC. The hydrodynamic diameter, indicating the apparent size of the dynamic hydrated/solvated particle (Kaszuba *et al.*, 2007; Mishchenko, 2009), is also estimated. A similar approach is nanoparticle tracking analysis (NTA). In NTA, Brownian motion of individual particles is analyzed by video where the individual particle positional changes are tracked step by step via light-scattering centres in two dimensions (Kendall *et al.*, 2009). Some DLS and NTA instruments can also be used for zeta potential measurements by applying an electric field across the dispersion and measuring particle mobility. Both methods have the advantage that they require minimum sample consumption (<0.5 ml), are cost-effective, and quick, providing information on the NP size distribution in a sample within a few minutes (Kendall *et al.*, 2009; Estevez *et al.*, 2009). The main disadvantage of DLS is the limitation in size analysis of polydispersed samples. The disadvantage of NTA is that it can only characterize particles down to 30 nm. Both techniques are unspecific so would not distinguish between man-made and natural particles of the same size. The methods do not provide any information on the chemical characteristics of particles.

The molecular weight (± 5%) and gyration radius of food or target NPs in food can be obtained by "classical light scattering" including static light scattering (SLS) and multiangle laser light scattering (MALLS) (Istarova *et al.*, 2005). These methods are designed to detect the scattered light at different discrete angles to measure both molar mass and average size of particles in liquids (Brar & Verma, in press).

Raman spectroscopy (RS) has been sub-characterized as both a light scattering and laser based technique. This technique is based on the Raman effect, which is a type of scattering formed after laser light impinges upon a molecule, which results in the energy of the laser photons being shifted up or down. This information can be collected for molecular identification, oxidation state, structure, and sizing analysis (Wong *et al.*, 2009). Similarly, laser-induced fluorenscence (LIF) employs a laser beam to excite the studied species. The excited species will de-excite and emit light which can be measured to provide information on the molecules structure, species detection, and flow visualization (Lombardo-Agüí *et al.*, 2010). Laser-induced breakdown detection (LIBD) is a new sensitive method for quantification of the size and number concentration of nanoparticles (< 50 nm) in aqueous systems at very low concentrations (Bundschuh *et al.*, 2001). The measurement is achieved through investigation of the breakdown probabilities of the test medium i.e. the breakdown of dielectric properties caused by laser irradiation. X-ray scattering techniques are a family of analytical techniques which can reveal information about chemical composition, crystallographic structure, and grain size of samples based on observation of the scattering intensity of an X-ray beam after it hits a sample. X-ray Diffraction (XRD) is commonly used to identify single substances or a mix of unknown substances, by comparing diffraction data against a database maintained by the international centre for diffraction data (Zabar *et al.*, 2008). With the advantages of minimal sample preparation, time efficiency (< 20 min per unknown mineral), wide availability and straight forward data interpretation, it has been widely used to characterize the crystallographic structure, grain size, and preferred orientation in

polycrystalline or powdered solid samples (Erdem *et al.*, 2009; Zabar *et al.*, 2008). However, the method is not very sensitive and has low resolution (100 - ~500 nm).

Small angle neutron and x-ray scattering (SANS and SAXS) can be used to record the scattering of neutrons/x-rays at very low angles (typically 0.1 – 10^{o}) which contains information about both the shape and size of particles (>1 nm), nanostrucutures and pore sizes (Zabar *et al.*, 2008; Weisman *et al.*, 2004). SANS can provide data on particle sizes in the range of 1 to a few hundreds nm (Lopez-Rubio & Gilbert, 2009) and SAXS 1-100 nm (Luykx *et al.*, 2008). The materials can be tested under realistic conditions, e.g. solid or liquid. The method is accurate, non-destructive and usually requires only a minimum amount of sample preparation (Lopez-Rubio & Gilbert, 2009; Bunjes & Unruh, 2007). SANS will be of particular interest in food science since it can easily differentiate various biological particles from the background (Li *et al.*, 2008: Jarvie *et al.*, 2009).

Other widely used X-ray spectroscopy techniques include X-ray photoelectron (XPS), X-ray fluorescence (XRF), and X-ray absorption spectroscopy (XAS). XPS is very useful for surface and coating characterization of solid samples (e.g. NPs) due to the short range of photoelectrons exciting from solid samples (Tiede *et al.*, 2008). XRF can be used to identify and quantify the element present in target samples e.g. solid, powdered or liquid samples.

Nuclear magnetic resonance (NMR) can provide information on the detailed molecular structure and size of particles based on the observation of specific quantum mechanical magnetic properties of an atomic nucleus in the presence of an applied external magnetic field (Carter *et al.*, 2005). Theoretically, NMR spectroscopy can be rapid, resolve almost any combination of compounds and most importantly it can detect a quantitative signal from nearly every food component with < 1 mg of sample. Ever since it was published as an ISO method for solid content measurement in 1993, NMR has been widely applied in a wide range of food safety applications broadly aimed at averting significant chemical, biological or microbiological threats to the food chain (Mariette, 2009). NMR has been used to explore the effects of NPs through integrated metabolomic analysis in heptotoxicity and nephrotoxicity studies (Lei *et al.*, 2008) and has been used to explore protein-NP interactions (Calzolai *et al.*, 2010), and intermolecular space characterization (Belotti *et al.*, 2010). NMR is however time consuming, expensive, has low resolution and is insensitive ((Calzolai *et al.*, 2010; le Feunteun & Mariette, 2007).

The last resonance technique to mention is surface plasmon resonance (SPR), which is based on the excitation of surface plasmon by light, from which the nano-sized metallic structures from food matrix can be measured (Chaurasia *et al.*, 2010).

Other methods that have been widely applied and routinely used for the chemical identification and quantification include atomic absorption spectrometry (AAS), optical emission spectroscopy (OES); inductively coupled plasma-OES (Escudero *et al.*, 2010); and ultraviolet-visible spectrophotometry (UV-VIS)

3.4.4 Mass spectrometry

Mass spectrometry (MS) is used in food analysis for quality and authenticity control of food products (Careri *et al.*, 2002). The technique allows chemical and molecular mass characterization of sample components and detection at concentrations as low as one part per trillion. In the method, a sample is ionized by means of some form of ionization technique, the resulting ions are separated by their mass-to-charge ratio in

a mass analyzer and qualitatively and quantitatively analyzed by the detector system. Frequently used ion sources in food analysis include electrospray ionization (ESI), matrix assisted laser desorption ionization (MALDI) and inductively coupled plasma (ICP).

ESI creates a spray of charged molecules from the dispersion. The technique allows ionization of large, non-volatile and ionisable particles like for example food macromolecules (Amad *et al.*, 2000; Luykx *et al.*, 2008). MALDI analyzes surface of the solid sample by applying laser irradiation in a focused point. The laser induces evaporation and charging of the sample components. MALDI and ESI are considered 'soft' ionization techniques- meaning that they do not fragment fragile molecules like organic food components. In contrast, ICP ionises atoms through application of a high temperature argon plasma. ICP is suitable for samples in the liquid state only and is broadly applied for trace metal analysis (Tiede *et al.*, 2008).

ESI, ICP and MALDI require a high vacuum for analysis. However, there are sources of ionisation available which can deal with the sample in ambient conditions and are suitable for all types of specimen - solid, liquid and gaseous. These techniques include desorption electrospray ionization (DESI) and direct analysis in real time (DART)). DESI and DART require no or minimal sample preparation. These methods were developed only recently and are promising solutions for *in situ* analysis of complex samples like food (Chen *et al.*, 2010).

There are several kinds of MS analyzers available e.g. time of flight (TOF), quadrupole, ion trap, Fourier transform, sector. They differ in resolution, mass accuracy and range of measured mass-to-charge ratios (Tiede *et al.*, 2008). MS performs analysis of the elemental composition and mass concentration of sample components. As an example of instrument performance, the ICP-MS can acquire the mass spectrum of the plasma for almost the entire periodic table in just minutes with detection limits below 0.1 ug/L.

Single particle mass spectrometry (SPMS) enables sizing of single particles. For example, in work on sodium chloride polydisperse NPs, SPMS provided data on both particle size and size distribution of NPs in a range of 30-150 nm (Lee *et al.*, 2005). SP-ICP-MS can be used in studies on metal based NP (e.g. Degueldre *et al.*, 2006)) to obtain size of particles as well as concentration measurements Low concentrations of samples are introduced to the ICP-MS, run in single particle mode, to achieve single particle spikes/events. MS systems can also be coupled with each other and used in tandem mode. This is done to achieve higher sensitivity of the method. In tandem setup, each MS isolates ions by their mass-to-charge ratio which allows more detailed analysis by the next MS in a sequence. This approach enables identification of individual subunits of the analyte. This method was used for the determination of surfactant NP fingerprints (Buse *et al.*, 2010).

MS can be combined with a range of size separation techniques (see section 4.1). A potentially useful combination for the characterization of organic NP could be the coupling of MS (usually employing MALDI or ESI depending on type of the sample) with ion-mobility spectrometry (IMS) (Luykx *et al.*, 2008; Peters *et al.*, in press). IMS separates ionised molecules based on their differential mobility in a carrier gas with an electric field applied. When joined with the MS technique, the method can separate the analyte based on size, shape and mass, providing chemical characterization at the same time.

3.4.5 Centrifugation, filtration and dialysis techniques

Filtration, centrifugation and dialysis in studies on NP containing food products can be utilized as separation techniques for sample preparation. Filtration and centrifugation might be also used themselves as analytical methods for the size fractionation of NPs.

Filtration is most commonly used as a preparative method for liquid foods, enabling investigation by other analytical techniques. Depending on the pore size filters may allow separation of NPs and other similar sized food components from larger solids. Nanofiltration with pore sizes below 1 nm can further separate the NP from dissolved substances such as salts (Hassellöv *et al.*, 2008) which are commonly present in food products. Filtration can process large volumes of the sample in a short time. Application of a tangential flow further improves the effectiveness of filtration by slowing down the effect of filter clogging. Tangential flow filtration (also called cross flow filtration), combined with centrifugation, can even pre-concentrate nanosized structures from 2 l of the sample down to 10-20 µl (Alonso *et al.*, 1999). Filtration enables size fractionation of NPs (Akthakul *et al.*, 2005), but because separation is only size-based, non-engineered food nanocomponents of similar sizes will always be retained in the purified phase with the NP of interest. In centrifugation, separation depends also on particle density. This offers improvement in NP separation from the food matrix especially for inorganic NPs which are made of heavier elements than the food components. Centrifugation as a sample preparation technique is applied in a range of analytical methods, separating coarse solids from supernatant containing NPs. For example, in microscopy, this approach can be employed as a preparation step for WetSEM^{TM} resulting in improved adhesion of specimen containing NP to the capsule membrane (Koh *et al.*, 2008). Conventional centrifugation operates at forces which are not sufficient for sedimentation of NPs. Therefore for further separation of NPs from similar size or weight components in the matrix, ultracentrifugation is necessary. This technique achieves forces of up to 1 000 000 g (Tiede *et al.*, 2008) and is able to fractionate NPs of different size, and even shape, chemical and physical properties in density gradient medium (Bai *et al.*, 2010). Ultracentrifugation is also used as a sample preparation method for NP characterization techniques. For example TEM grids can be placed at the bottom of an ultracentrifuge tube and centrifuged with the NP dispersion to both enhance the distribution of analyte and to concentrate the sample on the grid (Dudkiewicz *et al.*, 2011). Ultracentrifuges can also be equipped with optical detectors like refractive index or UV absorption. This method is called analytical ultracentrifugation (ANUC) and can characterize features of NP such as size, volume and density (Bootz *et al.*, 2004).

Dialysis separates sample components based on diffusion of the dissolved substances through a membrane. This technique is commonly used for purification of an NP dispersion form stabilising agents (e.g. Uboldi *et al.*, 2009). Dialysis has been applied for the assessment of NP dissolution rates (Franklin *et al.*, 2007). Like nanofiltration, this technique could be used for final purification of NPs from dissolved components of the food sample.

3.4.6 Other detection techniques

Brunanuer Emmett Teller (BET) can be used to measure the specific surface area of powdered nanoparticles (1 - >1000 nm) by adsorption of nitrogen gas onto the

particle surface and micropores. There are some other variants which are based on the adsorption of organic molecules (e.g. ethylene glycol monoethyl ether, EGME).

The Scanning Mobility Particle Sizer (SMPS) used information on the mobility of a charged particle in an electric field to measure the particle size distribution, charge, and central rod voltage of an aerosol, which is a suspension of fine solid particles or liquid droplets in a gas. The particles are classified according to their ability to traverse an electrical field and are then counted by a Condensation Particle Counter (CPC), which itself is an instrument to measure the number of ultrafine particles (3 to >5000 nm) by enlarging the particles through a condensing process. The number concentration within a certain size range can hence be determined within a few minutes. This instrument is able to measure particles with a size range of 3-1000 nm and a concentration range of 20-10,000,000 particles per ml^{-1}. The major advantage of SMPS is the ease of portability and significantly lower power consumption whilst the disadvantage is the sample has to be in the aerosol form.

Thermogravimetry (TG) is based on continuous recording of sample weight changes as a function of a combination of temperature with time, and additionally of pressure and gas composition. It is commonly employed to determine characteristics of materials, degradation temperatures, absorbed moisture content of materials, the level of inorganic and organic components in materials, decomposition points of explosives, and solvent residues.

Differential thermal analysis (DTA) and Differential scanning calorimetry (DSC) measure the temperature difference and the heat flow difference between a sample and a reference material (subjected to the same temperature variation in a controlled atmosphere). They can be used to measure phase changes, melting, purity, evaporation, sublimation, crystallization, pyrolysis, heat capacity, polymerization, aggregation, compatibility, etc. The methods can be used to track the degradation process of nanoparticles by identifying the formed by-product, and simultaneously to inspect the food quality change along with addition of nanoparticles.

Synchrotron is a powerful and expensive technique available for the nanoparticle detection, characterization, and quantification. Synchrotron radiation is generated by the acceleration of ultrarelativistic charged particles through the magnetic fields. The radiation produced may range over the entire electromagnetic spectrum (De Samber *et al.*, 2008). It hence can be combined with techniques such as X-ray spectroscopy, X-ray Diffraction and Imaging, Infrared spectroscopy and X-ray Lithography for the measurement of size distribution, number concentration, structure determination, orientation and crystallinity and even protein crystallography (Jackson *et al.*, 2009). With the high-energy electron beam, synchrotron can be used for structure characterization imaging, of either food or nanoparticles, from sub-nanometer level to micro and millimetre level.

3.5 Detection and characterization of engineered nanoparticles in foods, beverages and nutraceuticals

3.5.1 Sample preparation and digestion

Most of the analytical techniques described above require samples to be pre-treated prior to analysis. One should be aware that any additional step of sample preparation could introduce artefacts or alter the form of an NP in a sample. Therefore sample

preparation should be always kept to a minimum. The preparation method should be selected based on the type of NP, matrix and analytical technique used.

Separation techniques may simplify the detection of NPs. Restriction or exclusion of the food matrix from the NP suspension removes issues of sample homogeneity and may also concentrate the analyte, if the volume of the sample is significantly reduced without NP losses. Pre-concentration might be essential as a preparation step in cases where levels of NPs are likely to be low e.g. in food migration studies on NPs from food contact materials into the product. Also for some methods with high limits of detection (e.g. microscopy), pre- concentration is essential to allow detection and analysis of NPs.

Separation of NPs from liquid samples can be achieved by ultracentrifugation, filtration, and chromatography-based techniques (Tiede *et al.*, 2008). However these methods might not be able to exclude food components of the same size or similar dynamics from the NP of interest. Therefore other methods like extraction or digestion might need to be used to separate or aid separation by these techniques.

If NPs can be found in one of the fractions of the sample, extraction would be a good way of sample preparation. In the literature, examples of extraction of fullerene C_{60} from biological and environmental samples with toluene (Isaacson *et al.*, 2007) and by solid- phase extraction can be found (Chen *et al.*, 2008). The use of cloud point extraction has also been used as a pre-concentration method for silver NPs from environmental waters, which preserves the size and shape of the NPs (Liu *et al.*, 2009). However, extraction of organic NP can be more problematic, since the solvents used can disrupt their structure. The use of phase-transfer agents, which surround the particle and allow its relocation from an aqueous to an organic solvent environment may be suitable for extraction of organic NPs (Peters *et al.*, in press). Another option for sample preparation for organic NPs is mechanical separation from liquid food samples by filtration or ultracentrifugation (see section 4.5).

Separation of NP from solid samples may be difficult without changing their properties. For this purpose digestion methods can be used. Enzymatic hydrolysis is a very gentle method and can be applied for characterization of interactions of different fractions of an element with a food matrix (Bermejo *et al.*, 2004). However, enzymatic hydrolysis is a time consuming process. Acceleration can be achieved by sonication. This proved to shorten proteolysis in yeasts (Capelo *et al.*, 2004) and has been applied for recent studies on Selenium and its species in food supplements (Vale *et al.*, 2010). On the other hand use of sonication may change the agglomeration state of NP. Therefore the method, though gentle and able to separate components of interest from the matrix, might not fully reveal all NP characteristics. This method most likely would destroy organic NPs, especially carbohydrates, lipids or proteins.

Disintegration of sample structure and the dissolution of NPs by means of acid digestion might be also useful and is already practiced for NP mass concentration measurements. For example, for inorganic NP that are not commonly found in food products, like gold or silver, the sample can be fully digested and then analyzed for mass concentration of the element of interest by common available techniques. However, concentration measurements of nanoparticles based on total elemental quantification can lead to overestimates of NP concentrations as the measurement includes not only the NP form but also any non-NP form that is present in a sample. For example, silica NPs can be found in many food concentrates, but nanosilica constitutes only a part of the total silica content (Dekkers *et al.*, 2010). Furthermore

silica does not dissolve in low pH (except of when hydrofluoric acid is used) but requires an alkaline environment for extraction. Therefore, in the case of this particular NP, acid digestion might be useful for removal of the sample matrix to separate the nanosilica from the rest of the biological sample (Tadjiki *et al.*, 2008). However, it is anticipated that this method may also cause changes in NP characteristics.

3.5.2 Chemical analysis of nanoparticles in food products

The chemistry of an NP is a crucial characteristic influencing its properties. Depending on chemical composition, NPs can be used for food industry applications as antimicrobial agents (e.g. silver NPs), UV protection (e.g. TiO_2 NPs), nano delivery systems (NDS) for increased bioavailability of nutrients and their targeted delivery.

There are a number of methods that can help to characterize elemental composition of NPs which have already been discussed in section 4. However the problem is much more complex. Many NP systems are comprised of more than one element. These elements can be localised in different parts of the particle. For example the surface shell of the particle can consist of a different chemical from its core, or the whole NP can be divided into various chemical layers. Moreover NPs can be capped with stabilising agent or surrounded by residues of food matrix components after preparation of the sample. In terms of NP reactivity and potential toxicity these characteristics are also important and may require determination.

The most widely applied technique for NP chemical composition characterization is MS. By means of MS, evaluation of an NPs chemical formula is possible (Qian *et al.*, 2010). MS in combination with IMS is able to distinguish between chemically homogenous and complex NPs (Jackson *et al.*, 2005). Tandem MS can additionally provide fragmentation patterns characteristic for an analyzed NP indicating its fingerprint (Buse *et al.*, 2010). This might be of use especially for organic NPs. Organic NPs embedded in a food matrix can be difficult to analyze because of similarity in elemental composition with the food components. Therefore, they might need to be separated from the sample prior to analysis. Detection and characterization of inorganic and metal based NPs is less problematic and there is also a wider range of methods available. All techniques that atomise the sample for analysis like AAS, OES, ICP-MS, ICP-OES may be useful for characterization of inorganic and metal based NPs, especially if elements of interest are not commonly present in the food product. The drawback is that the NP structure is disrupted and characterization of other features- like existence of chemical layers is not possible. However, analytical techniques coupled to electron microscopes may enable visualization of element layers within the particle by elemental mapping as presented for multishell Au/Ag NPs imaged by STEM/EDS (Rodríguez-González *et al.*, 2005). Imaging techniques in combination with spectroscopic techniques such as EDS make it possible to localize chemically different NPs within a complex matrix and characterize their chemical composition as presented for industrial nano-contaminants in bread and biscuits (Gatti *et al.*, 2009). If an NP consists of high molecular weight elements, the contrast with the organic food matrix presented on the micrograph is also higher and this allows better imaging/detection. Detection of NPs in food by EM is often referred to as ‘looking for a needle in the haystack’ (Dudkiewicz *et al.* 2011). As discussed in section 4.2 these methods allow analysis of very scarce volume of the sample only and the limit of detection is quite high in

comparison to other analytical methods. Therefore, multi method analysis for chemical characterization of NP is a good solution. For example, asymmetrical flow FFF coupled to high resolution ICP-MS was applied for trace metal determination in NP extracted from riverbed sediment and TEM with EDS detection enabled analysis of single particles and interactions with heavy metals (Plathe *et al.,* 2010).

Since NPs are expected to interact with components of food matrices (EFSA, 2009) and easily adsorb proteins on their surfaces changing their composition (Lynch & Dawson, 2008), characterization of the surface chemistry of NPs is of particular interest. The surrounding layer of substances on the NP interface can be visualized with EM, however, characterisation of the chemical structure of the layer can be a problem. Analytical techniques coupled to EM can indicate elemental composition of this layer but are not able to identify its molecular structure. For this purpose NMR can be applied. This method has been used to identify acidic phosphorus-containing ligands on the surface of CdSe NPs (Kopping & Patten, 2008) and interactions of protein- human Ubiquitin with Au NPs (Calzolai *et al.*, 2010). NMR is an interesting technique for studies on food because it is non- destructive. Similarly, XRD does not require significant sample pre-treatment. This technique can identify crystalline molecules or mixtures of molecules based on their diffraction patterns (Luykx *et al.*, 2008). Therefore, XRD can be useful for characterization of chemically complex NPs and identification of molecules surrounding these NPs on condition that structures of interest are crystalline.

3.5.3 Size analysis of nanoparticles in food

Size distribution can be measured with chromatography, FFF, CE, light scattering, SPMS, ANUC and also microscopy methods. For chromatography based techniques calibration is a must, since particle size is calculated from retention time. There are many challenges connected with calibration. Calibration standards should comprise stable and inert particles of known size and concentration. The stabilising agent should not increase the diameter of the particles, and their shape should be the same, preferably spherical. A current problem faced by those using these chromatography methods is the availability of such standards.

In numerous studies methods enabling sizing of NPs are compared to each other and often provide different results. Various techniques may require different sample preparation which affects NP size and also expression of size itself varies between the methods. For example, methods like SEC, HDC, FFF, DLS, NTA measure the hydrodynamic diameter of NPs, whereas the radius of gyration is calculated from MALLS measurements (e.g.Fishman *et al.*, 1996)). Size separation and light scattering techniques are also not able to distinguish between particles and substances located on its surface. In this case, size measurements include any possible substances from the food matrix that could surround the NP. EM might be able to visualize the actual core of an NP and distinguish it from surrounding elements of the food matrix. There is a range of negative stains available for contrast enhancement and visualization of organic food components. Also sample preparation for EM and AFM involving removal of water or freezing might affect size of especially organic strongly hydrated nano-structures such as starch particles, which, measured by SEC and MALS, have a higher radius of gyration in comparison to data from TEM analysis (Fishman *et al.*, 1996). A similar effect was observed in studies on polyurethane NPs where data from DLS and AFM were compared (Zanetti-

Ramos *et al.*, 2009) and for poly (butyl cyanoacrylate) NP where SEM indicated a significantly shorter mean diameter than DLS and ANUC (Bootz *et al.*, 2004).

EM and AFM allow sizing of NPs within solid samples whereas other methods usually require separation of NP from the matrix, which also can affect NP size. Techniques like chromatography-based techniques use mobile phases to separate the sample, which might interact with NPs and affect their characteristics (Tiede *et al.*, 2008). Light scattering methods and ANUC can identify NPs in their original media, if liquid does not contain any other solids and colloidal particles which would cause false positives. Food matrices do not meet these requirements. Therefore ANUC, which separates particles also based on their density, mass and shape may enable controlled purification of NPs from food components and subsequent analysis of the particles of interest. Also SANS can discriminate the background from the particle and enable measurement of NPs even in turbid media as demonstrated for SiO_2 NPs with Fe_3O_4 core dispersed in real wastewater samples (Jarvie *et al.*, 2009). However, compared to ANUC, this technique cannot not separate an analyte during measurement. SANS, SAXS and also TEM can enable determination of core and shell thickness in relevant NP systems (Riley *et al.*, 2003; Kandar *et al.*, 2009; Martin *et al.*, 2008).

3.5.4 Imaging of nanoparticles in food products

A major drawback of imaging methods for characterization of NP in food products is the sampling, sample preparation and data interpretation, especially for electron microscopy techniques (Dudkiewicz *et al.*, 2011). Sampling for imaging is challenging because the volume of the sample introduced for the analysis is quite small in comparison to many other analytical methods. Furthermore, conventional EM techniques require extensive sample preparation. These sample preparation methods for SEM, TEM, FIB-SEM and STEM can employ various ways of water removal from the specimen. Drying causes alterations in food samples and may also influence NP features (Domingos *et al.*, 2009). Although chemical fixation followed by dehydration in ethanol/acetone and critical point drying or resin embedding better preserves the sample structure, it can also cause loss of food components (Kaláb & Larocque, 1996) and may remove NPs, especially if they are not associated with other sample components.

Some food products simply cannot be chemically fixed such as foods with high contents of saturated fat and carbohydrates. These products can be prepared for imaging by freezing and then imaged by cryo- EM. Freezing preserves well processed foods like cheese (Noronha *et al.*, 2008), bread (Bárcenas & Rosell, 2006) or chocolate (James & Smith, 2009). However, samples with intact cellular structures can suffer damage from growing ice crystals. This damage can be minimised by using optimal freezing conditions which ensure preservation of sample structure of the specimen in 5-10 μm depth due to formation of amorphous ice, allowing detailed observation of unaltered specimen in cryo-SEM and cryo-TEM.

A food sample in its unperturbed state can be viewed by environmental and liquid EM techniques. ESEM has found many applications for imaging of food products (James, 2009) and has been used for detection of metal based micro and nanosized contaminations in bakery products (Gatti *et al.*, 2009). Liquid and environmental EM offers lower resolution than conventional and cryo- techniques, even down to 100 nm, but provides important complementary information.

Light and x-ray microscopy as well as AFM do not need extensive sample preparation and therefore enable imaging of food samples close to their original status. Light microscopy even though its resolution is too low to image NPs can be useful as complementary imaging technique e.g. to check the homogeneity of the sample or select the area which may contain NP for high resolution imaging. Some NPs can be localized by light microscopy if their size is enhanced by deposition of silver ions – this method is called auto-metallography (Dudkiewicz *et al.* 2011).

X-ray microscopy enables observation of the specimen in the fully hydrated state and unlike SEM does not need sectioning for 3D imaging of the sample. X-ray microtomography finds numerous applications in food science, for example in measurements and distribution of pores in chocolate (Haedelt *et al.*, 2007), or bakery products (Adedeji & Ngadi, 2009; Babin *et al.*, 2006). In food analysis this method is advantageous over EM because it is non-invasive, involves less preparation than EM and can be used *in situ* (Babin *et al.*, 2006).

AFM is regarded as 'a powerful tool for nanofood production and research' (Yang *et al.*, 2007). It is widely used for characterization of natural food nanostructures and in nanomaterial science. AFM can characterize dry and fully liquid samples. Imaging of liquids, however, can pose a problem, because, if not fixed, particles will move and get attached to the tip causing imaging artefacts. Nevertheless the method provides high resolution imaging while avoiding many of the sample preparation challenges faced by EM.

A general issue for all the imaging techniques is the extraction of data from the obtained micrographs. Since microscopy is supposed to provide representative information about the size and size distribution of the NPs in the sample it is important to characterize as many particles as possible. The number of NPs required to be characterized to give sufficient information varies and in some cases, thousands of NPs may need to be analyzed. Therefore, manual interpretation of micrographs is almost impossible and automated image analysis tools have to be applied for this purpose. The Definiens Developer^{TM} software is an example of such a tool used for analysis of TEM micrographs for imaging of NPs and biological samples (Tiede *et al.*, 2009a; Tiede *et al.*, 2010).

3.5.5 Dissolution and aggregation measurement

Particle dissolution and interactions such as agglomeration are important variables that will need to be assessed in order to understand the behaviour and risks of NPs in food. Agglomeration is defined as clustering of particles which is reversible to well dispersed state, while in aggregates clustering is non reversible (Prestidge & Ametov, 2000). The change of NP aggregation state can be measured by determining the changes in shape and size over time.

EM techniques can be used to directly visualize NPs. Therefore EM can also indicate state of NP aggregation and agglomeration. As shown in Fig. 3.1, NP shape and size can be determined from EM images,. The distance between single particles, determined from micrographs by image analysis, can indicate agglomeration of nanoparticles in certain areas of the sample. Aggregation can be due to sample alterations introduced by the sample preparation methods used such as drying, during which suspensions of NPs tend to agglomerate and even aggregate due to the loss of dispersive phase and increases in attraction forces.

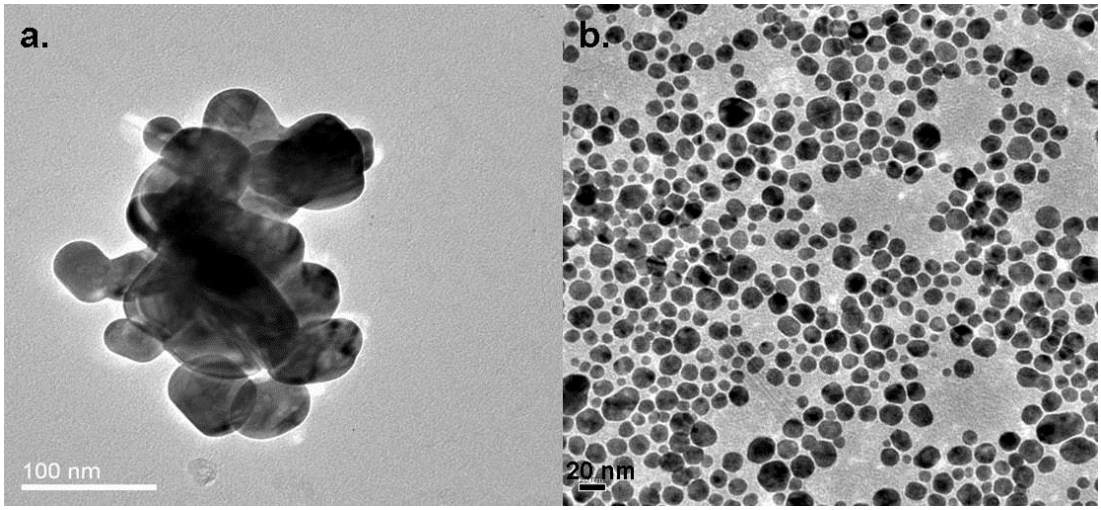

Fig. 3.1 TEM images present a. aggregation of silver nanoparticles and b. dispersed single silver nanoparticles

Techniques that are able to measure both size and particle number concentrations, e.g. NTA, CPS, and SMPS, can also be used to evaluate the state of aggregation/agglomeration of NPs. (Kendall *et al.*, 2009). Aggregation or agglomeration of NPs is indicated by a decrease in PNC and an increase in the mean diameter, while a break up of agglomerates will result in PNC increase and the mean NP diameter decrease. If the PNC is stable, but the NP mean diameter decreases then this can indicate dissolution of NPs.

In general, the measurement of dissolution and aggregation of NPs in food is complex, mainly due to the requirement for sample preparation, which often introduces sample alterations and therefore artefacts, and the difficulties in separating sample components, e.g. NPs from their ionic counterparts.

3.5.6 Determination of other important features of nanoparticles in food

Shape

The shape of a NP is usually determined by an imaging method. However, it is also possible to get a rough idea on NP shape by size fractionation techniques coupled to light scattering detectors (e.g. asymmetrical FlowFFF-MALLS applied for the characterization of riverbed sediment NP by Plathe *et al.* (2010)). Furthermore it is possible to fractionate NPs based on shape using density gradient separation by ultracentrifugation. This approach has been successfully been applied in the separation of gold nanospheres in a dispersion with gold nanowires (Bai *et al.*, 2010).

Surface charge

Surface charge of an NP has an effect on its stability and reactivity. It will also have an influence on NP stability in the food environment. Based on particle mobility, the overall charge of a colloidal system and therefore its stability can be determined (; (see section 3.4.3; Tiede *et al.*, 2008).

Surface area

Surface area of a NP will depend on its structural features, e.g. shape, porosity, crystallinity. Surface area can be determined by chemisorption based on methods like BET (See chapter 4.6). The higher the surface area to volume ratio, the higher the reactivity of an NP. The reactivity of an NP will have an impact on its fate in food products. A value of this property can be obtained by calculation as presented for gold NPs (Janz *et al.*, 2010). In this study the authors determined the concentration of thiol (often used as stabilizing agent) interacting with the surface of gold NPs to calculate the specific surface area and compared the data with measurements obtained by TEM imaging. A good correlation for these two methods was found. Surface-to-volume ratio can also be characterized by SAXS (Luykx *et al.*, 2008).

Structure

Structure of NP is a very broad term and some structural features like shape or chemical layers (see section 5.2) of NPs have already been discussed in previous sections. Most of the structural information can be obtained by imaging techniques. The popularity of these methods emerges from the fact that structure analysis has to be performed on a single particle basis. A method often applied for the identification of crystal structures is XRD. For example, XRD in combination with SAXS was applied to investigate nanostructures in resistant starch type III during thermal treatments and cycling (Zabar *et al.*, 2008).

3.6 Future Trends

Nanotechnology is still in the early stages of development in food industry applications. At the moment, the lack of knowledge concerning the risks of NPs in food and food related products: 1) potentially limits new product development; 2) means that consumers are concerned about the safety of NPs to their health; and 3) inhibits authorities in developing appropriate legislation. In order to develop knowledge on the risks of NPs, the development of methods for detecting and characterizing NPs in food is essential.

As pointed out in this chapter there is no one available technique able to detect and characterize all the important features of NPs used in food, nutraceuticals and food additives at once. The use of a combination of methods for characterisation of NPs in food matrices is usually necessary. Future work will have to focus on the development and validation of methods for *in situ* analysis of NPs in food and adequate sample preparation for the available techniques. Pre- treatment of especially solid food samples is in most cases unavoidable, but care has to be taken to choose appropriate methods and develop applicable protocols that result in minimal disturbance of the NPs within a sample. For the development of standardised analytical procedures and protocols, there is a need for size calibration standards and reference materials, which are not available at the moment.

3.7 References

Adedeji, A.A. and Ngadi, M.O. (2009), '3-D Imaging of Deep-Fat Fried Chicken Nuggets Breading Coating Using X-Ray Micro-CT', *International Journal of Food Engineering*, 5, 11.

Akthakul, A., Hochbaum, A.I., Stellacci, F. and Mayes, A.M. (2005), 'Size Fractionation of Metal Nanoparticles by Membrane Filtration', *Advanced Materials.*, 17, 532-535.

Alonso, M.C., Rodríguez, J. and Borrego, J.J. (1999), 'Enumeration and isolation of viral particles from oligotrophic marine environments by tangential flow filtration', *International Microbiology: The Official Journal of the Spanish Society for Microbiology*, 2, 227-232.

Amad, M.H., Cech, N.B., Jackson, G.S. and Enke, C.G. (2000), 'Importance of gas-phase proton affinities in determining the electrospray ionization response for analytes and solvents', *Journal of Mass Spectrometry*, 35, 784-789.

Auty, M., O'Kennedy, B., Allan-Wojtas, P. and Mulvihill, D. (2005), 'The application of microscopy and rheology to study the effect of milk salt concentration on the structure of acidified micellar casein systems', *Food Hydrocolloids*, 19, 101-109.

Babin, P., Dellavalle, G., Chiron, H., Cloetens, P., Hoszowska, J., Pernot, P., Reguerre, A., Salvo, L. and Dendievel, R. (2006), 'Fast X-ray tomography analysis of bubble growth and foam setting during breadmaking', *Journal of Cereal Science*, 43, 393-397.

Bai, L., Ma, X., Liu, J., Sun, X., Zhao, D. & Evans, D.G. (2010), 'Rapid Separation and Purification of Nanoparticles in Organic Density Gradients', *Journal of the American Chemical Society*, 132, 2333-2337.

Bárcenas, M.E. and Rosell, C.M. (2006), 'Effect of frozen storage time on the bread crumb and aging of par-baked bread', *Food Chemistry*, 95, 438-445.

Barnard, A.S., Feigl, C.A. and Russo, S.P. (2010), 'Morphological and phase stability of zinc blende, amorphous and mixed core–shell ZnS nanoparticles', *Nanoscale*, 2, 2294-2301.

Belotti, M., Martinelli, A., Gianferri, R. and Brosio, E. (2010), 'A proton NMR relaxation study of water dynamics in bovine serum albumin nanoparticles', *Physical Chemistry Chemical Physics*, 12, 516-522.

Bermejo, P., Capelo, J.L., Mota, A., Madrid, Y. and Cámara, C. (2004), 'Enzymatic

digestion and ultrasonication: a powerful combination in analytical chemistry', *Trends in Analytical Chemistry*, 23, 654-663.

Betzig, E., Trautman, J.K., Harris, T.D., Weiner, J.S. and Kostelak, R.L. (1991), 'Breaking the Diffraction Barrier: Optical Microscopy on a Nanometric Scale', *Science*, 251, 1468-1470.

Bootz, A., Vogel, V., Schubert, D. and Kreuter, J. (2004), 'Comparison of scanning electron microscopy, dynamic light scattering and analytical ultracentrifugation for the sizing of poly(butyl cyanoacrylate) nanoparticles', *European Journal of Pharmaceutics and Biopharmaceutics*, 57, 369-375.

Bouwmeester, H., Dekkers, S., Noordam, M., Hagens, W., Bulder, A., Deheer, C., Tenvoorde, S., Wijnhoven, S., Marvin, H. and Sips, A. (2009), 'Review of health safety aspects of nanotechnologies in food production', *Regulatory Toxicology and Pharmacology*, 53, 52-62.

Brar, S.K. and Verma, M. (2011), 'Measurement of nanoparticles by light-scattering techniques', *Trends in Analytical Chemistry*, 30, 4-7

Brewer, A.K. and Striegel, A.M. (2010), 'Characterizing a spheroidal nanocage drug delivery vesicle using multi-detector hydrodynamic chromatography', *Analytical and Bioanalytical Chemistry*, 399, 1507-1514

Bundschuh, T., Knopp, R. and Kim, J.I. (2001), 'Laser-induced breakdown detection (LIBD) of aquatic colloids with different laser systems', *Colloids and Surfaces A: Physicochemical and Engineering Aspects*, 177, 47-55.

Bunjes, H. and Unruh, T. (2007), 'Characterization of lipid nanoparticles by differential scanning calorimetry, X-ray and neutron scattering', *Advanced Drug Delivery Reviews*, 59, 379-402.

Buse, J., Badea, I., Verrall, R.E. and El-Aneed, A. (2010), 'Tandem Mass Spectrometric Analysis of the Novel Gemini Surfactant Nanoparticle Families G12-s and G18:1-s.', *Spectroscopy Letters: An International Journal for Rapid Communication*, 43, 447-457.

Calzolai, L., Franchini, F., Gilliland, D. and Rossi, F. (2010), 'Protein−Nanoparticle Interaction: Identification of the Ubiquitin−Gold Nanoparticle Interaction Site', *Nano Letters*, 10, 3101-3105.

Capelo, J.L., Ximénez-Embún, P., Madrid-Albarrán, Y. and Cámara, C. (2004), 'Enzymatic Probe Sonication: Enhancement of Protease-Catalyzed Hydrolysis of Selenium Bound to Proteins in Yeast', *Analytical Chemistry*, 76, 233-237.

Careri, M., Bianchi, F. and Corradini, C. (2002), 'Recent advances in the application of mass spectrometry in food-related analysis', *Journal of Chromatography A*, 970, 3-64.

Carter, L., Chen, W., Wu, H., Mehta, A., Hernandez, R., Ticku, M., Coop, A., Koek, W. and France, C. (2005), 'Comparison of the behavioral effects of gamma-hydroxybutyric acid (GHB) and its 4-methyl-substituted analog, gamma-hydroxyvaleric acid (GHV)', *Drug and Alcohol Dependence*, 78, 91-99.

Castaneda, L., Valle, J., Yang, N., Pluskat, S. and Slowinska, K. (2008), 'Collagen Cross-Linking with Au Nanoparticles', *Biomacromolecules*, 9, 3383-3388.

Chan, Q., Afton, S.E. and Caruso, J.A. (2010), 'Investigation of selenium metabolites in Se-enriched kale, Brassica oleracea A, via HPLC-ICPMS and nanoESI-ITMS', *Journal of Analytical Atomic Spectrometry*, 25, 186-192.

Chaudhry, Q. and Groves, K. (2010), 'Nanotechnology Applications for Food Ingredients, Additives and Supplements', In: Q. Chaudhry, L. Castle, R. Watkins (Ed.) *Nanotechnologies in food*, RSC Publishing, 69-84.

Chaurasia, V., Chand, N. and Bajpai, S.K. (2010), 'Water Sorption Properties and Antimicrobial Action of Zinc Oxide Nanoparticles-Loaded Cellulose Acetate Films', *Journal of Macromolecular Science, Part A*, 47, 309-317.

Chen, H., Hu, B. and Zhang, X. (2010), 'Principle and Application of Ambient Mass Spectrometry for Direct Analysis of Complex Samples', *Chinese Journal of Analytical Chemistry*, 38, 1069-1088.

Chen, X., Jo, C., Lee, J.I. and Ahn, D.U. (1999), 'Lipid Oxidation, Volatiles and Color Changes of Irradiated Pork Patties Affected by Antioxidants', *Journal of Food Science*, 64, 16-19.

Chen, Z., Westerhoff, P. & Herckes, P. (2008), 'Quantification of C60 fullerene concentrations in water', *Environmental Toxicology and Chemistry*, 27, 1852-1859.

Cieślik E., Niedośpiał A. and Mickowska B. (2008), 'Wykorzystanie elektroforezy kapilarnej w analizie żywności', *ŻYWNOŚĆ. Nauka. Technologia. Jakość,* 57, 5-14

CORDIS (2010), 'Nanoparticles in Food: Analytical methods for detection and characterisation (NANOLYSE)', Available from: http://cordis.europa.eu/fetch?CALLER=FP7_PROJ_FR&ACTION=D&DOC=6&CAT=PROJ&QUERY=01258d38da6b:97e6:04e5cdff&RCN=93181. (Accessed 14 November 2010).

De Samber, B., Evens, R., De Schamphelaere, K., Silversmit, G., Masschaele, B.,

Schoonjans, T., Vekemans, B., Janssen, C.R., Van Hoorebeke, L., Szalóki, I., Vanhaecke, F., Falkenberg, G. and Vincze, L. (2008), 'A combination of synchrotron and laboratory X-ray techniques for studying tissue-specific trace level metal distributions in Daphnia magna', *Journal of Anaytical. Atomic Spectrometry*, 23, 829-839.

Degueldre, C., Favarger, P. and Wold, S. (2006), 'Gold colloid analysis by inductively coupled plasma-mass spectrometry in a single particle mode', *Analytica Chimica Acta*, 555, 263-268.

Dekkers, S., Krystek, P., Peters, R.J.B., Lankveld, D.X.L.P.K., Bokkers, B.G.H., van Hoeven-Arentzen, P.H., Bouwmeester, H. and Oomen, A.G. (2010), 'Presence and risks of nanosilica in food products', *Nanotoxicology*, 5, 393-405.

Diplock, A.T., Charleux, J.L., Crozzier-Willi, G., Kok, F.J., Rice-Evans, C., Roberfroid, M., Stahl, W. and Vina-Ribes, J. (1998), 'Functional food science and defence against reactive oxidative species', *British Journal of Nutrition*, 80, S77-S112.

Dodds, J., Rasteiro, G., Scarlett, B., Weichert, R. and Williams, R. (2004), 'From Particle Size Analysis (PSA 1970) to Particulate Systems Analysis (PSA 2003)', *Chemical Engineering Research and Design*, 82, 1533-1540.

Domingos, R.F., Baalousha, M.A., Ju-Nam, Y., Reid, M.M., Tufenkji, N., Lead, J.R., Leppard, G.G. and Wilkinson, K.J. (2009), 'Characterizing Manufactured Nanoparticles in the Environment: Multimethod Determination of Particle Sizes', *Environmental Science and Technology*, 43, 7277-7284.

Doucet, F.J., Lead, J.R., Maguire, L., Achteberg, E.P. and Millward, G.E. (2005), 'Visualisation of natural aquatic colloids and particles a comparison of conventional high vacuum and environmental scanning electron microscopy' *Journal of Environmental Monitoring*, 7, 115-121.

Dubascoux, S., Le Hécho, I., Hassellöv, M., Von Der Kammer, F., Potin Gautier, M. & Lespes, G. (2010), 'Field-flow fractionation and inductively coupled plasma mass spectrometer coupling: History, development and applications', *Journal of Analytical Atomic Spectrometry*, 25, 613-623.

Dudkiewicz, A., Tiede, K., Loeschner, K., Soregaard Jensen, L.H., Jensen, E., Wierzbicki, R., Boxall, A.B.A. and Molhave, K. (2011), 'Characterisation of nanomaterials in food by electron microscopy- a review', *Trends in Analytical Chemistry*, 30, 28-43.

EFSA (European Food Safety Authority) (2009), 'Scientific Opinion of the Scientific Committee on a request from European Commission on the Potential

Risks Arising from Nanoscience and Nanotechnologies on Food and Feed Safety', *The EFSA Journal*, 958, 1-39.

Erdem, N., Cireli, A.A. and Erdogan, U.H. (2009), 'Flame Retardancy Behaviors and Structural Properties of Polypropylene/Nano-SiO2 Composite Textile Filaments', *Journal of Applied Polymer Science*, 111, 2085-2091.

Escudero, L.A., Cerutti, S., Olsina, R., Salonia, J. and Gasquez, J. (2010), 'Factorial design optimization of experimental variables in the on-line separation/preconcentration of copper in water samples using solid phase extraction and ICP-OES determination', *Journal of Hazardous Materials*, 183, 218-223.

Estevez, M., Vargas, S., Castaño, V. and Rodriguez, R. (2009), 'Silica nano-particles produced by worms through a bio-digestion process of rice husk', *Journal of Non-Crystalline Solids*, 355, 844-850.

Le Feunteun, S. and Mariette, F. (2007), 'Effect of casein structure on the diffusion of solutes in casein solution and gels as studied by pulsed field gradient NMR', *Magnetic Resonance Imaging*, 25, 568-591.

Fishman, M.L., Cooke, P., White, B. and Damert, W. (1995), 'Size distributions of amylose and amylopectin solubilized from corn starch granules', *Carbohydrate Polymers*, 26, 245-253.

Fishman, M.L., Rodriguez, L. and Chau, H.K. (1996), 'Molar Masses and Sizes of Starches by High-Performance Size-Exclusion Chromatography with On-Line Multi-Angle Laser Light Scattering Detection', *Journal of Agricultural and Food Chemistry*, 44, 3182-3188.

Franklin, N.M., Rogers, N.J., Apte, S.C., Batley, G.E., Gadd, G.E. and Casey, P.S. (2007), 'Comparative toxicity of nanoparticulate ZnO, bulk ZnO, and ZnCl2 to a freshwater microalga (Pseudokirchneriella subcapitata): the importance of particle solubility', *Environmental Science and Technology*, 41, 8484-8490.

Gatti, A.M., Tossini, D., Gambarelli, A., Montanari, S. and Capitani, F. (2009), 'Investigation of the Presence of Inorganic Micro- and Nanosized Contaminants in Bread and Biscuits by Environmental Scanning Electron Microscopy', *Critical Reviews in Food Science and Nutrition*, 49, 275-282.

Haedelt, J., Beckett, S. and Niranjan, K. (2007), 'Bubble-Included Chocolate: Relating Structure with Sensory Response', *Journal of Food Science*, 72, E138-E142.

Hassellöv, M., Readman, J.W., Ranville, J.F. and Tiede, K. (2008), 'Nanoparticle

analysis and characterization methodologies in environmental risk assessment of engineered nanoparticles', *Ecotoxicology*, 17, 344-361.

Isaacson, C.W., Usenko, C.Y., Tanguay, R.L. and Field, J.A. (2007), 'Quantification of Fullerenes by LC/ESI-MS and Its Application to in Vivo Toxicity Assays', *Analytical Chemistry*, 79, 9091-9097.

Istarova, T., Semenova, M., Sorokoumova, G., Selishcheva, A., Belyakova, L., Polikarpov, Y. and Anokhina, M. (2005), 'Effect of pH on the interactions of sodium caseinate with soy phospholipids in relation to the foaming ability of their mixtures', *Food Hydrocolloids*, 19, 429-440.

Ito, T., Ibrahim, S. and Grabowska, I. (2010), 'Chemical-force microscopy for materials characterization', *Trends in Analytical Chemistry*, 29, 225-233.

Jackson, B.P., Pace, H.E., Lanzirotti, A., Smith, R. and Ranville, J.F. (2009), 'Synchrotron X-ray 2D and 3D elemental imaging of CdSe/ZnS quantum dot nanoparticles in Daphnia magna', *Analytical and Bioanalytical Chemistry*, 394, 911-917.

Jackson, S.N., Wang, H.J., Woods, A.S., Ugarov, M., Egan, T. and Schultz, J.A. (2005), 'Direct tissue analysis of phospholipids in rat brain using MALDI-TOFMS and MALDI-ion mobility-TOFMS', *Journal of American Society for Mass Spectrometry*, 16, 133-138.

James, B. (2009), 'Advances in "wet" electron microscopy techniques and their application to the study of food structure', *Trends in Food Science & Technology*', 20, 114-124.

James, B.J. and Smith, B.G. (2009), 'Surface structure and composition of fresh and bloomed chocolate analysed using X-ray photoelectron spectroscopy, cryo-scanning electron microscopy and environmental scanning electron microscopy', *LWT - Food Science and Technology*, 42, 929-937.

Janz, A., Köckritz, A., Yao, L. and Martin, A. (2010), 'Fundamental calculations on the surface area determination of supported gold nanoparticles by alkanethiol adsorption', *Langmuir: The ACS Journal of Surfaces and Colloids*, 26, 6783-6789.

Jarvie, H.P., Al-Obaidi, H., King, S.M., Bowes, M.J., Lawrence, M.J., Drake, A.F., Green, M.A. and Dobson, P.J. (2009), 'Fate of Silica Nanoparticles in Simulated Primary Wastewater Treatment', *Environmental Science & Technology*. 43, 8622-8628.

Jiang, J., Oberdörster, G., Elder, A., Gelein, R., Mercer, P. and Biswas, P. (2008),

'Does nanoparticle activity depend upon size and crystal phase?', *Nanotoxicology*, 2, 33-42.

Kaláb, M., Allan-Wojtas, P. and Miller, S.S. (1995), 'Microscopy and other imaging techniques in food structure analysis', *Trends in Food Science & Technology*, 6, 177-186.

Kaláb, M. and Larocque, G. (1996), 'Research Note: Suitability of Agar Gel Encapsulation of Milk and Cream for Electron Microscopy', *Lebensmittel-Wissenschaft und-Technologie*, 29, 368-371.

Kandar, A.K., Srivastava, S., Basu, J.K., Mukhopadhyay, M.K., Seifert, S. and Narayanan, S. (2009), 'Unusual dynamical arrest in polymer grafted nanoparticles', *Journal of Chemical Physics*, 130, 121102-121107.

Karoui, R. and Debaerdemaeker, J. (2007), 'A review of the analytical methods coupled with chemometric tools for the determination of the quality and identity of dairy products', *Food Chemistry*, 102, 621-640.

Kaszuba, M., McKnight, D., Connah, M.T., McNeil-Watson, F.K. and Nobbmann, U. (2007), 'Measuring sub nanometre sizes using dynamic light scattering', *Journal of Nanoparticle Research*, 10, 823-829.

Katayama, Y., Burkacky, O., Meyer, M., Bräuchle, C., Gratton, E. and Lamb, D.C. (2009), 'Real-Time Nanomicroscopy via Three-Dimensional Single-Particle Tracking', *ChemPhysChem*, 10, 2458-2464.

Kendall, K., Dhir, A. and Du, S. (2009), 'A new measure of molecular attractions between nanoparticles near kT adhesion energy', *Nanotechnology*, 20, 275701-275705.

Kittler, S., Greulich, C., Diendorf, J., Köller, M. and Epple, M. (2010), 'Toxicity of Silver Nanoparticles Increases during Storage Because of Slow Dissolution under Release of Silver Ions', *Chemistry of Materials*, 22, 4548-4554.

Koh, A.L., Shachaf, C.M., Elchuri, S., Nolan, G.P. and Sinclair, R. (2008), 'Electron Microscopy Localization and Characterization of Functionalized Composite Organic-Inorganic SERS Nanoparticles on Leukemia Cells', *Ultramicroscopy*, 109, 111-121.

Kopping, J.T. and Patten, T.E. (2008), 'Identification of acidic phosphorus-containing ligands involved in the surface chemistry of CdSe nanoparticles prepared in tri-N-octylphosphine oxide solvents', *Journal of the American Chemical Soc*iety, 130, 5689-5698.

Lam, C. (2003), 'Pulmonary Toxicity of Single-Wall Carbon Nanotubes in Mice 7 and 90 Days After Intratracheal Instillation', *Toxicological Sciences*, 77, 126-134.

Lee, D., Park, K. and Zachariah, M.R. (2005), 'Determination of the Size Distribution of Polydisperse Nanoparticles with Single-Particle Mass Spectrometry: The Role of Ion Kinetic Energy', *Aerosol Science and Technology*, 39, 162-169.

Lei, R., Wu, C., Yang, B., Ma, H., Shi, C., Wang, Q., Wang, Q., Yuan, Y. and Liao, M. (2008), 'Integrated metabolomic analysis of the nano-sized copper particle-induced hepatotoxicity and nephrotoxicity in rats: A rapid in vivo screening method for nanotoxicity', *Toxicology and Applied Pharmacology*, 232, 292-301.

Lewinski, N.A., Zhu, H., Jo, H., Pham, D., Kamath, R.R., Ouyang, C.R., Vulpe, C.D., Colvin, V.L. and Drezek, R.A. (2010), 'Quantification of Water Solubilized CdSe/ZnS Quantum Dots in Daphnia magna', *Environmental Science and Technology*, 44, 1841-1846.

Li, Y., Lee, J., Lal, J., An, L. and Huang, Q. (2008), 'Effects of pH on the Interactions and Conformation of Bovine Serum Albumin: Comparison between Chemical Force Microscopy and Small-Angle Neutron Scattering', *Journal of Physical Chemistry B*, 112, 3797-3806.

Liu, J., Chao, J., Liu, R., Tan, Z., Yin, Y., Wu, Y. and Jiang, G. (2009), 'Cloud Point Extraction as an Advantageous Preconcentration Approach for Analysis of Trace Silver Nanoparticles in Environmental Waters', *Analytical Chemistry*, 81, 6496-6502.

Lombardo-Agüí, M., García-Campaña, A.M., Gámiz-Gracia, L. and Cruces Blanco, C. (2010), 'Laser induced fluorescence coupled to capillary electrophoresis for the determination of fluoroquinolones in foods of animal origin using molecularly imprinted polymers', *Journal of Chromatography A*, 1217, 2237-2242.

Lopez-Rubio, A. and Gilbert, E.P. (2009), 'Neutron scattering: a natural tool for food science and technology research', *Trends in Food Science & Technology*, 20, 576-586.

Lorenz, C., Tiede, K., Tear, S., Boxall, A., Von Goetz, N. and Hungerbuhler, K (2010) Imaging and characterization of engineered nanoparticles in sunscreens by electron microscopy, under wet and dry conditions. *International Journal of Occupational and Environmental Health*, 16, 406–428

Luykx, D.M.A.M., Peters, R.J.B., van Ruth, S.M. and Bouwmeester, H. (2008), 'A Review of Analytical Methods for the Identification and Characterization of Nano

Delivery Systems in Food', *Journal of Agricultural and Food Chemistry*, 56, 8231-8247.

Lynch, I. and Dawson, K.A. (2008), 'Protein-nanoparticle interactions', *Nano Today*, 3, 40-47.

Mariette, F. (2009), 'Investigations of food colloids by NMR and MRI', *Current Opinion in Colloid & Interface Science*, 14, 203-211.

Martin, J.E., Herzing, A.A., Yan, W., Li, X., Koel, B.E., Kiely, C.J. and Zhang, W. (2008), 'Determination of the Oxide Layer Thickness in Core−Shell Zerovalent Iron Nanoparticles', *Langmuir*, 24, 4329-4334.

McCormick, N., Velasquez, V., Finney, L., Vogt, S. and Kellher, S. (2010), 'X-Ray Fluorescence Microscopy Reveals Accumulation and Secretion of Discrete Intracellular Zinc Pools in the Lactating Mouse Mammary Gland', *PLoS ONE*, 5, e11078.

Meyer, V.R. (2000), Practical *High-Performance Liquid Chromatography*, John Wiley and Sons.

Mishchenko, M.I. (2009), 'Electromagnetic scattering by nonspherical particles: A tutorial review', *Journal of Quantitative Spectroscopy and Radiative Transfer*, 110, 808-832.

Noronha, N., Duggan, E., Ziegler, G., Stapleton, J., O'Riordan, E. and O'Sullivan, M. (2008), 'Comparison of microscopy techniques for the examination of the microstructure of starch-containing imitation cheeses', *Food Research International*, 41, 472-479.

Norwegian Pollution Control Authority (2008). *Environmental fate and ecotoxicity of engineered nanoparticles.* E.J. Joner, T. Hartnik and C.E. Amundsen. Bioforsk.

Peters, R.J.B., ten Dam, G., Bouwmeester, H., Helsper, H., Allmaier, G., von der Kammer, F., Ramsch, R., Solans, C., Tomaniová, M., Hajslova, J. and Weigel, S. (2011), 'Identification and characterization of organic nanoparticles in food', *Trends in Analytical Chemistry*, 30, 100-112

Plathe, K.L., von der Kammer, F., Hassellöv, M., Moore, J., Murayama, M., Hofmann, T. and Hochella, M.F. (2010), 'Using FlFFF and aTEM to determine trace metal–nanoparticle associations in riverbed sediment', *Environmental Chemistry*, 7, 82-93.

Prestidge, C.A. and Ametov, I. (2000), 'Cation effects during aggregation and agglomeration of gibbsite particles under synthetic Bayer crystallisation conditions', *Journal of Crystal Growth*, 209, 924-933.

Qian, H., Eckenhoff, W.T., Zhu, Y., Pintauer, T. and Jin, R. (2010), 'Total Structure Determination of Thiolate-Protected Au38 Nanoparticles', *Journal of the American Chemical Society*, 132, 8280-8281.

Relkin, P., Sourdet, S., Smith, A., Goff, H. and Cuvelier, G. (2006), 'Effects of whey protein aggregation on fat globule microstructure in whipped-frozen emulsions', *Food Hydrocolloids*, 20, 1050-1056.

Riley, T., Heald, C.R., Stolnik, S., Garnett, M.C., Illum, L., Davis, S.S., King, S.M., Heenan, R.K., Purkiss, S.C., Barlow, R.J., Gellert, P.R. and Washington, C. (2003), 'Core−Shell Structure of PLA−PEG Nanoparticles Used for Drug Delivery', *Langmuir*, 19, 8428-8435.

Rodríguez-González, B., Burrows, A., Watanabe, M., Kiely, C.J. and Liz Marzán, L.M. (2005), 'Multishell bimetallic AuAg nanoparticles: synthesis, structure and optical properties', *Journal of Materials Chemistry*, 15, 1755-1759.

Stokes, D. (2008), *Principles and Practice of Variable Pressure/ Environmental Scanning Electron Microscopy (VP-ESEM)*, New York: John Wiley.

Tadjiki, S., Assemi, S., Deering, C.E., Veranth, J.M. and Miller, J.D. (2008), 'Detection, separation, and quantification of unlabeled silica nanoparticles in biological media using sedimentation field-flow fractionation', *Journal of Nanoparticle Research*, 11, 981-988.

Tiede, K., Boxall, A., Tear, S., Lewis, J., David, H. and Hassellov, M. (2008), 'Detection and characterization of engineered nanoparticles in food and the environment', *Food Additives and Contaminants*, 25, 795-821.

Tiede, K., Boxall, A.B.A., Tiede, D., Tear, S.P., David, H. and Lewis, J. (2009a), 'A robust size-characterisation methodology for studying nanoparticle behaviour in 'real' environmental samples, using hydrodynamic chromatography coupled to ICP-MS', *Journal of Analytical Atomic Spectrometry*, 24, 964-972.

Tiede, K., Boxall, A.B.A., Wang, X., Gore, D., Tiede, D., Baxter, M., David, H., Tear, S.P. & Lewis, J. (2010), 'Application of hydrodynamic chromatography-ICP-MS to investigate the fate of silver nanoparticles in activated sludge', *Journal of Analytical Atomic Spectrometry*, 25, 1149-1154.

Tiede, K., Tear, S.P., David, H. & Boxall, A.B. (2009b), 'Imaging of engineered

nanoparticles and their aggregates under fully liquid conditions in environmental matrices', *Water Research*, 43, 3335-3343.

Uboldi, C., Bonacchi, D., Lorenzi, G., Hermanns, M.I., Pohl, C., Baldi, G., Unger, R.E. and Kirkpatrick, C.J. (2009), 'Gold nanoparticles induce cytotoxicity in the alveolar type-II cell lines A549 and NCIH441', *Particle and Fibre Toxicology*, 6, 6-18.

U.S. Food and Drug Administration (2010), 'Nanotechnology Task Force Report 2007' Available from: http://www.fda.gov/ScienceResearch/SpecialTopics/Nanotechnology/NanotechnologyTaskForceReport2007/default.htm. (Accessed 14 November 2010).

Vale, G., Rodrigues, A., Rocha, A., Rial, R., Mota, A., Gonçalves, M., Fonseca, L. and Capelo, J. (2010), 'Ultrasonic assisted enzymatic digestion (USAED) coupled with high performance liquid chromatography and electrothermal atomic absorption spectrometry as a powerful tool for total selenium and selenium species control in Se-enriched food supplements', *Food Chemistry*, 121, 268-274.

Valous, N.A., Mendoza, F. and Sun, D. (2010), 'Emerging non-contact imaging, spectroscopic and colorimetric technologies for quality evaluation and control of hams: a review', *Trends in Food Science & Technology*, 21, 26-43.

von der Kammer, F., Legros, S., Larsen, E.H., Löschner, K. and Hofmann, T. (2011), 'Separation and characterization of nanoparticles in complex samples (food/environment) by Field Flow Fractionation', *Trends in Analytical Chemistry*, 30, 425-436

Weisman, S., Hirschlerner, D., Barenholz, Y. and Talmon, Y. (2004), 'Nanostructure of Cationic Lipid-Oligonucleotide Complexes', *Biophysical Journal*, 87, 609-614.

Wong, H., Choi, S., Phillips, D. and Ma, C. (2009), 'Raman spectroscopic study of deamidated food proteins', *Food Chemistry*, 113, 363-370.

Yang, H., Wang, Y., Lai, S., An, H., Li, Y. and Chen, F. (2007), 'Application of atomic force microscopy as a nanotechnology tool in food science', *Journal of Food Science*, 72, 65-75.

Zabar, S., Shimoni, E. and Bianco-Peled, H. (2008), 'Development of nanostructure in resistant starch type III during thermal treatments and cycling.', *Macromolecular Bioscience*, 8, 163-170.

Zanetti-Ramos, B.G., Fritzen-Garcia, M.B., de Oliveira, C.S., Pasa, A.A., Soldi, V., Borsali, R. and Creczynski-Pasa, T.B. (2009), 'Dynamic light scattering and atomic

force microscopy techniques for size determination of polyurethane nanoparticles' *Materials Science and Engineering: C*, 29, 638-640.

Zhong, L., Liao, W., Wang, X. and Cai, J. (2008), 'Detection the specific marker of CD3 molecules of human peripheral blood T lymphocytes using SNOM and quantum dots', *Colloids and Surfaces A: Physicochemical and Engineering Aspects*. 313-314, 642-646.

3.8 Appendix: glossary

AAS	Atomic absorption spectroscopy
AFM	Atomic force microscopy
ANUC	Analytical ultracentrifugation
BET	Brunauer-Emmet-Teller chemisorption method
CE	Capillary electrophoresis
CFM	Chemical force microscopy
CLSM	Caonfocal laser scanning microscopy
CPC	Condensation particle counter
DART	Direct analysis in a real time
DESI	Desorption electrospray ionization
DLS	Dynamic light scattering
DSC	Differential scanning calorimetry
DTA	Differential thermal analysis
EDS	Energy-dispersive X-ray spectroscopy
EELS	Electron energy loss spectroscopy
EM	Electron microscopy
EPR	Electron paramagnetic resonance
ESEM	Environmental scanning electron microscopy
ESI	Electrospray ionization
ETEM	Environmental transmission electron microscopy
FIB	Focused ion beam
FFF	Field flow fractionation
HDC	Hydrodynamic chromatography
ICP	Inductively coupled plasma
IMS	Ion mobility spectrometry
LIBD	Laser-induced breakdown detection
LIF	Laser-induced fluorescence
MALDI	Matrix assisted desorption ionization
MALLS	Multiangle laser light scattering
MS	Mass spectrometry

NDS	Nanodelivery systems
NMR	Nuclear magnetic resonance
NP	Nanoparticle
NSOM	Near-field scanning optical microscopy
OES	Optical emission spectroscopy
PNC	Particle number concentration
RLS	Resonance light scattering
RS	Raman spectroscopy
SANS	Small angle neutron scattering
SAXS	Small angle X-ray scattering
SEC	Size exclusion chromatorgraphy
SEM	Scanning electron microscopy
SLS	Static light scattering
SMPS	Scanning mobility particle sizer
SPMS	Single particle mass spectrometry
SPR	Surface plasmon resonance
STEM	Scanning transmission electron microscopy
TEM	Transmission electron microscopy
TG	Thermogravimetry
TOF	Time of flight
UV-VIS	Ultraviolet-visible spectrophotometry
WDS	Wavelength-dispersive X-ray spectroscopy
XAS	X-ray absorption spectroscopy
XPS	X-ray photoelectron spectroscopy
XRD	X-ray diffraction
XRF	X-ray fluorescence spectroscopy
XRM	X-ray microscopy

Electron Microscopy and Analysis Group Conference 2013 (EMAG2013) IOP Publishing
Journal of Physics: Conference Series **522** (2014) 012057 doi:10.1088/1742-6596/522/1/012057

Sample preparation and EFTEM of Meat Samples for Nanoparticle Analysis in Food

L. Lari[1,2,3] **and A. Dudkiewicz**[4, 5]

[2]Department of Physics, University of York, Heslington, YO10 5DD, York, UK.
[3]The York JEOL Nanocentre, York Science Park, Heslington, YO10 5BR, York, UK
[4]Food and Environment Research Agency, YO41 1LZ, York,
[5]Department of Environment, University of York, Heslington, YO10 5DD, York, UK

E-mail: leonardo.lari@york.ac.uk

Abstract. Nanoparticles are used in industry for personal care products and the preparation of food. In the latter application, their functions include the prevention of microbes' growth, increase of the foods nutritional value and sensory quality. EU regulations require a risk assessment of the nanoparticles used in foods and food contact materials before the products can reach the market. However, availability of validated analytical methodologies for detection and characterisation of the nanoparticles in food hampers appropriate risk assessment. As part of a research on the evaluation of the methods for screening and quantification of Ag nanoparticles in meat we have tested a new TEM sample preparation alternative to resin embedding and cryo-sectioning. Energy filtered TEM analysis was applied to evaluate thickness and the uniformity of thin meat layers acquired at increasing input of the sample demonstrating that the protocols used ensured good stability under the electron beam, reliable sample concentration and reproducibility.

1. Introduction

The new emerging trend in the food industry exploits nanotechnology for versatile developments. One example is silver nanoparticles (NPs) used for food application. For their antimicrobial properties, silver nanoparticles (AgNPs) are used in food supplements and various food contact surfaces (e.g. packaging, cutting boards, cutlery)[1]. AgNPs are reported to be cytotoxic not only to bacterial but also human cells [2]. One of the reasons for this increased toxicity of AgNPs is associated with their size [2]. However, NPs size undergoes dynamic changes after spiking in complex matrices e.g. agglomeration/ aggregation, dissolution, deagglomeration [3-5]. Therefore The European Food Safety Authority emphasizes that for appropriate risk assessment of NPs in foods and feed, a particle size measurement in the hosting food products is necessary [6]. Of special interest among the methods allowing NP size measurement is electron microscopy (EM) coupled spectrometry methods. However, standard sample preparation protocol for solid food samples e.g. meat involves such methods as resin embedding or freezing and sectioning of frozen material [7]. Both methods are laborious, require sophisticated equipment and technical skills. Additionally the volume of the sample that can be

[1] To whom any correspondence should be addressed.

Content from this work may be used under the terms of the Creative Commons Attribution 3.0 licence. Any further distribution of this work must maintain attribution to the author(s) and the title of the work, journal citation and DOI.
Published under licence by IOP Publishing Ltd

Electron Microscopy and Analysis Group Conference 2013 (EMAG2013) IOP Publishing
Journal of Physics: Conference Series **522** (2014) 012057 doi:10.1088/1742-6596/522/1/012057

analysed in EM at once is very limited, making the method only useful for samples containing very high numbers of particles. In this study we test an alternative sample preparation protocol based on sedimentation of homogenized and highly diluted samples onto TEM grids. This approach allows a reduction in sample preparation time down to 1-2 hours and does not require skills necessary for thin sectioning of frozen or embedded material. The samples are dried prior to analysis and therefore it is possible to increase the analysed sample volume when compared to traditional approaches. In this work we report stability of the sample in the electron beam and summarize data regarding the sample layer thickness and its uniformity at increasing sample concentration. These parameters have a crucial meaning for the size measurement and quantification of NPs in food samples by EM. The study demonstrates application of powerful tools, energy filtered transmission electron microscopy (EFTEM) and electron energy loss spectrometry (EELS) for the measurement of the meat sample thickness.

2. Material and methods

Meat emulsion was obtained using the equipment and the methodology as described in [8]. However, at the final stage, the cryo-milled meat was not frozen and no AgNPs were added. The material was preserved using Proclin 150^{TM} at a concentration of 1.1 g/ kg and aseptically packed in 50 ml amber vials. The density of the meat emulsion was 1.006 g/ ml. Aqueous dispersion of AgNPs stabilized with polyvinylpyrrolidone at concentration of 0.1% m/m and nominal size of 42±10 nm was originally obtained from Nanogap (Milladoiro, Spain). AgNPs were mixed with the meat emulsion in a 1:1 ratio using a potter type homogenizer until visual homogeneity of the resulting viscous liquid was obtained.

TEM samples were prepared by dilution, homogenization and subsequent sedimentation of the AgNPs/meat viscous liquid on formvar-carbon coated, 400 mesh Cu TEM grids (Agar Scientific, Stansted, UK). A borate buffer at pH 8.0 (0.05M H_3BO_3, 0.05M KCl, 0.004M NaOH) was used for the dilution step for three dilution factors, 200 fold m/m (Sample *A*), 500 fold m/m (Sample *B*) and 2000 fold m/m (Sample *C*) respectively. The diluted emulsions were dispersed in the buffer using potter type homogenizer and subsequently homogenized with ultrasonic probe (Misonix, USA) in vials for 1 min at 100 W. During homogenization, vials were kept cool by immersion in water with ice. Lastly, 0.5 g of sample at each dilution level were transferred to polyallomer centrifuge tubes and topped up with the buffer to the level of 2-3 mm from the tube rim. The tubes were equipped with solid Agar 100 resin fillers (Agar Scientific, Stansted, UK) at the bottom to ensure flat support for the TEM grids. Samples were sedimented on the TEM grids in Beckman XL-100 ultracentrifuge (Beckman, California, USA), equipped with SW40Ti rotor and operating at RCF=100.000 g at 20^{0}C for 1h. Characterization by EFTEM was undertaken using a JEM-2200 FS (JEOL Ltd., Tokyo, Japan) field emission TEM operating at 200 kV, equipped with an in-column Omega-type energy filter, and CEOS image and probe 3rd order aberration correctors. Sample thickness was measured using the Digital Micrograph (DM) (Gatan, Pleasanton, USA) EFTEM thickness map routine.

3. Results and discussion

Figure 1 shows typical sample thickness analysis for the three samples. Bright field images in Fig. 1a), 1b) and 1c) show nanoparticles embedded in the dried emulsions. t/λ maps in Fig. 1e), 1f) and 1g) (where t is the sample thickness and λ is the electron mean free path for inelastic scattering) were obtained through acquisition and application of the log-ratio method [9] of an unfiltered bright field (BF) image followed by an elastic image with 10eV energy slit centred onto the zero loss peak (512x512 pxl, 3s acquisition). AgNPs were found positioned at different heights within the sample regardless of the dilution applied, demonstrating that the sample preparation method provided layers of significant thickness. The sample drift during the map acquisition was evaluated and removed using AgNPs as a reference for image correlation. Figure 1d)-f) show t/λ maps respectively for sample *A*, *B* and *C*. Cross correlation results from each map acquisition show an average drift of 2.4pxl (Sample *A*), 1.6 pxl (Sample *B*) and 4 pxl (sample *C*) corresponding to 3.2nm (0.5% of the field of view), 2.2nm (0.3%) and 5.4nm (0.8%). This shows that during the images acquisition, and regardless of the

Electron Microscopy and Analysis Group Conference 2013 (EMAG2013) IOP Publishing
Journal of Physics: Conference Series **522** (2014) 012057 doi:10.1088/1742-6596/522/1/012057

level of sample dilution, the samples were stable under the electron beam, *i.e.* no significant sample drift or shrinkage could be observed.

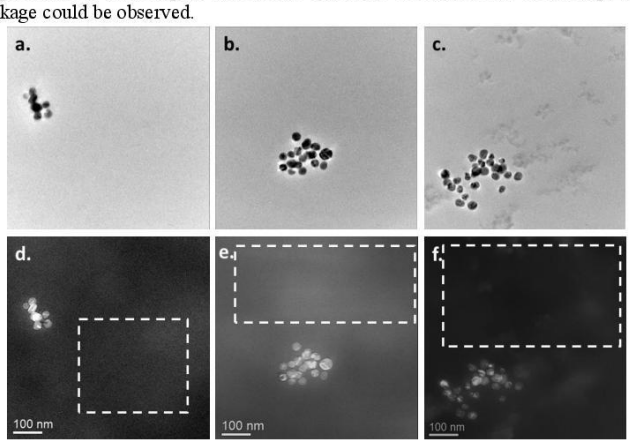

Figure 1. EFTEM analysis of *Ag NPs in 200 (a) and (d) (Sample A), 500 (b) and (e) (Sample B), and 2000 fold (c) and (f) (Sample C) with BF TEM images a.)-c.) and thickness maps d)-f); dashed boxes indicates typical areas of t/λ mean values measurement .*

The sample thickness was calculated from t/λ measurements on particle free areas and the results are reported in Table 1. λ was estimated using the following equations:

$$\lambda = \frac{106\,F\,\frac{E_0}{E_m}}{\ln(2\,\beta\,\frac{E_0}{E_m})} \quad (1)\,[9]; \qquad E_m = 7.6\,Z_{eff}^{0.36} \quad (2)\,[10]; \qquad Z_{eff} = \frac{(\sum Z_i\,f_i)^{1.3}}{(\sum Z_i\,f_i)^{0.3}} \quad (3)\,[9],$$

where F is-a relativistic factor (0.618 for 200kV electrons), E_0 the incident beam energy, E_m the mean energy loss (calculated using eq.(2)). The effective atomic number Z_{eff} is calculated according to fractions (f) of the (i) elements in the sample of atomic number Z as described in equation (3).

Table 1. EFTEM measurements of t/λ and mean values of calculated thickness

Dilution factor	$t/\lambda \pm$ s.d.	t (nm) ± sd
(**A**) 1 in 199	1.75 ± 0.31	260 ± 46
(**B**) 1 in 499	0.79 ± 0.26	118 ± 39
(**C**) 1 in 1999	0.50 ± 0.10	74 ± 15

Standard deviations (s.d.) are given from measurements in 5 different areas per sample.

β indicates the collection aperture, in our case no aperture was used and a value of 15mrad was chosen to feed into eq.(1) according to [10]. The sample (+support) composition was estimated by EELS spectroscopy (see Figure2a). A spectrum was acquired within a region comprising the main elements present in the meat (C, O, N) sample. Quantification was done using calculated cross sections in DM quantification routine producing the following elemental composition: C 88at%, N 7at% and O 5at%. λ value was estimated to be 149nm.

The mean sample thickness (see Table 1) varies with the sample dilution and increases with decreasing dilution factor. The measurements over 5 areas across the TEM grid point out good homogeneity of the sample thickness over the grid, potentially allowing quantification of homogenously distributed NPs in meat emulsion. However, the calculated sample thickness included the thickness of the formvar-carbon film initially present on the TEM grid. To estimate the film's thickness we used a linear fit of the measured sample+support thickness versus the quantity of sample applied in milligrams (see Figure 2b). The support thickness can be evaluated at

Electron Microscopy and Analysis Group Conference 2013 (EMAG2013) IOP Publishing
Journal of Physics: Conference Series **522** (2014) 012057 doi:10.1088/1742-6596/522/1/012057

the intercept on the x-axis (no sample applied) of the fitting function, which corresponds to a value of ~ 40 nm. This value is in good agreement with the value provided by the manufacturer: 30-40 nm of formvar and ~10 nm of carbon. Therefore the thickness for sample A, B and C is respectively about 220, 80, and 30nm. We have calculated that same samples in the hydrated state (based on meat emulsion density) would create 34±9 times thicker layer on the TEM grid. This figure also defines the level of the sample pre-concentration compared to the cryo- and resin embedding preparations where the volume changes in comparison to hydrated sample are minimal.

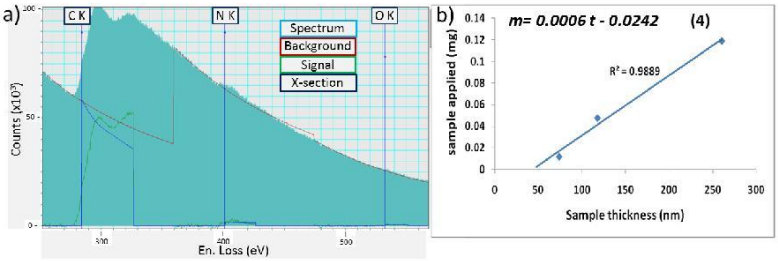

Figure 2. a) *Quantified EELS spectrum showing C, O and N K-edges. Red, green and blue lines represent background, net signal, and calculated cross section for quantification. b) Linear fit of sample applied versus sample thickness with linear fit equation (4) inset .*

4. Conclusions

In this paper we have evaluated a new sample preparation approach for potential quantification and measurement of NPs in food. EFTEM and EELS were successfully applied to measure the thickness of meat sample containing AgNPs. Using the described sample preparation protocol, we were able to obtain meat emulsion layers where the weight input of meat emulsion was linearly related to the TEM sample thickness and allowed to predict the support thickness for null input. This protocol provides a quicker and easier sample preparation method with respect to traditionally used solutions, such as resin embedding and cryo-sectioning, and allows increasing the amount of sample volume analysed.

Acknowledgements

The authors would like to acknowledge Prof. Kristian Mølhave from Danish Technical University (Lyngby, Denmark) for advice regarding experimental design, as well as Dr T. Linsinger and Dr R. Grombe at IRMM, JRC (Brussels, Belgium) for providing materials. Financial support from EU Programme NanoLyse (FP7/2007-2013) under grant agreement n° 245162 is gratefully acknowledged

References

[1] "PEN The Project on Emerging Nanotechnologies." http://www.nanotechproject.org/, 2013.
[2] Liu W. *et al.* 2010 Nanotoxicology **4** 319
[3] Luo P. *et al.*, J. 2013 Microsc **250** 32
[4] Zook J. M. *et al.* 2011 Anal. Bioanal. Chem. **401** 1993
[5] Peters R. *et al.* 2012 Acs Nano **6** 2441
[6] EFSA Scientific Committee, 2011 EFSA Journal **9** 1
[7] Dudkiewicz A. *et al.,* 2011 Trends in Analytical Chemistry **30** 28
[8] Grombe R. *et al.* "Production of Reference Materials for Analytical Method Development for Nanoparticles in Food. Part 2" submitted Anal. Bioanal. Chem.
[9] Egerton R. F., *Electron energy-loss spectroscopy in the electron microscope* (Plenum Press, New York, 1996).
[10] Malis T *et al.* 1988 J. Electron Microscopy Techniques **8** 193

Annex 4

Journal of Microscopy

Journal of Microscopy, Vol. 250, Pt 1 2013, pp. 32–41
Received 22 July 2012; accepted 5 January 2013

doi: 10.1111/jmi.12014

Visualization and characterization of engineered nanoparticles in complex environmental and food matrices using atmospheric scanning electron microscopy

P. LUO*, I. MORRISON†, A. DUDKIEWICZ*,‡, K. TIEDE‡, E. BOYES§, P. O'TOOLE†, S. PARK* & A.B. BOXALL*

**Environment Department, The University of York, Heslington, York, UK*
†*Department of Biology, The University of York, Heslington, York, UK*
‡*Ecological Chemistry, The Food and Environment Research Agency, Sand Hutton, York, UK*
§*York JEOL Nanocentre, Science Park, The University of York, Heslington, York, UK*

Key words. Atmospheric scanning electron microscope (ASEM), ASEM detection limit, nanoparticle characterization, nanoparticle tracking analysis (NTA), scanning electron microscopy (SEM), transimission electron microscopy (TEM).

Summary

Imaging and characterization of engineered nanoparticles (ENPs) in water, soils, sediment and food matrices is very important for research into the risks of ENPs to consumers and the environment. However, these analyses pose a significant challenge as most existing techniques require some form of sample manipulation prior to imaging and characterization, which can result in changes in the ENPs in a sample and in the introduction of analytical artefacts. This study therefore explored the application of a newly designed instrument, the atmospheric scanning electron microscope (ASEM), which allows the direct characterization of ENPs in liquid matrices and which therefore overcomes some of the limitations associated with existing imaging methods. ASEM was used to characterize the size distribution of a range of ENPs in a selection of environmental and food matrices, including supernatant of natural sediment, test medium used in ecotoxicology studies, bovine serum albumin and tomato soup under atmospheric conditions. The obtained imaging results were compared to results obtained using conventional imaging by transmission electron microscope (TEM) and SEM as well as to size distribution data derived from nanoparticle tracking analysis (NTA). ASEM analysis was found to be a complementary technique to existing methods that is able to visualize ENPs in complex liquid matrices and to provide ENP size information without extensive sample preparation. ASEM images can detect ENPs in liquids down to 30 nm and to a level of 1 mg L^{-1} (9×10^8 particles mL^{-1}, 50 nm Au ENPs). The results indicate ASEM is a highly complementary method to existing approaches for analyzing ENPs in complex media and that its use will allow those studying to study ENP behavior *in situ*, something that is currently extremely challenging to do.

Correspondence to: Ping Luo, Environment Department, The University of York, Heslington, *York YO10 5DD, UK*. Tel.: 0044-1904-462000 (ext 3538); fax: 0044-1904-322998; e-mail: ping.luo@live.cn.

Introduction

As a result of the increase in the usage of engineered nanoparticles (ENPs) in every day products, there are growing concerns about the safety of ENPs to humans and the environment (Hristozov & Malsch, 2009). A large number of studies have and are being performed to assess the risks of ENPs in the environment and food to human and ecological health (Green & Ndegwa, 2011). In order to understand levels of exposure in the environment and food stuffs and the mechanisms driving toxicity of ENPs, precise characterization of the concentrations and properties of the ENPs in their respective media is essential, which unfortunately remains a significant challenge (Tiede *et al.*, 2009a; Boxall *et al.*, 2007; Liu *et al.*, 2012). Although conventional analytical methods, e.g. inductively coupled plasma mass spectrometry (ICP-MS) and atomic absorption spectroscopy (AAS) and light scattering techniques have been commonly used in the analysis of ENPs (Tiede *et al.*, 2009b; Gillespie, Halling, & Edwards, 2011), these techniques only provide information on mass concentrations and/or particle size distributions of ENPs. They do not however provide information on e.g. the morphology of ENPs.

© 2013 The Authors
Journal of Microscopy © 2013 Royal Microscopical Society

Morphological information can be obtained using image-based approaches such as electron microscopy (Dudkiewicz *et al.*, 2011). In combination with methods for elemental analysis, e.g. energy dispersive X-ray spectroscopy (EDS), conventional electron microscopy can allow visualization of ENPs within a sample and can provide information on the chemical composition of the ENPs (Tiede *et al.*, 2008; Lorenz *et al.*, 2010). The vacuum environment inside the microscope chamber however dictates that samples usually need to be prepared in such a way that they are in a dry or solid state. This necessity can introduce artefacts during drying processes leading to erroneous results (Blasco & Picó, 2011). These artefacts can be avoided by e.g. using cryogenic preparation methodologies or wet scanning electron microscopy capsules (wetSEM; e.g. Tiede *et al.*, 2009b) or by the application of other imaging technologies such as environmental scanning electron microscopy (ESEM; e.g. Gatti *et al.*, 2008). However, cryogenic preparation is very time-consuming, ESEM does not work at 'real' atmospheric pressures which is very important for environmental studies, and the electron-transparent polymer QuantomiX capsule film used in wetSEM is vulnerable to electron beam damage (Tiede *et al.*, 2009b) and introduces the sample in an inverted scenario thus making sedimentary material difficult to image.

Due to the challenges around analysis of ENPs in complex media, and the limitations of different available methods, most researchers recognize that a suite of methods needs to be applied to a sample in order to produce useful data. Here we demonstrate a relatively new approach, atmospheric scanning electron microscope (ASEM), which is an instrument offering scanning electron imaging at atmospheric pressure. The use of a silicon nitride (SiN_x) membrane in the ASEM dish has drastically improved the stability of the sample enclosure when compared with the QuantomiX WetSEM capsule. It prevents the moisture from leaking into the vacuum chamber, is electron transparent, and it is stable up to 150°C in aqueous samples (Suga *et al.*, 2011).

An added advantage is that the system uses an inverted column, thus the samples are imaged from below. This allows for imaging of sedimentary materials. ASEM can therefore minimize artefacts introduced by sample preparation while avoiding some of the limitations and undesired sample handling problems associated with ESEM and WetSEM. So far, the method has been successfully used to visualize cell structure and nuclei (Nishiyama *et al.*, 2010), mycoplasma (Sato *et al.*, 2012), nitrate solution, silver paste, solder paste and the self-organization process of particles (Suga *et al.*, 2011). However, to the best of our knowledge, it has not yet been applied in the nanosafety research area. This study therefore investigated the application of ASEM to a range of environmental and food matrices and a range of ENPs. The results were compared to results obtained using TEM, SEM and nanoparticle tracking analysis (NTA) to evaluate the advantages and disadvantages of the method.

Methods and material

Study ENPs

Mercaptoundecanoic acid coated (MUDA) Au ENPs, with a nominal diameter of 30 nm, were obtained from Dr Jon Veinot at the University of Alberta (Edmonton, Canada). Citrate coated Au ENPs, with a nominal diameter of 50 nm, were purchased from BBInternational (Cardiff, UK; batch no. 10836). Titanium dioxide (TiO_2) nanopowder was purchased from Sigma Aldrich (UK, lot no. 637254, nominal diameter <25 nm). Spherical silica ENPs in dispersion were provided by AZ Electronic Material France SAS (Klebosol 30R50, nominal diameter 80 nm, concentration 29–31% w/w).

Study matrices

The natural sediment was selected to meet the criteria described in OECD guideline 106 (OECD, 2000) for sediment ecotoxicity testing and was collected from the river Derwent at Buttercrambe, York, UK (54° 0′59.04″ N, 0° 52′ 52.67″ W). The natural sediment had a pH value of 7.67, a composition of 4.2% clay (<2 μm), 2.8% silt (2~50 μm) 93% sand (>50 μm). Elendt M4 Daphnia culture medium was prepared according to OECD guideline 211 (OECD, 1998). Elendt medium is mainly used to culture *Daphnia magna* for ecological tests and is composed of various trace elements, macro-nutrients and vitamins. Tomato soup was obtained from Dr Thomas Linsinger and Dr Ringo Grombe at the Joint Research Centre (Brussels, Belgium). The tomato soup was prepared as a reference material under laboratory conditions for further ENPs fate studies. Bovine serum albumin (BSA) powder was purchased from Sigma Aldrich (UK); 10 g L^{-1} BSA made up in water is commonly used to stabilise nanoparticles for cell culture studies. Polylysine solution (P8920) and dextran-500 (31392) for ASEM dish treatment were obtained from Sigma Aldrich (UK).

Characterization of ENPs in stock solutions and environmental and food matrices by ASEM and other techniques

Stock dispersions of the MUDA and citrate coated ENPs were characterized by ASEM, FEG-SEM, TEM and NTA. ASEM, TEM and NTA were also applied to visualize citrate Au ENPs in the supernatant of natural sediment and in M4 medium; TiO_2 ENPs in BSA; and SiO_2 particles in tomato soup. An overview of the particle-matrix combinations that were characterized, the analytical approaches used and the concentrations of particles applied is given in Table 1.

ASEM Imaging

ASEM imaging was performed using a JEOL JASM-6200 ClairScope. The ClairScope consists of an upright optical

© 2013 The Authors

Table 1. Overview of the particle-matrix combinations that were characterized, the analytical approaches used and the concentrations of particles applied.

Nominal diameter	30 nm	50 nm	50 nm	50 nm	<25 nm	80 nm
Core	Au	Au	Au	Au	TiO_2	SiO_2
Coating material	11-MUDA*[1]	Citrate acid	Citrate acid	Citrate acid	n.a.	n.a.
Supplier	Edmonton, Canada	BBI, UK	BBI, UK	BBI, UK	Sigma Aldrich, UK	Sigma Aldrich, UK
Matrix	Stock	Stock	Daphnia medium	Natural sediment	BSA	Tomato soup
Mass [con]	40 mg L^{-1}	50 mg L^{-1}	50 mg L^{-1}	50 mg L^{-1}	n.a.	n.a.
Applied techniques	ASEM, TEM, NTA, FEG-SEM	ASEM, TEM, NTA, FEG-SEM	ASE, TEM, NTA	ASEM, TEM, NTA	ASEM, TEM, NTA	ASEM, TEM, NTA
Pre-treatment	n.a.	n.a.	$V_{ENPs}:V_{medium} = 1:3$ leave for 0.5 hr	$M_{ENPs}:M_{sedi} = 4:1$ leave overnight	10×10^3 mg L^{-1} of TiO_2 in BSA	2×10^3 mg L^{-1} of SiO_2 in tomato soup
ASEM	Step 1. add 200 μL of 0.01% w/v poly-L-Lysine solution to the ASEM dish for 10 min then washed with DI water Step 2. add 500 μL sample to ASEM dish*[2,3] Step 3. add 500 μL glutaraldehyde (this step only was applied to 30 nm AuMUDA) Step 4. add 500 μL dextran 500 (20 g L^{-1})					
FEG-SEM	Dry in an oven at 50 °C over night	n.a.	n.a.	n.a.	n.a.	
NTA	200 times dilution in water	n.a.	*[4]	100× in water	5000× in water	
TEM	Step 1. coat formvar-carbon coated copper grids with 0.01% w/v poly-L-Lysine solution Step 2. add 5 μL of the sample onto the treated grid, the excess moisture was blotted off using filter paper*[5].					

Note: [1] 11-MUDA, 11-mercaptoundecanoic acid.
[2] The TiO_2 ENPs in BSA solution were mixed with glucose solution in the volume ratio of 1:2 to reduce the beam damage to the BSA.
[3] Only the supernatant of the ENP-sediment system was imaged.
[4] Prior to ENPs dispersion, the sediment was pre-treated by vacuum filtration (11 μm filter pore size). After ENP spiking, the sample was centrifuged (rcf = 2000g, 2500 rpm×5 min, Hermle Z 513K). The supernatant was sampled and further diluted with water for 100 times (HPLC fluorescence grade water, Fisher scientific, UK).
[5] The ultracentrifugation of the ENPs in the supernatant of sediment onto TEM grids was performed on a Beckman XL-100 ultracentrifuge (Beckman, California) with a SW40Ti swing bucket rotor and polymer tubes, at 20°C for 1 h, with rcf = 100×10^3 g and $\omega = 128\times10^3$ rpm.

microscope (OM, not used in this study) and an inverted SEM with the specimen in a thin-film windowed dish, in the observation chamber under atmospheric conditions. The dishes are produced by depositing a 100 nm SiN_x film on a silicon substrate, etching the under-surface to leave a 250 μm square window, and inserting the chip into the base of a 35 mm diameter cell culture dish (Nishiyama *et al.*, 2010). The high-energy electrons travel through the SiN_x film of the open dish to interact with the specimen and backscattered electrons (BSE) are detected in the vacuum chamber to construct a SEM image of the specimen. An optical image can be taken by OM from the other side of the specimen. The ASEM was operated at 30 kV acceleration voltages and 30 spot size (8 nm beam diameter, Nishiyama *et al.*, 2010). This spot size was selected based on a compromise between the resolutions, signal to noise and heating. Larger spot sizes can provide more signal but at risk of reduced resolution and increased heating which would shorten the ASEM dish lifespan.

Prior to imaging, 200 μL of 0.01% w/v poly-L-Lysine (Sigma-Aldrich P8920, diluted 10-fold) solution was added to the ASEM dish to give a positive charge for better adhesion of the negatively charged ENPs (Table 1, Ramachandran *et al.*, 1998; Tiede *et al.*, 2009b). The positively charged poly-L-Lysine can properly neutralize the surface charge on the ASEM film window. The poly-L-Lysine was removed after 10 min, and the dish washed with pure water. This coating can be omitted if a neutral ASEM dish is required. Approximately 500 μL of each sample was then added to the centre of the ASEM dish and left to settle at room temperature for approximately 10 min. Sample preparation was completed by adding 500 μL of dextran 500 (20 g L^{-1}) on the top of the sample. The dextran acted as a free radical scavenger thus reducing the damage to the SiN_x membrane.

Scanning Electron Microscopy (SEM)

For SEM imaging, the same specimen as used in the ASEM was deposited on a silicon slab, allowed to dry in an oven (50°C) over night and was then imaged using a JEOL 7500F field emission gun-SEM (FEG-SEM) at 5.0 kV acceleration voltage and at a 4.3 mm working distance.

© 2013 The Authors

Annex 4

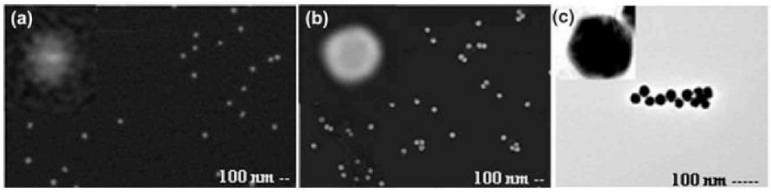

Fig. 1. Images of nominal 50 nm BBI Au obtained from ASEM (a), FEG-SEM (b) and TEM (c). Analysis showed that TEM, which has a greater resolution than ASEM and FEG-SEM gives the smallest mean particles size for a sample. Magnified images of single particles are presented in the top left corner of each image.

Transmission Electron Microscopy (TEM)

TEM images were acquired by a JEOL JEM-2010 microscope (200 kV) which was fitted with an energy dispersive X-ray spectrometer (EDS, Oxford Instruments, UK). Formvar-carbon coated copper grids (S162–4, Agar Scientific, UK) were coated with 0.1% w/v poly-L-Lysine solution (P8920, Sigma-Aldrich) to enhance the attraction of negatively charged particles. Dispersed ENPs (5 μL) were then applied to the copper grids and the excess moisture was blotted off with filter paper.

To increase the number of ENPs being visualized in the supernatant of natural sediment, ultracentrifugation, was applied to increase particle number concentration and hence improve imaging of particles. The ultracentrifugation was performed on a Beckman XL-100 ultracentrifuge (Beckman, California) with a SW40Ti swing bucket rotor and polymer tubes, at 20°C for 1 h, with rcf = 100×10^3 g and $\omega = 128 \times 10^3$ rpm. ENPs accumulated on the TEM grid located at the bottom of the centrifuge tube, with a flat bottom support of Agar 100 resin (Agar Scientific, UK).

Nanoparticle Tracking Analysis (NTA)

NTA was performed to monitor the ENP size distribution in liquid using a Nanosight-LM10 (NTA, Nanosight, UK). In order to meet the NTA ideal number concentration requirement ($1\sim25\times10^8$ particles per mL solution), samples were prepared differently. Stock solutions of the MUDA and citrate coated ENPs, TiO_2 ENPs in BSA and SiO_2 particles in tomato soup were further diluted in water prior to the analysis. A more extensive pre-treatment was carried out on the Au ENPs in natural sediment; the natural sediment was firstly treated by vacuum filtration (11 μm filter pore size). After mixing with ENPs, the ENP-sediment sample was centrifuged (rcf = 2000g, 2500 rpm × 5 min, Hermle Z 513K). The supernatant was sampled and further diluted (100 times) with water (HPLC fluorescence grade water, Fisher scientific, UK) for NTA analysis.

After sample preparation, 0.3 mL of each sample was injected into the NTA chamber using a BD Plastipak syringe (2 mL, lot number 300185, Spain) and 60 sec videos (frames per second = 60, viscosity = 0.95 at 22°C, 640 × 480 resolutions) were recorded. Videos were analyzed using NTA software 2.0 by calculating the sphere equivalent hydrodynamic diameter of each single particle via the Stokes-Einstein equation (Gillespie *et al.*, 2011).

Image Analysis

All the images acquired by TEM, ASEM and FEG-SEM were then analyzed by the eCognition Architect software (version 8.7) which has implemented solutions designed specifically for ENP characterization developed as part of the EU-FP7-funded project "Nanolyse". It is an object-based analysis software (OBIA), which groups pixels of the objects basing on color and shape (Blaschke, 2010; Tiede *et al.*, 2009c, 2010). Three representative images were collected from each sample. Each sample includes more than 50 particles that were measured for the mean equivalent circle diameter.

Result and discussion

Capability of ENP size measurement using ASEM

Images of the 50 nm Au ENPs were acquired by ASEM, FEG-SEM and TEM (Fig. 1). As expected, analysis showed that TEM, which has a greater resolution than ASEM and FEG-SEM gives the smallest mean particle size for a sample. The three methods all provide useful information for studying ENPs with various advantages and disadvantages. The ASEM images, seen in the top left corner, enables the samples to be simply imaged without any sample processing and while the ENPs are in their natural environment. However, the images of the ENPs in the ASEM appear blurry and the periphery lacks definition. This is because the electron beam scattering is broadened in solution and the electrons are absorbed during the pathway to and from a particle in a sample. Electron backscattering depends on the thickness of the scattering material, and thus differs between the centre and edge of the object. Moreover, Monte Carlo simulation shows that electron backscattering also depends on the location depth and the size of Au particles (Däbritz, Langer & Hauffe, 2001). Therefore, the beam broadening affects both the particle size and shape measurement.

© 2013 The Authors

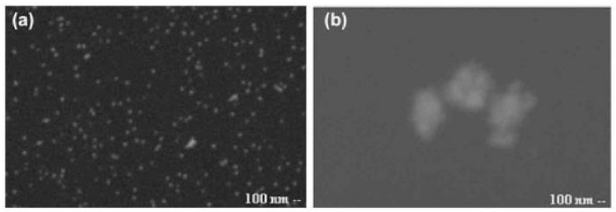

Fig. 2. Imaging of the smallest ENPs by ASEM in this study. The smallest round Au ENPs (a) detected by ASEM is 30 nm Au stock solution. The size of smallest irregular shaped TiO_2 aggregates (b) detected in BSA is 80 nm.

ASEM images showed an image size of 66 ± 6 nm, which is significantly larger ($p < 0.05$) than the ones acquired by the FEG-SEM (50 ± 6 nm), conventional TEM (41 ± 3 nm) and NTA (60 ± 39 nm, as shown in Fig. 3c). The difference between the NTA measurements and the TEM and SEM measurements are probably explained by the fact that NTA measures the hydrodynamic particle diameter whilst SEM and TEM detects the size of dry particle (Gittings & Saville, 1998).

The difference between FEG-SEM and TEM are probably due to the fact that high resolution FEG-SEM employs the secondary detector to acquire the image via detecting low energy secondary electrons ($\leq$50 eV, Goldstein *et al.*, 1981), primarily providing information on surface topology. Hence, both the core and coating material of the ENPs are imaged by FEG-SEM at 5 kV accelerating voltage. In a TEM, image acquisition is achieved by transmitted electrons. The core of the ENPs, Au, appears dark in the image whilst the shell regions (surface coating) of the ENPs appear grey or bright and the background appears bright at 200 kV (Fig. 1). Therefore the size of the core material and coating measured by FEG-SEM is larger than the size of the core measured by TEM.

The enlarged size measured by ASEM may be due to a range of different factors. The dominant factor is thought to be the increased electron scattering at the window and in the liquid environment, both to the incoming beam and in the BSE. Improved size measurement results could probably be obtained by deconvolution of these processes. However such estimation of particle sizes obtained from SEM in an aqueous medium behind a SiN_x window is a complex problem that is beyond the scope of this study. Another reason may be that the particles in liquid are able to undergo small movements which would reduce the image resolution. Similar conclusions were made by Tiede *et al.* (2009b) when using Quantomix capsules (WetSEM) in a conventional SEM to image ENPs under fully liquid conditions.

Optimising detection of ENPs

Size detection limit. Figure 2(a) shows the smallest Au ENPs detected by ASEM is 30 nm Au stock solution. The size of smallest TiO_2 aggregates detected in BSA is 80 nm (Fig. 2b) although TEM imaging suggests that the TiO_2 aggregates are down to ~30 nm (not shown). The detection limit might be improved through changes in the beam diameter and in sample preparation.

As illustrated in 'Capability of ENP size measurement using ASEM' section, electron beam broadening at the membrane and in the liquid are major factors in determination of particle size. The electron beam broadening effect is dependent on the beam diameter, sample preparation, film thickness of the ASEM dish, the operating voltage and current (Suzuki *et al.*, 2007). Theoretically, small beam diameter will enhance the electron interaction with the unit area of target sample, will limit the electron beam broadening effect, and ultimately will improve the size detection limit.

Sample preparation is another determinant of electron beam broadening. The effect of beam scattering can be minimized by using a short electron travel path. It is crucial to attract the ENPs close to the SiN_x film (3 μm). This is a key advantage of the ASEM over wetSEM where in ASEM gravity permits ENPs to settle on the surface of the SiN_x membrane, whereas the particles need to be physically attracted to the membrane used in wetSEM where the membrane is presented facing upwards. However to minimize movement of the particles whilst being examined, the SiN_x was also charged. On the ASEM dish, the behavior of ENPs under the electron beam is determined by the competition between different forces. One is the attractive force between the SiN_x membrane and ENPs, e.g. the ASEM dish was coated with positively charged poly-L-Lysine to attract the negatively charged ENPs (Ramachandran *et al.*, 1998; Tiede *et al.*, 2009b). The other force is the dispersive force of the ENP that is caused by Brownian motion, charging or thermal effects (Suga *et al.*, 2011) and the bonding force between each ENP. In this study, only a few of nominal 30 nm Au ENPs which were coated with 11-mercaptoundecanoic acid (11-MUDA) were observed using ASEM under liquid conditions. The negatively charged ENPs quickly drifted away from the position of the focused beam. Interestingly, this agrees with the phenomena reported by Suga *et al.* (2011), where the positively charged silica particles gathered toward the SiN_x

© 2013 The Authors

Annex 4

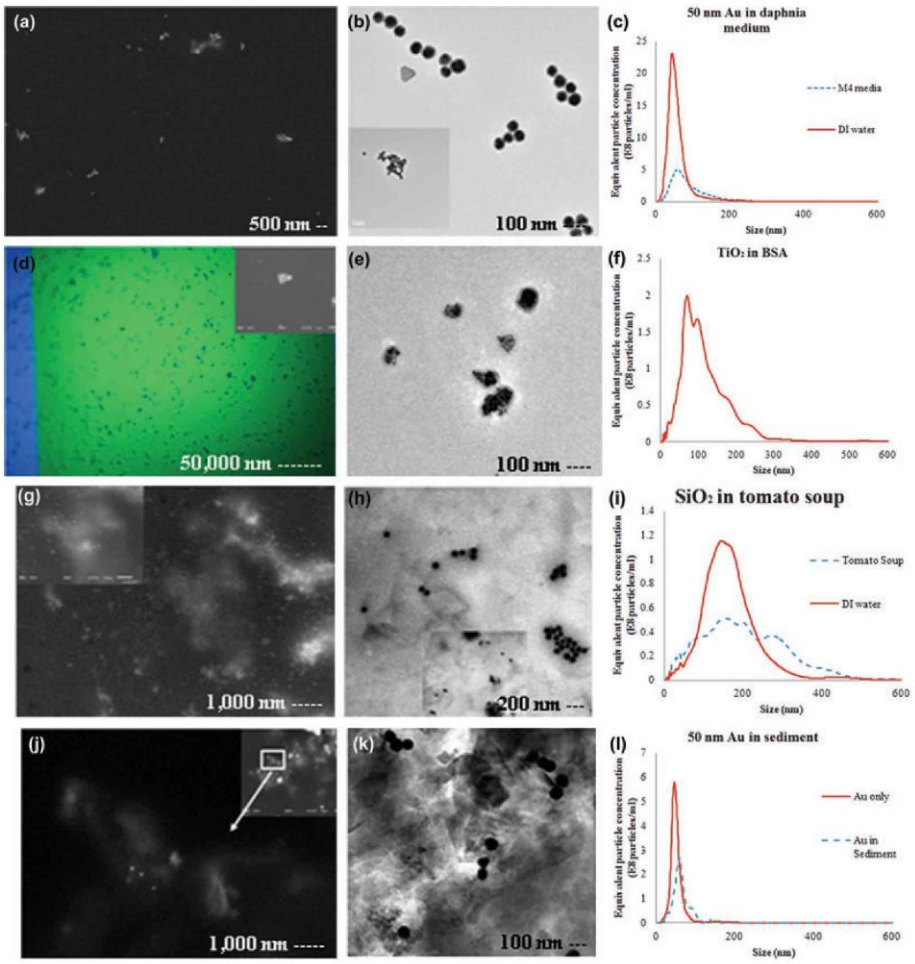

Fig. 3. Size distribution of ENPs in different sample matrices were acquired by ASEM, TEM and NTA, respectively (Fig. 3a–i). Large Au agglomerates in Daphnia culture medium is shown in the ASEM images due to the effect of gravity (Fig. 3a–c). ASEM shows the large TiO_2 aggregates in BSA which have been missed by TEM and NTA (Fig. 3d–f). The measurement of SiO_2 in tomato soup using ASEM (Fig. 3g) is slightly more difficult than TEM (Fig. 3h) and NTA (Fig. 3i) due to the low density. TEM images (Fig. 3k) mainly show Au agglomerates in sediment while ASEM images indicate that the Au ENPs associate with the natural sediment as singlets (Fig. 3j) which agrees with NTA data (Fig. 3l, 62 ± 21 nm)

film at the focus of the beam. Suga *et al.* (2011) explained that, the total sum of the secondary and BSE emitted from the SiN_x film is less than the total incident electrons which creates a potential difference in the water. This potential difference can attract the positive charged ENPs (e.g. Silica) while repel the negatively charged ENPs, e.g. 11-MUDA coated Au ENPs. If this repulsion force plus the dispersive force is weaker than the attraction force between the ENPs and ASEM dish, the

© 2013 The Authors

ENPs would be stable in the liquid and images of the ENPs can be obtained. The imaging of these 30 nm Au ENPs was highly improved by further treatment with glutaraldehyde. The covalent binding force between the glutaraldehyde (ENPs coating) can overcome the repulsion force and bring ENPs close to the SiN_x film (Fig. 2a). Another example is when Au ENPs are immobilized by an external matrix, e.g. by fixing in biological cells, then much smaller particles can be detected (<30 nm, C.L. Dennison, private communication). It is relatively straightforward to image 20 nm particles although the signal to noise of particles is lower and the precision of the size determination is correspondingly worse.

The operating voltage and film thickness of the ASEM dish, which controls the number of electrons and their path length through the film-windowed SiN_x ASEM dish, can play a role on the beam broadening. Generally the higher the voltage, the more electrons would hit the sample and minimize the broadening effect. Nishiyama *et al.* (2010) imaged 15 nm colloidal Au in liquid state through various SiN_x membranes, i.e. 150 nm, 100 nm and 30 nm at various accelerating voltages (20 and 30 kV). They suggested that the combination of 30 nm SiN_x film with higher voltage (30 kV) produced more sharply defined particles and the measured particle diameter is closer to the real value. However, 100 nm SiN_x film deposited ASEM dishes were used in this study since it offers a reasonable resolution and a longer lifetime than 30 nm film. All the specimens in this study were imaged at 30 kV. Therefore, the observable particle size is small when the beam diameter is small, acceleration voltage is high, when the film is thin, when the distance between the target and film is small.

The dose of the generated signal depends on the acceleration voltage and spot size, target atomic number, density, size and shape. Backscattered imaging at low accelerating voltages and large spot size (high current) results in enhanced specimen surface contrast and detail since the primary electrons penetrate less deep into the target and generate BSE closer to the original irradiated area (Richards *et al.*, 1999). The backscattering image contrast is reflecting the atomic number of the specimen composition. Therefore more BSE will be acquired with Au ($Z_{Au} = 79$) than for low atomic number samples such as Ti ($Z_{Ti} = 22$) (Nishiyama *et al.*, 2010). Figure 3(a) and (j) show the images of the nominal 50 nm Au ENPs in Daphnia culture medium and an extract of natural sediment, respectively. The presence of sand/organic matter in the sediment influenced the visualization of the Au ENPs. The greater the differences between the atomic numbers of the target object and sample matrix, the better the quality of images that can be obtained from ASEM, e.g. a dried sample is better than a wet one, a purified sample matrix is better than a crude one.

In addition, the size of signal generation area also depends on the size and shape of the sample. The minimum observable size of sphere particles (e.g. 30 nm Au ENPs) is smaller than the irregular shape of aggregates (e.g. 80 nm TiO_2). Therefore, the observable size is small when the acceleration voltage is low, the spot size is big, the atomic number and density of the sample is high and the sample shape is sphere. This explains smaller particle size was measured on spherical Au ENPs (30 nm) than the TiO_2 aggregates (80 nm).

Minimum particle number concentration

To achieve the ideal particle number concentration range for the ASEM imaging, theoretical calculations based on the experimental data were employed. Figure 1a shows an image of 5 μL of nominal 50 nm Au ENPs (50 mg L^{-1}), which is equivalent to 4.5×10^{10} particles mL^{-1}. About 50 ENPs are visible on the dish film at 50,000× nominal magnification and spot size 30. Assuming that the ideal particle number in an image for statistical analysis is between 5 and 100 particles, the ideal sample concentration for 50 nm Au ENPs would be 5–100 mg L^{-1} with a corresponding particle number concentration of 4.5×10^9–9×10^{10} particles mL^{-1} at the same magnification (50 k).

Evaluation of ASEM imaging for a range of ENPs in different sample matrices

Au ENPs in Daphnia culture medium

The elongated shape of agglomerated Au ENPs (nominal size of single ENP = 50 nm) was observed by ASEM after spiking into Daphnia culture medium for 20 min (Fig. 3a). Analysis by e-Cognition showed that the size of agglomerates was 230 ± 102 nm. This size measurement differed from results obtained by TEM imaging (85 ± 17 nm, Fig. 3b) and NTA (97 ± 73 nm, Fig. 3c). NTA analysis also showed that, after being spiked into Daphnia culture medium for 20 min, the hydrodynamic size of the ENPs increased from 60 ± 39 nm to 97 ± 73 nm along with an increased number of bigger particles (100 nm to 150 nm, Fig. 3c). It seems that ASEM indicates a larger size of agglomerates than TEM. This is possibly due to the fact that large agglomerates are easily to be seen under the effect of gravity.

TiO_2 ENPs in BSA solution

Results were obtained for the TiO_2 ENPs in BSA solution using similar methods. One of the ClairScope OM images of the TiO_2 ENPs (nominal <25 nm) in BSA is shown in Figure 3d (430×), with an insert showing the electron image. All the TiO_2 ENPs were observed as round firm aggregates with the size of 3822 ± 700 nm. The large aggregates are about 6 μm across while the small aggregates are down to ~80 nm. Only small aggregates were found by TEM imaging (127 ± 74 nm, Fig. 3e) and NTA (123 ± 75 nm, Fig. 3f). Various scenarios might contribute to these differences. First, NTA is incapable of detecting particles >1000 nm (Gillespie *et al.*, 2011). Second,

© 2013 The Authors

dilution (in deionized water) required by NTA might separate the agglomerates to constituent particles. NTA measurement of TiO_2 sample was performed in DI water due to the existence of large number of particles in the BSA solution. This indicates another drawback of NTA; it is unable to differentiate the target ENPs from other particles contained in the matrices. Third, the sample preparation required by TEM imaging (e.g. transferring with a pipette or blotting with filter paper) might lose the large agglomerates/aggregates. Larger particles are more likely to be lost if any part of the particles can be washed away from the grid surface during dry blotting. This is because, comparing with the smaller particles, the large ENPs have the lower surface-to-volume ratio and subsequent weak electrostatic attraction of particles toward the TEM grid. Lastly, the electron beam in ASEM might trigger the agglomeration/aggregation of ENPs in solution (Suga *et al.*, 2011), although at the used concentrations this is thought to be a low probability.

The main findings from the TiO_2 analysis are: (i) the nominal <25 nm TiO_2 nanopowders have been agglomerated into 80 nm $\sim$ 6000 nm particles after being dispersed into BSA. (ii) TEM and NTA overrated the small aggregates (up to 500 nm) whilst ASEM can provide a broad overview of the whole population ranging from nano to micro scale although it slightly overrated the large aggregates due to the effect of gravity. (iii) ASEM can provide a clear image of ENPs in a cloudy matrix which is incompatible with the NTA.

SiO_2 ENPs in tomato soup

The spherical SiO_2 ENPs were observed in tomato soup by ASEM imaging (Fig. 3g, 579 ± 370 nm). The bright cloud from the images (seen as arrow in Fig. 3g) may correspond to the loosely packed agglomerates in TEM images (Fig. 3h, 84 ± 15 nm). The large agglomerates observed by ASEM were a few μm in size, whereas the large agglomerates measured by TEM images were only about 600 nm in size. NTA showed the mean value of 126 ± 109 nm with the exception that a few agglomerates measured between 550 and 1000 nm in size. The explanation of the size differences between ASEM, TEM and NTA is similar to that given in 'TiO_2 ENPs in BSA Solution' section. Nevertheless, the measurement of SiO_2 ENPs (Fig. 3g) using ASEM is slightly difficult than TEM (Fig. 3h) and NTA (Fig. 3i) due to the low density.

Au ENPs in an extract of natural sediment

50 nm nominal size Au ENPs were imaged in an extract of natural wet pond sediment for the first time (Fig. 3j). The Au ENPs associated with the natural organic matter in the supernatant of the sediment as single particles. The size of the single ENPs in the extract was as 81 ± 3 nm, which is slightly larger than the size of the single Au ENPs measured in stock (66 ± 6 nm, Fig. 1). This is possibly due to the lower signal to noise of the ENP images as shown in section of minimum particle number concentration. Regarding the size distribution of ENPs in the sediment, TEM images (Fig. 3k) mainly show agglomerates, ASEM images indicate that the Au ENPs associate with the natural sediment as singlets which agrees with NTA data (Fig. 3l, 62 ± 21 nm)

Advantages and limitations of ASEM

ASEM offers imaging of dry, semi-dry and liquid samples in their original state and provides a broad overview of the whole population of particles ranging from the nano to micro scale. Furthermore, the alternative OM in the ClairScope will be convenient to check large aggregates in any depth which were washed out during sample preparation for TEM and SEM and which were underestimated by NTA. Minimum sample preparation is required and can be achieved using simple approaches such as the application of poly-L-Lysine solution to attract ENPs to the ASEM dish, use of dextran 500 or glucose to neutralize the free radicals, use of glutaraldehyde to cross link the coating of ENPs. Although, it is worth noting that even this minimal preparation can potentially alter the dispersion state of the ENPs. With necessary sample preparation, the minimum measurable concentration of the ENPs in liquid is 1 mg L^{-1} (9×10^8 particles mL^{-1}) for 50 nm nominal Au ENPs.

The ASEM dish is not reusable or recyclable. Care must be taken when viewing hard materials to ensure that the fine membrane is not compromised. Similar to the Quantomix capsules in WetSEM, the ASEM dish film may deteriorate during exposure to the electron beam due to the free radical or other mechanical damages (Tiede, *et al.*, 2009b). The free radicals, which are induced by electron beam irradiation, can instigate complex chemical reactions with the SiN_x dish film and eventually will cause failure of the film integrity. Addition of free radical scavengers (Dextran) to the specimen can somewhat reduce these effects. After comparison studies, these effects can be effectively minimised by the selection of a spot size of 30 which can maximize the resolution. Nevertheless, a 100 nm SiN_x film is recommended which provides a <1 hr lifespan, where the beam can focus on one area for maximum 35 mins, which is enough for observation. New developments such as multi-windowed film dishes are expected to ease this restriction.

Some researchers have highlighted the need for analysis of the chemical composition of particles during imaging of samples. Current developments allow the combination of TEM and SEM with EDS, Electron energy loss spectroscopy (EELS), Selected area electron diffraction (SAED), Wavelength dispersive spectroscopy (WDS) or High angle annular dark field (HAADF) to obtain elemental information. No chemical analysis can be achieved by ASEM based on the current design. However, the OM fitted on the top of specimen does allow various kinds of fluorescent and bright-field imaging which could provide useful additional information on the

© 2013 The Authors

composition of a sample (Murai *et al.*, 2011), which not readily achieved using the other techniques. The OM can also be of great use to identify regions of interest prior to using the scanning electron mode and can also provide a corresponding field of view with ASEM.

Conclusions

This study has demonstrated the application of ASEM to the analysis of environmental and food samples. While measured mean sizes for the samples tested were higher than those obtained by TEM, FEG-SEM and NTA, the fact that ASEM is able to measure particles in the liquid phase with minimum preparation provides a number of advantages over the other methods and means that data can begin to be generated on the behaviour of an ENP *in situ*. With necessary sample preparations, ASEM images can provide the information of ENPs down to at least 30 nm, 1 mg L^{-1} (9×10^8 particles mL^{-1}, 50 nm Au ENPs). The ASEM was successfully applied to a range of different core/shell ENPs, e.g. metal (Au), metal oxide (TiO_2) and semiconductor oxide (SiO_2) with different coating materials in complex wet matrices, such as Daphnia culture medium, BSA and tomato soup.

Overall, we believe that ASEM is a valuable addition to the existing 'tool kit' that is available for understanding the occurrence and behaviour of ENPs in complex media. While the results are by no means perfect, the fact that ENPs can be visualised with ease in 'wet' complex samples offers a number of advantages over some of the existing techniques. When used in combination with other methods, ASEM should provide useful additional knowledge on the characteristics of ENPs in environmental matrices and food.

Acknowledgments

The authors wish to express their appreciation to CEFIC for funding this project. Part of the work leading to this publication has received funding from the European Union Seventh Framework Program (FP7/2007–2013) under grant agreement n° 245162. We would like to acknowledge JEOL for loaning this ClairScope ASEM to the Technology Facility of the Department of Biology, the University of York (UK). We also would like to thank Mr Andy Yarwood from JEOL (UK) for technical support, inspiring discussion and professional advices about this study, Dr Guibin Ma and Dr Jonathan G. C. Veinot from the Chemistry Department, University of Alberta (Canada) for supplying 30 nm Au ENPs, Dr Alan MacNicoll from the EcoChemistry Team at the Food and Environment Research Agency (FERA, UK) for preparing TiO_2 in BSA, Ian Wright, Gonzalo Vallejo Fernandez, Michael Walsh and Michael Ward from the York JEOL Nanocentre, York (UK) for providing help with operation of SEM and TEM, Dr Thomas Linsinger and Dr Ringo Grombe from Joint Research Centre (Brussels, Belgium) for providing SiO_2 dispersions and preparing tomato soup matrix. The authors would like to express gratitude to Dr Peter Hofmann and Dr Dirk Tiede from the Geographic Information Science department in the Austrian Academy of Sciences, Salzburg for granting access to the solutions for nanoparticle measurement implemented in e-Cognition software. The authors are further grateful to Jonathan Smith from Nanosight, UK and to Meg Stark from the Biology Department, University of York (UK) for technical support.

References

Blasco, C. & Picó, Y. (2011) Determining nanomaterials in food. *Trac-trend Anal. Chem.* **30**, 86–99.

Blaschke, T. (2010) Object based image analysis for remote sensing. *ISPRS J. Photogramm* **65**, 2–16.

Boxall A.B.A., Chaudhry, Q., Sinclair, C., Jones, A., Aitken, R., Jefferson, B. & Watts, C. (2007) *Current and Future Predicted Environmental Exposure to Engineered Nanoparticles*. Central Science Laboratory, York, UK.

Däbritz, S., Langer, E. & Hauffe, W. (2001) Kossel and pseudo Kossel CCD pattern in comparison with electron backscattering diffraction diagrams. *Appl. Surf. Sci.*, **179**, 38–44.

Dudkiewicz, A., Tiede, K., Loeschner, K., Jensen, L.H.S., Jensen, E., Wierzbicki, R., Boxall, A.B.A. & Molhave, K. (2011) Characterization of nanomaterials in food by electron microscopy. *Trac-Trend Anal. Chem.* **30**, 28–43.

Gatti, A., Kirkpatrick, J., Gambarelli, A., Capitani, F., Hansen, T., Eloy, R. & Clermont, G. (2008) ESEM evaluations of muscle/nanoparticles interface in a rat model. *J. Mater. Sci.: Mater. Med.* **19**, 1515–1522.

Gillespie, C., Halling, P. & Edwards, D. (2011) Monitoring of particle growth at a low concentration of a poorly water soluble drug using the NanoSight LM20. *Colloid Surf. A: Physicochem. Eng. Aspects*, **384** (1–3), 233–239.

Gittings M.R. & Saville D.A. (1998) The determination of hydrodynamic size and zeta potential from electrophoretic mobility and light scattering measurements. *Coll. Surf. A: Physicochem. Eng. Aspects* **141**, 111–117.

Green, C. & Ndegwa, S. (2011) *Nanotechnology*: A Review of Exposure, Health Risks and Recent Regulatory Developments, National Collaborating Centre for Environmental Health. Accessed by 20th February, 2012. [http://www.ncceh.ca/sites/default/files/Nanotechnology_Review_Aug_2011.pdf]

Goldstein J.I., Newbury D.E., Echlin P, Joy D.C., Fiori C.E. & Lifshin E. (1981) Scanning electron microscopy and X-ray microanalysis, Plenum Press, New York.

Hristozov, D. & Malsch I. (2009) Hazards and risks of engineered nanoparticles for the environment and human health, *Sustainability* **1**, 1161–1194.

Liu, J., Legros, S., Ma, G., Veinot, J.G.C., Kamme, F.v.d. & Hofmann, T. (2012) Influence of surface functionalization and particle size on the aggregation kinetics of engineered nanoparticles, *Chemosphere* **87**, 918–924.

Lorenz, C., Tiede, K., Tear S., Boxall, A.B.A., Von Goetz, N. & Hungerbühler, K. (2010). Imaging and characterisation of engineered nanoparticles in sunscreens by electron microscopy, under wet and dry conditions. *Int. J. Occup. Environ. Health* **16**, 406–428.

Murai, T., Maruyama, Y., Mio, K., Nishiyama, H., Suga, M. & Sato, C. (2011) Low cholesterol triggers membrane microdomain-dependent CD44 shedding and suppresses tumor cell migration. *J. Biol. Chem.*, **286**(3) 1999–2007.

© 2013 The Authors

Annex 4

Nishiyama, H., Suga, M., Ogura, T., Maruyama, Y., Koizumi, M., Mio, K., Kitamura, S. & Sato, C. (2010) Atmospheric scanning electron microscope observes cells and tissues in open medium through silicon nitride film. *J Struct. Biol.* **172**, 191–202.

OECD/OCDE (1998) Guideline for the testing of chemicals 211: Daphnia magna Reproduction Test.

OECD/OCDE (2000) Guideline for the testing of chemicals 106: Adsorption–Desorption Using a Batch Equilibrium Method.

Richards, R.G., Owen, G. Rh, & ap Gwynn, I. (1999) Low voltage backscattered electron imaging (<5 kV) using field emission scanning electron microscopy. *Scanning Microsc.* **13**, 55–60.

Sato, C., Manaka S., Nakane, D., Nishiyama, H., Suga, M., Nishizaka, T., Miyata, M. & Maruyama, Y. (2012) Rapid imaging of mycoplasma in solution using atmospheric scanning electron microscopy (ASEM). *Biochem. Biophys. Res. Commun.* **417**, 1213–1218.

Suga, M., Nishiyama, H., Konyuba, Y., Iwamatsu, S., Watanabe, Y., Yoshiura, C., Ueda, T. & Sato, C. (2011) The atmospheric scanning electron microscope with open sample space observes dynamic phenomena in liquid or gas. *Ultramicrocopy* **111**,1650–1658.

Suzuki,M., Kitsuki, H., Ngo, Q., *et al.* (2007) Image formation mechanisms in scanning electron microscopy of carbon nanofibers on substrate. *Microsc. Microanal.* **13**, 580–581.

Wilson, M.A., Tran, N.H., Milev, A.S., Kannangara, G.S.K., Volk H. & Lu, G.Q.M. (2008) Nanomaterials in soils. *Geoderma* **146**, 291–302.

Ramachandran,T.R., Baur, C., Bugacov, A., Madhukar, A., Koel, B.E., Requicha, A. & Gazen, C. (1998) Direct and controlled manipulation of nanometer-sized particles using the non-contact atomic force microscope. *Nanotechnology* **9**, 237–245.

Tiede, K., Boxall, A.B.A., Tear, S.P., Lewis, J., David, H. & Hassellöv, M. (2008) Detection and characterization of engineered nanoparticles in food and the environment. *Food Addit. Contam.* **25**, 795–821.

Tiede, K., Hassellö v, M., Breitbarth, E., Chaudhry, Q. & Boxall, A.B.A. (2009a) Considerations for environmental fate and ecotoxicity testing to support environmental risk assessments for engineered nanoparticles. *J. Chromatogr. A* **1216**, 503–509.

Tiede, K., Tear, S.P., David, H. & Boxall, A.B.A. (2009b) Imaging of engineered nanopartlicles and their aggregates under fully liquid conditions in environmental matrices. *Water Res.* **43**, 3335–3343.

Tiede, K., Boxall, A.B., Tiede, D., Tear S.P., David, H. & Lewis, J. (2009c) A robust size-characterisation methodology for studying nanoparticle behaviour in "real" environmental samples, using hydrodynamic chromatography coupled to ICP-MS. *J. Anal. Atom. Spectrom.* **24**, 964–972.

Tiede, K., Boxall, A.B.A., Wang, X.M., *et al.* (2010) Application of hydrodynamic chromatography-ICP-MS to investigate the fate of silver nanoparticles in activated sludge. *J. Anal. Atom. Spectrom.* **25**, 1149–1154.

© 2013 The Authors

Anal Bioanal Chem (2014) 406:3895–3907
DOI 10.1007/s00216-013-7554-1

RESEARCH PAPER

Production of reference materials for the detection and size determination of silica nanoparticles in tomato soup

Ringo Grombe · Jean Charoud-Got · Håkan Emteborg · Thomas P. J. Linsinger · John Seghers · Stephan Wagner · Frank von der Kammer · Thilo Hofmann · Agnieszka Dudkiewicz · Meritxell Llinas · Conxita Solans · Angela Lehner · Günter Allmaier

Received: 20 October 2013 / Revised: 1 December 2013 / Accepted: 3 December 2013 / Published online: 5 January 2014
© European Union 2013

Abstract A set of four reference materials for the detection and quantification of silica nanoparticles (NPs) in food was produced as a proof of principle exercise. Neat silica suspensions were ampouled, tested for homogeneity and stability, and characterized for total silica content as well as particle diameter by dynamic light scattering (DLS), electron microscopy (EM), gas-phase electrophoretic molecular mobility analysis (GEMMA), and field-flow fractionation coupled with an inductively coupled mass spectrometer (FFF-ICPMS). Tomato soup was prepared from ingredients free of engineered nanoparticles and was spiked at two concentration levels with the silica NP suspension. Homogeneity of these materials was found sufficient to act as reference materials and the materials are sufficiently stable to allow long-term storage and distribution at ambient temperature, providing proof of principle of the feasibility of producing liquid food reference materials for the detection of nanoparticles. The spiked soups were characterized for particle diameter by EM and FFF-ICPMS (one material only), as well as for the total silica content. Although questions regarding the trueness of the results from EM and FFF-ICPMS procedures remain, the data obtained indicate that even assigning values should eventually be feasible. The materials can therefore be regarded as the first step towards certified reference materials for silica nanoparticles in a food matrix.

Keywords Engineered nanoparticles · Colloidal silica · Reference material production

Published in the topical collection *Characterisation of Nanomaterials in Biological Samples* with guest editors Heidi Goenaga-Infante and Erik H. Larsen.

R. Grombe · J. Charoud-Got · H. Emteborg · T. P. J. Linsinger (✉) · J. Seghers
European Commission, Joint Research Centre, Institute for Reference Materials and Measurements (IRMM), Retieseweg 111, 2440 Geel, Belgium
e-mail: thomas.linsinger@ec.europa.eu

S. Wagner · F. von der Kammer · T. Hofmann
Department of Environmental Geosciences, University of Vienna, Althanstrasse 14, 1090 Vienna, Austria

A. Dudkiewicz
The Food and Environment Research Agency, Sand Hutton York YO41 1LZ, UK

A. Dudkiewicz
Environment Department, University of York, Heslington York YO10 5DD, UK

M. Llinas · C. Solans
Institute of Advanced Chemistry of Catalonia, Consejo Superior de Investigaciones Científicas (IQAC-CSIC) and Centro de Investigaciones Biomédica en Red en Bioingeniería, Biomateriales y Nanomedicina (CIBER-BBN), Barcelona, Spain

A. Lehner · G. Allmaier
Institute of Chemical Technologies and Analytics, Research Group Bio- and Polymer Analysis, Vienna University of Technology, Getreidemarkt 9/164-IAC, 1060 Vienna, Austria

Introduction

Nanotechnology holds great promise for conservation of resources and better products, but—like any new technology—has potential risks connected to it. The European Commission has stepped forward to propose a definition of "nanomaterial" to be used in legislative context [1] and legislation requiring food producers to inform consumers if ingredients are present in the nano-form [2] has been passed. According to [1], a nanomaterial is defined as a material where 50 % of the number of particles have external diameters between 1 and 100 nm. The definition explicitly mentions that this criterion applies not to the overall size of agglomerates or aggregates, but to the constituent particles of potential agglomerates and

aggregates. Implementation of this legislation requires reliable methods to detect and quantify nanomaterials in foodstuff. The project NanoLyse, funded under the European Union's 7th Framework Programme (grant agreement 245162), aims to provide proof of principle that such methods are feasible, as there are currently no validated methods for this purpose available.

Reference materials play a crucial role in the development and validation of analytical methods. Two sorts of reference materials exist:

- Pure calibration standards, where the analyte is present either in its pure form or is dispersed in a solvent.
- Matrix reference materials, where the analyte in question is contained in the type of material to be measured (food, soil, human serum etc.).

Calibration standards are used to establish traceability and are also often used for preliminary method development, as they are the simplest conceivable samples. In a second step, matrix reference materials are required for establishing precision during method validation, and if a certified value is available, also for demonstrating method trueness and method proficiency. Therefore, the project also foresaw development of reference materials along with method development for specific nanoparticle–food combinations, as currently no certified nanoparticle reference materials with particles having a broad size distribution in complex matrices exist [3].

Development of certified reference materials for emerging measurands is a classic case of a chicken and egg problem: reliable analytical methods are required to assess not only homogeneity and stability of the candidate certified reference materials, but also to characterize them in a way that a reliable value can be assigned in a metrologically valid way. At the same time, exactly such certified reference materials are required for the development and validation of reliable methods. It is therefore acknowledged that production of certified reference materials and method development have to be approached in a stepwise fashion, starting with certified reference materials that are not perfect but allow development of the first methods, which are in turn used to develop and characterize certified reference materials of a better quality. The very first step in such an iterative process is the production of non-certified reference materials, i.e., materials for which homogeneity and stability have been assessed, but for which no value has been assigned. Reaching this stage is usually easier than production of certified RMs, as homogeneity and stability assessment can be done on a relative basis and does not require absolute method trueness. This manuscript describes the first step of such an iterative process for the development of reference materials for silica nanoparticles in food, namely the production of non-certified RMs and indicates that even the production of certified RMs should be eventually feasible.

Concept

Silicon dioxide ("silica") is together with carbon black the nanomaterial currently used in the highest quantities [4]. As silica is also an approved food additive in Europe (E551), silica was chosen as one of the nanomaterials to be investigated. One of the uses of silica is as anticaking agent, i.e., to ensure that dried powders remain free-flowing. For this reason, vegetable soup was chosen as matrix for the determination of the silica NPs.

The project foresaw development of one screening method (electron microscopy) and one confirmation method (field-flow fractionation coupled to an inductively coupled plasma mass-spectrometer (FFF-ICPMS)) for silica particles in soup. As it was deemed unlikely that an unambiguous value assignment could be achieved using the results from these methods alone, a characterization approach was necessary that allowed assessment of the particle diameters in the matrix independently from the analytical measurements on the matrix. Determination of particle sizes in pure suspensions is analytically much less challenging than in matrices. It was therefore decided to produce matrix materials by spiking a blank matrix with characterized pure suspensions. In this way the particle size distribution in the matrix should resemble the one in the suspension, allowing checking for biases in the particle size distribution and for recovery.

For this approach to be successful, silica particles must not dissolve in the food matrix. In addition, particles in the pure suspensions should (ideally) be not agglomerated or aggregated. If aggregation is not avoidable, the aggregates should not disaggregate in the food matrix, so that pure suspensions and food matrix still contain the same particles. Therefore, the following choices were made:

- A suspension rather than a dry powder was used as source material for the nanoparticles. In this way problems of incomplete deagglomeration and disaggregation can be minimized or avoided.
- Fumed silica was preferred over precipitated silica. While this material is certainly aggregated, aggregation at high temperatures should prevent disaggregation in suspension or in the food matrix. The high temperature of synthesis should also prevent dissolution in the matrix.
- Liquid soup was preferred over powdered soup, again to prevent formation of agglomerates that are difficult to resuspend.
- The liquid soup had to be prepared from base ingredients to avoid incidental presence of silica from bouillon stock etc.

Processing

Aqueous silica suspensions

Aqueous silica dispersion Aerodisp® W7520 N was purchased from Evonik (Hanau, Germany). Two custom-made batches of 30 kg each were obtained, subsequently named NanoLyse01 and NanoLyse02, having silica mass fractions of 10 and 40 g/kg, respectively. The suspensions were adjusted from pH 9 to pH 8 to fit better the pH of the foodstuff to be spiked. The suspensions were ampouled as received into precleaned and dried amber glass ampoules on an automatic ampouling machine (ROTA Verpackungstechnik, Wehr, Germany). Each ampoule contained 25 mL suspension in a sealed ampoule flushed with Ar to minimize degradation. The ampoules were labeled displaying a unique sample number in the order of the filling sequence.

Silica spiked tomato soup

Tomato soup was produced from fresh ingredients in order to obtain a food matrix with low silica nanoparticle background. Therefore, a 30-L tomato soup was produced by a local catering service according to IRMM's specifications (adopted from [5]):

Thirty-kilogram beef bones were added to 70 L water, brought to boil and emerging foam was skimmed off. Two-kilogram onions were cut in half, roasted with a little fat until brown and added to the boiling water/bone mixture. After another 1.5 h, 1.4 kg of carrots and some salt was added. The soup was left to boil for another hour, then onions, bones, and carrots were filtered off and the volume was adjusted to 30 L. This bouillon was further processed with 50 kg fresh tomatoes (non-processed) and 5 L cream. In order to minimize heterogeneity within the soup matrix, fat was skimmed from cold bouillon, seeds were removed from the tomatoes, and no additional spices were added. A corresponding flow chart is depicted in Fig. 1.

Tests were performed to find the right conditions to obtain a homogenous spiked material. Adjusting the pH was considered the most important parameter affecting inhomogeneity. Rapid precipitation upon spiking of small test batches with silica suspension was observed in all cases irrespective of pH adjustment or formulating strategy. As there are several reasons for such behavior like matrix clearing due to agglomeration or segregation of fatty from non-fatty parts, at least pH induced agglomeration was prevented by adjusting 30 L soup to pH 8 by means of addition of 140 mL of a 12.5-M NaOH solution.

The pH-adjusted soup matrix was filtered (1.4 mm, Analysensieb, Haver&Boecker, Oelde, Germany) before blending with the aqueous silica dispersions also used for the preparation of the materials NanoLyse01 and NanoLyse02. Aerodisp® W7520 N dispersions of 10 and 40 g/kg were added over 30 min to the soup matrix under constant stirring at 50 revolutions per min (rpm), using a laboratory stirrer designed for simple stirring tasks of up to 10 L with a speed range from 40 to 1,200 rpm. The resulting materials were filled into 25 mL clear glass jars on an automated filling machine (All-Fill model SHA, Allfill, Sandy, United Kingdom) and sealed with a twist-off lid on an automated filling and sealing machine (model TO-05-06, Lensen Vul en Sluittechniek, Sevenum, the Netherlands). The spiked soup was continuously stirred during the filling process to avoid segregation and the mass of the filled jars was monitored to ensure constant amounts per jar. Closing of jars was performed under a constant steam flow and a slight vacuum kept the lid tightly closed. The flowchart in Fig. 1 shows the processing steps of the material labeled NanoLyse09. An equivalent scheme was followed for the production of NanoLyse10. In addition to the spiked material, non-spiked tomato soup was filled for blank determinations and spiking experiments.

The samples needed to be sterilized to prevent matrix degradation induced by bacterial contamination. Steam water spray sterilization was not suitable as silica nanoparticles were observed to change slightly in size upon heat treatment (see the "Assessment of stability" section). Thus, the samples were γ-irradiated on a GS6000 pallet irradiator at SynergyHealth Ede (Etten-Leur, the Netherlands) with an average dose of 10.8 kGy within 24 h after processing. The success of the irradiation was checked by means of plating *Escherichia coli* CIP 106878 spiked samples for viable bacteria. There was no bacterial activity detectable after the irradiation. As a consequence, users have two ways of checking for the validity of the material: (a) the dark color of the glass indicating a successful sterilization by means of γ-irradiation and (b) the typical sound of vacuum sealed jars during opening.

Measurement and statistical methods

Determination of dissolved silica

Ultrafiltration was the method chosen as it is straightforward and readily available compared to approaches such as cloud point extraction [6]. Potential biases from this method come from adsorption of dissolved silica to the filter as well as migration of silica nanoparticles through the filter. Nevertheless, the method should give a sufficiently accurate estimate of dissolved silica.

The determination of dissolved silica in the dispersions was done in two steps:

1. Separation of solute from colloids using ultrafiltration

For the separation of dissolved silica, three samples of each material were randomly chosen from stock and aliquoted (5 mL, two of each sample) into ultrafiltration spin columns

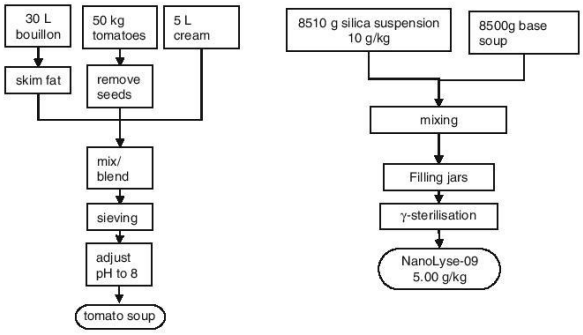

Fig. 1 Flowchart of the processing of tomato soup (*left*) and silica doped tomato soup NanoLyse09 (*right*)

(VS0611, 5,000 g/mol MWCO PES, Sartorius, Göttingen, Germany). The tubes were centrifuged at 5,000 rpm (20 °C) for 15 min.

2. Analysis of the filtrate of NanoLyse01 and NanoLyse02 by ICP-OES (described below).

Dynamic light scattering (DLS)

DLS measurements for homogeneity and stability of the aqueous suspensions were performed on a Malvern Zetasizer Nano ZS (Malvern Instruments, Malvern, UK). The scattering angle was 173°, the measuring position was 4.65 mm inside the cuvette, and the measuring temperature was set to 25 °C. The liquid viscosity was set to 0.89 mPa·s (25 °C) and the liquid refractive index 1.33 (25 °C). The silica nanoparticle refractive index and absorption was set to 1.46 and 0.00, respectively. For homogeneity and stability, three replicate measurements using the cumulants method were performed.

For characterization, additional measurements on a Malvern 41700C (Malvern Instruments, Malvern, United Kingdom), an LS Spectrometer (LS Instruments, Fribourg, Switzerland) both with samples in NMR or Pyrex tubes, and a Horiba LB-550 (Horiba, Longjumeau Cedex, France) were performed.

Zeta potential by electrophoretic light scattering (ELS)

ELS measurements were performed on a Malvern Zetasizer Nano ZS. The scattering angle was 13°, the measuring position was 2.00 mm inside the cuvette, and the measuring temperature was set to 25 °C. The liquid viscosity used was 0.89 mPa·s (25 °C) and the liquid refractive index 1.33 (25 °C). The dispersant dielectric constant was 78.5 (25 °C). The zeta potential values were obtained from 3 consecutive measurements. Measurement uncertainties are given as standard deviations.

Inductively coupled plasma optical emission spectroscopy (ICP-OES)

The mass fraction determination of the silica dispersions was performed at Solvias (Kaiseraugst, Switzerland). Thirty to 40 mg of two duplicate samples was digested using the Wurzschmitt procedure (fusion melting with Na_2O_2 with subsequent dissolution of the digest in water [7]). The silicon mass fraction of the resulting solution was quantified on a Thermo Iris Intrepid II ICP-OES.

Scanning electron microscopy (SEM)

The silica dispersions and soup samples were investigated by means of SEM (FEI Sirion S FEG, Hillsboro, OR, USA). The microscope was equipped with a lens detector used for the image acquisition in this study and energy dispersive X-ray spectroscopy system (Thermo Fisher NS7 system with NSS112E NORAN operating software). All the samples were diluted (200-fold-particle suspensions, 100-fold-soup reference materials) with a 0.05-M borate buffer at pH 8 (BB8.0). Diluted samples were equilibrated at this pH for 6 h by mixing with a magnetic stirrer. Particles from the samples were then transferred onto the formvar-carbon-coated TEM grids (Agar Scientific, Stansted, UK) by means of electrostatic attraction. The protocol comprised of four stages:

1. Grid placed for 5 min floating on the drop of freshly prepared gelatin (Gelatin from porcine skin Type A, Sigma-Aldrich, St. Louis, MO, USA) 0.1 % solution in demineralized water (DMW);
2. Excess of gelatin removed by blotting with the filter paper and surface of the grids washed with a drop of DMW

three times followed by blotting off the moisture with the filter paper;
3. Grid placed floating on the drop of the sample for 2 min;
4. Sample blotted off and grid rinsed in two drops of DMW followed by blotting off the moisture with the filter paper;

The prepared grids were attached to standard SEM aluminum stubs using carbon tape and coated with a nominal 10 nm layer of Pt/Pd using 2300HR High Resolution Fine Coater with a JEOL FC-TM20 Thickness Controller. The coating was used in order to improve the imaging conditions—they reduce charging and increase particle contrast but also increased the size of the particles given in this study as equivalent circle diameter (ECD). Calibration on spherical mercaptoundecanoic acid coated gold ENPs (University of Alberta, Edmonton, Canada) by imaging particles before and after coating indicated that this increase was close to 8 nm. Therefore, this value was subtracted in all of the particle measurements.

The imaging was carried out using the same micrograph size for all of the samples (6.3 μm × 4.73 μm). For sizing of the particles, object based image analysis software (eCognition Architect, version 8.7.2, Trimble, Munich, Germany) with a specially designed application facilitating the measurement of NPs in complex matrices (Centre for GeoInformatics, Paris Lodron University of Salzburg, Salzburg, Austria) was used. The accepted limit for the particle size measurement from the image was 15 pixels which was equivalent of 30 nm particle ECD after subtraction of the coating thickness.

Solid content determination (dry mass, ashing)

The silica mass fractions of NanoLyse01 and NanoLyse02 were determined gravimetrically. Duplicates of 10 samples of each material were dried at 85 °C for 4 h in a drying oven (Heraeus model WV 6100, Hanau, Germany). The samples were weighed after cooling to room temperature in a dessicator. Absence of residual moisture was confirmed by additional drying of the samples for 1 h at 105 °C and additional 30 min at 170 °C. The dry mass also includes reagents for adjusting the pH value (NaOH). However, the purpose of homogeneity testing is to demonstrate equivalence of each ampoule, so that a slight analytical bias is acceptable.

The silica mass fractions of NanoLyse09 and NanoLyse10 were determined gravimetrically after sample ashing [8] on 10 different jars with three independent subsamples per sample. Samples were placed in a pre-heated Carbolite furnace (RWF 1100, Sheffield, United Kingdom) and kept at 550 °C for 2 h. The resulting samples were stored at room temperature to cool down and weighed afterwards. An identical procedure was applied to blank tomato soup (three determinations) to determine its solid content. Ashing accounts for all mineralic substances in the soup, but it is still suitable for demonstrating the homogeneity of the jars. Ash content was corrected for the ash content of the blank soup to be able to compare the target silica mass fraction with the measured mount of non-combustible solids.

FFF-ICPMS

The system consisted of an Eclipse Dualtec AF^4 flow control module with a flat AF^4 separation channel (Superon, Dernbach, Germany, length 275 mm, wide spacer). A 350-μm spacer was used and a 10-kg/mol nominal cut-off regenerate cellulose membrane (Millipore, Billerica, MA, USA) was used as the accumulation wall. Detector flow was set to 1 mL/min and cross flow was set to 0.6 mL/min. Flows were controlled using an Agilent Technologies 1200 Series quaternary pump equipped with a micro-vacuum degasser. The detection chain consisted of a diode-array ultraviolet/visible detector (UV-DAD, Agilent Technologies 1200 Series, primary detection wavelength λ=254 nm), a multi-angler laser light scattering detector MALS (Dawn Heleos II, Wyatt Technology, Santa Barbara, CA, USA) and an inductively coupled plasma mass spectrometer ICP-MS (Agilent Technologies 7700x). All injections were performed using an autosampler (Agilent Technologies 1200 Series, large volume kit); injection volumes were 50 μL. As carrier liquid a mixture of 0.025 % FL70 (alkaline detergent; Fisher Scientific, Waltham, MA, USA) and 0.25 mM NaCl was used. The method was calibrated with latex beads as size standards (Thermo Fisher Scientific, Dreieich, Germany), themselves calibrated against NIST certified reference materials . The reported size distributions from the FFF-ICPMS method are ^{28}Si-concentration particle mass-based size distributions assuming a constant stoichiometry of the SiO_2 particles.

Silica nanoparticles were isolated from tomato soup applying a multiple step sample preparation, consisting of heating the soup for 30 min at 50 °C, homogenization in a glass beaker (Ultra Turrax, IKA-T10; 30 s at 20,000 to 25,000 rpm), removal of the organic material by acid digestion and stabilization of the remaining particle suspension by pH adjustment and probe sonication [9]. Subsequently separation by FlowFFF was used for the determination of size distributions.

Gas-phase electrophoretic molecular mobility analysis (GEMMA)

Measurements on the neat silica NP suspensions were performed by GEMMA [10] using a nano electrospray/charge reduction (Po-210) unit type 3480 (TSI, Shoreview, MN, USA) coupled to a nano DMA unit type 3080 (TSI, Shoreview, MN, USA) and an ultralow condensation particle counter type 3025A (TSI, Shoreview, MN, USA). The electrospray unit was run in the positive ion mode with a mixture of 0.5 L/min compressed air supplied by a table top

compressor (Dürr-Technik, Bietigheim-Bissingen, Germany) and 0.1 L/min CO_2 (99.995 %, Air Liquide, Schwechat, Austria) and an applied spraying voltage of 2.5 kV resulting in an electrical current of 360–470 nA. A cone-tipped-fused silica capillary with 40 μm inner diameter was used and the pressure difference along the capillary was 4 psid. The nano DMA was run with a sheath flow of 3 L/min and the condensation particle counter used butanol in the high flow mode. Samples were diluted prior to analysis in 20 mM CH_3COONH_4.

Three measurement series consisting of 4–10 measurements each were performed for NanoLyse01 (24 measurements in total) and 5 measurement series consisting of 5–10 measurements each (36 measurements in total) were performed for NanoLyse02.

Density of silica particles

The density of silica particles was determined by isopycnic centrifugation performed by Dr. Lerche (Berlin, Germany) [11].

Study designs and statistcial methods

Assessment of homogeneity

Nanomaterial related measurands are method-defined, so each method, while analyzing the same particles, measures different material properties (sedimentation velocity, transmission of electrons etc.). This means that a material could be homogeneous for one method but not for another method. Ideally, homogeneity would therefore be assessed using a number of methods to obtain method independent information on the homogeneity. However, such practice was not feasible within the frame of the project. Hence, it was decided that homogeneity data on mass fraction and particle size should be obtained from one appropriate method each.

Homogeneity was tested on 10 samples using drying/ashing and DLS and on 9 samples using FFF-ICPMS. Results of the homogeneity tests were evaluated using one-way analysis of variance (ANOVA) as described in [12]. Standard deviations within ampoule (s_{wb}, repeatability) and between ampoule variation (s_{bb}) were calculated. In addition, the maximum heterogeneity that could be hidden by method repeatability (u^*_{bb}), the "limit of detection of the homogeneity study," was calculated as described in [13].

Assessment of stability

Stability testing was performed to assess stability during transport (short-term stability) and stability during storage (long-term stability). As the transport time is very limited (1–2 days in Europe, 3–4 days world-wide), stability studies for assessing transport stability only need to be of a short duration. On the other hand, transport conditions such as temperature may vary. Therefore, a typical short-term stability study lasts 4 weeks, but includes the conditions that cover the "worst-case" scenario (low and high temperatures). The goal of the study is to identify transport conditions where a potential change during transport is absent or negligible.

Analytical variation should be reduced to a minimum when assessing stability. Therefore, stability studies were carried out using an isochronous design [14]. In that approach, samples randomly selected from the stock are stored for a certain time at different temperature conditions. After each time point, the samples are moved to conditions where further degradation can be assumed to be negligible ("reference conditions"), effectively "freezing" the degradation status of the materials. The definition of such conditions is difficult for the characterization of nanoparticles, as little information on their stability is available so far, but all possible degradation processes will lead to different rates of change at different conditions. Absence of any change of the measurand (here particle diameter) is therefore a clear indication of stability. At the end of the isochronous storage, the samples are analyzed simultaneously under repeatability conditions eliminating day-to-day variations. Analysis of the material (after various exposure times and temperatures) under repeatability conditions greatly improves the sensitivity of the stability tests.

Regarding the methods employed, ideally each stability parameter would be assessed using a number of methods. However, that would cause an unrealistic work load. Stability was therefore assessed using only one method per parameter and material.

The results were evaluated by trend analysis as described in [15]: Linear regressions were performed and the slopes of the regressions were tested for significance. If the slope was found insignificant, uncertainties of long-term stability (u_{lts}) were calculated from the standard uncertainty of the slope for a shelf life of 2 years.

Value assignment

As the materials are not certified reference materials, value assignment is in principle not required. However, using the value obtained in the assessment of homogeneity and stability and the data provided for characterization allows an indication about the feasibility of the production of CRMs in the future.

As is common practice for certified reference materials (CRMs) [16], uncertainty contributions of homogeneity (u_{bb}), long-term stability (u_{lts}) and characterization (u_{char}) were combined and multiplied with a coverage factor of $k=2$ to obtain an idea of which uncertainties would be achievable for an assigned value of a CRM. The following data were used:

All uncertainties of homogeneity (u_{bb}) were based on the larger value of s_{bb} or u^*_{bb} for each of the suspensions. The

homogeneity data for NanoLyse10 from FFF-ICPMS was also used as homogeneity contribution to the median diameter by EM for both soup materials.

The uncertainty of long-term stability for particle size was in all cases based on the u_{lts} estimated for NanoLyse01 and NanoLyse02 for a storage period of 2 years. This could be an underestimation for the soup material, but, given the high homogeneity contribution, should not influence the result too much. Based on the high chemical stability of silica, uncertainties for the time variation of silica mass fractions are assumed to be negligible. Uncertainties of characterization were in all cases estimated as the standard error of the mean of results.

Results and discussion

Assessment of homogeneity

Aqueous suspensions NanoLyse01 and NanoLyse02

Homogeneity of the silica mass fraction was determined gravimetrically by oven drying. Homogeneity in terms of particle size was determined by DLS on a Malvern Zetasizer Nano ZS (Malvern Instruments, Malvern, United Kingdom). The results were calculated using the cumulants method [17]. One replicate measurement per ampoule of NanoLyse01 and NanoLyse02 was performed, as the measurements were repeatable enough to set narrow limits for repeatability. For NanoLyse02, data were also available from the validation of the FFF-ICPMS method. On three different days, seven measurements were performed on three units each.

The results of the homogeneity assessment (s_{wb}, s_{bb}, and u^*_{bb}) are shown in Table 1. Relative variations (s_{wb}[%], s_{bb}[%], u_{bb}[%]) of NanoLyse01 were smaller than 1 %. For NanoLyse02, the relative between bottle variation s_{bb} % and the relative hidden uncertainty u^*_{bb} for the dry mass and the diameter as determined were below or around 1 %, respectively. Between-unit standard deviation as obtained by FFF-ICPMS was with 4.6 % significantly higher [18]. The results show that the between-unit variations are sufficiently small to make NanoLyse01 and NanoLyse02 suitable as reference materials.

Spiked soups NanoLyse09 and NanoLyse10

Homogeneity of silica mass fractions was determined by ashing at 550 °C. Homogeneity of particle size distribution of NanoLyse 10 was assessed by FFF-ICPMS on 9 jars, with 7 replicate determinations performed on each jar. The results for s_{wb}, s_{bb}, and u^*_{bb} are shown in Table 1.

Blank-corrected ash mass fractions of 5.4±0.2 and 19.2± 0.2 g/kg (uncertainties are single standard deviations) were measured for NanoLyse09 and NanoLyse10, respectively. The within and the between bottle variations of NanoLyse09 are below 2 %. For NanoLyse10, a within bottle variation of 3.5 % was obtained. This, as well as the lower between bottle variation matches the homogeneity characteristics of NanoLyse01/02. Such match indicates an insignificant heterogeneity contribution of the soup as far as mass fractions are concerned. The total silica mass fraction of NanoLyse09 and NanoLyse10 was also determined in duplicate using ICP-OES. The obtained values were 6.2 and 19.3 g/kg, respectively, which agree with the values obtained by ashing within the respective uncertainties of the measurement results.

The median particle diameter as measured by FFF-ICPMS scatters significantly more: a between-unit variation of 16 % was observed [18]. Nevertheless, the variation is still significantly smaller than method reproducibility and the material is therefore fit for purpose as reference material.

Assessment of stability

Aqueous suspensions NanoLyse01 and NanoLyse02

For the aqueous silica nanoparticle systems (NanoLyse01, NanoLyse02), the short-term stability was assessed using an isochronous scheme with testing times of 0, 1, 2, and 4 weeks at 4 °C and 60 °C. The materials were measured by DLS using the cumulants method with relative standard deviations for the silica dispersions were below 1 %, thus allowing a good assessment of the stability of the materials.

A statistical analysis of the data revealed that the slopes of the regression lines for NanoLyse01 (both temperatures) and of NanoLyse02 (4 °C) were not different from zero on a 95 % confidence level. Although the slope of the regression line for NanoLyse02 (60 °C) differed from zero on a 95 %, but not on a 99 % confidence level, the extent of the potential change during transport even at 60 °C (observed change: 0.02 % per week) is technically negligible. The long-term stability data demonstrate that the materials remain stable when stored at ambient temperatures. Uncertainties of stability for storage of 2 years at 18 °C were calculated as 0.43 % (NanoLyse01) and 0.99 % (NanoLyse02) as described in [15].

DLS measurements on autoclaved samples (20 min at 121 °C on an AR092, JBTC, Sint Niklaas, Belgium) of NanoLyse01 and NanoLyse02 showed a reduction of the particle diameter to 85 and 95 nm, respectively. Thus, a thermal sterilization of materials containing silica nanoparticles is inappropriate.

Additionally, the silica dispersions were frozen at −70 °C for 10 min causing irreversible sedimentation (data not shown). The samples therefore should not be exposed to such condition. The results of all stability studies are summarized in Table 2.

Table 1 Homogeneity data on a) silica mass fraction of NanoLyse01 and NanoLyse02 by dry mass, silica mass fraction of NanoLyse09 and NanoLyse10 by ashing; b) silica nanoparticle size of NanoLyse01 and NanoLyse02 by DLS, silica nanoparticle size of NanoLyse09 and NanoLyse10 by FFF-MALLS; n.c.—not calculated as only one replicate analysis per sample was performed

		NanoLyse01	NanoLyse02	NanoLyse09	NanoLyse10
[a)] Mass fraction	Nominal [g/kg]	10	40	5	20
	Average [g/kg]	10.4	40.5	5.4	19.2
	s_{wb} [%]	0.97	2.2	1.9	3.5
	s_{bb} [%]	0.85	0.63	1.8	1.0
	u^*_{bb} [%]	0.46	1.04	0.6	1.1
[b)]Diameter	Average [nm]	135	135	Not measured	103
	s_{wb} [%]	n.c.	n.c.		15
	s_{bb} [%]	0.27	0.59		16
	u^*_{bb} [%]	n.c.	n.c.		2.3

Spiked soups NanoLyse09 and NanoLyse10

Only a tentative assessment of the stability of the soups can be given, as no real reference conditions for long-term stability are available, precluding therefore the use of an isochronous design. Nevertheless, several independent indications are available supporting the assumption of sufficient stability of the nanoparticles in soup:

- Addition of the silica to the soup led to a rapid precipitation of soup components. Particle size distributions obtained by FFF-ICPMS (see section below) after storage of the soup for several months still show similar particle size distributions for aqueous suspensions and soup, indicating reversible agglomeration and no severe ageing effects.
- Measurements by electron microscopy also show no reversible agglomeration after several months, also indicating absence of severe ageing.

The fact that addition of the silica led to precipitation is certainly a major drawback, but, as explained in the Section "concept", using suspensions is currently the only realistic way to allow assessment of trueness of methods. The results from the characterization (see below) show that the precipitate is re-suspendible by heating and ultrasonication. It is therefore possible to re-create the soup in its initial state. Unfortunetaly, the measurement methods are currently not accurate enough to assess whether this is also true after extended storage periods. While there is little doubt about the chemical stability of silica, the stability of the particle size distribution still requires further studies with more precise methods. Nevertheless, despite of the absence of any measurements shortly after processing, there is indication that the materials are unchanged after several months of storage at 4 °C.

Characterization

Two parameters (mass fraction, particle size) were characterised in dedicated studies. The mass fraction was determined by ICP-OES for NanoLyse01 and NanoLyse02 as well as NanoLyse09 and NanoLyse10.

Aqueous silica suspensions NanoLyse01 and NanoLyse02

Total and dissolved silica mass fractions For the aqueous silica nanoparticle systems (NanoLyse01, NanoLyse02), the total silica mass fraction as determined by ICP-OES was 11.9 ±1.4 and 41.2±1.4 g/kg (uncertainties are single standard deviations) for NanoLyse01and NanoLyse02, respectively. This is in accordance with the results of the gravimetrical determination. Therefore, the standard error of the dry mass determinations were adopted as uncertainty of characterization (u_{char}).

Ultrafiltration gave clear and colorless filtrates. Their SiO_2 concentrations as determined by ICP-OES were 90.3±2.0 and

Table 2 Summary of the results of the stability studies of NanoLyse01 and NanoLyse02

Storage condition	NanoLyse01	NanoLyse02
<0 °C	Irreversible sedimentation	Irreversible sedimentation
4 °C (4 weeks)	Stable	Stable
60 °C (4 weeks)	Stable	Particle diameter decreases by 0.02 % per week
18 °C (46 weeks)	Stable	Stable
	$u_{lts,2\ years}$ is 0.4 %	$u_{lts,2\ years}$ is 1.0 %

90.6±0.8 mg/L (uncertainties are single standard deviations) for NanoLyse01 and Nanoyse02, respectively. These values are negligible compared to the total silica mass fractions. Therefore, practically all silica is present in particulate form.

Particle size by DLS Different methods (cumulants, frequency, cross-correlation) at three different laboratories were used to conduct DLS measurements. On each of 3 days, one ampoule of NanoLyse01 and NanoLyse02 were measured in duplicate. A certified reference material (ERM-FD100; IRMM, Geel, Belgium) was measured on the first day to establish traceability and to demonstrate proper functioning and calibration of the equipment used. Representative particle diameter distribution graphs for silica dispersions as obtained by DLS are shown in Fig. 2 and the characterization results are shown in Table 3.

For NanoLyse01 and NanoLyse02, the results from Malvem Zetasizer using cumulants analysis differ significantly from results obtained with the other DLS instruments (see Table 3). Particle-particle interactions may partly explain this difference: measurements were performed undiluted, but also diluted to 2.5 g/kg. There was no difference for NanoLyse01, but a particle diameter of about 142 nm on the undiluted suspension of NanoLyse02 was obtained. However, the main reason for the difference is most likely the mode of evaluation, which yields different results from the cumulants method, frequency analysis and cross-correlation analysis as they show different sensitivities for deviation from monodispersity. While this may be surprising, as the analytical instruments are based on the same measurement principle and all report the hydrodynamic diameter, this observation has been already reported previously [19]. However, as the results differed not too widely (difference max-min is about 15 %), a general overall average over all methods was calculated. Also frequency analysis as performed by the Horiba LB-550 gave results that agreed with the other measurements and the results were therefore pooled with those from correlation analysis. Using the standard error of the mean of means as estimate of u_{char}, relative uncertainty values of 2.2 % (NanoLyse01) and 2.3 % (NanoLyse02) were obtained for the intensity weighted harmonic mean hydrodynamic diameter.

Particle size by FFF-ICPMS The size information for NanoLyse02 is again derived from the measurements obtained in the method validation study [18]. On three different days, three different samples were analysed in 7 replicates each, yielding 9 datasets of 7 individual results. An average mass-based median diameter of 58.1 nm was obtained for the average over all samples and days. The variation between datasets was significantly larger than the one within each dataset, so it was decided to base an uncertainty estimation on the variation of the means of datasets. The standard deviation of the mean results of the 9 datasets was 2.7 nm. Using the standard error of the mean values, a u_{char} of 1.5 % is obtained.

Particle size by electron microscopy The SEM images show irregular particles in various agglomeration/aggregation states, which may be due to the sample preparation (Fig. 3). The higher concentration of NanoLyse02 is reflected in a higher particle density on the grid.

The median diameter of NanoLyse01 and NanoLyse02 was obtained by performing duplicate SEM measurements on each of the two materials on 10 different days (20 results per material). Average median particle diameters of 57.2±3.4 and 59.9±2.7 nm were obtained for NanoLyse01 and NanoLyse02 (uncertainties are single standard deviations). Using the standard error of the mean as estimate of u_{char}, uncertainty contributions of 1.3 % and 1.0 % were obtained for NanoLyse01 and NanoLyse02. These low uncertainties stem from the fact that because the grand mean value is based on a high number of individual measurement averages (20), so the contribution of repeatability and between-run variation to the measurement uncertainty becomes very small. This estimate most likely underestimates the true uncertainty, as only one laboratory performed the characterization measurements, which by definition excludes any possibility to quantify a between-laboratory effect.

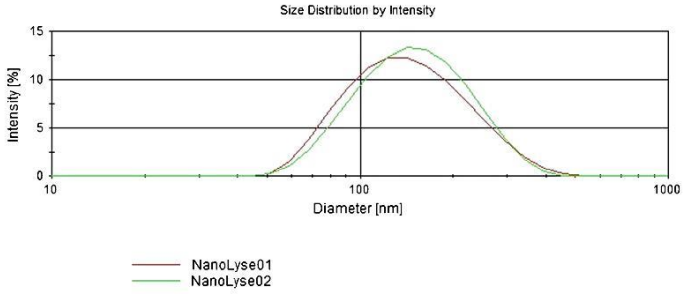

Fig. 2 Representative DLS intensity-weighted size distribution graphs for NanoLyse01 and NanoLyse02

Table 3 Results of the DLS characterisation study of the neat dispersions (NanoLyse01, NanoLyse02)

DLS method	Instrument	NanoLyse01	NanoLyse02
Correlation analysis, cumulants method	Malvern Zetasizer	133.2±1.3	133.3±1.4
	Nano ZS	134.2±1.7	135.5±1.2
	Malvern 41700C	152.1±5.8	142.3±2.9
Cross-correlation	LS Spectrometer 3D; NMR tubes	149.3±1.9	154.1±1.8
	LS Spectrometer 3D; Pyrex tubes	145.5±3.6	150.4±2.5
Frequency analysis	Horiba LB-550	146.1±6.6	142.9±6.7
	Average	143.4±7.9	143.1±8.1

The certified value for ERM-FD100 is 19.0±0.7 nm (cumulants analysis). Size is diameter average; uncertainties are single standard deviations

Particle size by GEMMA Particle diameters determined by GEMMA are based on sizing of several ten thousand particles at minimum. Mean number-based particle diameter as determined by GEMMA were 61.4±1.7 nm for NanoLyse01, 58.8±1.8 nm for NanoLyse02 (uncertainties are single standard deviations). The two results are not statistically significantly different on a 95 % confidence level. The diameters as determined at atmospheric pressure (no vacuum at all) by GEMMA agree very well with the results obtained by SEM. Using the standard error of the mean as estimate of u_{char}, uncertainty contributions of 1.6 % and 1.4 % were obtained for NanoLyse01 and NanoLyse02. Representative GEMMA spectra of NL01 and NL02 can be seen in Fig. 4.

Zeta potential and particle density The zeta potential of the silica colloidal dispersions were analyzed by means of ELS. NanoLyse01 and NanoLyse02 had a zeta potential of −44.7± 0.7 and −46.2±0.7 mV, respectively (uncertainty are single standard deviations).

Measurements of the density of 18 subsamples gave an average density of 2.010±0.042 g/cm^3 (uncertainty is a single standard deviation).

Soup materials NanoLyse09 and NanoLyse10

Particle size by electron microscopy Images by SEM clearly show increased agglomeration of silica NPs (Fig. 3), but a large number of NPs is still present as individual particles. Measurements by SEM indicate a shift of the number-based particle diameter distribution towards smaller particles with, compared to the pure suspensions, more particles in the range of 30–50 nm and fewer particles above 60 nm (Dudkiewicz et al., manuscript submitted). This results in lower median particle diameters for the silica in soup than in the neat suspension as shown in Fig. 5.

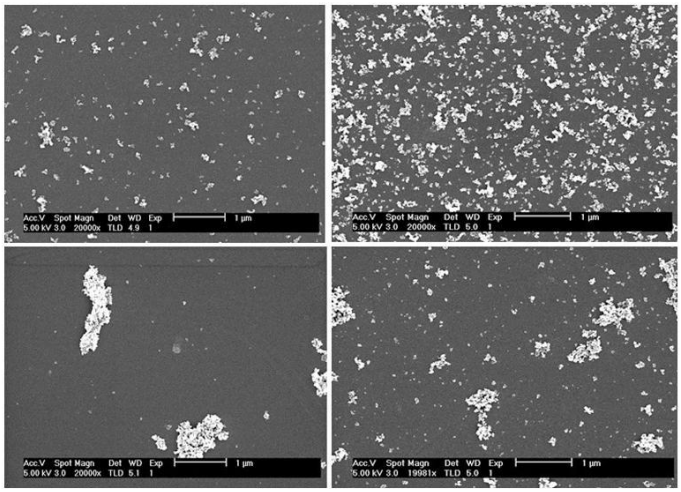

Fig. 3 SEM images of NanoLyse01 (*top left*), NanoLyse02 (*top right*), NanoLyse09 (*bottom left*), and NanoLyse10 (*bottom right*). *Size bars* are 1 μm

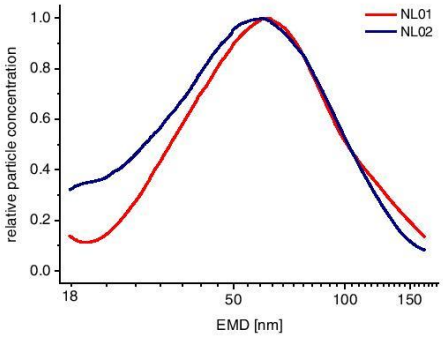

Fig. 4 GEMMA spectra of NanoLyse01 and NanoLyse02

The data from the method validation study were used for a tentative characterization of particle diameter by SEM. The average number-based median diameters of 20 replicate determinations were 43.7 (NanoLyse09) and 43.5 nm (NanoLyse 10) with standard deviations of 8.7 and 8.0 nm, respectively. These values are roughly in agreement with the number-weighted distributions as obtained by DLS for the spiking suspensions, especially taking into consideration the rather low reliability of the conversion between intensity to number based distributions for polydisperse, non-spherical particles. Using the standard error of the mean as estimate of u_{char}, uncertainty contributions of 4.5 % and 4.1 % were obtained for NanoLyse09 and NanoLyse10. Again, very low uncertainties were obtained due to the high number of average results on which the grand mean is based (20 individual median sizes).

Particle size by FFF-ICPMS The data from the homogeneity testing were also used for characterization of NanoLyse10 [18]. The average median particle diameter of the 63 measurements was 207.6 nm with a standard deviation of 42 nm. Again, using the standard error of the mean as estimate of u_{char}, an uncertainty contribution of 2.6 % was obtained.

The sizes obtained for NanoLyse10 differ significantly from those obtained on the neat suspension. This difference is an effect of the sample preparation by acid digestion. It is hypothesized that the time-lab between digestion and measurement is important with longer time-lags resulting in smaller differences, but also lower recoveries.

As is the case for EM, also here the high number of measurements result in a very small standard error of the mean, which is an underestimation of the true uncertainty. As there is currently no possibility to assess a potential between-laboratory effect, this is the best estimate available.

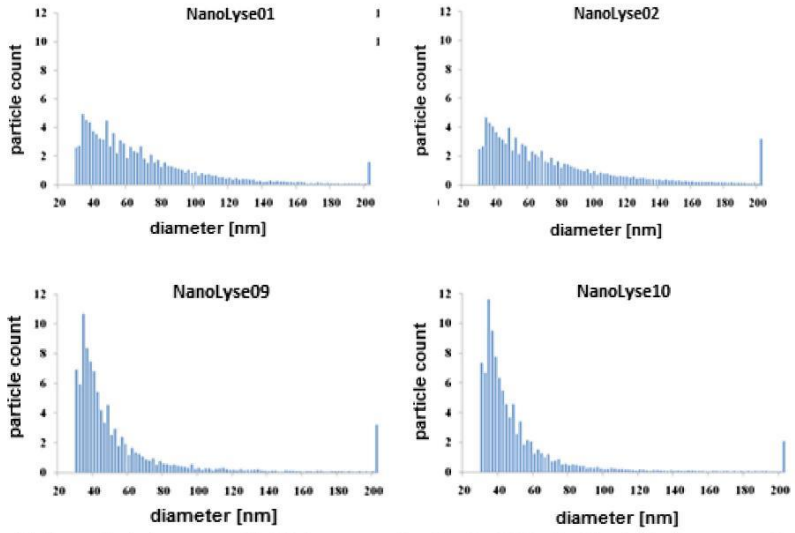

Fig. 5 Particle diameter distribution as measured by EM for neat suspensions (NanoLyse01, NanoLyse02) and silica in tomato soup (NanoLyse09, NanoLyse10) from. Size-cut off of the measurements is 30 nm

Tentative value assignment

The uncertainty budgets and assigned values are shown in Table 4. For the neat suspensions NanoLyse01 and NanoLyse02, the median diameters obtained by SEM, GEMMA, and FFF-ICPMS agree with each other. This agreement is surprising, as these methods are based on completely different method principles. FFF-ICPMS and GEMMA are influenced by the movement of the particles in a liquid or gas phase, whereas EM evaluates a static image. GEMMA and EM produce number based median diameters, whereas FFF-ICPMS produced mass-based median diameters. Finally, GEMMA is run at atmospheric pressure whereas EM under vacuum.

The results from these three methods differed from the average diameter obtained by DLS. This is expected, as the intensity-weighted mean value as obtained by DLS is much more influenced by a few large particles than the median diameters obtained by the other methods. Using the instrument software to convert the intensity-weighted diameters into number-weighted diameters gives averages of about 65 nm, i.e., in much closer agreement with the results obtained from the other methods (data not shown).

The work described here shows that the production of RMs, eventually even CRMs is feasible if the remaining issues regarding mainly stability and characterization are solved:

With respect to stability, the uncertainty of stability for the soup materials, currently used from the neat suspension, is only a first estimation. Measurements with more precise methods are required to assess whether the particles remain re-suspendable for extended time periods.

The second major question concerns the trueness of results. Data for GEMMA, FFF-ICPMS, and SEM were obtained by one laboratory only. The detection of unrecognized laboratory bias is the reason why many reference materials are characterized by a collaborative study involving multiple laboratories performing independent measurements [16]. The situation is less severe for the neat suspensions, where the agreement of the data from SEM and GEMMA indicates absence of major bias, but no such check is available for the soup materials. It is therefore not clear whether the change in the median particle diameter found by FFF and SEM is due to a method bias or due to real changes. Repeated measurements in several laboratories would be required to clarify this issue.

The values listed in Tables 3 and 4 therefore are tentative only and they must not be considered certified or even indicative values. This tentative nature of the these values has important consequences for the use of the materials: As no values are assigned, the materials cannot be used as ultimate proof of method accuracy. It should, however, be pointed out that the aim of this part of the project was a proof of principle of RM production and not the actual production of certified reference materials. The materials produced demonstrate the possibility of producing reference materials and indicate that even the production of certified RMs should be feasible. In addition, in the absence of any other RMs for nanoparticles in complex matrices, they do allow laboratories to compare their values with those obtained by other methods and laboratories. The materials therefore form the first step in the iterative process of improving analytical methods and reference materials.

Conclusion

This work highlighted some of the problems in developing reference materials for NPs in complex matrices. A major

Table 4 Uncertainty budget and assigned values for NanoLyse01, NanoLyse02, NanoLyse09, and NanoLyse10

		u_{bb} [%]	u_{hs} [%]	u_{char} [%]	Assigned value[e]
NanoLyse01	Mass fraction	0.89	0	0.29	10.4±0.2 g/kg
	Mean diameter by DLS[a]	0.3	0.4	2.2	135±7 nm
	Median diameter by SEM[b]	0.3	0.4	1.3	57±2 nm
	Median diameter by GEMMA[c]	0.3	0.4	1.6	61±2 nm
NanoLyse02	Mass fraction	1.0	0	0.5	40.5±1.0 g/kg
	Mean diameter by DLS[a]	0.6	1.0	2.3	135±7 nm
	Median diameter by SEM[b]	0.6	1.0	1.0	60±2 nm
	Median diameter by GEMMA[c]	0.6	1.0	1.4	59±2 nm
	Median diameter by FFF-ICPMS	4.6	1.0	1.5	58±6 nm
NanoLyse09	Mass fraction	1.8	0	0.47	5.4±0.2 g/kg
	Median diameter by SEM[b]	16	0.4	4.5	44±15 nm
NanoLyse10	Mass fraction	1.1	0	0.66	19.2±0.5 g/kg
	Median diameter by SEM[b]	16	1.0	4.1	44±15 nm
	Median diameter by FFF-ICPMS[d]	16	1.0	2.6	208±68 nm

[a] Intensity-weighted harmonic mean diameter as determined by DLS

[b] Number-weighted median diameter as determined by SEM

[c] Number weighted mean electrophoretic mobility diameter as determined by GEMMA

[d] Mass-weighted hydrodynamic diameter as determined by FFF-ICPMS

[e] Uncertainties are expanded uncertainties with a coverage factor $k=2$ corresponding to a level of confidence of about 95 %

issue for food materials is homogeneity, as silica acts as clarifying agent, leading to considerable precipitation of food components. Processing of the materials was made more difficult by the lack of methods for suitable process control. Existence of analytical methods are expected to lead to improved materials in the future.

Information on stability is limited, based on the only recently developed analytical methods. In addition, the application of isochronous measurements is not straightforward, as little information is currently available on what would be suitable reference conditions for nanoparticles in food. Also here, further knowledge will lead to more robust assessments of stability.

Finally, more extensive data on the reliability of methods for the characterization of nanoparticles in food matrices are necessary. Interlaboratory comparisons should help establishing reproducibility limits for the individual methods, allowing more reliable characterization.

Despite of these challenges, the work has demonstrated that development and characterization of reference materials for the detection and quantification of silica nanoparticles in liquid food is possible and that it should be feasible to assign values with acceptable uncertainties. The materials developed in this project might be the first step in the iterative improvement of methods and RMs for the analysis of nanoparticles in complex matrices.

Acknowledgments The work leading to these results has received funding from the European Union Seventh Framework Programme (FP7/2007–2013) under grant agreement no. 245162. The authors thank Mrs. Meeus (EC JRC IRMM) for conducting the microbiology tests.

References

1. Recommendation 2011/696/EU of the European Commission on the definition of nanomaterial
2. Regulation 1169/2011 of the European Parliament and of the council on the provision of food information to consumers
3. Linsinger TPJ, Roebben G, Solans C, Ramsch R (2010) Reference materials for size measurements of nanoparticles. Trends Anal Chem 30:18–27. doi:10.1016/j.trac.2010.09.005
4. Schlag S, Suresh B, Yoneyama M, Yang V (2010) Nanoscale Chemicals and Materials, Report by SRI Consulting, 2010
5. Plachutta E, Wagner C: Die gute Kueche, Orac, Vienna, Austria, 1993, ISBN 3701503109; p160 "Rindsknochensuppe" and p. 170 "Tomatensuppe"
6. Liu J, Chao J, Liu R, Tan Z, Yin Y, Wu Y, Jiang G (2009) Cloud Point Extraction as an Advantageous Preconcentration Approach for Analysis of Trace Silver Nanoparticles in Environmental Waters. Anal Chem 81:6496–6502
7. Latscha HP, Klein HA (2004) Analytische Chemie, Basiswissen III. Springer Verlag, Berlin Heidelberg
8. Matissek M, Steiner G (2006) Lebensmittelanalytik, Grundzüge, Methoden, Anwendungen, 3rd edn. Springer Verlag, Berlin Heidelberg
9. Wagner S, v.d. Kammer F, Legros S, Larsen EH, Loeschner K, Navratilova J, Hofmann T Sample preparation for detection of silica NPs in soup by AF4-ICP-MS (manuscript in preparation)
10. Kaufman SL, Skogen JW, Dorman FD, Zarrin F (1996) Macromolecule Analysis Based on Electrophoretic Mobility in Air: Globular Proteins. Anal Chem 68:1895–1904
11. Wohlecke H, Lerche D, Detloff T, Franks K, Kestens V, Roebben G (2013) In-situ determination of the effective particle density of suspended colloidal silica particles by means of analytical centrifugation, Poster at Partec 2013, Nuremberg, April 23-25 2013. Abstract available via http://www.partec.info/en/review/review2013/
12. Van der Veen AMH, Linsinger TPJ, Pauwels J (2001) Uncertainty calculations in the certification of reference materials. 2. Homogeneity study. Accred Qual Assur 6:26–30
13. Linsinger TPJ, Pauwels J, van der Veen AMH, Schimmel H, Lamberty A (2001) Homogeneity and stability of reference materials. Accred Qual Assur 6:20–25
14. Lamberty A, Schimmel H, Pauwels J (1998) The study of the stability of reference materials by isochronous measurements. Fres J Anal Chem 360:359–361
15. Linsinger TPJ, Pauwels J, Lamberty A, Schimmel H, van der Veen AMH, Siekmann L (2001) Estimating the Uncertainty of Stability for Matrix CRMs. Fres J Anal Chem 370:183–188
16. ISO Guide 35 (2006) Reference materials — General and statistical principles for certification, International Organization for Standardization, Geneva, Switzerland
17. ISO 13321(1996) Particle size analysis – Photon correlation spectroscopy, International Organization for Standardization, Geneva, Switzerland
18. Wagner S, von der Kammer F (2013) Final report of the FP7 project "NanoLyse Nanoparticles in Food: Analytical methods for detection and characterisation", Collaborative project 245162. A peer-reviewed publication on the FFF-ICPMS work on the method development and validation for silica NPs in soup is planned for 2014
19. Braun A, Kestens V, Franks K, Roebben G, Lamberty A, Linsinger TPJ (2012) A new certified reference material for size analysis of nanoparticles. J Nanoparticle Res 14:1012–1023

References

Aitchinson, J. (1982), "The statistical analysis of compositional data", *Journal of the Royal Statistical Society. Series B (Methodological)*, Vol. 44 No. 2, pp. 139–177.

Aitchinson, J. (2013), "A concise guide to compositional data analysis", CDA Workshop, Girona. Available from: http://www.leg.ufpr.br/lib/exe/fetch.php/pessoais%253Aabtmartins%253Aa_concise_guide_to_compositional_data_analysis.pdf (accessed 7 March 2014)

Al-Amoudi, A., Chang, J.-J., Leforestier, A., McDowall, A., Salamin, L.M., Norlén, L.P.O., Richter, K., Sartori Blanc N., Sturder D. and Cubochet J. (2004), "Cryo-electron microscopy of vitreous sections", *The EMBO Journal*, Vol. 23 No. 18, pp. 3583-3588

Anderson, W., Kozak, D., Coleman, V.A., Jämting, Å.K. and Trau, M. (2013), "A comparative study of submicron particle sizing platforms: Accuracy, precision and resolution analysis of polydisperse particle size distributions", *Journal of Colloid and Interface Science*, Vol. 405, pp. 322–330.

Asghari, S., Johari, S.A., Lee, J.H., Kim, Y.S., Jeon, Y.B., Choi, H.J., Moon, M.C., Je Yu, I. (2012), "Toxicity of various silver nanoparticles compared to silver ions in Daphnia magna", *Journal of Nanobiotechnology*, Vol. 10 No. 1, pp. 1-11.

Auty, M.A.E., O'Kennedy, B.T., Allan-Wojtas, P. and Mulvihill, D.M. (2005), "The application of microscopy and rheology to study the effect of milk salt concentration on the structure of acidified micellar casein systems", *Food Hydrocolloids*, Vol. 19 No. 1, pp. 101-109.

Bacher, G., Szymanski, W.W., Kaufman, S.L., Zollner, P., Blaas, D. and Allmaier, G. (2001), "Charge-reduced nano electrospray ionization combined with differential mobility analysis of peptides, proteins, glycoproteins, noncovalent protein complexes and viruses", *Journal of Mass Spectrometry*, Vol. 36 No. 9, pp. 1038–1052.

Balmes, O., Malm, J.O., Pettersson, N., Karlsson, G. and Bovin, J.O. (2006), "Imaging atomic structure in metal nanoparticles using high-resolution cryo-TEM", *Microscopy and Microanalysis*, Vol. 12 No. 2, pp. 145–150.

Balnois, E. and Wilkinson, K.J. (2002), "Sample preparation techniques for the observation of environmental biopolymers by atomic force microscopy", *Colloids and Surfaces A: Physicochemical and Engineering Aspects*, Vol. 207 No. 1–3, pp. 229–242.

Barcenas, M. and Rosell, C. (2006), "Effect of frozen storage time on the bread crumb and aging of par-baked bread", *Food Chemistry*, Vol. 95 No. 3, pp. 438-445.

Barnard, A.S., Feigl, C.A. and Russo, S.P. (2010), "Morphological and phase stability of zinc blende, amorphous and mixed core–shell ZnS nanoparticles", *Nanoscale*, Vol. 2 No. 10, pp. 2294-2301.

Barthel, H., Heinemann*, M., Stintz, M. and Wessely, B. (1999), "Particle sizes of fumed silica", *Particle & Particle Systems Characterization*, Vol. 16 No. 4, pp. 169–176.

Bergh, O., BOrsheim, K.Y., Bratbak, G. and Heldal, M. (1989), "High abundance of viruses found in aquatic environments", *Nature*, Vol. 340 No. 6233, pp. 467–468.

Bettarel, Y., Sime-Ngando, T., Amblard, C. and Laveran, H. (2000), "A comparison of methods for counting viruses in aquatic systems", *Applied and Environmental Microbiology*, Vol. 66 No. 6, pp. 2283–2289.

Bijl, E., de Vries, R., van Valenberg, H., Huppertz, T. and van Hooijdonk, T. (2014), "Factors influencing casein micelle size in milk of individual cows: Genetic variants and glycosylation of κ-casein", *International Dairy Journal*, Vol. 34 No. 1, pp. 135–141.

Blasco, C. and Picó, Y. (2011), "Determining nanomaterials in food", *Trends in Analytical Chemistry*, Vol. 30 No. 1, pp. 84–99.

Bogner, A., Thollet, G., Basset, D., Jouneau, P.H. and Gauthier, C. (2005), "Wet STEM: A new development in environmental SEM for imaging nano-objects included in a liquid phase", *Ultramicroscopy*, Vol. 104 No. 3-4, pp. 290–301.

Boldridge, D. (2010), "Morphological characterization of fumed silica aggregates", *Aerosol Science and Technology*, Vol. 44 No. 3, pp. 182–186.

Boque, R., Maroto, A., Riu, J. and Rius, F. (2002), "Validation of analytical methods", *GRASAS Y ACEITES*, Vol. 53 No. 1, pp. 128–143.

Bouwmeester, H., Dekkers, S., Noordam, M., Hagens, W., Bulder, A., de Heer, C., ten Voorde, S., Wijinhoven S. W., Marvin H. J. and Sips A. J. (2009), "Review of health safety aspects of nanotechnologies in food production", *Regulatory Toxicology and Pharmacology*, Vol. 53 No. 1, pp. 52–62.

Bowen, P. (2002), "Particle size distribution measurement from millimeters to nanometers and from rods to platelets", *Journal of Dispersion Science and Technology*, Vol. 23 No. 5, pp. 631–662.

Bozzola, J.J. (2007), "Conventional specimen preparation techniques for scanning electron microscopy of biological specimens", in J. Kuo (Ed.), *Electron microscopy methods and protocols*, Humana Press, Second Edition., pp. 449-466.

Branton, D. (1966), "Factur faces of frozen membranes", *Proceedings of the National Academy of Sciences of the United States of America*, Vol. 55 No. 5, pp. 1048-1056

Braun, A., Couteau, O., Franks, K., Kestens, V., Roebben, G., Lamberty, A. and Linsinger, T.P.J. (2011), "Validation of dynamic light scattering and centrifugal liquid sedimentation methods for nanoparticle characterisation", *Advanced Powder Technology*, Vol. 22 No. 6, pp. 766–770.

Braun, A., Kestens, V., Franks, K., Roebben, G., Lamberty, A. and Linsinger, T.P.J. (2012), "A new certified reference material for size analysis of nanoparticles", *Journal of Nanoparticle Research*, Vol. 14 No. 9,

Bruggeller, P. and Mayer, E. (1980), "Complete vitrification in pure liquid water and dilute aqueous solutions", *Nature*, Vol. 288 No. 5791, pp. 569-571.

Buffet, P.-E., Tankoua, O.F., Pan, J.-F., Berhanu, D., Herrenknecht, C., Poirier, L., Amiard-Triquet, C., Amiard, J. C., Bérard, J. B., Risso, C., Guibbolini M., Roméo, M., Reip, P., Valsami-Jones, E. and Mouneyrac C. (2011), "Behavioural and biochemical responses of two marine invertebrates

Scrobicularia plana and Hediste diversicolor to copper oxide nanoparticles", *Chemosphere*, Vol. 84 No. 1, pp. 166–174.

Calzolai, L., Gilliland, D. and Rossi, F. (2012), "Measuring nanoparticles size distribution in food and consumer products: a review", *Food Additives & Contaminants: Part A*, Vol. 29 No. 8, pp. 1183–1193.

Carr, B. and Malloy, A. (2013), "NanoParticle Tracking Analysis – The NANOSIGHT system.", Available from: http://f-praktikum.physik.uni-greifswald.de/Anleitungen/nanopartikel.pdf. (accessed 8 July 2013).

Carr, M.E., Cromartie, R. and Gabriel, D.A. (1989), "Effect of homo poly(L-amino acids) on fibrin assembly: role of charge and molecular weight", *Biochemistry*, Vol. 28, pp. 1384–1388.

Castaneda, L., Valle, J., Yang, N., Pluskat, S. and Slowinska, K. (2008), "Collagen cross-linking with Au nanoparticles", *Biomacromolecules*, Vol. 9 No. 12, pp. 3383–3388.

Cavalier, A., Spehner, D. and Humbel, B.M. (2009), *Handbook of cryo-preparation methods for electron microscopy*, CRC Press.

Chaudhry, Q. and Castle, L. (2011), "Food applications of nanotechnologies: An overview of opportunities and challenges for developing countries", *Trends in Food Science & Technology*, Vol. 22 No. 11, pp. 595–603.

Chaudhry, Q., Castle, L., Bradley, E., Backburn, J., Aitken, R. and Boxall, A. (2008), "Assessment of current and projected applications of nanotechnology for food contact materials in relation to consumer safety and regulatory implications", Food Standard Agency, Available from: http://www.foodbase.org.uk//admintools/reportdocuments/346-1-648_A03063_Final_Report.pdf (accessed 7 March 2014)

Chaudhry, Q. and Groves, K. (2010), "Nanotechnology applications for food ingredients, additives and supplements", in Q. Chaudhry, L. Castle, R. Watkins (Ed.) *Nanotechnologies in food*, RSC Publishing, pp. 69–84.

Chen, X., Jo, C., Lee, J.I. and Ahn, D.U. (1999), "Lipid oxidation, volatiles and color changes of irradiated pork patties affected by antioxidants", *Journal of Food Science*, Vol. 64 No. 1, pp. 16–19.

CPS Instruments, Inc. (2005), "CPS Disc Centrifuge Operating Manual", CPS Instruments Inc., Available from: http://www.cpsinstruments.eu/pdf/Manual.pdf (accessed 8 July 2013).

Cushen, M., Kerry, J., Morris, M., Cruz-Romero, M. and Cummins, E. (2012), "Nanotechnologies in the food industry – Recent developments, risks and regulation", *Trends in Food Science & Technology*, Vol. 24 No. 1, pp. 30–46.

Danscher, G. and Stoltenberg, M. (2006), "Silver enhancement of quantum dots resulting from (1) metabolism of toxic metals in animals and humans, (2) in vivo, in vitro and immersion created zinc-sulphur/zinc-selenium nanocrystals, (3) metal ions liberated from metal implants and particles", *Progress in Histochemistry and Cytochemistry*, Vol. 41 No. 2, pp. 57–139.

DeCarlo, P.F., Slowik, J.G., Worsnop, D.R., Davidovits, P. and Jimenez, J.L. (2004), "Particle morphology and density characterization by combined mobility and aerodynamic diameter measurements. Part 1: theory", *Aerosol Science and Technology*, Vol. 38 No. 12, pp. 1185–1205.

Dekkers, S., Krystek, P., Peters, R.J.B., Lankveld, D.P., Bokkers, B.G., van Hoeven-Arentzen, P.H., Bouwmeester, H. Oomen, A.G. (2010), "Presence and risks of nanosilica in food products", *Nanotoxicology*, Vol. 5 No. 3, pp. 393–405.

Denk, W. and Horstmann, H. (2004), "Serial block-face scanning electron microscopy to reconstruct three-dimensional tissue nanostructure", *Plos Biology*, Vol. 2 No. 11, pp. 1900–1909.

Diplock, A.T., Charleux, J.L., Crozzier-Willi, G., Kok, F.J., Rice-Evans, C., Roberfroid, M., Stahl, W. and Viña-Ribes, J. (1998), "Functional food science and defence against reactive oxidative species", *British Journal of Nutrition*, Vol. 80, pp. S77–S112.

Domingos, R.F., Baalousha, M.A., Ju-Nam, Y., Reid, M.M., Tufenkji, N., Lead, J.R., Leppard, G.G., Wilkinson, K.J. (2009), "Characterizing manufactured nanoparticles in the environment: multimethod determination of particle sizes", *Environmental Science & Technology*, Vol. 43 No. 19, pp. 7277–7284.

Donaldson, K., Aitken, R., Tran, L., Stone, V., Duffin, R., Forrest, G. and Alexander, A. (2006), "Carbon nanotubes: A review of their properties in

relation to pulmonary toxicology and workplace safety", *Toxicological Sciences*, Vol. 92 No. 1, pp. 5–22.

Doren, E.A.V., Temmerman, P.-J.R.D., Francisco, M.A. and Mast, J. (2011), "Determination of the volume-specific surface area by using transmission electron tomography for characterization and definition of nanomaterials", *Journal of Nanobiotechnology*, Vol. 9 No. 1, p. 17.

Doucet, F.J., Lead, J.R., Maguire, L., AchterbergPresent address: Southamp, E.P. and Millward, G.E. (2005), "Visualisation of natural aquatic colloids and particles - a comparison of conventional high vacuum and environmental scanning electron microscopy", *Journal of Environmental Monitoring*, Vol. 7 No. 2, p. 115-121.

Draft ISO/WD 14411-2. (In preparation), "Preparation of particulate reference materials - Part 2: Poly-disperse spherical particles".

Du, S., Kendall, K., Morris, S. and Sweet, C. (2010), "Measuring number-concentrations of nanoparticles and viruses in liquids on-line", *Journal of Chemical Technology & Biotechnology*, Vol. 85 No. 9, pp. 1223–1228.

Dubochet, J. (2009), "Vitreous water", in A. Cavallier, D. Spehner, B. M. Humbel (Ed.), *Handbook of cryo-preparation methods for electron microscopy*, CRC Press, pp. 3-18.

Dudkiewicz, A., Luo, P., Tiede, K. and Boxall, A.B.A. (2012), "Detecting and characterizing nanoparticles in food, beverages and nutraceuticals", in Quingrong Huang (Ed.) *Nanotechnology in the food, beverage and nutraceutical industries*, Woodhead Publishing, pp. 53–80.

EFSA Scientific Committee. (2011), "Guidance on the risk assessment of the application of nanoscience and nanotechnologies in the food and feed chain", *EFSA Journal*, Vol. 9(5):2140, pp. 1–36.

Egelandsdal, B., Christiansen, K.F., Høst, V., Lundby, F., Wold, J.P. and Kvaal, K. (1999), "Evaluation of scanning electron microscopy images of a model dressing using image feature extraction techniques and principal component analysis", *Scanning*, Vol. 21 No. 5, pp. 316–325.

Elias, H. and Hyde, D.M. (1980), "An elementary introduction to stereology (quantitative microscopy)", *The American Journal of Anatomy*, Vol. 159, pp. 411-446.

European Commission. (2012), "Second regulatory review on nanomaterials", *Communication from the Commission to the European Parliament, the Council and the European Economic and Social Commitee*, Vol. COM(2012) 572, pp. 1–15.

Fayek, M., Utsunomiya, S., Pfiffner, S., White, D.C., Riciputi, L.R., Ewing, R.C., Anovitz, L.M. and Stadermann, F.J. (2005), "The application of HRTEM techniques and NanoSIMS to chemically and isotopically characterize Geobacter Sulfurreducens surfaces", *The Canadian Mineralogist*, Vol. 43, pp. 1631–1641.

Fede, C., Selvestrel, F., Compagnin, C., Mognato, M., Mancin, F., Reddi, E. and Celotti, L. (2012), "The toxicity outcome of silica nanoparticles (Ludox(R)) is influenced by testing techniques and treatment modalities", *Analytical and Bioanalytical Chemistry*, Vol. 404 No. 6-7, pp. 1789–1802.

Federer, W. t. (1968), "Non-negative estimators for components of variance", *Journal of the Royal Statistical Society: Series C (Applied Statistics)*, Vol. 17 No. 2, pp. 171–174.

Filipe, V., Hawe, A. and Jiskoot, W. (2010), "Critical evaluation of nanoparticle tracking analysis (NTA) by NanoSight for the measurement of nanoparticles and protein aggregates", *Pharmaceutical Research*, Vol. 27 No. 5, pp. 796–810.

Fishman, M.L., Cooke, P., White, B. and Damert, W. (1995), "Size distributions of amylose and amylopectin solubilized from corn starch granules", *Carbohydrate Polymers*, Vol. 26 No. 4, pp. 245–253.

Gallego-Urrea, J.A., Tuoriniemi, J. and Hassellöv, M. (2011), "Applications of particle-tracking analysis to the determination of size distributions and concentrations of nanoparticles in environmental, biological and food samples", *Trends in Analytical Chemistry*, Vol. 30 No. 3, pp. 473–483.

Gatti, A.M., Tossini, D., Gambarelli, A., Montanari, S. and Capitani, F. (2009), "Investigation of the presence of inorganic micro- and nanosized

contaminants in bread and biscuits by environmental scanning electron microscopy", *Critical Reviews in Food Science and Nutrition*, Vol. 49 No. 3, pp. 275–282.

Giannuzzi, L.A. and Stevie, F.A. (1999), "A review of focused ion beam milling techniques for TEM specimen preparation", *Micron*, Vol. 30 No. 3, pp. 197-204.

Gmachowski, L. (2000), "Estimation of the dynamic size of fractal aggregates", *Colloids and Surfaces A: Physicochemical and Engineering Aspects*, Vol. 170 No. 2–3, pp. 209–216.

Gomes, J., Rocha, S., Pereira, M., Peres, I., Moreno, S., Toca-Herrera, J. and Coelho, M. (2010), "Lipid/particle assemblies based on maltodextrin-gum arabic core as bio-carriers", *Colloids and surfaces B-biointerfaces*, Vol. 76 No. 2, pp. 449-455.

Gray, E.P., Bruton, T.A., Higgins, C.P., Halden, R.U., Westerhoff, P. and Ranville, J.F. (2012), "Analysis of gold nanoparticle mixtures: a comparison of hydrodynamic chromatography (HDC) and asymmetrical flow field-flow fractionation (AF4) coupled to ICP-MS", *Journal of Analytical Atomic Spectrometry*, Vol. 27 No. 9, pp. 1532–1539.

Grombe, R., Charoud-Got, J., Emteborg, H., Linsinger, T.P.J., Seghers, J., Wagner, S., von der Kammer, F., Hofmann, T., Dudkiewicz, A., Llinas, M., Solans C., Lehner, A. and Allmaier, G. (2014), "Production of reference materials for the detection and size determination of silica nanoparticles in tomato soup", *Analytical and Bioanalytical Chemistry*, Vol. 406 No. 16, pp. 3895-3907.

Grombe, R., Allmaier, G., Charoud-Got, J., Dudkiewicz A., Emteborg, H., Hofman, Huusfeldt Larsen, E., Lehner, A., Llinas, M., Loeschner, K., Molhave, K., Peters, R.J., Seghers, J., Solans, C., von der Kammer, F., Wagner, S., Weigel, S. and Linsinger, T.P.J. (In preparation), "Feasibility of the development of reference materials for the detection of Ag nanoparticles in food: neat dispersions and spiked chicken meat".

Gun'ko, V.M., Zarko, V.I., Leboda, R. and Chibowski, E. (2001), "Aqueous suspension of fumed oxides: particle size distribution and zeta potential", *Advances in Colloid and Interface Science*, Vol. 91 No. 1, pp. 1–112.

Hagendorfer, H., Kaegi, R., Parlinska, M., Sinnet, B., Ludwig, C. and Ulrich, A. (2012), "Characterization of silver nanoparticle products using asymmetric flow field flow fractionation with a multidetector approach--a comparison to transmission electron microscopy and batch dynamic light scattering", *Analytical chemistry*, Vol. 84 No. 6, pp. 2678–2685.

Haham, M., Ish-Shalom, S., Nodelman, M., Duek, I., Segal, E., Kustanovich, M. and Livney, Y.D. (2012), "Stability and bioavailability of vitamin D nanoencapsulated in casein micelles", *Food & Function*, Vol. 3 No. 7, pp. 737–744.

Hallar, A.G., Chirokova, G., McCubbin, I., Painter, T.H., Wiedinmyer, C. and Dodson, C. (2011), "Atmospheric bioaerosols transported via dust storms in the western United States", *Geophysical Research Letters*, Vol. 38 No. 17, pp. 1-6

Hassellöv, M., Readman, J.W., Ranville, J.F. and Tiede, K. (2008), "Nanoparticle analysis and characterization methodologies in environmental risk assessment of engineered nanoparticles", *Ecotoxicology*, Vol. 17 No. 5, pp. 344-361.

Hayashi, Y., Okado, K., Ashimine, I. and Shoji, M. (2002), "The Baylis-Hillman reaction under high pressure induced by water-freezing", *Tetrahedron Letters*, Vol. 43 No. 48, pp. 8683-8686.

Hayat, M.A. (1989a), "Support films", in Hayat M.A. (Ed.) *Principles and techniques of electron microscopy biological applications*, Macmillan Press Scientific and Medical, Third Edition., p. 376.

Hayat, M.A. (1989b), *Principles and techniques of electron microscopy biological applications*, The Macmillan Press Ltd, Third Edition.

Hillyer, J.F. and Albrecht, R.M. (2001), "Gastrointestinal persorption and tissue distribution of differently sized colloidal gold nanoparticles", *Journal of Pharmaceutical Sciences*, Vol. 90 No. 12, pp. 1927–1936.

ISO/IEC Guide 98-3:2008. (2008). "Uncertainty of measurement- Part 3: Guide to the expression of uncertainty in measurement (GUM:1995)", International Organization for Standarization.

James, B.J. and Smith, B.G. (2009), "Surface structure and composition of fresh and bloomed chocolate analysed using X-ray photoelectron spectroscopy, cryo-scanning electron microscopy and environmental scanning electron microscopy", *LWT - Food Science and Technology*, Vol. 42, No. 5, pp. 929–937.

Jarvis, B. and Hedges, A.J. (2011), "The effect of the number of sample units tested on the precision of microbial colony counts", *Food Microbiology*, Vol. 28 No. 6, pp. 1211–1219.

Jiang, J., Oberdörster, G. and Biswas, P. (2008a), "Characterization of size, surface charge, and agglomeration state of nanoparticle dispersions for toxicological studies", *Journal of Nanoparticle Research*, Vol. 11 No. 1, pp. 77–89.

Jiang, J., Oberdörster, G., Elder, A., Gelein, R., Mercer, P. and Biswas, P. (2008b), "Does nanoparticle activity depend upon size and crystal phase?", *Nanotoxicology*, Vol. 2 No. 1, pp. 33–42.

Jores, K., Mehnert, W., Drechsler, M., Bunjes, H., Johann, C. and Mäder, K. (2004), "Investigations on the structure of solid lipid nanoparticles (SLN) and oil-loaded solid lipid nanoparticles by photon correlation spectroscopy, field-flow fractionation and transmission electron microscopy", *Journal of Controlled Release*, Vol. 95 No. 2, pp. 217-227.

Jóźwiak, K. (2007), "Budowa i działanie elektronowego mikroskopu skaningowego (SEM)", in A. Barbacki (Ed.), *Mikroskopia elektronowa*, Wydawnictwo Politechniki Poznańskiej, pp. 84-92.

Kachlicki, T. (2007a), "Fizyczne podstawy mikroskopii elektronowej", in A. Barbacki (Ed.), *Mikroskopia elektronowa*, Wydawnictwo Politechniki Poznańskiej, pp. 7-15.

Kachlicki, T. (2007b), "Elektronowy mikroskop transmisyjny", A. Barbacki (Ed.), *Mikroskopia elektronowa*, Wydawnictwo Politechniki Poznańskiej, pp. 30-46.

Kaiser, D.L. and Watters, R.L. (2007a), "Report of investigation reference material 8012 gold nanoparticles, nominal 30 nm diameter", National Institute of Standards & Technology, Available from: https://www-s.nist.gov/srmors/view_report.cfm?srm=8012 (accessed 7 March 2014).

Kaiser, D.L. and Watters, R.L. (2007b), "Report of investigation reference material 8013 gold nanoparticles, nominal 60 nm diameter", National Institute of Standards & Technology, Available from: http://www.dunesciences.com /files/SRM8013.pdf (accessed 7 March 2014).

Kaláb, M., Allan-Wojtas, P. and Miller, S.S. (1995), "Microscopy and other imaging techniques in food structure analysis", *Trends in Food Science & Technology*, Vol. 6 No. 6, pp. 177–186.

Kaláb, M. and Larocque, G. (1996), "Research Note: Suitability of agar gel encapsulation of milk and cream for electron microscopy", *Lebensmittel-Wissenschaft und-Technologie*, Vol. 29 No. 4, pp. 368–371.

Kamiti, M., Boldridge, D., Ndoping, L.M. and Remsen, E.E. (2012), "Simultaneous absolute determination of particle size and effective density of submicron colloids by disc centrifuge photosedimentometry", *Analytical chemistry*, Vol. 84 No. 24, pp. 10526–10530.

Kasper, G. (1982), "Dynamics and measurement of smokes. I size characterization of nonspherical particles", *Aerosol Science and Technology*, Vol. 1 No. 2, pp. 187–199.

Kesten, J., Reineking, A. and Porstendörfer, J. (1991), "Calibration of a TSI model 3025 ultrafine condensation particle counter", *Aerosol Science and Technology*, Vol. 15 No. 2, pp. 107–111.

Kittler, S., Greulich, C., Diendorf, J., Köller, M. and Epple, M. (2010), "Toxicity of silver nanoparticles increases during storage because of slow dissolution under release of silver ions", *Chemistry of Materials*, Vol. 22 No. 16, pp. 4548–4554.

Knoll, G., Oebel, G. and Plattner, H. (1982), "A simple sandwich-cryogen-jet procedure with high cooling rates for cryofixation of biological materials in the native state", *Protoplasma*, Vol. 111 No. 3, p. 161.

Knudsen, J.C. and Skibsted, L.H. (2010), "High pressure effects on the structure of casein micelles in milk as studied by cryo-transmission electron microscopy", *Food Chemistry*, Vol. 119 No. 1, pp. 202-208.

Koh, A., Shachaf, C., Elchuri, S., Nolan, G. and Sinclair, R. (2008), "Electron microscopy localization and characterization of functionalized composite

organic-inorganic SERS nanoparticles on leukemia cells", *Ultramicroscopy*, Vol. 109 No. 1, pp. 111–121.

Kousaka, Y., Endo, Y., Ichitsubo, H. and Alonso, M. (1996), "Orientation-specific dynamic shape factors for doublets and triplets of spheres in the transition regime", *Aerosol Science and Technology*, Vol. 24 No. 1, pp. 36–44.

Laborda, F., Jiménez-Lamana, J., Bolea, E. and Castillo, J.R. (2013), "Critical considerations for the determination of nanoparticle number concentrations, size and number size distributions by single particle ICP-MS", *Journal of Analytical Atomic Spectrometry*, Vol. 28 No. 8, pp. 1220–1232.

Lam, C.-W. (2003), "Pulmonary toxicity of single-wall carbon nanotubes in mice 7 and 90 days after intratracheal instillation", *Toxicological Sciences*, Vol. 77 No. 1, pp. 126–134.

Lari, L. and Dudkiewicz, A. (2014), "EFTEM of meat samples for nanoparticle analysis in food", *Journal of Physics: Conference Series*, Vol. 522 No. 1, pp. 012057.

Larrea, V., Perez-Munuera, I., Hernando, I., Quiles, A. and Lluch, M. (2007), "Chemical and structural changes in lipids during the ripening of Teruel dry-cured ham", *Food Chemistry*, Vol. 102 No. 2, pp. 494-503.

Leforestier, A., Richter, K., Livolant, F. and Dubochet, J. (1996), "Comparison of slam-freezing and high-pressure freezing effects on the DNA cholesteric liquid crystalline structure", *Journal of Microscopy*, Vol. 184 No. 1, pp. 4-13.

Leppard, G.G., Heissenberger, A. and Herndl, G.J. (1996), "Ultrastructure of marine snow. I. Transmission electron microscopy methodology", *Marine Ecology Progress Series*, Vol. 135 No. 1-3, pp. 289–298.

Leunissen, J.L.M. and Yi, H. (2009), "Self-pressurized rapid freezing (SPRF): a novel cryofixation method for specimen preparation in electron microscopy", *Journal of Microscopy*, Vol. 235 No. 1, pp. 25-35.

Li, W., Matyjaszewski, K., Albrecht, K. and Moller, M. (2009), "Reactive surfactants for polymeric nanocapsules via interfacially confined miniemulsion ATRP", *Macromolecules*, Vol. 42 No. 21, pp. 8228-8233.

Lienemann, C.-P., Heissenberger, A., Leppard, G.G. and Perret, D. (1998), "Optimal preparation of water samples for the examination of colloidal material by

transmission electron microscopy", *Aquatic Microbial Ecology*, Vol. 14, pp. 205–213.

Linsinger, T.P.J. (2010), "ERM Application Note 1- Comparison of a measurement result with the certified value", pp. 1–2.

Linsinger, T.P.J., Chaudhry, Q., Dehalu, V., Delahaut, P., Dudkiewicz, A., Grombe, R., von der Kammer, F., Huusfeldt Larsen, E., Legros, S., Loeschner, K., Peters, R., Ramsch, R., Roebben, G., Tiede, K. and Weigel, S. (2013), "Validation of methods for the detection and quantification of engineered nanoparticles in food", *Food chemistry*, Vol. 138 No. 2-3, pp. 1959–1966.

Linsinger, T.P.J., Pauwels, J., Veen, A.M.H. van der, Schimmel, H. and Lamberty, A. (2001), "Homogeneity and stability of reference materials", *Accreditation and Quality Assurance*, Vol. 6 No. 1, pp. 20–25.

Linsinger, T.P.J., Roebben, G., Gilliland, D., Calzolai, L., Rossi, F., Gibson, N. and Klein, C. (2012), "Requirements on measurements for the implementation of the European Commission definition of the term 'nanomaterial'.", *JRC Refernce Reports*, Vol. EUR 25404 EN, pp. 1–56.

Liu, J. (2005), "Scanning transmission electron microscopy and its application to the study of nanoparticles and nanoparticle systems", *Journal of Electron Microscopy*, Vol. 54, pp. 251-278.

Liu, K.-L., Wu, C.-C., Huang, Y.-J., Peng, H.-L., Chang, H.-Y., Chang, P., Hsu, L. and Yew, T.R. (2008), "Novel microchip for in situ TEM imaging of living organisms and bio-reactions in aqueous conditions", *Lab on a Chip*, Vol. 8 No. 11, pp. 1915-1921.

Liu, W., Wu, Y., Wang, C., Li, H.C., Wang, T., Liao, C.Y., Cui, L., Zhou, Q.F., Yan, B. and Jiang, G.B. (2010), "Impact of silver nanoparticles on human cells: effect of particle size", *Nanotoxicology*, Vol. 4 No. 3, pp. 319–330.

Loeschner, K., Hadrup, N., Qvortrup, K., Larsen, A., Gao, X., Vogel, U., Mortensen, A., Lam, H.R. and Huusfeldt Larsen E. (2011), "Distribution of silver in rats following 28 days of repeated oral exposure to silver nanoparticles or silver acetate", *Particle and Fibre Toxicology*, Vol. 8 No. 1, pp. 1-14.

Loeschner, K., Navratilova, J., Købler, C., Molhave, K., Wagner, S., von der Kammer, F. and Huusfeldt Larsen, E. (2013a), "Detection and

characterization of silver nanoparticles in chicken meat by asymmetric flow field flow fractionation with detection by conventional or single particle ICP-MS", *Analytical and bioanalytical chemistry*, Vol. 405 No.25, pp.8185-8195

Loeschner, K., Navratilova, J., Legros, S., Wagner, S., Grombe, R., Snell, J., von der Kammer, F. and Huusfeldt Larsen E. (2013b), "Optimization and evaluation of asymmetric flow field-flow fractionation of silver nanoparticles", *Journal of Chromatography A*, Vol. 1272, pp. 116–125.

López-Viota, J., Mandal, S., Delgado, A.V., Toca-Herrera, J.L., Möller, M., Zanuttin, F., Balestrino, M. and Krol, S. (2009), "Electrophoretic characterization of gold nanoparticles functionalized with human serum albumin (HSA) and creatine", *Journal of Colloid and Interface Science*, Vol. 332 No. 1, pp. 215–223.

Lorenz, C., Tiede, K., Tear, S., Boxall, A., von Götz, N. and Hungerbühler, K. (2010), "Imaging and characterisation of engineered nanoparticles in sunscreens by electron microscopy, under wet and dry conditions", *International Journal of Occupational and Environmental Health*, Vol. 16 No. 4, pp. 406–428.

Luo, P., Morrison, I., Dudkiewicz, A., Tiede, K., Boyes, E., O'Toole, P., Park, S. and Boxall, A.B. (2013), "Visualization and characterization of engineered nanoparticles in complex environmental and food matrices using atmospheric scanning electron microscopy", *Journal of microscopy*, Vol. 250 No. 1, pp. 32–41.

Luykx, D.M.A.M., Peters, R.J.B., van Ruth, S.M. and Bouwmeester, H. (2008), "A review of analytical methods for the identification and characterization of nano delivery systems in food", *Journal of Agricultural and Food Chemistry*, Vol. 56 No. 18, pp. 8231–8247.

Lynch, I. and Dawson, K.A. (2008), "Protein-nanoparticle interactions", *Nano Today*, Vol. 3 No. 1-2, pp. 40–47.

Mahdi, S.S., Vadood, R. and Nourdahr, R. (2012), "Study on the antimicrobial effect of nanosilver tray packaging of minced beef at refrigerator temperature", *Global Veterinaria*, Vol. 9 No. 3, pp. 284–289.

Mahl, D., Diendorf, J., Meyer-Zaika, W. and Epple, M. (2011), "Possibilities and limitations of different analytical methods for the size determination of a bimodal dispersion of metallic nanoparticles", *Colloids and Surfaces A: Physicochemical and Engineering Aspects*, Vol. 377 No. 1–3, pp. 386–392.

Maricq, M.M. and Xu, N. (2004), "The effective density and fractal dimension of soot particles from premixed flames and motor vehicle exhaust", *Journal of Aerosol Science*, Vol. 35 No. 10, pp. 1251–1274.

Mast, J. and Demeestere, L. (2009), "Electron tomography of negatively stained complex viruses: application in their diagnosis", *Diagnostic Pathology*, Vol. 4 No. 5, pp. 1-7.

Maunsbach, A.B. and Afzelius, B.A. (1999), *Biomedical Electron Microscopy*, Academic Press.

Mayhew, T.M., Mühlfeld, C., Vanhecke, D. and Ochs, M. (2009), "A review of recent methods for efficiently quantifying immunogold and other nanoparticles using TEM sections through cells, tissues and organs", *Annals of Anatomy - Anatomischer Anzeiger*, Vol. 191 No. 2, pp. 153-170.

McIntosh, R., Nicastro, D. and Mastronarde, D. (2005), "New views of cells in 3D: an introduction to electron tomography", *Trends in Cell Biology*, Vol. 15 No. 1, pp. 43-51.

Melas, A.D., Konstandopoulos, A.G., Isella, L. and Drossinos, Y. (2012), "The friction coefficient of fractal aggregates in the continuum and transition regimes", *Excerpt from the Proceedings of the 2012 COMSOL Conference in Milan*, pp. 1–4.

Messaud, F.A., Sanderson, R.D., Runyon, J.R., Otte, T., Pasch, H. and Williams, S.K.R. (2009), "An overview on field-flow fractionation techniques and their applications in the separation and characterization of polymers", *Progress in Polymer Science*, Vol. 34 No. 4, pp. 351–368.

Micheel, C.M., Zanchet, D. and Alivisatos, A.P. (2008), "Correlation analysis of TEM images of nanocrystal molecules", *Langmuir*, Vol. 24 No. 18, pp. 10084–10088.

Misra, S.K., Dybowska, A., Berhanu, D., Luoma, S.N. and Valsami-Jones, E. (2012), "The complexity of nanoparticle dissolution and its importance in

nanotoxicological studies", *Science of The Total Environment*, Vol. 438, pp. 225–232.

Molero, J.C., Lee, S., Leizerman, I., Chajut, A., Cooper, A. and Walder, K. (2009), "Effects of rosiglitazone on intramyocellular lipid accumulation in Psammomys obesus", *Biochimica et Biophysica Acta - Molecular Basis of Disease*, Vol. 1802 No. 2, pp. 235-239.

Molhave, K. (2004), "Nanomanipulation systems", *Tools for In-situ Manipulation and Characterization of Nanostructures*, MIC - Department of Micro and Nanotechnology Technical University of Denmark., pp. 7–27.

Moor, H. and Muhlethaler, K. (1963), "Fine structure in frozen-etched yeast cells", *Journal of cell biology*, Vol. 17 No. 3, pp. 609-628.

MRC. (2009), "A Response from the MRC Human Nutrition Research Unit to the House of Lords Science and Technology Select Committee Call for Evidence on Nanotechnologies and Food", MRC Collaborative Centre for Human Nutrition Research. Available from:http://www.parliament.uk/documents/lords-committees/science-technology/st148supplementaryevmrc.pdf (accessed 7 March 2014).

Mühlfeld, C., Rothen-Rutishauser, B., Vanhecke, D., Blank, F., Gehr, P. and Ochs, M. (2007), "Visualization and quantitative analysis of nanoparticles in the respiratory tract by transmission electron microscopy", *Particle and Fibre Toxicology*, Vol. 4 No. 1, pp. 1-17.

Musyanovych, A., Schmitz, J., Mail,,nder, V., Walther, P. and Landfester, K. (2008), "Preparation of biodegradable polymer nanoparticles by miniemulsion technique and their cell interactions", *Macromolecular Bioscience*, Vol. 8, pp. 127–139.

Naito, M., Hayakawa, O., Nakahira, K., Mori, H. and Tsubaki, J. (1998), "Effect of particle shape on the particle size distribution measured with commercial equipment", *Powder Technology*, Vol. 100 No. 1, pp. 52–60.

Niels de Jonge, R.S. (2007), "Three-dimensional aberration-corrected scanning transmission electron microscopy for biology", in Vo-Dinh T. (Ed.) *Nanotechnology in biology and medicine – methods, devices, and applications*, CRC Press, p. 13-I

Nisman, R., Dellaire, G., Ren, Y., Li, R. and Bazett-Jones, D.P. (2004), "Application of quantum dots as probes for correlative fluorescence, conventional, and energy-filtered transmission electron microscopy", *Journal of Histochemistry and Cytochemistry*, Vol. 52 No. 1, pp. 13–18.

Noronha, N., Duggan, E., Ziegler, G.R., Stapleton, J.J., O'Riordan, E.D. and O'Sullivan, M. (2008), "Comparison of microscopy techniques for the examination of the microstructure of starch-containing imitation cheeses", *Food Research International*, Vol. 41 No. 5, pp. 472–479.

Norwegian Pollution Control Authority. (2008), "Environmental fate and ecotoxicity of engineered nanoparticles.". Available from: http://www.bioforsk.no/ikbViewer/Content/49692/SFTs%20rapport.pdf (accessed 7 March 2014).

Novak, J.P., Nickerson, C., Franzen, S. and Feldheim, D.L. (2001), "Purification of molecularly bridged metal nanoparticle arrays by centrifugation and size exclusion chromatography", *Analytical Chemistry*, Vol. 73 No. 23, pp. 5758–5761.

Palka, K. (2003), "The influence of post-mortem ageing and roasting on the microstructure, texture and collagen solubility of bovine semitendinosus muscle", *Meat Science*, Vol. 64 No. 2, pp. 191–198.

Pan, J.F., Buffet, P.E., Poirier, L., Amiard-Triquet, C., Gilliland, D., Joubert, Y., Pilet, P., Guibbolini, M., Risso de Faverney, C., Roméo, M., Valsami-Jones, E., Mouneyrac, C. (2012), "Size Dependent Bioaccumulation and Ecotoxicity of Gold Nanoparticles in an Endobenthic Invertebrate: The Tellinid Clam Scrobicularia Plana". *Environmental Pollution* Vol 168, pp. 37–43.

Park, S., Woodhall, J., Ma, G., Veinot, J.G., Cresser, M.S. and Boxall, A.B. (2013), "Regulatory ecotoxicity testing of engineered nanoparticles: are the results relevant to the natural environment?", *Nanotoxicology*, pp. 1–10.

Peckys, D.B., Veith, G.M., Joy, D.C. and de Jonge, N. (2009), "Nanoscale imaging of whole cells using a liquid enclosure and a scanning transmission electron microscope", *PLoS ONE*, Vol. 4 No. 12, pp. 1-7

"PEN The Project on Emerging Nanotechnologies". (2013). Available from: http://www.nanotechproject.org/ (accessed 7 March 2014).

Perret, D., Leppard, G.G., Müller, M., Belzile, N., DeVitre, R. and Buffle, J. (1991), "Elecron-microscopy of aquatic colloids: non-perturbing preparation of specimens in the field", *Water Research*, Vol. 25 No. 11, pp. 1333-1343.

Peters, R., Kramer, E., Oomen, A.G., Herrera Rivera, Z.E., Oegema, G., Tromp, P.C., Fokkink, R., Rietveld, A., Marvin, H.J.P., Weigel, S., Peijinenburg A.A.C.M., Bouwmeester, H. (2012), "Presence of nano-sized silica during in vitro digestion of foods containing silica as a food additive", *ACS Nano*, Vol. 6 No. 3, pp. 2441–2451.

Plathe, K.L., von der Kammer, F., Hassellöv, M., Moore, J., Murayama, M., Hofmann, T. and Hochella, M.F. (2010), "Using FlFFF and aTEM to determine trace metal–nanoparticle associations in riverbed sediment", *Environmental Chemistry*, Vol. 7 No. 1, pp. 82–93.

Porter, A.E., Gass, M., Muller, K., Skepper, J.N., Midgley, P. and Welland, M. (2007), "Visualizing the uptake of C60 to the cytoplasm and nucleus of human monocyte-derived macrophage cells using energy-filtered transmission electron microscopy and electron tomography", *Environmental Science & Technology*, Vol. 41 No. 8, pp. 3012–3017.

Pouchou, J.-L., Boivin, D., Beauchêne, P., Besnerais, G.L. and Vignon, F. (2002), "3D reconstruction of rough surfaces by SEM stereo imaging", *Microchimica Acta*, Vol. 139 No. 1-4, pp. 135-144.

Principe, E.L. (2007), "High-density FIB-SEM 3D nanotomography with applications of real-time imaging during FIB milling", in N. Yao (Ed.), *Focused ion beam systems*, Cambridge University Press, pp. 146-186.

Quantomix. (2011,September19), ":: QuantomiX WETSEM® Technology ::". Available from: http://www.quantomix.com/ (accessed 19 September 2011).

Rahman, I.A., Vejayakumaran, P., Sipaut, C.S., Ismail, J. and Chee, C.K. (2008), "Effect of the drying techniques on the morphology of silica nanoparticles synthesized via sol-gel process", *Ceramics International*, Vol. 34 No. 8, pp. 2059–2066.

Raja Mohd Hafidz, R.N., Yaakob, C.M., Amin, I. and Noorfaizan, A. (2011), "Chemical and functional properties of bovine and porcine skin gelatin", *International Food Research Journal*, Vol. 18, pp. 813–817.

Small, J.A. and Watters, R.L. (2012), "Report of investigation reference material® 8011 gold nanoparticles, nominal 10 nm diameter", National Institute of Standards & Technology. Available from: http://www.dunesciences.com/files/SRM8011.pdf (accessed 7 March 2014)

Ström, G., Öhgren, C. and Ankerfors, M. (2013), "Nanocellulose as an additive in foodstuff Innventia Report No.: 403 Nanocellulose as an additive in foodstuff", Inventia. Available from: http://www.innventia.com/Documents/Rapporter/Innventia%20report403.pdf (accessed 7 December 2013).

TEAM. (2013), "The TEAM Project: What is the TEAM microscope?". Available from: http://ncem.lbl.gov/TEAM-Project/Files/What.html (accessed 15 December 2013).

The European Commission. (2011), "Commission recommendation of 18 October 2011 on the definition of nanomaterial (Text with EEA relevance)", *Official Journal of the European Union*, Vol. 275, pp. 38–40.

Thiel, B.L., Bache, I.C., Fletcher, A.L., Meredith, P. and Donald, A.M. (1997), "An improved model for gaseous amplification in the environmental SEM.", *Journal of Microscopy*, Vol. 187, pp. 143-157.

Tiede, K., Boxall, A., Tear, S., Lewis, J., David, H. and Hassellov, M. (2008), "Detection and characterization of engineered nanoparticles in food and the environment", *Food Additives & Contaminants: Part A*, Vol. 25 No. 7, pp. 795–821.

Tiede, K., Boxall, A.B.A., Tiede, D., Tear, S.P., David, H. and Lewis, J. (2009a), "A robust size-characterisation methodology for studying nanoparticle behaviour in 'real' environmental samples, using hydrodynamic chromatography coupled to ICP-MS", *Journal of Analytical Atomic Spectrometry*, Vol. 24 No. 7, pp. 964-972.

Tiede, K., Boxall, A.B.A., Wang, X., Gore, D., Tiede, D., Baxter, M., David, H., Tear, S.P. and Lewis J. (2010), "Application of hydrodynamic chromatography-ICP-MS to investigate the fate of silver nanoparticles in activated sludge", *Journal of Analytical Atomic Spectrometry*, Vol. 25 No. 7, pp. 1149-1154.

Tiede, K., Hassellov, M., Breitbarth, E., Chaudhry, Q. and Boxall, A. (2009b), "Considerations for environmental fate and ecotoxicity testing to support environmental risk assessments for engineered nanoparticles", *Journal of Chromatography A*, Vol. 1216 No. 3, pp. 503–509.

Tiede, K., Tear, S.P., David, H. and Boxall, A.B.A. (2009c), "Imaging of engineered nanoparticles and their aggregates under fully liquid conditions in environmental matrices", *Water Research*, Vol. 43 No. 13, pp. 3335–3343.

In 't Veld, P.H., van Strijp-Lockefeer, N.G., Havelaar, A.H. and Maier, E.A. (1996), "The certification of a reference material for the evaluation of the ISO method for the detection of Salmonella", *The Journal of applied bacteriology*, Vol. 80 No. 5, pp. 496–504.

Villiger, W. and Bremer, A. (1990), "Ultramicrotomy of biological objects: From the beginning to the present", *Journal of Structural Biology*, Vol. 104 No. 1-3, pp. 178-188.

Vogelgesang, J. and Hädrich, J. (1998), "Limits of detection, identification and determination: a statistical approach for practitioners", *Accreditation and Quality Assurance*, Vol. 3 No. 6, pp. 242–255.

Wagner, T., Wiemann, M., Schmitz, I. and Lipinski, H.-G. (2013), "A cluster-based method for improving analysis of polydisperse particle size distributions obtained by nanoparticle tracking", *Journal of Nanoparticles*, Vol. 2013, pp. 1-9.

Wahlund, K.G. and Giddings, J.C. (1987), "Properties of an asymmetrical flow field-flow fractionation channel having one permeable wall", *Analytical Chemistry*, Vol. 59 No. 9, pp. 1332–1339.

Weir, A., Westerhoff, P., Fabricius, L., Hristovski, K. and von Goetz, N. (2012), "Titanium dioxide nanoparticles in food and personal care products", *Environmental Science & Technology*, Vol. 46 No. 4, pp. 2242–2250.

Weiss, V.U., Subirats, X., Pickl-Herk, A., Bilek, G., Winkler, W., Kumar, M., Allmaier, G., Blaas, D. and Kenndler E. (2012), "Characterization of rhinovirus subviral A particles via capillary electrophoresis, electron microscopy and gas-phase electrophoretic mobility molecular analysis: Part I", *Electophoresis*, Vol. 33 No. 12, pp. 1833–1841.

Win, K. and Feng, S. (2005), "Effects of particle size and surface coating on cellular uptake of polymeric nanoparticles for oral delivery of anticancer drugs", *Biomaterials*, Vol. 26 No. 15, p. 2713-2722.

Winter, D.A.M.D., Schneijdenberg, C.T.W.M., Lebbink, M.N., Lich, B., Verkleij, A.J., Drury, M.R. and Humbel, B.M. (2009), "Tomography of insulating biological and geological materials using focused ion beam (FIB) sectioning and low-kV BSE imaging", *Journal of Microscopy*, Vol. 233 No. 3, pp. 372-383.

Woehlecke, H., Lerche, D., Detloff, T., Franks, K., Kestens, V. and Roebben, G. (2013), "In-situ determination of the effective particle density of suspended colloidal silica particles by means of analytical centrifugation", *International Congress on Particle Technology (PARTEC) Abstracts and Proceedings*.

Won, Y.-Y., Brannan, A.K., Davis, H.T. and Bates, F.S. (2002), "Cryogenic transmission electron microscopy (Cryo-TEM) of micelles and vesicles formed in water by poly(ethylene oxide)-based block copolymers", *The Journal of Physical Chemistry B*, Vol. 106 No. 13, pp. 3354-3364.

Wriedt, T. (2012), "Mie theory: a review", in Hergert W. and Wriedt T. (Ed.), *The Mie theory basics and applications*, Springer Series in Optical Sciences, Springer, pp. 53–71.

Zelenyuk, A., Cai, Y. and Imre, D. (2006), "From agglomerates of spheres to irregularly shaped particles: determination of dynamic shape factors from measurements of mobility and vacuum aerodynamic diameters", *Aerosol Science and Technology*, Vol. 40 No. 3, pp. 197–217.

Zhang, X., Jin, L., Fang, Q., Hui, W.H. and Zhou, Z.H. (2010), "3.3 Å Cryo-EM structure of a nonenveloped virus reveals a priming mechanism for cell entry", *Cell*, Vol. 141 No. 3, pp. 472-482.

Zheng, H., Smith, R.K., Jun, Y., Kisielowski, C., Dahmen, U. and Alivisatos, A.P. (2009), "Observation of Single Colloidal Platinum Nanocrystal Growth Trajectories", *Science*, Vol. 324 No. 5932, pp. 1309–1312.

Zheng, Y.Z., Webb, R., Greenfield, P.F. and Reid, S. (1996), "Improved method for counting virus and virus like particles", *Journal of Virological Methods*, Vol. 62 No. 2, pp. 153–159.

Zook, J.M., Long, S.E., Cleveland, D., Geronimo, C.L.A. and MacCuspie, R.I. (2011), "Measuring silver nanoparticle dissolution in complex biological and environmental matrices using UV–visible absorbance", *Analytical and Bioanalytical Chemistry*, Vol. 401, pp. 1993–2002.